THE EFFECT OF STIMULUS LOCATION ON THE MAJOR COMPONENTS OF THE VISUAL EVOKED RESPONSE

CATHERYN JANE NESFIELD

Doctor of Philosophy

ASTON UNIVERSITY, BIRMINGHAM

MAY 1992

Aston University

The Effect of Stimulus Location on The Major Components of the Visual Evoked Response

Catheryn Jane Nesfield

Doctor of Philosophy

1992

The topographical distribution of the pattern reversal Visual Evoked Response (VER) was recorded from a localised montage of 20 electrodes over the visual cortex. The response was recorded after stimulation with a black and white checkerboard stimulus. The effect of field location on the major components was investigated in 11 subjects (age range (23-55). The major components of the half field response were; a negative around 75ms (N75) followed by a positivity around 80ms (P80), then a positivity around 100ms (P100) followed by another positivity at around 120ms (P120) and a negativity at approximately 145ms (N145). No effect of field size could be demonstrated on either the amplitude or latency of the late negativity, N145. No significant effect of field size or location was shown on the latency of the P100 response. A delay previously shown in the upper half field response was therefore not substantiated. In contrast the amplitude of the major positivity, P100 was significantly affected by the field size and location. The amplitude of both P100 and N145 were significantly reduced following upper field stimulation when compared with the lower field response. No significant amplitude difference between the upper and lower field responses was demonstrated using electroretinography, the amplitude may therefore be reduced as a result of the ventral position of the upper field representation on the visual cortex.

The lateral half field VEP was compared with the distribution of the visual evoked magnetic response (VEMR). The distribution of the VEMR supported the proposal that the paradoxical lateralisation of the VEP half field response is the result of the source being directed ipsilaterally.

The morphology of the VEP following octant and double octant stimulation suggests that the response is generated in the striate cortex, with a reversal in response distribution following stimulation of the upper vertical and horizontal meridia.

Key Words: pattern reversal, visual evoked potential, visual evoked magnetic response, visual field, mapping, major components.

Acknowledgements

I would like to acknowledge the guidance, support and encouragement from my supervisor Professor Graham Harding.

I am indebted to Antoinette Slaven for all her help with the Biomagnetometry and Dr Richard Armstrong for his advice and statistical expertise. I also wish to thank Antoinette for permitting me to include in my thesis the full field recordings made using the magnetometer.

I would also like to thank all the staff in the Clinical Neurophysiology unit, especially Paul Furlong and Vivica Tipper, for their help and assistance.

I am grateful to all those who gave up many hours to sit as subjects for me.

I also want to thank Mark Brown for not only sitting as a subject but for also putting up with me in the past months.

List of Contents

List of Figures

List of Tables

List of Appendices

CHAPTER 1

Introduction

Much of the critical information gathered on brain function is based on results from experiments on animals, mainly monkeys. The enthusiasm for study of functioning of the human brain has fuelled the necessity for the development of noninvasive techniques.

The first major advance came with the recording of electrical activity generated in the brain but detected on the scalp surface. Initially only passive ongoing activity could be recorded, then with the introduction of averaging a whole new field of human brain research was opened. Averaging provided a means for extracting stimulus related activity from the much larger background activity. Visual evoked activity is recorded after stimulation of the visual system with either a pattern or uniform light.

The visual evoked potential (VEP) is recorded from scalp electrodes attached over the visual cortex. The latency and morphology of the response can be recorded from a limited number of electrode placements. Greater information regarding the source may however be gained by topographic mapping which produces a distribution of potential over the scalp surface. From investigation of the potential gradients in these distributions the area of activation and nature of the source can be indicated. Localised montages of electrodes may increase the accuracy of source prediction by enhancing the topographic distribution.

The visual evoked response to a pattern stimulus is dependent upon the mode of stimulation. A reversing checkerboard stimulus produces a waveform with three quantifiable features, the latency of the first negative peak, the latency of the positive peak and the latency of the second negativity. On half field stimulation the negative, positive, negative response is recorded over the midline and ipslateral hemisphere, a response with opposite polarities of similar latencies is recorded over the contralateral hemisphere. A comparison of the topographical distribution at these three latencies could indicate whether the cortical region of generation is similar or different.

Other methods are available to investigate the functional brain activity. Research into PET (positron emission tomography) scanning as a method of showing the

source of brain activity has shown it to be a valid approach. A map of the region of highest activity after stimulation using this method is compared with an anatomical picture of the brain to determine the region of activation. This technique is however not truly noninvasive as a tracer must first enter the blood supply and, in addition, the temporal resolution is inadequate.

Recent advances in noninvasive techniques have meant that more accurate modelling of the sources of physiological events can be made. In the past thirty years biomagnetism has become recognised as a practical procedure to investigate electrical events in the brain. By recording the magnetic field around a current source the generator of that current can be more accurately located and an approximate depth estimated. Biomagnetism evades two of the major problems encountered with the VEP, that of the reference electrode and smearing and reduction of the response by multiple interfaces and resistance, respectively, within and between the cortical tissues and scalp.

A paradox found in the occurence of the maximum positive component of the visual evoked potential (VEP) over the wrong hemisphere, when using a half field stimulus, is now well established. This is thought to be the result of a tangentially oriented source located in the correct hemisphere. Biomagnetometry is more sensitive to tangential sources and should therefore be unaffected by this source orientation so producing a distribution over the correct hemisphere. The VEP and VEMR (visual evoked magentic response) therefore contain complementary information regarding the same cortical source.

There has been much deliberation over the cortical generator of the VEP, both striate and extrastriate generators have been proposed. The cortical representation of the visual field in the striate cortex and along the calcarine fissure is simplistically modelled as a cross (+), termed the 'cruciform model'. The distribution of the response following localised stimulation may assist in predicting the origin and orientation of the source, by investigating both the waveform morphology and peak components topographic distribution.

CHAPTER 2

THE VISUAL SYSTEM

2.1 Introduction

The visual system consists of a pathway of neurons projecting from the photoreceptors in the retina to the cerebral cortex. The photoreceptors stimulate first order neurons; bipolars which then synapse with ganglion cells, these are all situated within the retina. The ganglion cells constitute the second order neurons and their axons project to at least 6 different areas of the brain, the main area being the dorsal Lateral Geniculate Nucleus (LGNd). In mammals and marsupials the ganglion cells also project to:

1.The Superior Colliculus

2.The Accessory Optic System

3.The Hypothalamus

4.The Pretectal Complex

1. This area is the mesencephalic root of the optic tract (diencephalic root to the LGNd), the projection is very small in Man (Davson 1984). From this region there is a projection to the pulvinar or lateral posterior nucleus of thalamus (Kaas 1977) and then onto the extrastriate areas. The function is related to visual attention and in primates to the control of eye movements (Schiller 1977). In primates there is also a pathway to the occipital and temporal extrastriate areas (Lin and Kaas 1979) and a lesser projection to the striate cortex layers I and II. The major functions of the superior colliculus will be discussed in more detail later in this chapter.

2. The accessory optic system can be divided into the inferior and superior optic tracts (Hayhow et al 1960). Fibres in the inferior tract project to a dorsal portion of a prominent terminal nucleus in the midbrain tegentum. The majority of the superior tract terminates in the dorsal and lateral nuclei of the optic tract, however some fibres also end in the basal portion of the medial terminal nucleus. A hypothalamic termination has also been described which may influence non circadian rhythmic effects of continuous light or dark exposure (Stephen and Zucker 1972).

3.The circadian rhythm is influenced by the light input through this pathway (Moore and Klein 1974).

4.Fibres from this region carry input to pupillomotor and accomodative eye muscles.

2.2 Gross Anatomy of the Visual System

2.2.1 Optic Nerve Fibres

The axons of the ganglion cells in the optic nerve remain roughly grouped through to the LGNd according to their site of origin in the retina. There are five main groups:

1.Macular

2.Upper temporal

3.Lower temporal

4.Upper nasal

5.Lower nasal

When the optic nerve leaves the eye the macular fibres are bundled together in the temporal portion of the nerve but, as the nerve extends, these fibres become more diffuse and some migrate into the centre. At the optic chiasm the fibres from the nasal halves of each retina decussate so that each cerebral hemisphere receives inputs from the contralateral half of the visual field (or ipsilateral half of the retinae).

In the optic tract the majority of the macular fibres are situated in the superior portion but there are also fibres distributed throughout the tract. Fibres representing the temporal crescent of the visual field are located in both the dorsal and ventral areas of the tract (Harrington 1981).

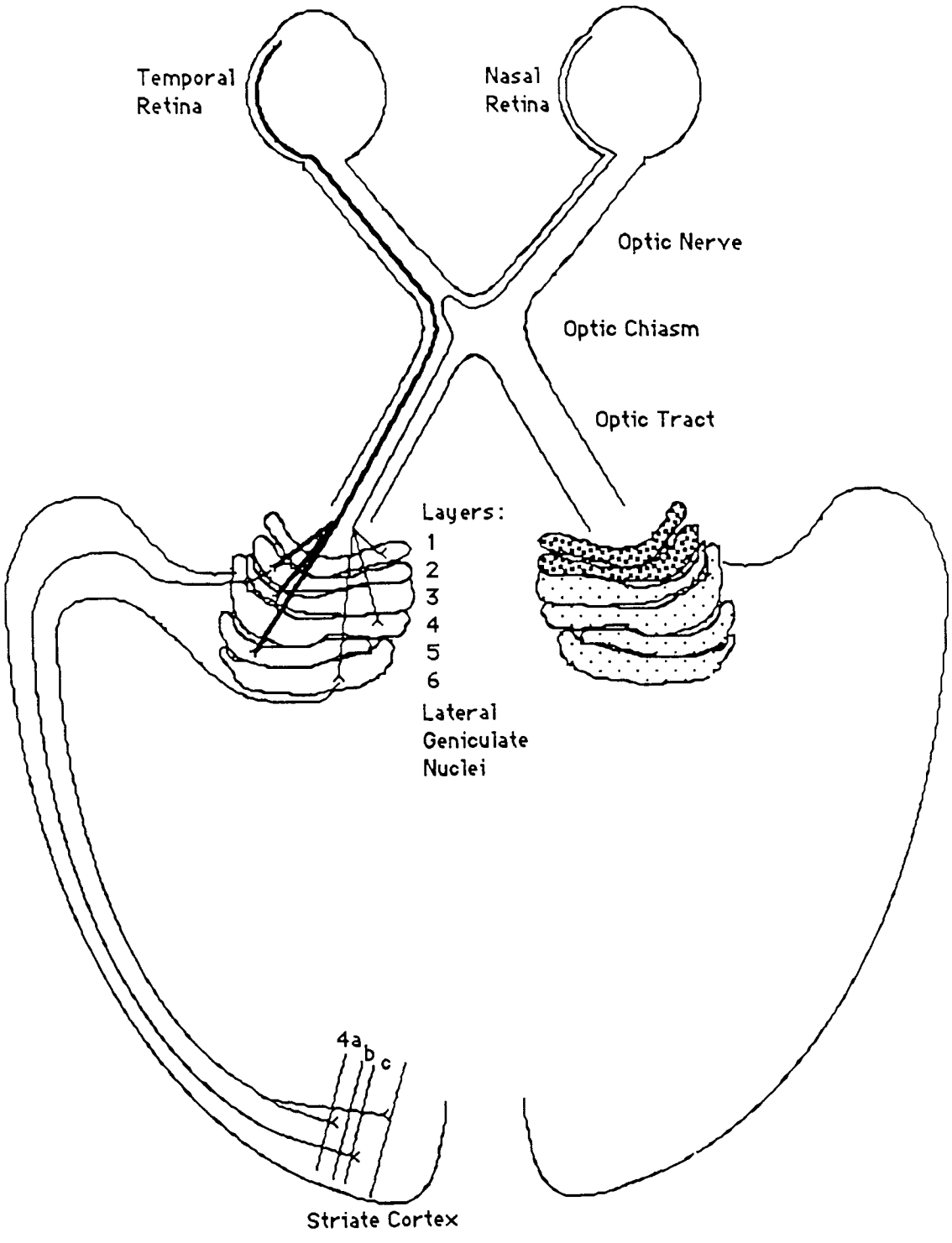

Fig 2.1. Diagrammatic illustration of the visual pathway from the retina to the striate cortex.

2.2.2 The Lateral Geniculate Nucleus

This should be considered as the dorsal Lateral Geniculate Nucleus (LGNd) since the ventral nucleus, or pregeniculate nucleus (PGN) in primates receives retinal input which is not projected to the cerebral cortex. Approximately 80% of axons from the optic tract synapse in the LGNd (Harrington 1981). The neurons can be classed in two groups; those in which the axons project to the visual cortex, and a small number with short axons which terminate within the LGNd. The LGNd is made up of 6 layers, see fig.2.2, although the four dorsal layers may actually be the result of folding in two layers (Kaas 1972, 1978). The crossed fibres from the nasal retina synapse in layers 1, 4 and 6, whereas the uncrossed fibres from the temporal retina synapse in layers 2, 3 and 5. The fibres from the two eyes are therefore segregated and no binocular driven cells are found. The fibres are also further segregated; cells with large axons are found in the two ventral layers (the magnocellular layers), and cells with small axons are found in the remaining four dorsal layers (the parvocellular layers).

The third order neurones' axons pass from the LGNd to the striate cortex, Brodmann's area 17.

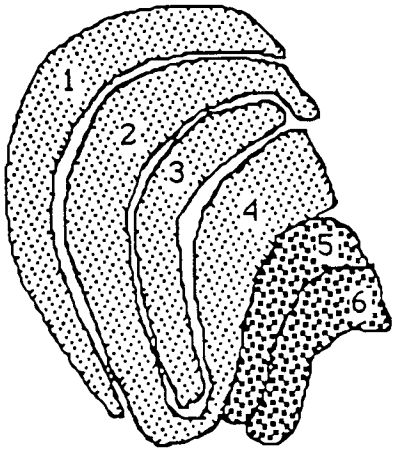

Fig.2.2 Illustration of the Macaque LGN. After Hubel (1989).

2.2.3 Striate Cortex

The striate cortex receives and processes information from the LGNd and subsequently integrates the inputs from the two eyes. The striate cortex or V1 lies

within Brodmann's area 17. It is located on the occipital lobe of each hemisphere around the calcarine fissure, usually over half of the striate cortex is located within the calcarine fissure (Polyak 1957). The area is defined by the white line of Gennari (Holmes 1918) formed by axons of the optic radiation and axons of association fibres passing to the adjacent cortex. The anterior boundary is usually located just in front of the junction of the inner parieto-occipital sulcus and the calcarine fissure. From studies on soldiers with gunshot wounds after the First World War, Holmes (1919) predicted that the projections from the geniculocalcarine pathways were retinotopically mapped onto the striate cortex,see fig.2.3. The fibres from the macular terminate most posteriorly and the periphery anteriorly, with the fibres from the monocular temporal crescent projecting most anteriorly (Holmes 1919,Dobelle et al 1979). The upper quarter of the visual field is projected to cortex below the calcarine fissure and the lower quarter to the cortex above (Holmes 1919). The horizontal meridian is represented within the calcarine fissure whereas the vertical meridian is represented on the lip of the calcarine fissure (Holmes 1918).

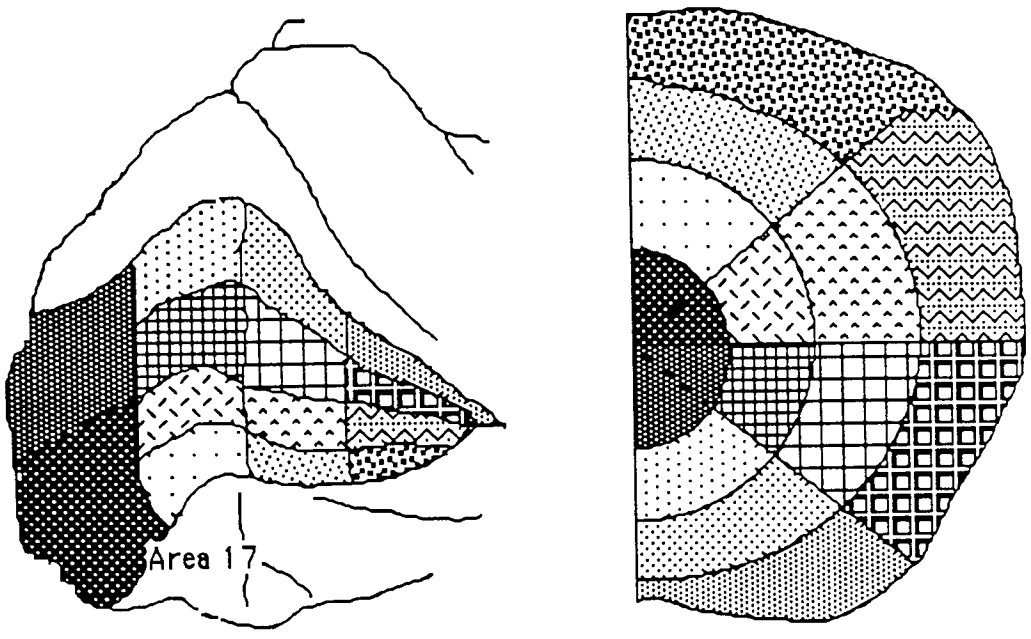

Fig.2.3. Representation of the projection of the visual field onto the striate cortex After G.Holmes (1945).

Eliot-Smith (1907) divided the calcarine fissure into two regions; posterior and anterior. The posterior calcarine fissure has striate area on both superior and inferior banks whereas the anterior calcarine fissure possesses striate cortex only on the floor. This was quantified by Zeki (1977) who stated that, after the first 25mm the upper lip of the calcarine fissure did not represent the striate cortex.

Holmes (1918) observed that the position of the striate area could be approximately located from the position of the inion, or boney occipital protruberence, the posterior end of the calcarine fissure was positioned roughly 2cm above the inion's tip. The fissure then extended forward and up at an angle of about 25° to a depth of approximately 4cm. The projection was uniform in the sense that each portion of the visual field projected to the same area of striate cortex. The thinnest cortex is the most posterior portion in the pocket of the lateral or posterior calcarine fissure near or at the occipital pole. The thickest area is in the anterior projection where the monocular nasal portion of the contralateral half field is represented.

Stensaas et al (1974) demonstrated that the striate cortex extends about 5cm from the pole, with the area below the calcarine fissure extending most anteriorly. The area exposed on the mesial surface below the calcarine fissure was on average greater (271mm^2) than that above (148mm^2).

2.2.4 Variability of the Striate Cortex

The position, shape and extent of the striate cortex varies greatly between individuals (Eliot-Smith 1906, Brindley 1972, Stensaas et al 1974). Stensaas et al (1974) showed, in 52 hemispheres a three fold difference in the amount of striate cortex present and a four fold difference in the amount of cortex exposed. The striate area not only varied between individuals but also between paired hemispheres, in 46 paired hemispheres only 2 were symmetrical, in 15 the left hemisphere possessed more striate cortex, a greater area of this being exposed. The striate cortex was not always situated on the pole as is the classical conception, in some cases it was totally represented around the calcarine fissure.

Le May and Kido (1978) described cerebral asymmetries from computed tomograms of 165 patients (80 right handed and 85 left handed). In seventy-one percent of the right handers the left parieto-occipital area was wider than the right, in only nine percent was the right occipital lobe larger than the left. In seventy-five percent the left hemisphere was found to extend more posteriorly than the right. In the left handed group the asymmetries tended to be less obvious. However, widening of the right occipital area was more common in left handers. The right occipital area was wider in thirty-two percent, the same in thirty-four percent and smaller in thirty-four percent. The left hemisphere was shown to extend more posteriorly in fortytwo percent, be equal in forty percent and the right extended more posteriorly in fourteen percent.

Subjects	Lt Occiput Wider	Equal	Rt Occiput Wider
Right Handers			
40M	29	9	2
40F	28	7	5
Left Handers			
48M	16	19	13
37F	13	10	14

Table 2.1. Comparative widths of the occipital cerebral hemispheres (in the left handed group 10 of the males and 17 of the females had other family members who were left handed). Table after LeMay and Kido (1978)

In 1982, Weinberger et al demonstrated a 20% greater volume in the right occipital region compared with the left, although the region referred to as the occiput was not demonstrated cytoarchitectonically. Murphy (1985) measured the volume asymmetry of the two striate cortices, the right striate cortex was found to be larger in 77% of the cases examined. This may appear contradictory to the results of Stenaas et al (1974), this is because they calculated the area whereas Murphy (1985) and Weinberger et al (1982) recorded the volume of the striate cortex.

2.2.5 Cortical Representation of the Visual Field

There have been many conflicting reports as to the amount of striate cortex devoted to a certain defined area of the visual field. Lenz (1914) calculated that the first 2-3cms of striate cortex anterior to the occipital pole were devoted to the central 30°. However Holmes (1919) , Spalding(1952) and Teuber et al (1960) proposed that the first cm represents the central 8-10°; 2.5cm represents 30°; 3.5cm, 50°; and 4.5cm, 70°. Polyak (1957) claimed that the first cm is the macular representation of 2-3°, this was however disputed by Duke-Elder and Wybar (1961) who proposed that the macular area is represented in the first 3 cms. The first 2.5cms has been calculated to represent 15° (Brindley 1972) and 25-50° (Stensaas 1974).

It is obvious that a disproportionately large amount of cortex is required in processing the central visual field. The value of this is greatest at the macular and falls steeply to the periphery. The linear extent of the cortex devoted to each linear degree on the retina has been termed the magnification factor (Daniel and Whitteridge 1961). The linear factor is adequate providing that the magnification is

approximately the same at a certain eccentricity. In the peripheral retina the magnification factor is proportional to the ganglion cell density (Rolls and Cowey 1970). Transposing this into ganglion receptive field density (Dr), Drasdo (1977) showed that the magnification factor (M) was proportional to $\sqrt{Dr}$. In the human it was calculated that the maximal value of M, which is at the fovea, was 11.5mm/°. The value of M for the peripheral visual field subsequently declines and can be computed by using the following equation with different 'S' values for the different retinal areas:

$$V=k[1+S\emptyset(1+3\emptyset^2 x10^{-5}+8(S\emptyset)5.5x10^{-10}]$$

$V=1/\sqrt{Dr}$, and $k=1/\sqrt{Dr}$ for the fovea

$S=(0.46-0.00043\emptyset)$ for temporal meridian

$S=(0.50+0.0019\emptyset)$ for nasal meridian

$S=(0.62+0.0033\emptyset)$ for superior meridian

$S=(0.6-0.0006\emptyset)$ for inferior meridian

can be approximated to : $V=k(1+0.59\emptyset)$ for $\emptyset < 30°$

The same formula, $M^2=gDr$ was used by Rovamo and Virsu (1979) they however inputed a different value for Dr. An average of the direct counts of Polyak and Osterberg was used, this value being approximately half that used by Drasdo (1977). Their value of 7.99mm/° for the foveal magnification factor was therefore significantly less than that of Drasdo. Four seperate equations were computed for deriving the value of M at various locations in the visual field, as above. Using M scaled targets they recorded the contrast sensitivity and resolution of different areas of the visual field. All contrast sensitivity results were within a factor of +/-2, with a higher sensitivity being observed from the temporal and inferior fields. The resolution of the retina could be computed by the equation; R=rM c/°. In support of his higher value for the foveal M Drasdo (1989) showed that his model was probably the best for the estimation of Dr for all types of ganglion cells. The slope of the Drasdo model is close to that of the parvocellular ganglion cells which represent about eighty percent of the total population of ganglion cells (Perry and Cowey 1985), whereas that of the Rovamo and Virsu model falls midway between the parvocellular and magnocellular ganglion cells. Consequently any visual test that stimulates either population of cells independently will not be appropriate to their model. To overcome this a correction factor for spatial summation was introduced by Rovamo and Raninen (1984).

In 1985 Perry and Cowey attempted to calculate the linear radial representation of each degree of the visual field of the Macaque monkey. The ganglion cell distribution was shown to decline less steeply in the nasal direction than in any

other, and the cone distribution along the nasal meridian was also greater than any other. The dorsal retina possessed a slightly lower density of both cones and ganglion cells over the first few mm from the fovea as compared to the ventral area. In the central 2° the ratio of the nasal to temporal ganglion cells was approximately 1 whereas between 20° and 40° the ratio was approximately 1.5, this is reflected in the width of the ocular dominance columns in the striate cortex. They failed to demonstrate a simple relationship between the ganglion cell density and the cortical or subcortical magnification factors. The first step in the overemphasis of the central visual field was shown to occur in the LGNd; the Pß ganglion cells in the central 5° showed expansion in the LGNd whereas in the periphery the opposite occured, the Pa ganglion cells showed compression at all eccentricities. The overrepresentation of the central field therefore occurs in two steps, the retinogenicular projecton being the first and the next involving the geniculo cortical projection.

2.2.6 Prestriate Cortex

Surrounding V1 in the cortex is an area known as the prestriate cortex. Because of its ill-defined cyto-architecture this was previously thought to be one area but with more anatomical and functional evidence it has been shown to be a composite of several distinct areas involved with visual processing.

A visual area is defined by Zeki (1978) as having :

1. A well defined cytoarchitecture

2. A complete map of the visual field

3. A well defined anatomical input

4. Distinct functional properties

5. Callosal connections

The first definition cannot be applied to the prestriate cortex, the visual field may be multiply mapped in one area or not completely mapped. Boundary evidence can sometimes be shown by the reversal of the meridian mapped e.g horizontal-vertical-horizontal, this may also be accompanied by a change in the cell's characteristics. Some areas may, however contain maps with a number of reversals. The prestriate area of the monkey can be divided into at least 6 areas e.g. V2, V3, V3A, VP, V4, V4A all, except the motion area of the superior temporal sulcus (V5) which lies within area 19, lie within Brodmann's area 18, see fig.2.4

and fig.2.5. Each area may be involved in processing a different part of the visual scene and so it is obvious that a whole map of the visual field may not required in each area e.g. for colour analysis only the central retina would be required and for motion analysis it would be more relevant to have information from the periphery, although each area may not only have one function. The functions of these various areas will be dealt in more detail later in this chapter. Much of the functional analysis of the striate and extrastriate cortex has been performed on the monkey. It has previously been demonstrated that the rhesus monkey is an excellent model for the human visual system (Harwerth and Smith 1985).

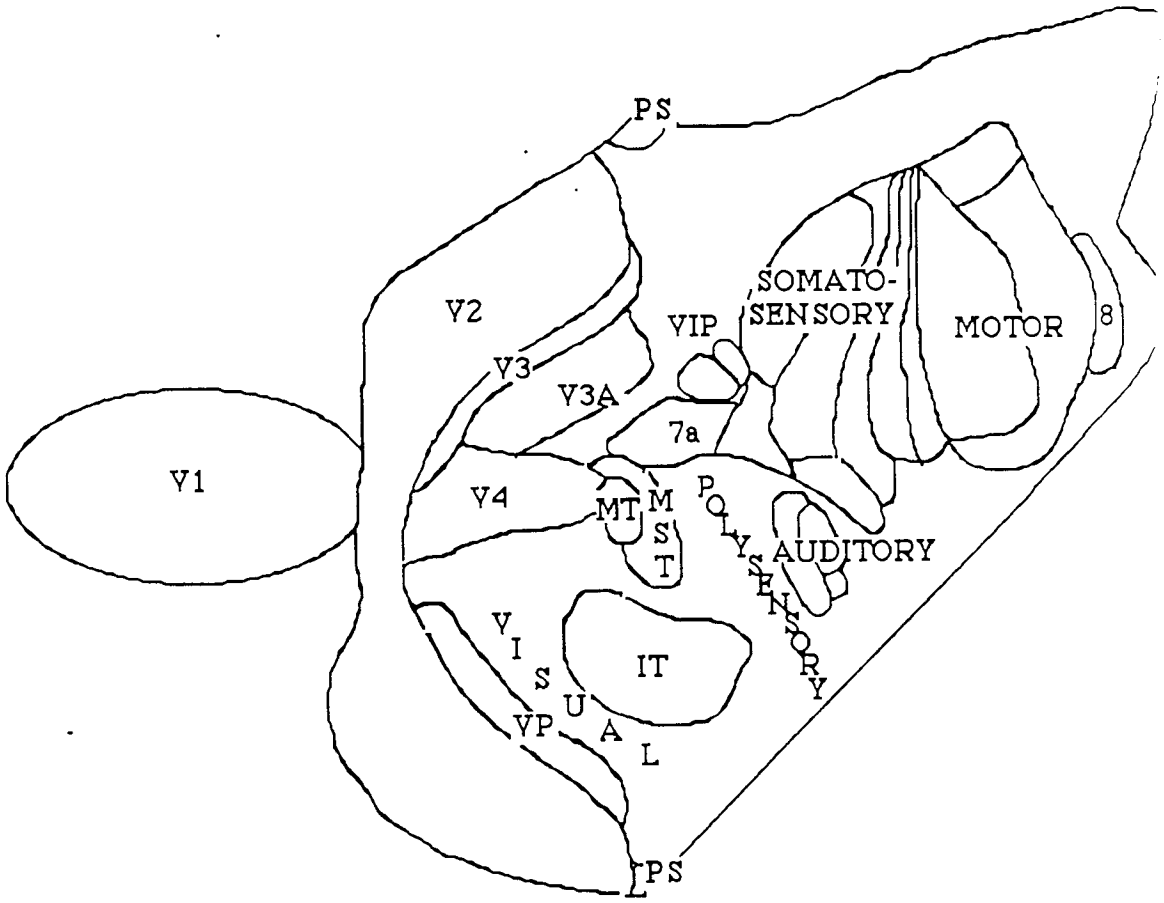

Fig 2.4.Position of the extrastriate visual areas on the unfolded macaque cortex. IT = inferotemporal cortex, MST = medial superior temporal cortex, MT = middle temporal area, PS = prostriate area, VIP = ventral intraparietal area, VP = ventral posterior area. After van Essen (1985).

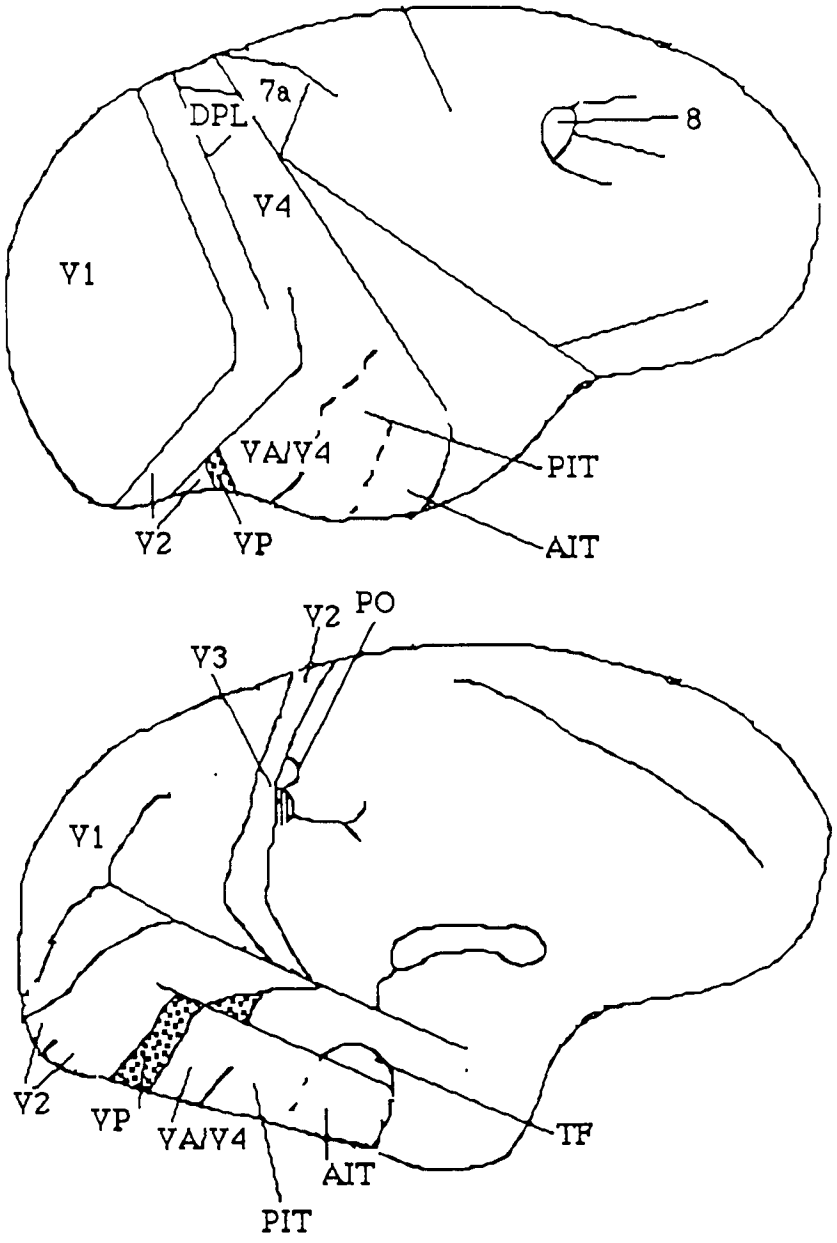

Fig 2.5. Position of the extrastriate visual areas on the folded macaque cortex. AIT = anterior inferotemporal area, DPL = dorsal prelunate area, TF = area TF of Bonin and Bailey, PIT = posterior inferotemporal area, PO = parieto-occipital area, VP = ventral posterior area. After van Essen (1985).

2.3 Physiology of the Visual System

2.3.1 The Retina

The retina forms the first processing level in the visual pathway and the photoreceptors (rods and cones) are the first to be activated by incoming light. These are connected to bipolar cells which in turn synapse with ganglion cells. Three types of cones are present in the primate retina, these are sensitive to different wavelengths of the incoming light. The rods contain only one

photopigment and therefore possess no colour sensitivity. The rods function in low levels of illumination and will not be discussed further.

The axons of the ganglion cells form the optic nerve. There are approximately $1x10^6$ fibres in the optic nerve and approximately $150x10^6$ receptors, a high degree of convergence must therefore be required. A single optic nerve fibre may have connections with many bipolar cells which will in turn connect with many photoreceptors, the 'receptive field' of a single optic nerve fibre may therefore be quite large. The term receptive field was first described by Hartline (1938): as the area of retina over which a response in a single axon/cell can be provoked by a visual stimulus. Hartline investigated the ganglion cells of the Bullfrog with a spot of light, he described cells which responded if the light was switched on ,off, and both on and off. The response was however not uniform, it was maximum towards the centre and reduced towards the edge. On careful examination of the receptive fields of the intact cats retina Kuffler (1953) showed that the centre of the receptive field gave the opposite response to the periphery i.e. if the centre gave an ON response the periphery gave an OFF response so illumination by a large spot of light gave a weaker response than a small spot. This is known as the centre-surround mechanism. There are two classes of bipolar cells, those which hyperpolarise to light (OFF) and those which depolarise to light (ON). The dendrites of ON- and OFF-centre ganglion cells receive their inputs from the corresponding bipolar cells.

The first step in the retina is therefore to compare the amount of light at each point in the retina with the amount of light in the surrounding area, this process results in constancy i.e. if a newspaper is viewed under reduced illumination and then the illumination is increased the paper will still look white and the print black due to constancy. The centre surround mechanism therefore converts the visual input of absolute light units into information about the relative brightness at any point compared with its immediate surround.

The receptive fields of the ganglion cells in the central area of the cat retina have been shown to cover a much smaller area than those in the periphery (Wiesel 1960). Hubel and Wiesel (1960) have pursued these observations in the monkey retina where they found a similar pattern of receptive fields, the receptive fields were however smaller and possessed colour sensitivity.

Two areas of thought have led to the analysis of ganglion cell's properties being approached in different ways:

2.3.1.i Parametric Analysis

This type of analysis investigates the properties of the cells using specific stimuli e.g.spot lights, bars and gratings.

Rodieck and Stone (1965) made two findings in their investigations of the cat retina:

1.The responses of the cat retinal ganglion cell to stationary and moving stimuli can be regarded as the product of a single receptive field mechanism.

2. A population of ganglion cells distributed over the retina can give more information about contrast, width, length, velocity and direction than just one cell.

2.3.1.i Feature Extraction Analysis

Natural stimuli instead of spots of light are used for cell activation. The function of the particular cell is to detect a particular feature in the visual scene and signal this occurence to the brain.

Lettvin (1961) described the following cell groups:

I. Boundary detectors

II. Movement gated, dark convex boundary detectors

III. Movement or changing contrast detectors

IV. Dimming detectors

V. Unclassified

2.3.2 Ganglion Cell Classification

2.3.2.i Parametric Analysis; Y/X/W Classification of Retinal Ganglion Cells in the Cat.

Ganglion cells can be classed into groups by their morphology, receptive field physiology, axonal calibre, conduction velocity, relative numbers, retinal distribution, central projection and perhaps phylogenetic history. Ganglion cells are classified into three groups: α, ß and γ. Enroth-Cugell and Robson (1966) were the first to classify the ganglion cells in the cat by measuring their individual contrast sensitivity to various spatial frequencies. They found this function could

only be plotted for approximately twenty-five percent of the cells investigated, the remaining cells gave two functions, an unmodulated and a modulated response, as the spatial frequency increased the response became unmodulated. They termed these two groups X and Y respectively. The X group had linear summation over the receptive field so that if both the centre and surround were stimulated with symmetrically opposite stimuli no response was observed. The Y group possessed non linear summation and as a result no null point could be observed.

Other distinguishing properties were reported:

1. The receptive field centres of the Y cells were greater than the X cells

2. The X cells were more frequent in the central area of the cat's retina

3. It was predicted that the Y cells had larger diameter axons

Fukada (1971) demonstrated that the Y cells' axons had a faster conduction velocity. From these properties it was postulated that X cells subserve high resolution pattern vision and Y cells subserve movement vision or perhaps low resolution pattern vision.

In 1972 Stone and Hoffman recorded from cells that possessed different receptive field properties to both X and Y cells and slower conducting axons than X cells. These are classed as W cells (to retain the progression of X and Y in terms of the conduction velocity). The W cells exhibited a variety of receptive field properties including fields with ON/OFF centres and also non-concentric properties. The X, Y, W cell classification was related to the morphological classes of retinal ganglion cells described by Boycott and Wassle (1974). Three types were identified α, ß, and γ. The 'α' class possessed the largest dendritic field diameters and the thickest axons, ß had the smallest dendritic fields and thinnest axons. The dimensions of the α and ß cells increased from the central retina to the periphery whereas the γ cells were found at all eccentricities with similar field dimensions. They suggested the following correlations between X and ß cells, Y and α cells and W and γ cells.

2.3.2.ii Feature Extraction Analysis of Cat Retinal Ganglion Cells

Cleland and Levick (1971) classified cells according to the duration of their responses i.e. sustained and transient these are probably equivalent to the X and Y cells, respectively. The sustained cells gave a modulated discharge, whereas the discharge from the transient cells continued when modulation ceased, while the grating continued to move.

In 1974 they introduced a further subgrouping of brisk and sluggish for the concentrically organised receptive fields, this resulted in 8 classes of cells with respect to type: centre on or off, sluggish or brisk response, and, sustained or transient. The sluggish cells had a slower conduction velocity than both the brisk sustained or the transient whereas the brisk transient gave the fastest response and projected to the pretectal regions and superior colliculus. The brisk sustained group constituted the major input to the LGNd.

2.3.3 Classification of Monkey Ganglion Cells

DeMonasterio et al (1975) recorded responses from the ganglion cells in the central 40° of the rhesus monkey. Three classes of cells were found; class I was termed colour opponent comprising cells with concentric receptive fields and a sustained colour opponent response. Few cells had non-concentric (co-extensive) receptive fields. Class II was termed broad band transient and comprised cells with concentric receptive fields, some had colour opponent responses. Class III cells had non concentric receptive fields, one group was phasic ON, OFF or ON-OFF with no spontaneous activity another group had regular spontaneous activity and were responsive only to moving stimuli. Cells of class I with concentric fields had the smallest receptive field centre sizes, whereas cells of class III with phasic responses had the largest. There were also distinctions based on retinal location and projection; a high proportion of the colour opponent cells were found near the foveola and a high proportion of broad band cells were found in the periphery, the class III cells appeared to be evenly distributed over the whole retina. The majority of class I cells terminated in the parvocellular layers of the LGNd whereas a greater proportion of cells of class II terminated in the magnocellular layers. None of the class III cells projected to the LGNd, they projected to the superior colliculus and the accessory optic system.

These classes of cells are not directly equivalent to the X, Y, and W cells of the cat retina. Leventhal et al (1981) determined morphologically 4 groups of retinal ganglion cells groups A,B,C,and E. 'A' group projects to the magnocellular layers of the LGNd, these have large cell bodies and the thickest axons and are Y-like, class II. B group projects to the parvocellular layers of the LGNd, these are X-like, class I. C group have small cell bodies and the thinnest axons, W-like. E group have medium to large bodies, fine to medium axons and project to the pretectum. The X cells are more numerous and the W cells less numerous in the monkey retina compared with the cat retina and the difference in properties between the X and Y cells were shown to be more strongly developed in the monkey.

2.3.4 Colour Processing in the Retina

The centre surround layout is developed for the assessment of contours but colour information must also be conveyed. The human retina is made up of three types of cones that contain photopigment that absorb maximally at 419nm(B), 531nm(G) and 559nm(R) (Lennie 1984). R and G cones are found in a proportion of 4:3, the B cones are much rarer. The centre of the receptive field is stimulated by a type of cone sensitive to one wavelength with the surround being colour opponent. To be colour sensitive the cell must work on the theory of subtraction, i.e. the responses of one cone are compared with those of another to the same incoming light. This process is the first step in the parvocellular system.

There are at least 11 different types of ganglion cells receptive fields acting in parallel over a small area of the primate retina, see table 2.2.

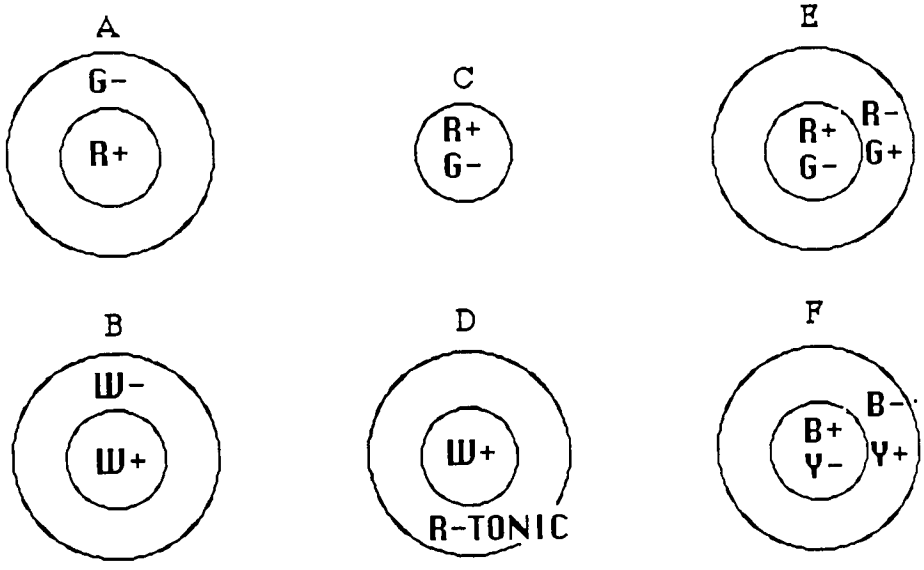

Fig 2.6. Organisation of the circular receptive fields of the ganglion and lateral geniculate cells. A. Colour opponent centre surround. B.Broad band. C. Colour opponent centre only. D. Broadband tonic red surround. E. Double opponent. F. Double opponent. After Regan (1989).

Tonic	Red	On centre	Green Off surround	Weak	Colour Opponency	15%
Tonic	Green	On centre	Red Off surround	Weak	Colour Opponency	9%
Tonic	Red	Off centre	Green On surround	Weak	Colour Opponency	7%
Tonic	Green	Off centre	Red On surround	Weak	Colour Opponency	6%
Tonic	Red	On centre	Green Off surround	Strong	Colour Opponency	8%
Tonic	Green	On centre	Red Off surround	Strong	Colour Opponency	9%
Tonic	Blue	On centre	Yellow Off surround	Strong	Colour Opponency	6%
Tonic	BrB	On centre	BrB Off surround	No	Colour Opponency	7%
Tonic	BrB	Off centre	BrB On surround	No	Colour Opponency	4%
Phasic	BrB	On centre	BrB Off surround	No	Colour Opponency	16%
Phasic	BrB	Off centre	BrB On surround	No	Colour Opponency	10%

Table 2.2. Classifications of the types of receptive fields of the ganglion cells. BrB- BroadBand, also 2% strongly colour opponent red/green antagonistic Off centre and 4% unclassified. After Gouras and Zrenner (1981).

2.3.5 The Lateral Geniculate Nucleus (LGNd)

The receptive fields of the LGNd have the same basic organisation as the ganglion cells of the retina, e.g. ON or OFF centre and ON or OFF surround but they are not exactly the same e.g. accentuation of the inhibitory response. Investigations of the LGNd have shown a division into four magnocellular and two parvocellular layers which correlate with the X/Y division of function. The parvocellular laminae relay X like ganglion cells to the visual cortex and the magnocellular laminae relay Y like ganglion cells.

Kaplan and Shapley (1982) classified the cells in the Macaque LGN using spatial summation and demonstrated 2 classes of X cells. There were both magnocellular

and parvocellular X cells, the magnocellular X possessed greater contrast sensitivity. Approximately ninety-nine percent (225/226) of the parvocellular layer and approximately seventy-five percent (59/77) of the magnocellular layer were of the X type the remaining tweny-five percent of the magnocellular layer cells were Y type. Both the magnocellular X and Y cells had greater contrast sensitivity than the parvocellular X cells. The cells were classified as follows:

X: 1.Cells have a null response when gratings spatial phase is shifted 90° from the peak response.
2.Cells response modulated at the local flicker frequency
3.Cells responded to low and high spatial frequencies as if they received an input from a linear receptive field mechanism.

Y: 1.Strong response at 2x the local flicker frequency, responded to low spatial frequencies in the same way as the X type.
2.The frequency doubled component is approximately independent of the spatial phase.

This categorisation gave a poorer judge of homologies than earlier studies which used several parameters e.g. axon conduction, receptive field size and velocity selectivity to classify the cells, this accounts for the greater number of X cells (Stone 1972).

2.3.5.i Lesion Studies in the LGN

Lesions of the magnocellular layer define this layer as being responsible for contrast sensitivity at low spatial frequencies and high temporal frequencies (Merigan and Maunsell 1990, Merigan, Katz and Maunsell 1991). The magnocellular system is also responsible for motion perception, flicker detection and low contrast stereopsis (Schiller, Logothetis and Charles 1990).

The parvocellular system is essential for colour discrimination, and responsible for pattern, size and fine shape discrimination, texture perception and fine stereopsis (Schiller, Logothetis and Charles 1990). Parvocellular lesions have been shown to result in a 3-4 fold drop in acuity and severely reduce contrast detection at high spatial frequencies (Merigan, Katz and Maunsell 1991). Visual perception in the entire high spatial frequency portion of the spatiotemporal frequency space (at least down to a spatial frequency 4 fold lower than the acuity) is mediated by the parvocellular pathway (Merigan, Katz and Maunsell 1991). Selective stimulation of the parvocellular pathway can therefore be obtained with luminance stimuli of only high spatial frequencies (Merigan, Katz and Maunsell 1991).

Except for colour vision both types of cells can process all attributes (pattern, texture and form discrimination, motion and flicker perception, stereopsis and contrast sensitivity) but they do so in different parts of the range of both spatial and temporal domains, interaction of the two systems was demonstrated when one system alone could not fully analyse the task (Schiller, Logothetis and Charles 1990). Lesions of both the magnocellular and parvocellular systems to the same area of the visual field result in total blindness (Schiller, Logothetis and Charles 1990).

2.3.5.ii Psychophysical Studies

Psychophysical experiments have investigated the functions of the magnocellular system by utilising the fact that this system cannot operate at equiluminance. Cavanagh, Tyler and Favreau (1984) have shown that speed of movement perception is greatly reduced or abolished with equiluminance. Stereopsis and other depth cues are also lost suggesting that all aspects of depth and distance perception are processed by the magnocellular system (Lu and Fender 1972). Figure ground segregation and spatial relationships of objects are also broken down. Ingling and Grigsby (1990) have shown that one can see excellent depth using monocular cues in afterimages and because afterimages last for longer than a few seconds this must be the result of the sustained parvocellular system. Hubel and Livingstone (1991) have disputed the fact that all magnocellular cells are transient, as some do show sustained responses. In reply to Hubel and Livingstone, Ingling and Grisby (1991) quoted Kelly and Martinez-Uriegas (1990) who concluded that the afterimage was confined to the parvocellular channel and patients with loss of the parvocellular channel tend not to see afterimages, although these were tested with different paradigms.

2.3.5.iii Projections of the LGN

There is evidence in the Macaque monkey of a projection from the LGNd to the prestriate cortex. Injection of Horseradish peroxidase (HRP) into the prestriate cortex, highlighted cells which are sparsely distributed throughout the LGN. They had a large soma size which was constant over the LGN and were mainly interlaminar originating from both magnocellular and parvocellular layers. It was not clear if these cells received a direct retinal input.

Most afferents of the LGN terminate in layer IVc of the striate cortex, these cells are monocular with circular receptive fields. The parvocellular projection terminates in layer IVcß and IVA and also those distributing to layers 6 and 1. The

which sends minor or no collaterals to layer 6, the minority of the magnocellular projections arborize in the upper half of 4Ca with major collaterals to layer 6B (Blasdel and Lund 1983). Afferents to layer 4Ca cover approximately 6x as much surface area as those to 4Cb, the layer 4Cb is more consistent with that of retinotopic specificity.

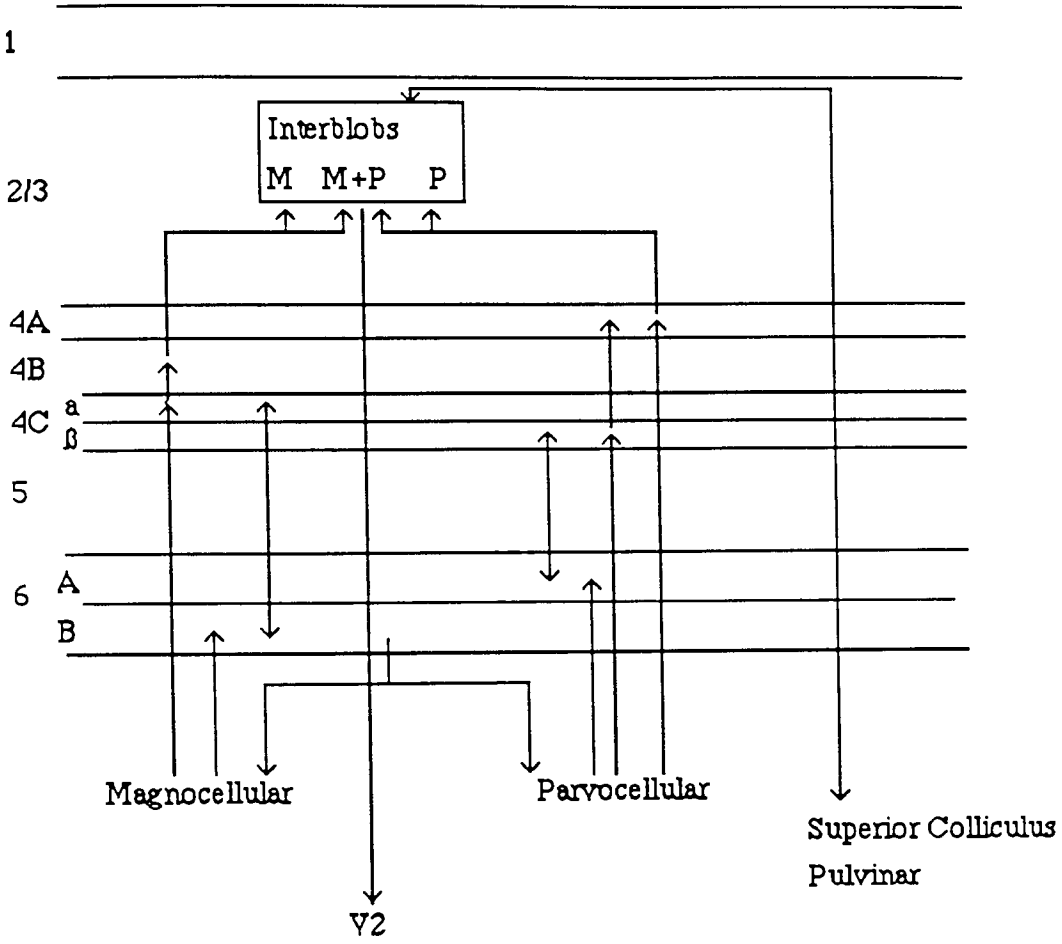

Fig.2.7. Projections of the magnocellular and parvocellular pathways to the striate cortex.After van Essen D.C.(1985).

2.3.5.iv Colour Processing in the LGNd

Cell types A,B,and C (see fig.2 6) are found in the parvocellular layer neurons with the type A being most common, accounting for approximately 80%. Type E is not found.(Creutzfeldt et al 1979).

Work by DeValois, Abramov and Jacobs (1966) demonstrated spectrally opponent cells and also cells which were excited by light of all colours. Later work showed that the cells could transmit more than one piece of information in addition cells were shown that possessed low pass spatial tuning for chromatic gratings and

bandpass for achromatic gratings. The properties of these cells could be important for figure ground segregation.

The achromatic mechanism is thought to receive signals from only red and green cones (Elsner and MacLeod 1980), see fig 2.8. The capacity to resolve spatial detail is poorer when the detail is presented in chromatic contrast than when it is represented by brightness contrast. Chromatic opponent units could resolve an achromatic (but not a chromatic) grating in the fovea of upto 40 cpd (Blakemore and Vital-Durand 1979). The capacity to resolve temporal detail is also poorer when presented in chromatic contrast (Lennie 1984).

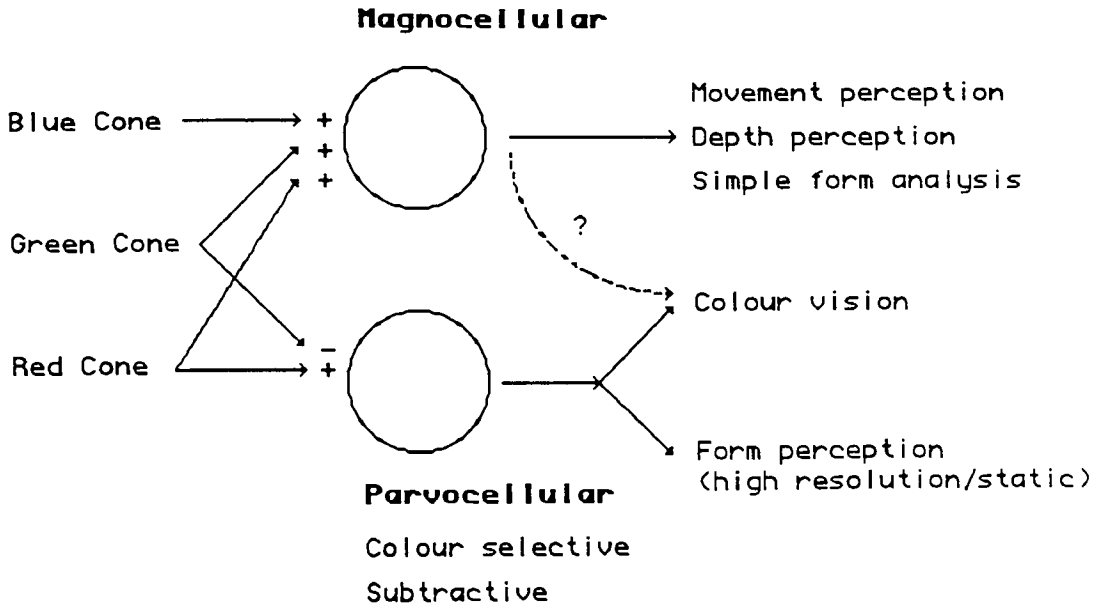

Fig 2.8 Diagram to illustrate the retinal origin of both the magnocellular and parvocellular pathways. After Livingstone (1990).

It has been suggested that the magnocellular/parvocellular distinction corresponds to separate processing channels for colour and contrast, the magnocellular dealing with contrast and the parvocellular dealing with colour (Shapley 1986). The parvocellular system is made up of approximately 80% R-G units and 10-20% B-Y units, the B-Y units tend to have larger receptive fields in which the antagonistic mechanism is often co-extensive (Lennie 1984).

Further analysis of the information must be carried out to distinguish the responses of the parvocellular units as they respond to both achromatic and chromatic stimuli, this is achieved later in the visual pathway, the next stage being the striate cortex.

Krauskopf and Farell (1990) used psychophysiological experiments involving moving plaid patterns produced by the superposition of two drifting sine wave

gratings. If the colours making up the gratings activated one colour processing channel i.e. red and green then the plaid appeared to move along the vector sum of the movement of the gratings. If the colours were not related i.e. orange and turquoise then the plaid appeared to be made up of two separate gratings. They proposed, that to be integrated by the second cortical stage of motion processing, the motion signals must be processed through the same chromatic and luminance channels. The pathway along which this is achieved and value of this processing in the functional sense has not been established (Albright 1991).

2.3.6 Striate Cortex

2.3.6.i Cellular layers of the Striate Cortex (V1)

The striate cortex is thin compared with other regions of cerebral cortex, it consists of 6 layers, layer 4 being split into three: 4A,4B and 4C. Layers 2, 3, 4A, 4C and 6, are the most densely packed, layers 1,4B and 5 are the most loosely packed (Polyak 1957).

Layer 1: This is the plexiform layer, there are few true nerve cells. The cells are mostly irregular shapes including some pyramidal.

Layer 2: Outer granular layer contains short pyramidal type whose dendrites spread into layer 1.

Layer 3: The pyramidal cell layer and contains approximately 25% of the cells in the striate cortex. The cells are usually joined in clusters.

Layer 4A: Outer layer of the inner granular layer, most of the cells are uniform with few pyramidal type.

Layer 4B: Middle layer of the inner granular layer, contains a small number of cells of various shapes ; spherical, ellipsoid, ovoid and some are multipolar.

Layer 4C: Inner layer of the inner granular layer, contains granular small spherical or irregular cell shapes.

Layer 5: Ganglion cell layer.Large and medium cell size.

Layer 6: Multiform cell layer small and irregular with long dendrites maybe pyramidal.

Using Golgi stain to determine the extent of the cells axons and dendrites two major classes of cells are described (Sventagothia,1973):

2.3.6.ia Class I: Pyramidal Type Cells

These cells are defined by shape and the pattern of dendritic arborisation. The apex points toward the cortical surface and dendrites arise from the basal part of the body and run in a radiate direction. Small pyramidal type cells can be found in layer II but most pyramidal type cells are found in the deeper layers of the cortex. The axon normally projects toward the white matter but it can occasionally ascend and loop back in an arc. Pyramidal type cells are also found in layer 4 and layer 5. Other forms found are inverted pyramidal type cells and fusiform with their cell bodies parallel to the cortical surface. Stellate neurons with long axons may also be found in layer 4 .

2.3.6.ib Class II: Stellate Type Cells

These cells are characterised by axons which branch and terminate in neighbouring layers. There are various types, the classical type being found in layer 4. Stellate type cells are found in all layers of the striate cortex except layer I.

The layers of the visual cortex differ in both their inputs and their projections. Most connections in the cortex run vertically but there are some diagonal connections that run for approximately 1-2mm.

2.3.6.ii Properties of the Cells in V1

In the heirarchical model of the visual system the information is thought to be processsed by one set of cells first which extract details relating to one feature of the visual scene, the same information is then processed by cells specific for another feature. This theory transcribes into the form of simple, complex, and hypercomplex cells. Cells in layer 4C of the striate cortex receive monocular inputs from the LGNd. The cells in 4Cß all seem to have centre surround properties without any orientation selectivity whereas those in 4Ca have centre surround fields and some appear to be orientation specific with simple receptive fields. In all other layers of the striate cortex the cells are no longer organised with concentric fields and are as follows:

2.3.6.iia Simple Cells

These receptive fields possess an excitatory and inhibitory region. They are however, not circular but oblong, the centre is in the form of a stripe with an adjoining parallel periphery. These cells respond to a slit parallel to the long axis of

the receptive field and are therefore very orientation selective, there are four different types, see fig.2.9.

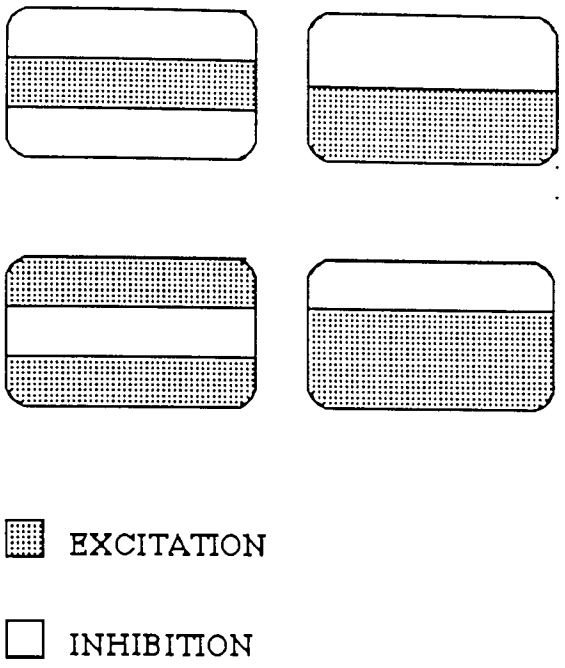

Fig.2.9. Receptive field organiation of the simple cells in the striate cortex.After Hubel (1988).

The maximum response is obtained with movement in one direction with the cell being unresponsive in the opposite direction, slow moving stimuli are preferred 2-4° per second, intermediate directions will actually inhibit the cell's activity. The size of the receptive field depends alot on the position of the projections from the retina relative to the fovea. These cells are most freqently found in layer 4 of the striate cortex and only in the striate cortex. It is postulated by Hubel and Wiesel (1968) that the simple cell's receptive field can be constructed from concentric receptive fields arranged in a straight line.

2.3.6.iib Complex Cells

This is the commonest cell type in the cortex, they respond (as with simple cells) to specifically orientated lines although they are not as selective as simple cells, they will respond to a moving slit wherever it is placed in the receptive field as long as it's orientation is approximately correct (Hubel 1988). These cells are found in area 17 (layers 2,3,5,and 6),18 and infrequently in 19. Complex cells have larger receptive fields than simple cells but possess an equivalent resolving power. They may be built up from many simple cells with receptive fields of the same orientation, however not all complex cells receive inputs from simple cells, some have a direct input from layer 4C (Kandel 1985).

2.3.6.iic Direction Selectivity

Many complex cells respond maximally to only one direction of movement. About 10-20% of the cells in the upper layers of the striate cortex have this property (Hubel and Wiesel 1968).

2.3.6.iid Hypercomplex

These cells are found in Brodmann's areas 18 (areas V2 and V3, Hubel and Wiesel 1968) and 19. There is a low and high order classification: the low order possess properties of complex cells but are end stopped whereas the higher order show double end stopping and are only excited by stimuli in the centre of the receptive field (Kandel 1985). They may also respond to two lines orientated 90° apart.

2.3.6.iie Endstopping

An ordinary simple or complex cell usually shows length summation i.e. as the length is increased the response improves until the line is as long as the receptive field, an increase in length will now produce no change to the response. In end stopped cells however, increasing the length only improves the response to a certain limit, any subsequent increase actually inhibits the response. As a result end stopped cells are sensitive to corners, curvature, or sudden breaks in lines (Hubel 1988). End stopping is thought to be produced through the projections of layer six, this layer projects to layer four of the striate cortex (Bolz and Gilbert 1986), the LGN (Tsumoto 1978) and the Claustrum (Sherk and Levay 1983) through these layer six may inhibit the cells in the upper striate layers.

Simple cells act in a similar way to retinal and LGN parvocellular cells to counterphase modulated and drifting gratings (DeValois et al 1982).

The response of complex cells to a grating is unmodulated, they also possess non linear spatial summation as do magnocellular cells.

2.3.7 Columnar Organisation of the Striate Cortex

The striate cortex is thought to be segmented into blocks of ocular dominance and orientation slabs or 'columns' orientated perpendicular to the cortex. Orientation specific cells are arranged into a unit for each point of the visual field. In a pentration perpendicular to the cortical surface all the cells have the same orientation, in a pentration tangential to the surface the neighbouring slabs change

in orientation, a shift in 0.05mm results in the preferred orientation shifting through 10°. These slabs are duplicated so that there is a representation for each eye in neighbouring slabs. In layer 4 all cells are monocularly driven and if an electrode is passed parallel to the cortex in layer 4C the ocular dominance changes from one eye to the other, in contrast in layers 2/3 the dominance alternation is not as abrupt resulting in varying degrees of dominance. Each ocular dominance slab is about 0.5mm wide but the width varies depending on whether it is representing the contra or ipsilateral eye. Perry and Cowey (1985) showed a difference in the number of ganglion cells of the Macaque monkey projecting from the nasal and the temporal retina the ratio was 1.5 for cells representing the central 20° to 40°, this asymmetry is reflected in the ocular dominance column widths.

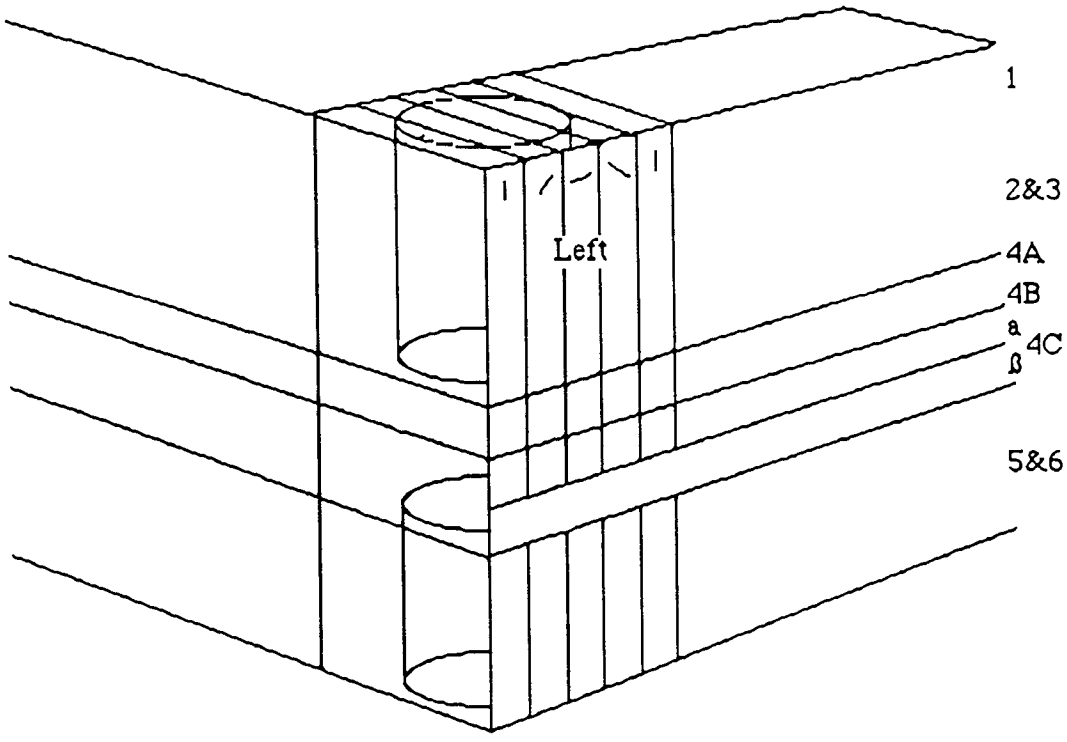

Fig.2.10. Illustration of ocular dominance columns in the Macaque showing the area stained for cytochrome oxidase (represented by the cylinders, possessing processing for colour). After Livingstone and Hubel (1984).

Doubt has been cast as to whether the cortex is modular (Swindale 1990). Arguments against the existence of minicolumns were based on the facts that many of the properties of the cortex do not correltate spatially e.g.in the monkey the eye preference changes every 800μm whereas the preferred orientation changes every 570μm, the cytochrome oxidase concentration changes every 250-350μm and the size of processing unit suggested by the degree of receptive field scatter was estimated by Hubel and Wiesel to be 1-2mm. The number of cells within a column

is also not constant, some cell types have sparser distributions than others. The relationships between the horizontal shifts in function and the vertical striations are unclear, continuous change can not be ruled out. The cell groupings are unlikely to be defined by common clonal origins. The cytochrome oxidase patches are however the most powerful indication of cortical modularity due to their regular spacing and the fact that many properties also correlate with them. The argument against macrocolumns is based on the fact that their size can not be agreed.

It was proposed that the organisation of the cortex may be presented by maps for different stimulus parameters, these being overlaid in such a way as to ensure that varied combinations of features are represented. The use of a modular term may actually simplify the cortex too much and fail to represent the diversity of the forms of columnar order that are actually present.

2.3.8 Colour Processing in V1

In psychophysical studies the visual system has been shown to possess low pass tuning for colour varying stimuli and band pass tuning for luminance varying stimuli (Thorell et al 1984). In single cell studies they showed that seventy-nine percent of cells tested were definitely colour cells, with fifty-three percent responding equally well to colour and luminance, twenty-six percent preferred colour stimuli and twenty-on percent preferred achromatic stimuli. A colour cell was considered so if it responded to an isoluminant colour change.

Some cells possessed a property not seen in the LGN, that of double opponency. This type were found near the termination of the LGN afferents and were also seen in layers 2 and 3. These cells respond well to chromatic contrast within the receptive field but not so well to luminance contrast. Simple cells showed excitation to white bars and small off responses to black bars, they also showed excitation to some wavelengths and inhibition with off responses to others (81% were double opponent), in addition they were phase selective. In contrast the complex cells excited to both black and white bars, to all wavelengths but more to some than others and were not phase selective. The frequency preference for colour gratings was lower than that for luminance gratings (2.63 c/deg compared with 3.5 c/deg) and some cells possessed different tuning for colour and luminance gratings. In the extreme a number of cells were low pass filters for colour gratings and bandpass filters for luminance gratings. It was concluded that most cells in the fovea and parafovea of the Macaque respond to pure colour stimuli in addition to luminance varying stimuli, cells which preferrred a yellow-blue variation were also observed (Thorell et al 1984).

Michael (1985) argued that the processing of both luminance contrast and colour contrast is along separate parallel channels. The colour cells are restricted to columns which are separated from areas that respond to both white and colour stimuli, the columns contain cells excited by monochromatic stimuli with a full range of receptive field types and may vary in axis orientation or eye preference. Nearly all the opponent colour cells in the monkey LGNd are confined to the parvocellular layers which project primarily to 4Cß and 4A. Concentric and double opponent colour cells are restricted to these layers but complex and end stopped cells are found in layers above and below these. It is suggested that the serial processing of colour is just one of a number of separate parallel pathways processing colour contrast, luminance contrast, orientation selectivity, eye preference and spatial frequency.

This parallel system for colour processing found in the visual pathway is not tuned to orientation and has been shown to terminate in blobs revealed by cytochrome oxidase. The blobs are found centred along the ocular dominance columns and contain a high proportion of double opponent cells and an absence of colour opponent centre surround cells (Livingstone and Hubel 1984). Some broad band cells were also demonstrated with a greater number of ON centres (ratio of ON to OFF centres was 2:1). About 12% of the cells were colour opponent centre only, about the same percentage as found in the LGNd. Most of the cells in the interblob regions are orientation selective but not all of these cells are broadband with respect to colour processing, many are highly selective in their colour properties, these are most probably used for form processing. Cytochrome oxidase staining in V2 reveals alternating wide and narrow stripes separated by paler interstripes. There is a projection from the blobs in V1 to the thin cytochrome oxidase stripes in V2 and from the interblob regions in V1 to the pale interstripes in V2.

There are two conflicting porposals as to the organisation of the visual system when processing the incoming information:

1.Parallel: different properties of the visual scene are processed simultaneously.

2.Serial: different properties of the visual scene are processed consecutively.

Bullier and Henry (1985) categorised the monkey afferents reaching cortical cells as slow conducting (X like) and fast conducting (Y like). There was no evidence of cells receiving both X and Y inputs , the separate X and Y input cells were found in the layers in which the X and Y afferents terminated. Some of the

receptive field properties of the cortical cells matched those of the geniculate cells providing their input.

Malpeli et al (1981) showed that a proportion of both simple and complex cells lost their responsiveness when an area of the LGNd including both magnocellular and parvocellular projections was blocked, suggesting these cells may receive a joint X and Y cell input.

If the X and Y channels converge then the end of parallel processing is located in the striate cortex. According to Van Essen the magnocellular and parvocellular cells converge in layers 2 and 3 at the orientation tuned interblob areas, the magnocellular fibres then project to V2 and the parvocellular fibres to layer 5.

It is now becoming increasingly apparent that the processing in the visual system is made up of both parallel and serial processing. This aspect will be dealt with in more detail later in this chapter.

2.3.9 Properties of the cells in the separate regions of the extrastriate cortex.

2.3.9.i V2

V2 adjoins V1 along the portion representing the vertical meridian and is situated on the posterior bank of the lunate sulcus, see fig 2.11. V2 is smaller than V1 and contains a coarser representation of the visual field. V2 is included in both the object and visuospatial pathways of Mishkin et al (1983), which will be discussed later in this chapter. Cells in V1 and V2 respond to a range of spatial frequencies middle to high being preferred by V1 and low to middle by V2.

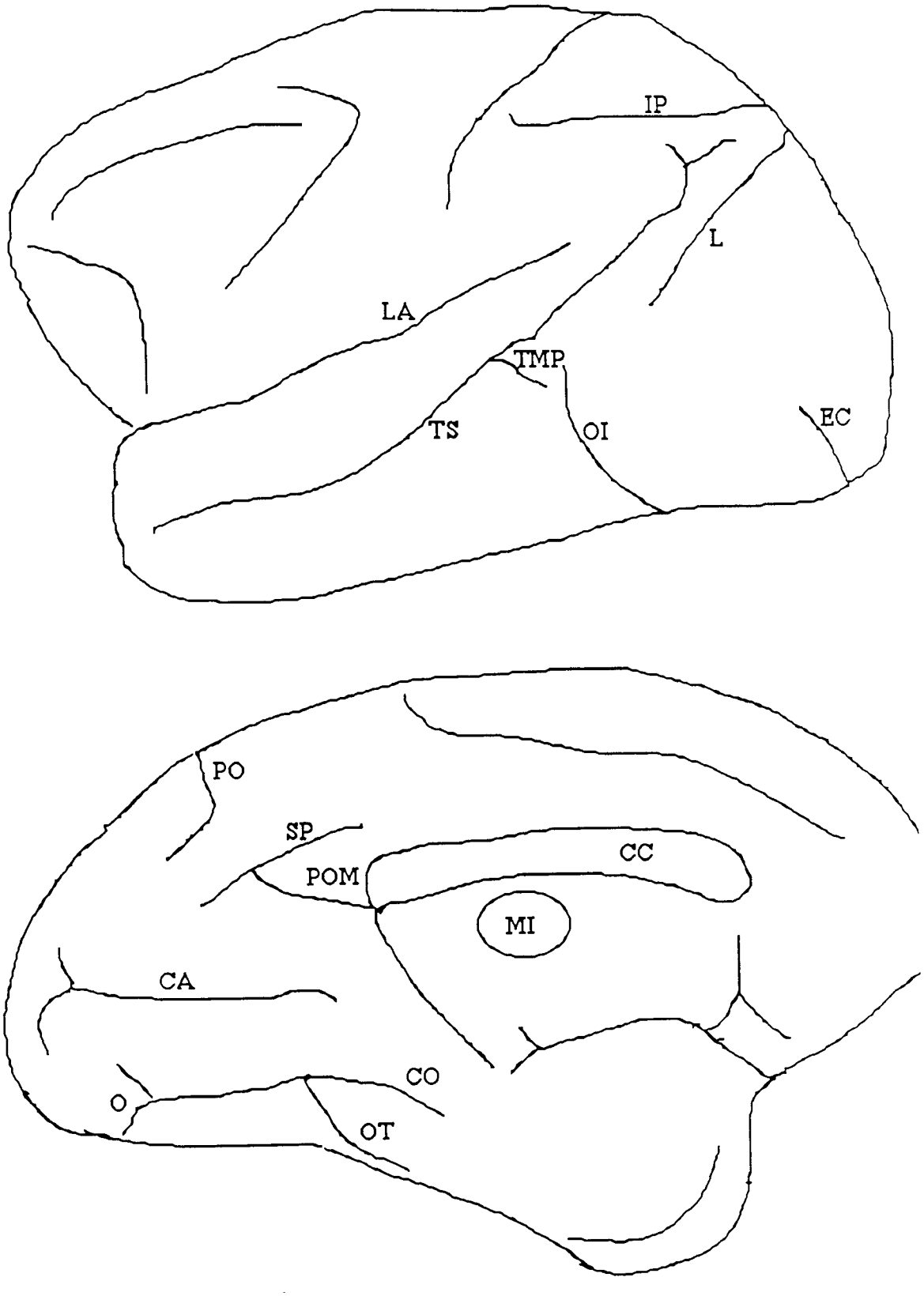

Fig 2.11. The positions of the sulci on the cerebral cortex of the macaque monkey. Abbreviations: CA, calcarine fissure; CC, corpus callosum; CO,collateral sulcus; EC, ectocalcarine sulcus; IP, intraparietal sulcus; L, lunate sulcus; MI, massa intermedia; OI, inferior occipital sulcus; OT, occipitotemporal sulcus; PO, parieto occipita sulcus; POM, medial parieto occipital sulcus; SP, subparietal sulcus; TMP, posterior middle temporal sulcus; TS, superior temporal sulcus. After van Essen, Maunsell and Bixby.

Zeki (1978) investigated the properties of V2 cells: 70% were orientation selective, <15% were direction selective and about 8% were colour opponent, most were binocularly driven. The receptive fields were larger than in V1 but little difference was found in the receptive field positions, they appeared directly opposite to one another, Van Essen and Zeki (1978). Hubel and Wiesel (1970) demonstrated that 60% of the cells in V2 show disparity sensitivity.

In the owl monkey the representation of the upper and lower visual quadrants in V2 are separated by V1 (Kaas 1977). The lower visual field is represented dorsally and the upper field is represented ventrally. The vertical meridian is positioned at the posterior border adjacent with V1 whereas the horizontal meridian is represented twice in the dorsal and ventral areas.

When staining for cytochrome oxidase in V2 Hubel and Livingstone (1985) demonstrated that the stains formed stripes of 0.5-1.0mm width, alternating thick and thin. In the Squirrel monkey the thin stripes contained complex unorientated cells which were connected to the blobs in V1. In the Macaque the distinction between the stripes was difficult to discern but usually alternate stripes contained colour coded and unorientated cells. In the interstripe region the cells were endstopped and connected to the interblob region in V1, the connections of the thick stripes were not known.

Hubel and Wiesel (1970) showed that approximately half (57%) of the cells in area 18 react to simultaneous stimulation of the two eyes and are similar to the complex and hypercomplex cells of V1. Most of these cells also respond to stimulation of each eye individually although there is moderate summation with binocular stimulation. The remainder of the cells are more specialised; these are depth cells and will therefore not respond to monocular stimulation. The cells respond to varying degrees of disparity and were found mainly in the lunate sulcus.

Most V2 cells respond best to motion along a perpendicular line.(Burkhalter and Van Essen 1986) the modal preference for V2 is 32°/sec which is the same as VP and MT but is faster than V1 (8°/sec).

2.3.9.ii V3 and VP

V3 is considered to be divided into 2 areas V3 and VP (ventral posterior area), this distinction is based on; the projections from V1, asymmetrical callosal inputs, differences in myelination (VP lacks heavy myelination) and also differences in cell properties. The receptive fields are larger than V2 but with similar properties to

V1. There is a high percentage of orientation and direction selective (40%) cells and a few colour selective cells (21%) in V3 with the reverse for VP: 13% directional selective cells and 64% colour selective (Burkhalter et al 1986). The receptive field size is also larger in VP (3.0-8.1° compared with 1.25°-5.5° for V3) (Burkhalter et al 1986). The topographic organisation of V3 and VP is a mirror image of V2 with the inferior contralateral quadrant adjoining that of the dorsal V2 in the lateral sulcus and postero-occipital sulcus and the superior contralateral quadrant adjoining that of the ventral V2 in the infero-occipital sulcus, occipito-temporal gyrus and occipito-temporal sulcus. The lower half field is represented in V3 and the upper half field in VP, there is a full representation of the contralateral quadrant in both areas. A projection from V1 to V3, but not to VP, has been demonstrated (Burkhalter et al 1986) the projection from V1 originates in layer 4B, the same layer that projects to V5. Retrograde projections from V3 to V1 have been shown to terminate in layers 6,4B and 1 (Felleman and Van Essen 1984). Some cells in VP are selectively sensitive to motion along one direction and respond only to a limited number of speeds the modal preference being approximately 32°/sec. Both V3 and VP have several projections in common: V2, V3A and V5, in addition there are projections from V3 to V4 and VP to VA/V4.

2.3.9.iii V3A

This area is situated on anterior bank of the lunate sulcus and floor of the postero-occipital sulcus. Properties of the cells in V3A are similar to V3, V3A however differs from V3 and V2 in that both the superior and the inferior quadrants of the visual field are represented in a single region of the dorsal occipital lobe rather than separate dorsal and ventral subdivisions. The inferior vertical meridian is represented along the V3/V3A border and the superior vertical meridian is represented along the V3A/V4 border. V3A doesnot receive a direct input from V1 (Zeki 1978). Fields further than 20-25° from the fovea were not found in V3A (Van Essen and Zeki 1978).

Galletti et al (1990) studied 87 neurons in area V3A of the Macaque monkey, in 48% (42/87) there was a significant difference in the response to stimulus movement compared with that to eye movement. The majority of these (36/42) were termed real-motion cells i.e. the response was greatest to stimulus movement. These cells could be involved in distinguishing real from self induced movements of the retinal image i.e. actual movements of the object of regard. The cells were also found to be very sensitive to orientation with a range for 119 cells of +/-42.6° (+/-18.3° SD), this was a greater sensitivity than recorded from neurons in either V1 or V2 (the mean range for V1 was 50.4°+/-24.8SD and V2 50.1°+/-24.8SD,

these are not significantly different). Twenty-six percent were direction selective and almost all the cells were activated by moving targets upto and greater than 50°/sec, some were activated by stimulus velocities over 100°/sec. When the real motion cells were tested in the dark some no longer possessed the real motion effect. The results from Galletti et al (1990) suggest that area V3A possesses a variety of functions : form analysis, space localisation and motion detection.

2.3.9.iv V4

V4 is situated on the anterior bank of the lunate sulcus, bordering V3A. It receives a direct projection from V1 (Kennedy and Bullier 1985, Zeki 1978), and also projections from V2 and V3 (van Essen and Maunsell 1983). V4 is considered to be a part of the pathway for the analysis of form and colour which originates in V1 and includes V4, VP and the infero-temporal cortex (IT). V4 is included in the pathway crucial for object identification (Mishkin et al 1983) . Dorsally V4 borders V3 and receives projections from the lower field representation of V2 and V3. The cortex adjacent to V3 on the ventral side is thought to be the upper field representation of V4 as it receives upper field projections from V2 and V3. The central representation of V4 is lateral and the peripheral is medial (Desimone et al 1985). The central representation has a minor projection to MT and a small zone in the parietal cortex, but the major output is to the IT. V4 is the primary source of lower field input into IT (van Essen and Maunsell 1983).

From the analysis of awake monkeys it has been shown that most of V4 is retinotopically organised, with 2 representations of the contralateral lower visual quadrant one anterior and lateral to the other, the other representation may belong to V4A (Baiser and Maguire 1983). Van Essen and Zeki (1978) described multiple representations of the vertical meridian whereas Gattam et al (1985) reported that V4 contained only one visual field representation. Ungerleider et al (1983) demonstrated that single points in V2 usually projected to single points in V4.

There has been much controversy as to the function of V4. It was initially suggested that V4 was a colour processing area with the majority of the cells (54%) having colour oppponent properties (Zeki 1978). Experimental work presented by Van Essen and Zeki (1978) showed that 32% of the cells were colour coded or biased, 42% were orientation selective and only 3% were direction selective, 100% were binocularly driven. The colour coded cells responded to a small part of the visual spectrum whereas the biased cells responded to all colour and white light but displayed a strong preference for a small range of colours. In 1985 Wild et al

demonstrated, after removal of the V4 complex in the Macaque monkey that V4 was necessary for colour constancy and not hue discrimination .

After staining for cytochrome oxidase in V2 it has been shown that the thin interstripe regions project to V4 and connect with the wavelength selective blobs of V1 (Shipp and Zeki 1985). The interstripe regions contained orientation selective cells. Wavelength selective cells were positioned in or at the borders of the thin stripes, some being double opponent cells.

The receptive fields of V4 in anaesthetised monkeys have been found to be larger than those in V1 (Desimone et al 1985). A proportion of the cells were sensitive to the length, width, and direction of the motion of a bar stimulus. The peak spatial frequencies of the neurons tested were 0.12 - 8.0 cycles per degree. A higher proportion of cells in V4 were tuned to lower spatial frequencies, some responding to a narrow phase range, others showing no phase sensitivity. The properties of the cells fell into a range from simple through to complex. Surrounding the receptive fields were large areas of suppression which could be shown to be greater than 30° in diameter and could extend upto 16° into the ipsilateral visual field. Maximum suppression was exhibited when the spectral or spatial content of the centre and surround were equal and a maximum response was shown when there was a spectral difference between the receptive field stimulus and the surround. The surround mechanism may be utilised for figure ground segregation or colour constancy. The cells were not found to be narrowly tuned but most showed evidence of colour bias and colour opponent properties, a failure to respond to white light was also uncommon.

Some of the visual properties could be modified by the monkey's task and by incoming signals of other modalities. V4 can exhibit a form of short term visual memory. V4 has also been shown to respond poorly to sine wave gratings but respond well to bars or square wave gratings i.e. edge sharpness may be represented in V4 (Desimone and Schein 1987).

2.3.9.v Middle Temporal Cortex, MT (V5)

This region lies in the floor and adjacent portion of the lower bank of the caudal third of the superior temporal sulcus and occupies a small part of area 19, responding only to visual stimuli (Gross 1981). This area forms part of the visuo-spatial pathway : V1--V2--V5--four areas in the upper superior and intraparietal sulcus. There is a direct projection from V1 to V5 (Kennedy and Bullier 1985). The fibres originate in the middle and deep layers of V1 and the connections are retinotopically matched (Krubitzer and Kaas, 1990). The backward projections

from V5 to V1 terminate in the superficial layers (Krubitzer and Kaas, 1990). Area V5 also receives projections from V2 (Zeki 1976) and anterior parts of the inferior and lateral Pulvinar (Benevento 1976). The projections from V2 originate in the thin cytochrome bands whereas the backward projections terminate in both the thick and thin bands (Krubitzer and Kaas, 1990).

In the squirrel monkey the caudal parts of V5 represent central vision and these connect more densely to the area DL and the inferotemporal cortex (Krubitzer and Kaas, 1990).

Ungerleider (1985) demonstrated projections from V5 to four areas located dorsally in the occipito-parietal cortex, IP1,IP2,ST2 and ST3. IP1 begins in the annectant gyrus caudally and extends along the fundus of the posterior third of the intraparietal sulcus, this may be equivalent to the area V3A of Zeki (1978) and IPa and VIP of van Essen and Maunsell (1983). IP2 lies in the anterior two thirds of the sulcus extending from the fundus to the posterior bank in the area PG. ST2 borders V5 medially in the superior temporal sulcus and contains directionally selective units. ST3, also located in the superior temporal sulcus borders V5 anteriorly. One of the areas in the superior temporal sulcus is related to tracking eye movements and therefore direction of motion information may be used by the oculomotor system.

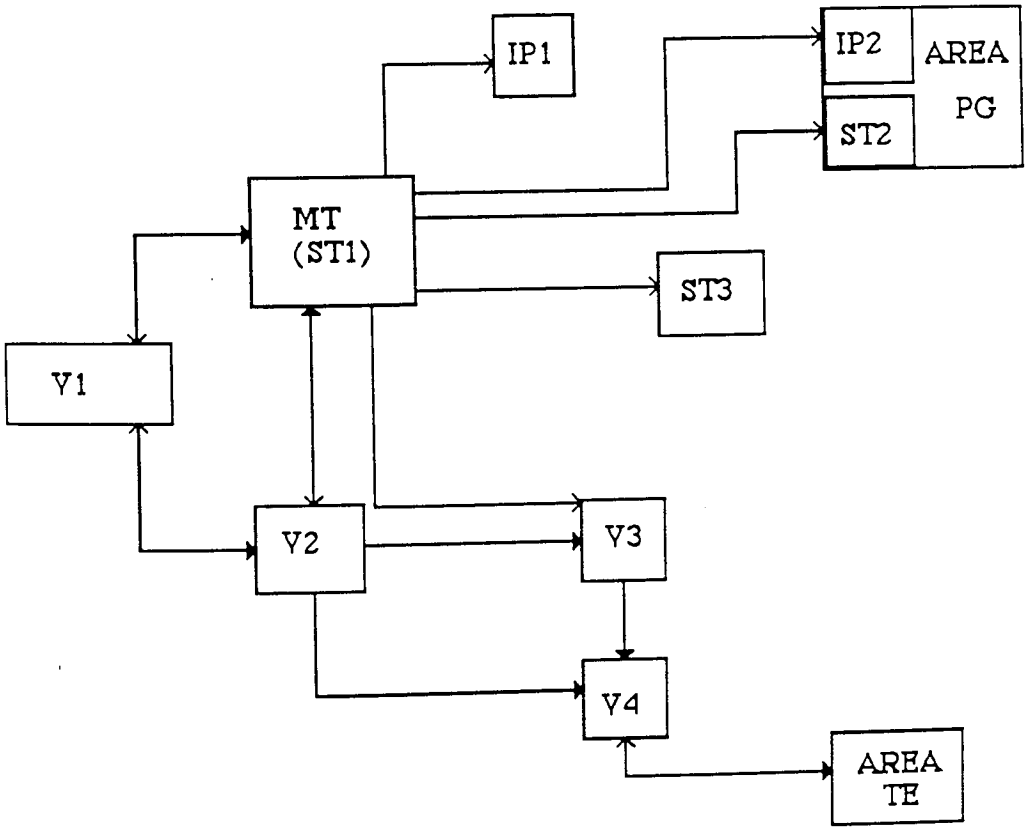

Fig.2.12. The connections of the middle temporal cortex of the macaque monkey After Ungerleider (1985).

Most of the cells in V5 show a strong preference for stimuli moving in a certain direction either within the plane of fixation, towards or away from the subject (Zeki 1974 a,b). The direction selective cells in V1 are especially concentrated in layer 4 B, which forms the major projection to V5 (Van Essen 1979). Most V5 cells are selective for speed and binocular disparity as well as direction and the cells show no selectivity for stimulus shape or colour. A large proportion of the cells were velocity tuned with a wide range of velocities (2°-256°/sec). Desimone et al (1985) observed from electrode penetrations in the macaque MT, indications of a systematic representation of the direction of motion. In some penetration discontinuities were apparent, however if the axis of motion was taken instead of the direction of motion these were nearly always avoided. A vertical columnar organisation of the axis of motion was proposed with 180° of axis of motion represented in 400-500 microns (similar to the size representing 180° of orientation in the ocular dominance columns of the striate cortex). The direction of motion information may be used for information about motion toward or away from the centre of gaze.

In V5 of the Owl monkey it has been demonstrated that some cells are surrounded by a suppressive region the size of which is in the order of 7-10 times the receptive field diameter (Allman et al 1985). Suppression was maximal when the stimuli in the receptive field and surround matched the optimal velocity and the optimal direction, as in V4.

V5 contains a representation of only the central 30-40° of the contralateral field , the peripheral field is represented medial to V5 in the area MTp which receives a projection from the far periphery of V1 and V2 (Desimone and Ungerleider 1986). The areas medial superior temporal and posterior parietal medial to V5 and MTp contain a high percentage of direction selective cells. The MST and fundus superior temporal (FST) also have a direct projection from V5. It is suggested that the MT, MTp, MST and PP with the superior polysensory area are all concerned with motion analysis. The macaque MT contains a high proportion of velocity tuned cells, approximately half of which are disparity selective. In the squirrel monkey Krubitzer and Kaas (1990) found dense connections from V5 to the frontal ventral area, FV, but not to the frontal eye fields.

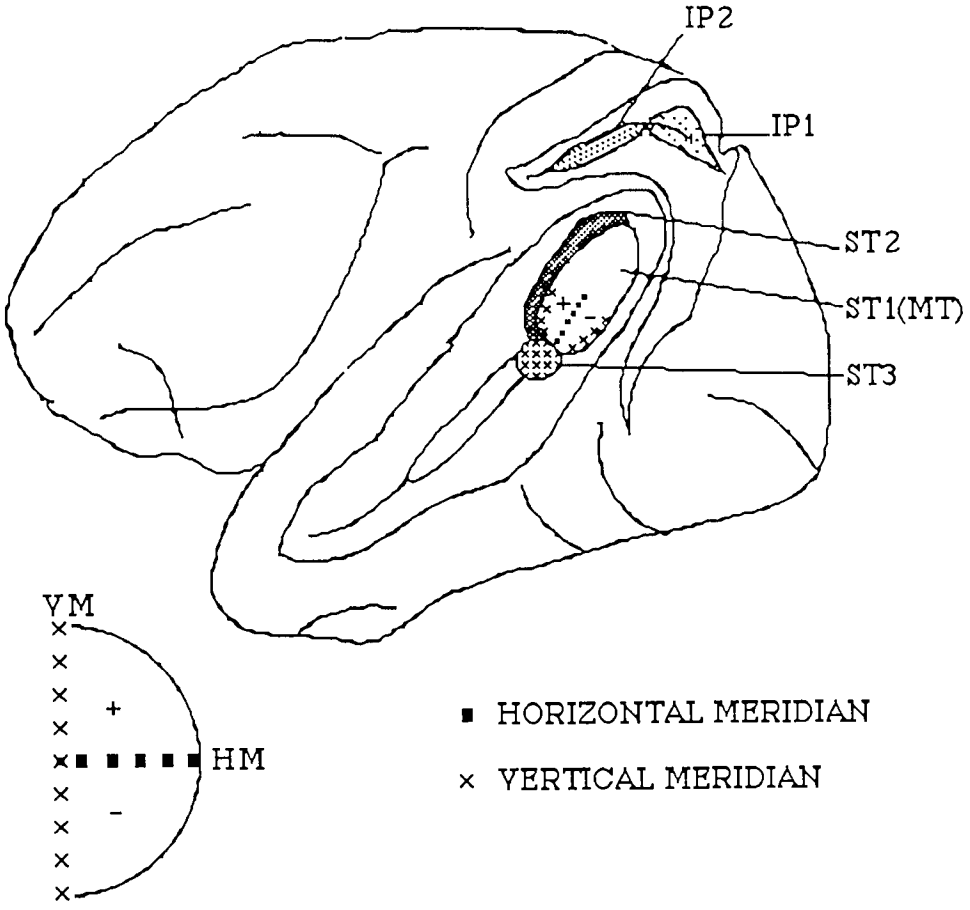

Fig. 2.13. The position on the cerebral cortex of the projections of the middle temporal area (MT). IP = the intraparietal sulcus, ST = the superior temporal sulcus. After Ungerleider (1985).

2.3.9.vi Inferotemporal Cortex

This area is situated on the inferior convexity of the temporal lobe. The macaque IT can be divided into a posterior area TE which receives an input from V4 and an anterior area TE which receives an input from the posterior TE, see fig.2.15 (Mishkin 1982).

Removal of this area results in a deficit in visually guided behaviour and a reduction in visual learning ability. The deficits of posterior inferotemporal lesions are characterised as perceptual whereas anterior lesions appear to be mnemonic (Gross 1973, Manning and Mishkin 1976). The effects of temporal lobectomy in man depends on which side is removed, the left lobe results in language disturbances whereas the right produces a range of deficits on non verbal tasks both auditory and visual (Milner 1968). No projections from the LGNd to the IT have been demonstrated. The IT does however receive projections from the prestriate and lateral frontal cortex, pulvinar and the contralateral temporal cortex.

It transmits fibres to the prestriate cortex, frontal lobe and several sub cortical regions including the basal ganglia, dorsomedial nucleus, pulvinar and the superior colliculus. The cortex dorsal, ventral and rostral to the IT contains many neurones with polysensory properties i.e. auditory, somatic and visual.

Mishkin et al (1983) include the IT in the pathway for visual identification of objects, this pathway includes the striate and prestriate areas the IT then links with limbic structures in the temporal lobe and ventral portions of the frontal lobe.

Gross (1972) recorded responses of neurons in the macaque Monkey IT, they responded only to visual stimuli and possessed a long response latency. The receptive fields have several unique characteristics, they were found to be large with a median value of 25°x25° and included the fovea, over half of which extended into both visual half fields. No map of the visual field or retina was present in the IT and the stimulus selectivities of the IT neurones remained similar throughout the receptive field. As a result of the large receptive fields and stimulus selectivity equivalence this area may also be responsible for the phenomenon of stimulus equivalence across the visual field i.e. being able to recognise an object as the same if it is moved to a different part of the visual field. To achieve this there must be a loss of information, concerning the position of the object within the visual field, along the occipito-temporal pathway (Mishkin et al 1983).

Gross et al (1985) tested for stimulus selectivity using fourteen different stimuli including a face, hand, banana, shape, contrast, size , orientation, direction and wavelength. Thirteen percent of the neurons tested could not be driven and in 14% the responses were too weak to be investigated. Thirty percent were found to respond to all stimuli and therefore had no selectivity. In the remaining forty-three percent were selective, twenty-eight percent of these being selective for shape,sixteen percent for colour, seven percent for texture and seven percent for faces or hands. Configuration of the internal features was essential to gain responses from the face cells . The neurons responded to both human and monkey faces and front views or profiles. The hand selective units were also tested with fourier descriptors and it was established that the response was independent of the size, retinal position or contrast reversal of the stimulus. As the amplitude of the fourier descriptor was increased the amplitude of the response increased.

The IT is involved closely in the processing of pattern perception and pattern discrimination learning (Iwai 1985). On recording from cells in the Macaque monkey IT they found good transfer of learning from lower halves of the pattern stimuli only. It was proposed that the anterior IT is involved mainly in visual

cognition or memory and the posterior IT is predominantly involved in pattern perception. The IT may also be dependant on the tectofugal system for information about the location of a stimulus relative to the animal and the significance of that stimulus (Gross 1974). Gross considered the IT to be a further stage in the hierarchical stimulus feature detection system and the final stage in the process of visual pattern recognition.

2.3.9.vii The Superior Temporal Polysensory Area (STP)

This area is situated in the upper bank of the middle and rostral portions of the superior temporal sulcus immediately dorsal to the IT cortex. Anteriorly it crosses the floor of the superior temporal sulcus and extends onto the lateral surface of the temporal lobe. Virtually all the cells respond to visual stimuli but some also respond to somatosensory and auditory stimuli. The receptive fields are large; the median value for the contralateral field is 80°, 70° for ipsilateral, 55° for superior and 50° for inferior. The cells respond well to movement and 50% show direction selectivity, a minority are sensitive to complex stimuli e.g. a face (Gross et al 1981).

This area receives inputs from the IT, superior temporal and posterior parietal cortex as well as other cortical and subcortical areas e.g.frontal eye fields (area 8), cingulate cortex, parahippocampal region, amygdala and the medial pulvinar. The connections between the frontal eye fields and the posterior parietal cortex are reciprocal (Gross et al 1981). Both V1 and the superior colliculus contribute to the visual properties of the STP neurons.

Gross et al (1981) suggested that together with the frontal eye fields the superior temporal polysensory and posterior parietal areas form a system for linking sensory inputs with action. Lesions in the STP result in a deficit in visuospatial task performance (Petrides et al 1979) and in multimodal task performance involving visuo-auditory association (Petrides et al 1978).

2.3.9.viii Posterior Parietal Cortex

Lesion experiments in monkeys (Bates and Ettinger 1960, La Motte and Acuna 1978) and observations in human subjects (Balint 1909, Hecaen and De Ajuriaguerra 1954, Randot et al 1977) have proposed that the posterior parietal cortex is concerned with control of visual reaching. Parietal lesions also result in disturbances in the formation of grip and adjustment of hand orientation (Sakata et al 1985). Taira et al (1991) using microelectrodes implanted into the parietal cortex investigated hand manipulation. Fifty-one penetrations were performed in the

inferior parietal lobule of 5 hemispheres of the Macaca Fuscata monkey. The penetrations were located in the posterior bank of the intraparietal sulcus (area 7 or area POa of Pandya and Seltzer 1980). Forty-one percent (55/124) of the recorded cells were termed hand movement related and were activated equally well in the dark and the light. Most of these neurons gave an initial transient increase and then maintained this discharge rate during the object manipulation. Many were selective for the orientation and configuration of the manipulated object. The visual input was thought to be processed within this area as neurons related to visual space perception have also been recorded (Motter and Mountcastle 1981). Visual dominant neurones were those which gave no response when tested in the dark, and motor cells where those which gave a reduced response in the dark. It was postulated that the visual dominant neurons in this area and the motor cells of the premotor cortex (area 6) provide inputs to the combined visual and motor cells.

Pandya and Seltzer (1982) divided the parietal area into two constituent parts :

1. The superior parietal lobule and medial surface of the parietal lobe

2. The inferior parietal lobule and parietal operculus.

The inferior parietal lobule has a direct input from V1 via the extrastriate cortex and also from the superior colliculus and pretectal regions. It contains cells with giant bilateral receptive fields which may extend far into the periphery. The inferior parietal cortex contains four zones: PF, PFG, PG and Zone Opt.

Iwai (1985) demonstrated in the Macaque monkey that the area PG is involved in the process of attending selectively to a visual stimulus in irrelevant back ground or visual space.

2.3.9.ix Area PO

This area described by Gattass et al (1985) borders V2 on the medial cortical surface, V5 dorsally and V3 ventrally and posteriorly. It is located on the anterior bank of the parieto-occipito sulcus and extends onto adjacent portions of the precuneate gyrus and the adjacent portion of the medial bank of the intraparietal sulcus. The upper visual field is represented medially and the lower visual field laterally. The representation of the periphery is large compared with the centre and often discontinuous and the magnification factor actually increases in the periphery. The receptive field size is large compared with other visual areas, see fig 2.14. This area receives projections from the periphery of V1 and V2 and also maybe from the posterior part of the superior temporal sulcus and the intraparietal sulcus.

This area could be homologous to the area M described by Allman and Kaas (1976) in the owl monkey.

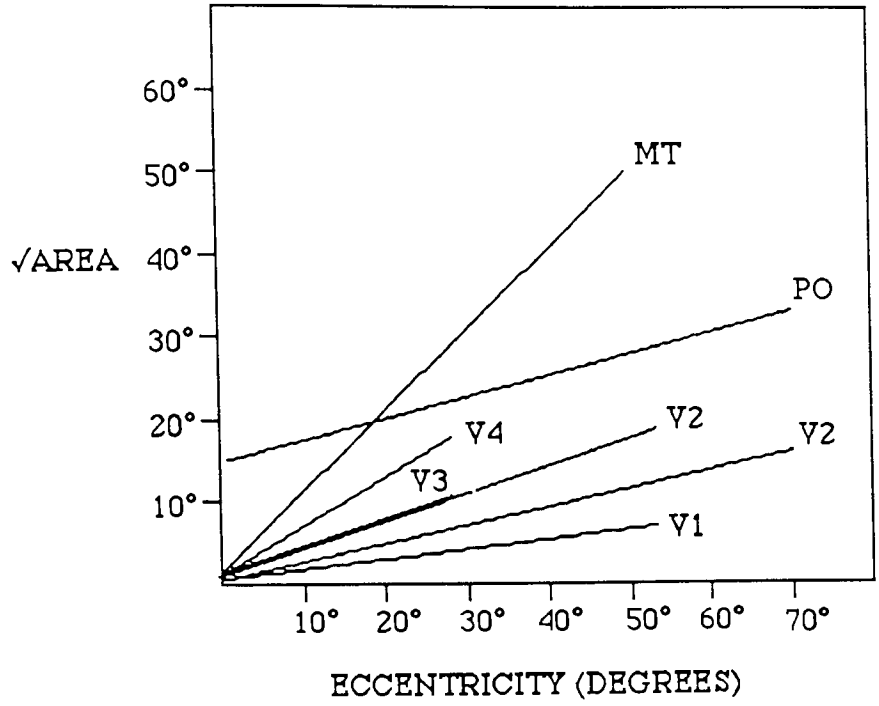

Fig.2.14. Receptive field size (√area) as a function of eccentricity for V1, V2, V3, V4, V5 and PO. Lower V2 line and PO data from same animal different to animal for other areas. After Gattass et al (1985).

2.3.9.x Area VF

This is located anterior to V3 and V4 and lateral to V2. The lower visual field is only represented. The receptive fields are larger than those of V4 at a given eccentricity (Gattass et al 1985).

2.3.9.xi Pulvinar

This area has 3 subdivisions: the inferior (PI) , the lateral (PL) and the dorsomedial (Pdm), the former 2 are retinotopically organised with well defined receptive fields increasing in size with eccentricity whereas the latter has a crude retinotopic organisation with varying receptive field sizes (Benevento and Miller 1981).

Petersen et al (1985) studied the neurons in the Macaque pulvinar and found all areas contained cells which were sensitive to orientation and direction, the majority were broad tuned to these stimuli.

The tectal and cortical pathways converge in this area and then relay back to the cortex. The caudal portion has a convergent input from several regions of the visual cortex. The cells in this area respond to moving bars and flashing lights and

also possess non linear binocular interaction. Pdm may play a role in selective visual attention while PI and PL are responsible for other aspects of visual perception.

2.3.9.xii The Claustrum

A reciprocal retinal projection has been demonstrated in the squirrel monkey from the Claustrum to areas 17,18,19 and V5, but it receives no direct retinal input (Olson and Graybiel 1980). Olson and Graybiel (1980) studied the cat claustrum with lesions and injection of HRP and nuclear yellow. Most cells studied could be activated by either eye and the best response was observed to moving bars and spots, the receptive fields ranged in area from a few degrees to a few 100 degrees. The cells also showed broad tuning for bar orientation or axis of motion. The claustrum was shown to have projections to V1 which terminate in layer 1 and the deeper layers including layer 4, a reciprocal projection from layer 6 was also demonstrated.

2.3.9.xiii The Amygaloid Complex

There is a direct connection of area 20 (inferior temporal cortex) with the amygdala which furnishes a route into the hypothalamus for visual cortical influences (Jones 1973). This area also has sensory and visceral inputs associated with emotional states (Tigges and Tigges 1985).

2.4 Connections Between Visual Areas

Ungerleider and Mishkin (1983) proposed the striate cortex as the source of two pathways: the ventral and dorsal pathways.

The ventral pathway is a colour opponent system fed by the parvocellular system and projects from V1 via V2 and V4 to the inferotemporal cortex in the temporal lobe, this pathway is crucial for object recognition.

The dorsal pathway consists of achromatic broadband cells and is fed by the magnocellular system projecting from V1 via V2 and the MT (V5) to the inferior parietal area, this is concerned with space and movement.

Inputs from the central visual field are important for the occipito-temporal pathway whereas, inputs from both central and peripheral visual fields are important for the occipito-parietal pathway.

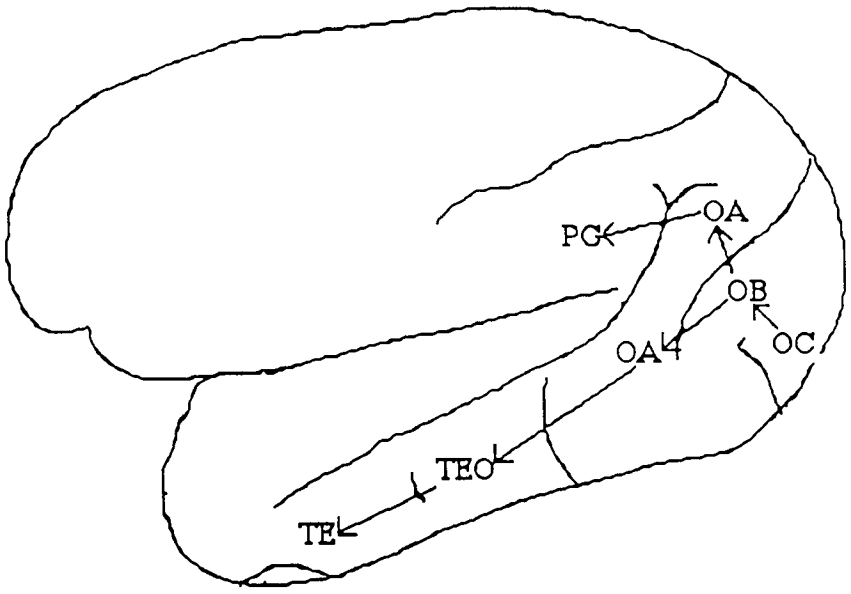

Fig. 2.15. Representation of the two pathways. OB is equivalent to V2 and V3. V4 and V5 are contained within OA,PG = parietal area and TEO and TE are the temporal cortex. After Mishkin, Ungerleider and Macko (1983).

The occipito-temporal pathway makes subsequent links with limbic structures in the temporal lobe and with ventral portions of the frontal lobe, these connections may make possible the cognitive association of visual objects with other events such as emotional and motor acts. The occipito-parietal pathway may also continue with connections to the dorsal limbic and dorsal frontal cortex, these pathways could enable the cognitive construction of spatial maps and the guidance of motor acts. The later sections of this pathway may connect with polysensory areas.

The two pathways have been shown to be mainly independent (Morel and Bullier 1990, Baizer, Ungerleider and Desimone 1991) after injection of retrograde tracers in the parietal and temporal areas of the monkey, the areas were slightly different between the two studies. Small regions of overlap were observed, particularly at the margins. One zone of overlap included V4, V3 (V3A, Morel and Bullier 1990 but not Baizer, Ungerleider and Desimone 1991) and TEO (Baizer, Ungerleider and Desimone 1991). Certain areas in the parietal and temporal cortex received afferents from common areas in the anterior superior temporal sulcus, this area may therefore act as an integation area, with its complex receptive fields. Reciprocal connections were demonstrated between the infero-temporal cortex and area POa in the parietal cortex (Morel and Bullier 1990). Very few double labelled cells were observed i.e. project to both the parietal and temporal cortex, this would suggest that different cell populations in similar areas send projections along the two pathways.

The projections to the inferior temporal cortex were shown throughout the remainder (not injected) of TEO and TE including the portions of TE in the superior temporal sulcus. Other areas included FST, TG, TF and TH on the parahippocampal gyrus. In the prestriate cortex cells were found in V4, V4t, DP, the foveal representation of V2 and the central field representations of V3d and V3v. Some labelled cells were also observed in the frontal eye fields. The primary source of inputs to area TE was shown to be area V4.

Cells projecting to the parietal cortex were observed in areas V2, V3 and V4. In V2 the cells were limited to the far peripheral field representations of the upper and lower visual field, the cells in V3 and V4 were also more concentrated in the peripheral representations. Cells also found in PO, V3A and DP and in the posterior superior temporal sulcus such as areas MT, MST and FST and the anterior portions of the sulcus.

Due to the fact that V4 projects to both areas it is suggested that this area contains two sets of cells processing different aspects of the visual stimulus. The results support the concept that the parietal cortex is preferentially stimulated by the peripheral field (Ungerleider and Desimone 1986 and Ungerleider et al 1986) and also suggest that the temporal cortex receives preferential inputs from the central visual field. Physiological evidence suggests that the central and peripheral fields are processed differently in the posterior parietal cortex. The results are also consisitent with the proposal of magnocellular and parvocellular roots for the two pathways (Livingstone and Hubel 1988) it is however, unlikely that the all the information processed in the parietal and temporal cortex can be traced back to the different layers in the LGN. Interconnectons between the two systems occur along the dorsal and ventral pathways, it is therefore unlikely that the temporal or parietal cortex will be completely isolated following a lesion in either the magnocellular or parvocellular system.

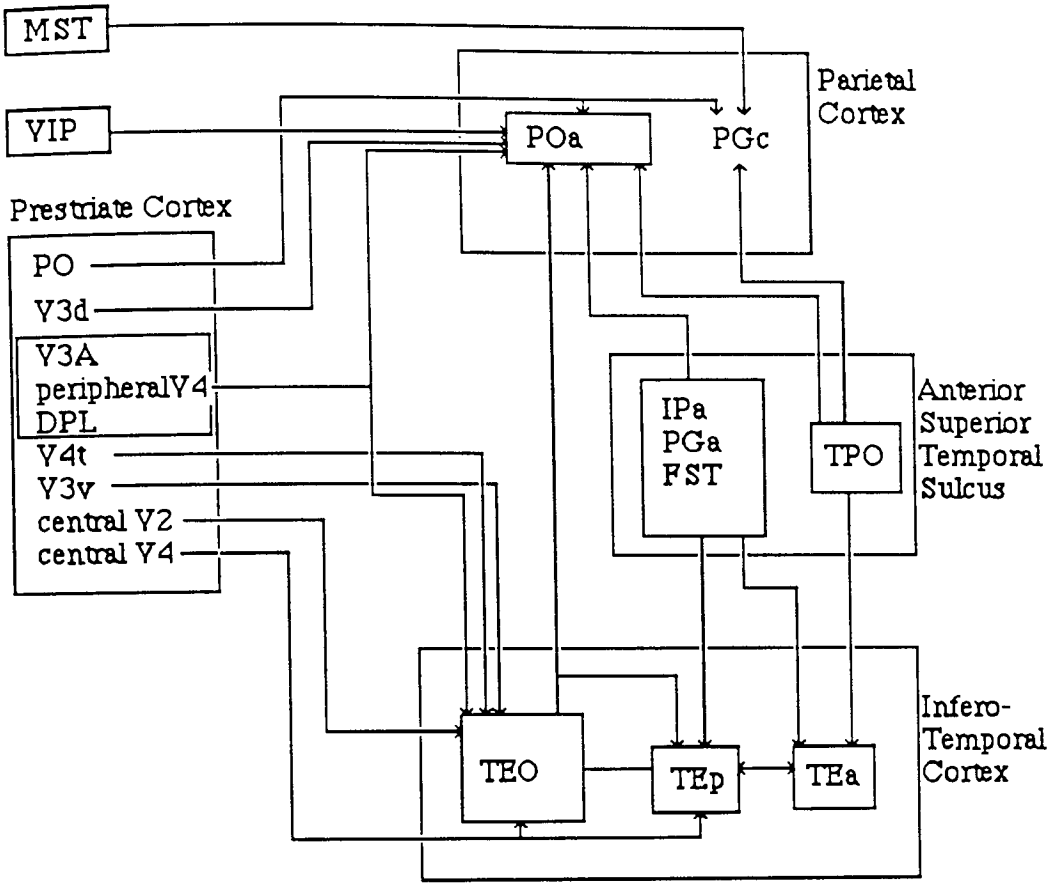

Fig 2.16. Diagrammatic illustration of the prestriate and anterior superior temporal sulcus connections with the inferior parietal and inferotemporal cortex. The central V2 and V4 refer to the region coding for the central visual field and the periphery refers to that coding for the peripheral visual field. DPL = dorsal prelunate area, FST = fundus superior temporal, IPa = , MST = medial superior temporal, PGa = , PGc = , POa = , PO = , TEO = , TEa = , TEp = , TPO = , VIP = ventral intraparietal area. After Morel and Bullier (1990).

Using fluorescent dyes Kennedy and Bullier (1985) investigated the afferent connections of V1 and V2 of the Macaque monkey. They showed that V3, V3A and V4 projected more heavily to V2 than V1. There were also projections to V1 and V2 from the STS, IT cortex and the parahippocampal gyrus. In V1 the cells projecting to V2 were located mainly in layers 2/3, 4b and some in the lower section of layer 5 and upper section of layer 6, the latter two connections were not previously reported. The projections from V2 to V1 were found in layers 2,5 and 6. In the LGNd cells located within the laminae projected to V1 whereas cells projecting to V2 were more scattered and located in the interlaminar zone. The lateral pulvinar had a greater projection to V2 than V1. V1 was shown to project to V2, V3, V3A, V4 and V5 this they stated would be irreconcilable with the

heirarchical model of the visual processing. To further support their argument they demonstrated that V1 and V2 share alot of information from both subcortical and cortical sources, also double labelled neurones having a projection to both V1 and V2 from branches of the same axon were reported.

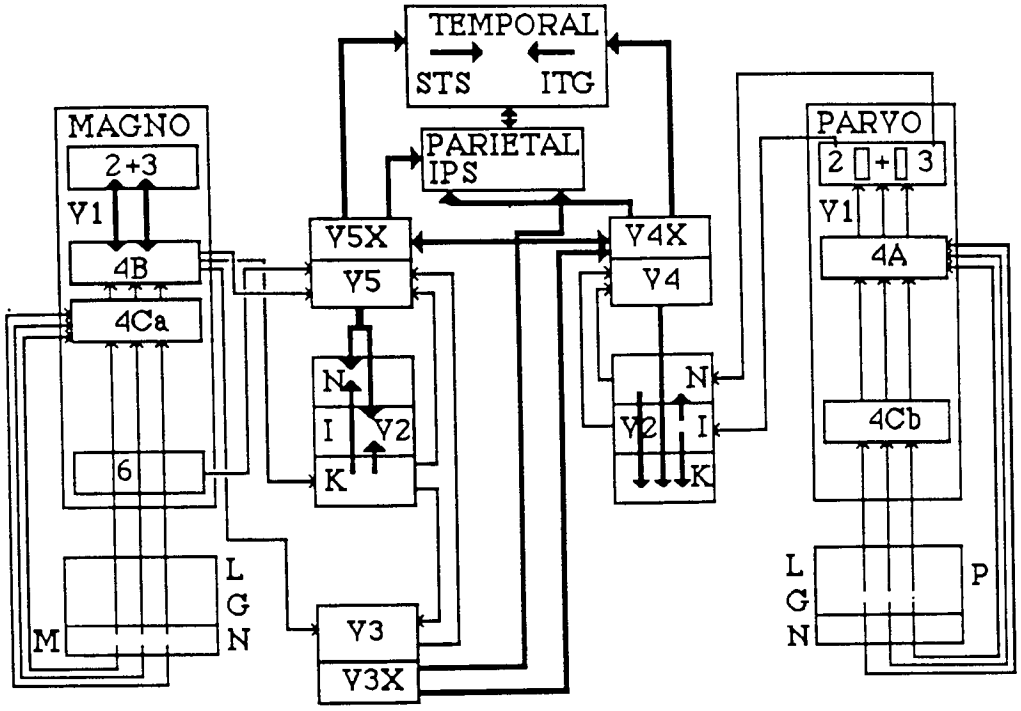

Fig.2.17. Connections between the lateral geniculate, the striate cortex and the extrastriate visual areas. Cytochrome oxidase blobs are represented by small cylinders in layers 2 and 3 of the striate cortex. The cytochrome oxidase bands in V2 are thick, K thin ,N and inter,I. V3, V4 and V5 are part of the third fourth and fifth visual complexes denoted by V3X, V4X and V5X. Connections shown to arise from V3X, V4X and V5X include the whole complex and do not exclude V3, V4 and V5. ITG is the infero temporal gyrus. After Zeki and Shipp (1988).

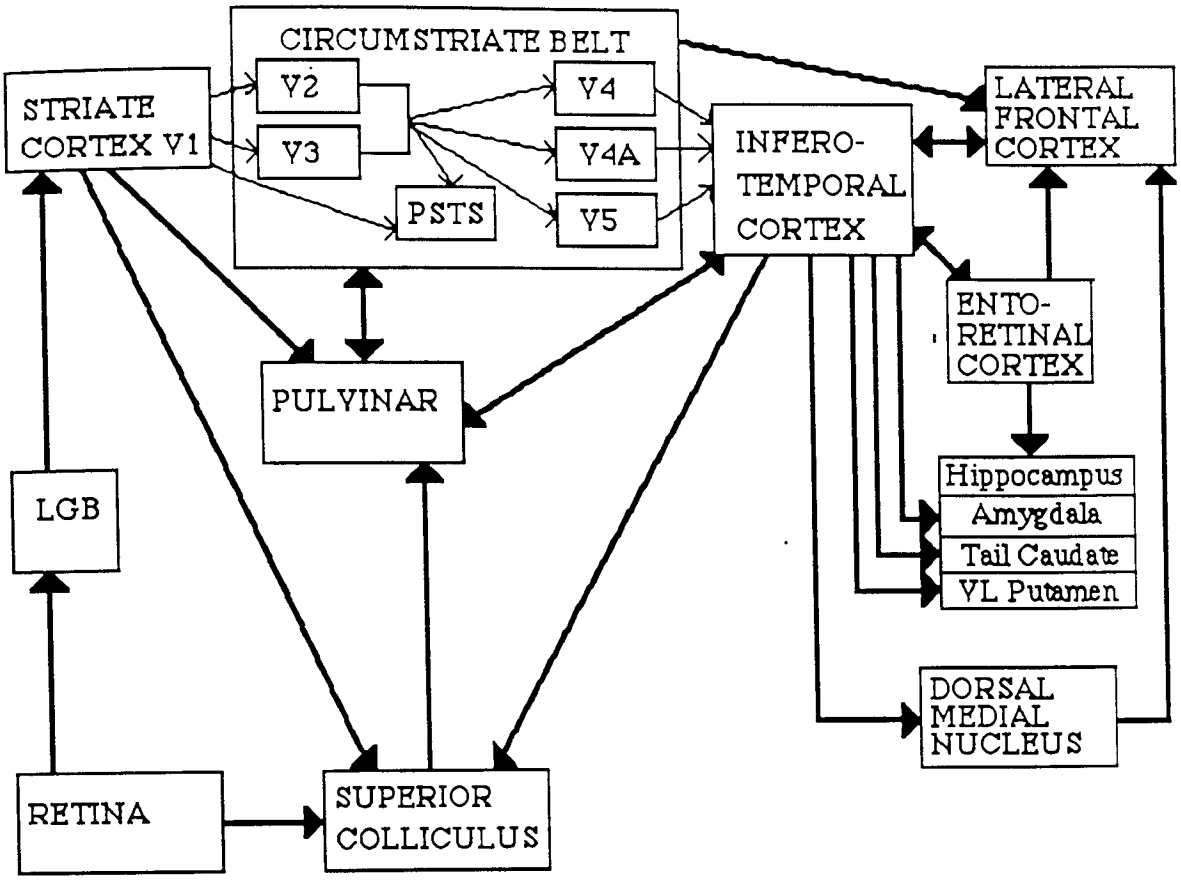

Fig.2.18. Further connections of the extrastriate visual areas. After Gross, Bender and Rocha-Miranda (1974).

It is evident that specialisation occurs within the each visual area but each area is not totally independent. By virtue of the complex interactions between areas and between neurons common to more than two areas the visual areas can not remain independent. The neural pathways in the visual system accumulate information by means of convergence. Zeki and Shipp (1988) cited two types of convergence: topical and confluent. Confluence defines the merging of information from two separate pathways whereas topical defines operations within a pathway. These are further categorised as forward, backward, intrinsic and lateral.

	Topical	Confluent
Forward	Blobs V1-->thin stripes V2-->V4	V2 (thin) + V3 -->V4
	V1 --> V5	V4 + V5 -->IPS + STS
Intrinsic	in V4	in V1,V2 and IPS
Lateral		V4 -- V5
Backward	V5 -->V1	V3 +V5 --> V1(layer 4B)
		V4 + V5 --> V2 (thick, thin and interstripes)

Forward topical convergence occurs when a larger part of a lower area projects to a smaller part of a higher area, so resulting in cells with larger receptive fields typical in the pathways of the visual system e.g. V4, V2 and V1. These larger receptive fields are vital for processes such as colour constancy in V4 and stimulus equivalence in IT. Intrinsic connections are those in the same area but between different layers. Most projections are reciprocal but the location of the forward and backward projections within the same area do not necessarily coincide. Some areas can therefore be influenced indirectly by backward projections from other visual areas although they may have no direct connections with this area. For example backward projections of V5 can influence projections to V4 from V2 as these backward projections terminate in all layers of V2 including those that project to V4. These will influence V4 before the lateral connections of V4 and V5 can act.

It may therefore be concluded that a simplistic model of the processing of a visual signal is of various serial pathways acting in parallel. Superimposed on this model are other more complicated projections. V1 processes the information with regard to its relative attributes, this is then transmitted along various pathways. V2 further processes information from V1 which is fed back to modulate other outputs of V1 (Kaas 1992). Integration of these various pathways occurs at higher levels in the visual system.

2.5 Functions of the Superior Colliculus

In lower animals the superior colliculus is the chief information processing unit, in primates the geniculostriate system is more dominant. Although in the owl monkey retinal projections have been found in the superficial layers of the superior colliculus these are mainly Y cells and also some W cells (Marocco and Li 1977, Schiller and Malpeli 1977). Input to the rhesus superior colliculus has been demonstrated from layer 5 of V1 (Schiller 1977). In the owl and rhesus monkey (Schiller 1977) the superior colliculus projects to two of the three subdivisions of the inferior pulvinar: posterior IPp and central IPc nuclei (Kass 1977). The relay from the IPc is primarily to the prestriate cortex and IPp appears to project to visually responsive areas of the temporal lobe (Lin and Kaas 1979). In old world monkeys the inferior pulvinar has not been subdivided but it has been shown that the macaque IP projects to the striate cortex (Benevento and Resak 1976). The superior colliculus is composed of several layers, the cells in the deeper layers are selective to saccade eye movements and respond prior to certain saccades (Schiller 1977). There is a representation of the visual half field in each colliculus, the left superior colliculus represents the right visual half field. The anterior superior

colliculus represents central vision and the periphery is represented posteriorly, receptive field size increases with eccentricity (Schiller 1977).

Hoffman and Stone (1973) demonstrated three pathways from the retina to the colliculus:

1.Direct via the W cells to 73% of the colliculi cells.

2.Direct via the Y cells to 9% of the colliculi cells.

3.Indirect involving a cortical loop consisting of a retinal Y cell, a geniculate Y cell and a cortical complex cell sending it's axon through the corticotectal pathway.

If the pathway from the striate cortex to the colliculus is interrupted then the colliculus becomes undrivable by visual stimuli. Subsequently if both the colliculus and the frontal eye fields are ablated then there is no ability to form visually guided eye movements.

Sterling and Wickelgren (1969) examined the receptive fields of the cat's colliculi and found their properties similar to the complex and hypercomplex units of the monkey however orientation was not as critical and was, largely confined to the horizontal.

2.6 Functions of the Corpus Callosum

The corpus callosum is made up of myelinated fibres linking both hemispheres, these fibres join homologous areas. Myers (1962) demonstrated the transfer of visual information across the corpus callosum. In addition Choudhury et al (1965) showed that it was the vertical midline of the visual field that was connected, receptive fields could therefore span the midline.

CHAPTER 3

Methods of Recording Activity in the Visual Cortex on the Scalp

3.1 The Origin of the Scalp Recorded Activity

The evoked response recorded at the scalp is the result of activation of neurons in the cerebral cortex. Neurons convey information along their axons and dendrites from one cell to another. This information is in the form of impulses.

3.1.1 Transmission of a Neuronal Impulse

In the resting state of a nerve there is a charge of +70mV outside the neuron membrane, this is the result of a concentration gradient of Na+ and K+ ions across the membrane. A higher concentration of Na+ ions is present outside the cell, the K+ ions being present within the cell. Channels selective for either Na+ or K+ are present within the membrane, these open or close to allow or prevent the passage of the appropriate ion. In the resting state the Na+ channels are closed and most of the K+ channels are open. When an impulse arrives the Na+ channels open, Na+ enters the cell and the membrane potential reverses polarity to become -40mV outside. The Na+ channels then close and the rest of the K+ channels open to bring the membrane back to its resting potential. This depolarisation of the membrane spreads along the fibre at a rate of 0.1-10m/sec. Once the Na+ channels have closed they are unable to open for a few thousandths of a second resulting in a maximum firing rate of approximately 800/sec, although the usual rate is 100-200/sec. To increase the speed of the impulse some nerve cells are covered with myelin, breaks (nodes of Ranvier) are present in the myelin sheath to allow the passage of Na+ ions.

The impulse is transferred from one cell to another over a synaptic junction. When a neuronal impulse arrives at a junction Ca+ channels open at the pre-synaptic membrane resulting in the release of a neurotransmitter, this acts on receptors of the post-synaptic membrane to open either Na+, K+ or Ca+ channels depending on whether the synapse is excitatory (Na+) or inhibitory (K+). A nerve cell is connected by many synapses, the resulting membrane potential is therefore the sum of excitatory and inhibitory impulses. An impulse is usually generated where the axon leaves the cell body. A cell can receive inputs from more than one cell, this is termed convergence however if the cell's axon branches and stimulates many other

nerve cells this is termed divergence. Convergence can be seen to operate on a wide scale in the visual system.

3.1.2 Classification of Impulse Resulting in a Recordable Response.

Neurons respond to action potentials reaching them via synaptic connections in one of three ways (Regan 1989) :

1. A relatively slow reduction (depolarisation) in the magnitude of the transmembrane resting potential.

2. A relatively slow increase (hyperpolarisation) in the magnitude of the transmembrane resting potential.

3. The triggering of an action potential which propogates automatically once the threshold depolarisation is complete.

All three of these will give rise to recordable extracellular currents but the scalp recorded responses (Electroencephalogram (EEG) and Magnetoencephalogram (MEG)) are thought to be due to graded potentials which are the result of 1 and 2.

The evoked response is most probably the result of postsynaptic potentials and not action potentials due to the fact that;

1. Action potentials are too fast, postsynaptic potentials have an average duration of approximately 17ms for the excitatory phase compared with 1ms from an action potential (Vvendenski 1985, Gloor 1985). Summation of action potentials does not occur because the potentials must be perfectly synchronised to overlap or coincide, however synaptic potentials last for between 10-30ms and so lack of synchronisation could still allow them to overlap for most of their duration leading to a time coherent potential change large enough to be recorded (Gloor 1985).

2. Postsynaptic potentials generate large extracellular loops and are normally monophasic, whereas action potentials are biphasic with more localised current loops. Temporal scatter of the action potentials and spatial scatter of the activated soma result in the cancelling of opposite membrane currents (Mitzdorf 1986).

Excitatory synaptic activities are thought to be the dominant cause of the sinks and sources in the cerebral cortex which result in the evoked response (Mitzdorf 1986).

3.1.3 Most Probable Class of Neurons Producing the Response

The cells most likely to produce a response outside the head are termed open field. Two major classes of cells are present in the visual cortex; pyramidal and stellate, these produce different electrical fields after activation by postsynaptic potentials, see fig 3.1.

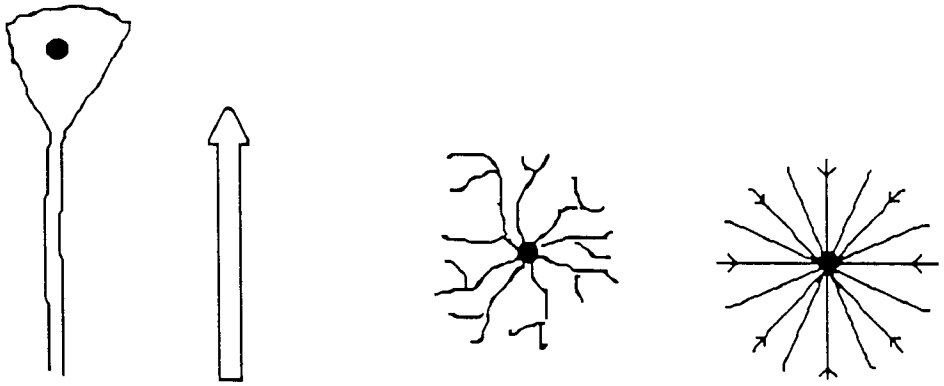

A B

Fig 3.1. The two groups of cells in the visual cortex, A the pyramidal cells (open field) and B the stellate cells (closed field). A diagrammatic representation of the cell and a representation of the dipole configuration.

Stellate cells give rise to a 'closed field' in which the dipoles set up act in opposition, the resultant sum of the total field approximates zero. If, however a pyramidal cell is stimulated the field more approximates a dipole with a positive and negative pole. The neuronal activity generated may therefore be represented in simplified terms as an equivalent dipole. These cells are oriented normal to the cortical surface and parallel to one another, simultaneous activation of a large number will therefore lead to a measurable potential. The third type of configuration is an open-closed field, in which both types of the previous cells are present. This class is most common but, since the closed fields should not contribute to the response the form can be simplified into an open field. Fusiform cells are an example of cells which will produce an open-closed field.

3.1.4 Intracellular, Extracellular and Transmembrane Currents

When a dendrite is activated through a postsynaptic potential the cellular membrane and charge change and an intracellular, extracellular and transmembrane current are produced, see fig.3.2. The current density of the extracellular current is small compared with that of the intracellular current as it can disperse over a relatively large area.

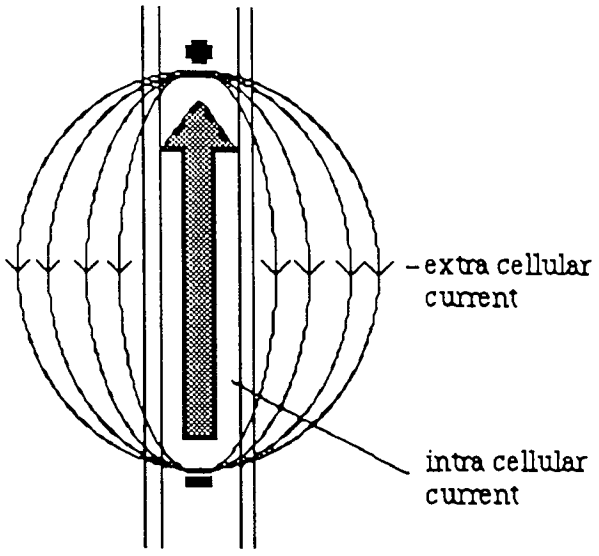

Fig.3.2. Diagram to illustrate the relationship between the intra and extracellular currents produced by activation of a single neuron.

If an extracellular current meets a boundary between two areas of differing electrical conductivities e.g. between the dura mater and the skull, secondary sources will be evoked. The secondary source will be directed normally to the scalp i.e. in a radial direction. The magnitude of the secondary source is equal to $(\partial 1-\partial 2)V$, where ∂ represents the conductivities on the two sides of the boundaryand V is the electrical potential at the boundary (Geselowitz 1970). The secondary sources may increase or reduce the magnitude of the evoked resposne depending on whether the conductivity in the region of the primary source is lower or higher than that of the surrounding region.

3.2 The Evoked Potential (EP)

The recorded electrical potential is the sum of the potential due to three components of the source, i.e. the radial and tangential components (Okada 1989, Rose 1987). The evoked potential recorded from the scalp is assumed to be the result of extracellular currents from the dendrites and not the intracellular currents. The extracellular currents are attenuated and/or smeared by the tissues and skull surrounding the brain before being recorded at the scalp (Cohen and Cuffin 1979). As a result of being sensitive to the radial components of the electric field the potential can be affected by secondary sources set up at boundaries of differing conductivity. The evoked potential is therefore strongly dependent on the conductivity of structures surrounding the source, this can lead to gross distortions

of the spatial pattern and make it difficult to relate the magnitude of the surface potential to that of the primary source (Okada 1989). It has also been shown that large dipole layers (several 10's of cms) produce scalp potentials that are attentuated by factors of roughly 2-4 between the cortex and the scalp. In contrast to this small dipoles are attenuated by factors of 100 or more (Nunez 1981, 1988). The skull and the spatial separation between the sources and the electrode also act so as to selectively attenuate short wavelength activity (Nunez 1988). Due to the smearing effect of the cortical structures a source located by the EP recording will be computed to lie deeper than it does in reality (Cuffin 1985). It is therefore suggested that the MEG, being less sensitive to smearing, will be more accurate at source localisation than the EP.

Cuffin (1985) also investigated the effect of fissures on the EEG. For a radial dipole the potential is reduced with the introduction of a fissure. In contrast for a tangential dipole (directed towards the fissure) the potential is larger with a fissure except for points on or adjacent to the fissure. For a dipole directed parallel to the fissure the potential is generally smaller. Moving the source closer to the fissure or increasing the conductivity in the fissure had little effect on the distribution of the recorded potential.

3.3 The Evoked Magnetic Field (EMF)

A magnetic field associated with a current dipole encircles the dipole and flows in a direction perpendicular to that of the dipole, see fig.3.3.

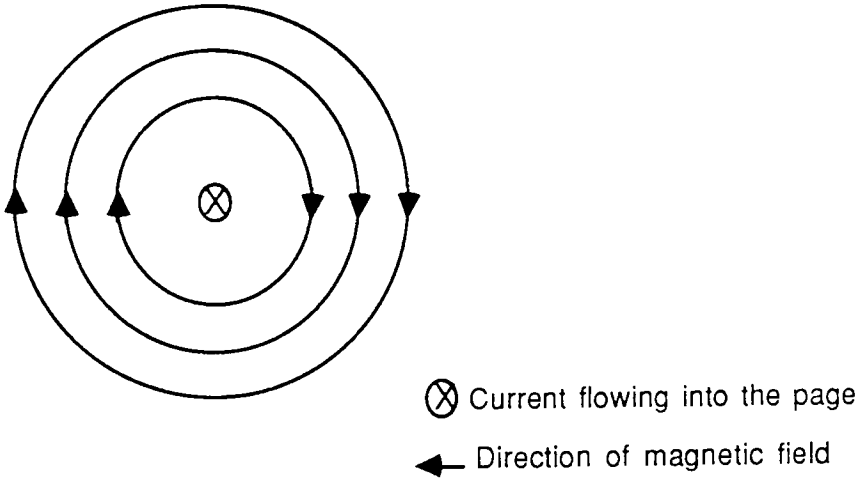

Fig.3.3. If a current is flowing down a straight wire then a magnetic field will be produced and will surround the wire in concentric field lines

When a dipole as such is located in the cortex and oriented in a direction tangential to the scalp a magnetic field can be recorded whose field lines will 'cut' the scalp and leave and enter the brain. This gives rise to the radial and tangential components of the magnetic field. The radial components are positioned where the field enters and leaves the cortex, the tangential component is situated above the dipole. If the radial component of the field is recorded a distribution of the field will be represented by two maxima, the dipole can be approximatley located between the maxima. The recorded evoked field is the result of the tangential components of the source, if the head is spherical then we expect no external field due to a radial source (Okada 1989).

The strength of the magnetic field at the recording site is very dependent on distance of the source from the recording site. An action potential set up in an axon leads to a current quadrupole being set up and this could produce a magnetic field. This is, however unlikely to be recorded on the scalp as the rate of signal amplitude fall off from a quadrupole is related to the inverse cube law. In contrast the rate of fall off of a current dipole is related to the inverse square law, and is therefore more likely to produce a signal that can be recorded (Okada 1982). In addition to this the cross sectional area of an axon is much less than the total cross sectional area of the dendrites, the resistence is therefore greater in an axon resulting in a reduction in the current density (Rall et al 1962). To produce a magnetic field the current density has to be high, a low current density results from the extracellular currents and these are therefore not thought to contribute significantly to the recorded field. The transmembrane current also provides a negligible contribution to the evoked field because of its radial symmetry and thinness (Plonsey 1981). Intracellular currents produce higher current densities so resulting in larger magnetic fields. In an excitatory input the current in the dendrite flows toward the lower electrical resistance i.e toward the soma whereas the extracellular current flows in the opposite direction. The direction is reversed for an inhibitory input (Okada 1982). The current density of the intracellular current is higher for excitatory inputs, and will presumably give rise to a stronger magnetic field (Okada 1982).

3.4 A Comparison of the Evoked Field and the Evoked Potential

The magnetic and electrical field differ in many respects;

a) Differences in conductivity have a greater effect on the evoked potential, thus reducing the spatial resolution.

b) The evoked potential field is more sensitive to radial sources and the potentials produced by these may obscure the potentials set up by tangential sources. The MEG, being more sensitive to tangential sources, may therefore record that which could be obscured in the EP map (Cohen and Cuffin 1983). Using both the MEG and evoked potential recordings it may be possible to distinguish between a tangential dipole and two radial dipoles postioned in the same area but with opposite polarity (Wood 1985).

c) Evoked potentials are relatively more sensitive to deep sources (Wood 1985).

d) The maxima of the magnetic field are rotated by 90° compared with the maxima of the electrical field, see fig.3.4.

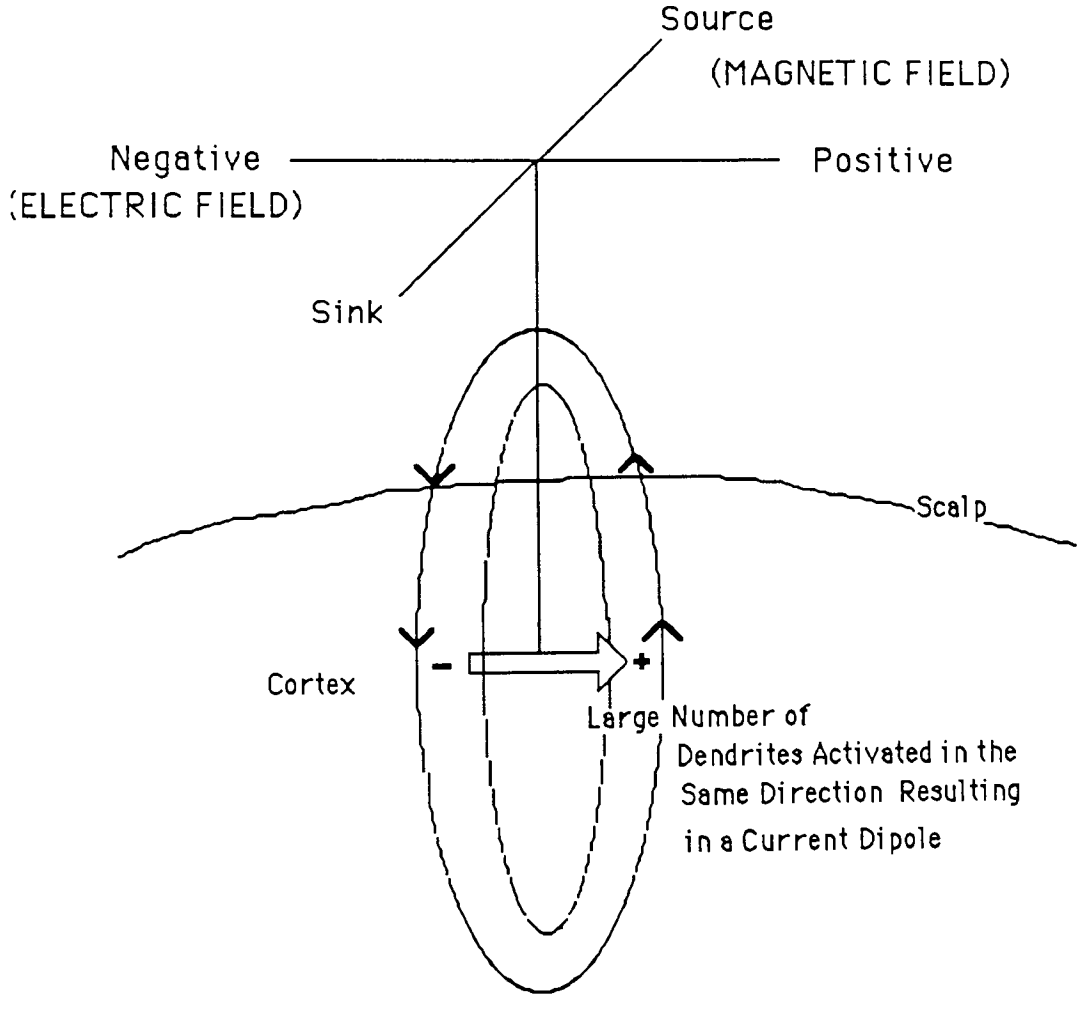

Fig 3.4. Illustration of the relationship of the magnetic and electrical fields evoked by a current dipole.

In theory the evoked potential and the evoked field are measurements of the same electrical event but recording the different cellular currents.

The magnetic field is presumed to be less affected by inhomogeneities in the head compared with the electrical field, this therefore results in an increase in the accuracy of source localisation obtainable with the magnetic field. For spherical head models the magnetic field recorded at the scalp from a primary radial dipole is zero, as both the tangential and radial components of the magnetic field are zero. Hr (radial component), is zero because perfect spherical symmetry causes both the primary and secondary contributions to be zero. Ht (tangential component), is zero because the spherical symmetry causes the secondary sources to contribute a tangential component equal in magnitude but opposite in sign to the primary source (Baule and McFee 1965, Grynspan and Geselowitz 1973). If the head were made up of perfectly spherical surfaces then the volume currents which are radially oriented would not contribute to the recorded magnetic field outside the head. However, as the cortex is not smooth, volume currents may affect the response.

The radial component of the magnetic field is less affected by volume currents when compared with the tangential component. For the tangential component the contribution of the primary source (intracellular current) is counteracted by the contribution from the secondary source (volume currents) so much so that the recorded field may be a greater reflection of the secondary and not the primary source (Meijs 1987). It is therefore unwise to record the tangential components. The effect of secondary sources is partly dependent on the method used for recording the magnetic field, this will be dealt with in more detail later in the chapter.

Since the head is, however not a spherical surface the radial component of the magnetic field will have a limited contribution from secondary sources, at least over the upper parts of the head which are not too close to the non spherical parts of the head (Nunez 1986). The effect of non sphericity of the head on the magnitude of the secondary sources was investigated by Cuffin and Cohen (1977). They found that for shallow sources the distortions due to secondary sources although not completely absent appeared to be within acceptable limits.

The radial magnetic field appears to be mainly due to tangential dipoles and the EEG appears to be more sensitive to radially oriented dipoles. Although the MEG can be compared to the EEG directly the EEG is influenced by the position of the

reference electrode. Consequently, an improved comparison may be that of the radial current estimate with the magnetic field. This is not dependent on the reference, it represents the radial component of the source and is biased towards the detection of shallower sources.

The effect of different conductivities of the medium surrounding a dipolar source in a computer model of the head has been studied (Ueno, Wakisako and Harada 1985). The effect of inhomogeneities due to brain lesions and also the inclusion of the ventricles was investigated. The head was modelled by a spherical volume conductor with a conductivity, $\partial 1$ which remained constant, into which an area of inhomogeneous conductivity, $\partial 2$ was placed. In the first model the brain was modelled with conductivity, $\partial 1$ and occupied the top half of the sphere, the rest, occupied by the nasal and oral cavities, was filled with conductivity $\partial 2$. A current dipole was located tangentially in the brain area. The second model consisted of a brain lesion which was modelled by a sphere, the current dipole was located under the lesion. The conductivity of the lesion was varied to model oedema, with high conductivity and calcification, with low conductivity. The third model was the ventricles, a current dipole was again placed beneath the modelled area. Electrical potentials and magnetic fields were recorded over the surface of the head after changing the ratio of $\partial 1/\partial 2$. In the case of the hemispherical model, (model 1) the value of the electrical potential increased as the value of $\partial 2$ decreased and the maxima appeared to become less separated. The magnetic field values were not so influenced by the change. For the brain lesion model the potential distribution resembled that from the homogenenous state ($\partial 1/\partial 2 = 1$) , however the amplitude decreased as the value of $\partial 2$ increased and the maxima appeared to move closer together. In contrast the magnetic field distributions were very dependent on the ratio of $\partial 1/\partial 2$. There was reversal in the flow of the field between $\partial 1/\partial 2 = 10$ and $\partial 1/\partial 2 = 0.1$, i.e. when going from oedema to calcification. In the ventricular model the potential distribution again resembled that from the homogenenous state, whereas the magnetic distribution again reversed as $\partial 1/\partial 2$ varied, this time from 10 to 1. They postulated that the change in the magnetic distribution was the result of changes in the secondary sources set up by the volume currents flowing through areas with differing conductivities. The variation was dependent on the inhomogenities and also the position of the source with respect to the boundaries.

Iramina and Ueon (1988) proceeded to investigate the effect of inhomogeneties on the magnetic field from a radial dipole. A simple inhomogeneous sphere model was used, and the magnetic and electrical field were calculated. The sphere was

split into two, as before, with the upper region representing the brain and the lower the nasal and oral cavities. The upper conductivity, ∂1 was kept constant and the lower conductivity, ∂2 varied. The net result was a variation in the ratio of ∂1/∂2 from 0.01 to 100. Radial dipoles were placed at different depths in the sphere see fig.3.5.

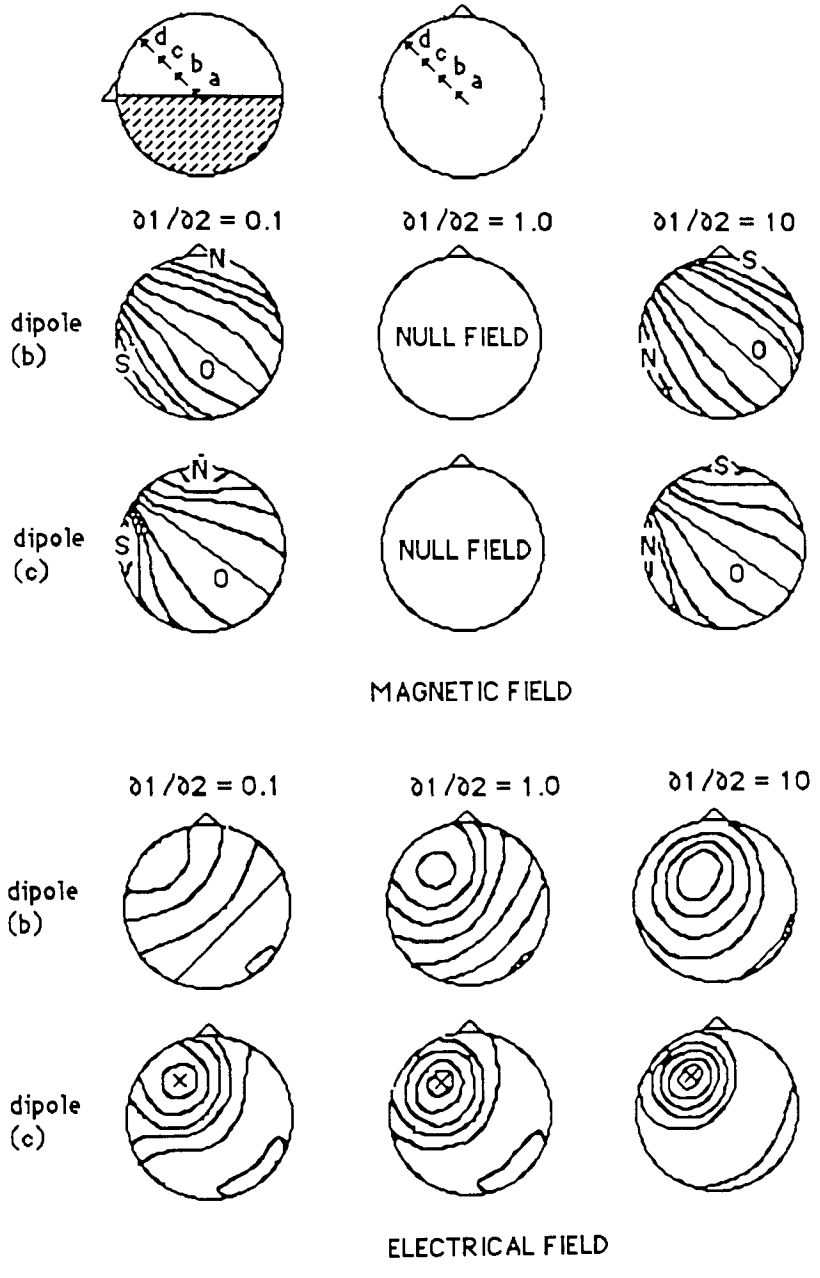

Fig 3.5. Spatial distributions of the normal component of the magnetic field and the electrical potential over the surface of a sphere generated by a current dipole. Positions of dipoles in the sphere as illustrated. (After Iramina and Ueno 1988.)

The magnetic field flow reversed when the conductivity ratio changed from 0.1 to 10, or from 10 to 0.1. When the ratio was equal to 1.0 no magnetic field could be detected. The flow of volume currents is therefore strongly affected by changes in homogeneity and for radially oriented dipoles the magnetic field recorded is the result of these volume currents and not related to the dipole. The magnetic field amplitude increased when the dipole approached the boundary. The effect on the potential distribution was also dependent on the position of the dipole with respect to the boundary, when the dipole was positioned near the boundary the amplitude became influenced by the conductivity ratio, the amplitude reduced as the ratio increased. The effect of dipole rotation was also investigated, this was found to be dependent on the recording site position. Recording sites positioned nearest the boundaries of conductivity were more affected by a change in $\partial 1/\partial 2$, whereas those furthest from the boundaries were more affected by the rotation.

Wikswo and Roth (1988) proposed that homogeneity in a source model can be assumed if the depth of the source is small compared with the radius of curvature of the skull. If this is so the boundaries between the inhomogeneities can be represented by plane surfaces, resulting in the normal component of the magnetic field remaining unaffected by the inhomogeneities.

Magnetic recordings were found to be 6x more sensitive to tangential dipoles compared with radial dipoles (Melcher and Cohen (1988). The fields from radial dipoles can be detected outside a head because it is not a perfect spherical shell. A dipole was oriented radially and tangentially in the head of a rabbit and the magnetic field was measured in the z, x and y directions. For the dipole locations chosen relatively small z components were expected and they therefore concentrated on the responses in the x and y direction, although the z component was still recorded to check the field gradient. Theoretical distributions were also calculated to see how well the rabbit head could be approximated by a sphere. The tangential dipole behaved roughly as a tangential dipole in a conducting sphere. The electric potential distribution was also recorded and matched for the radial dipole giving a maximum over the dipole. The factor of 6 for the suppression was derived from a raw value of 4 and increased with correction factors allowing for the fact that the dipoles were not oriented exactly tangentially or radially. The dipoles were only placed near the skull surface and no attempt was made to calculate the effect of deeper dipoles. As a tangential dipole approaches the centre of sphere its magnitude approximates zero. Unless the magnetic field for a radial dipole decreases proportionally with the reduction in strength of the tangential dipole, the

Figure 3.6. The location of electrodes over the scalp when positioned according to the 10-20 system. Key; F = frontal, C = central, T = temporal P = parietal and O = occipital. After Jasper (1958).

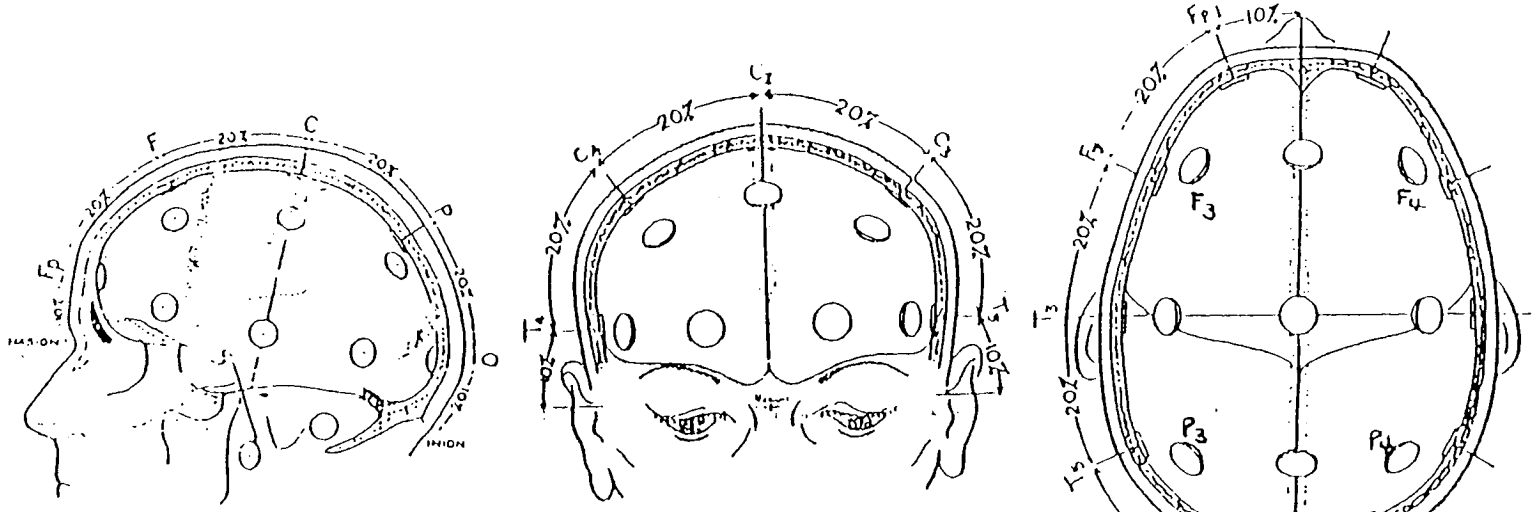
F
C
P
Fp
O
INION
Cz
T3
T4
Fp1
F3
F4
P3
P4
T5
T6
10%
20%

suppression will not be as great for deeper dipoles. Significantly greater suppression was not expected for the human head although this was only supposition.

3.5 Recording the Evoked Potential

3.5.1 Electrodes

The point of connection between the scalp and the recording equipment is at the electrode. Silver-silver chloride electrodes are used as they can not be polarised, this would lead to noise in the output. Cup electrodes are adequate when the components of interest have frequencies less than 2Hz (Regan 1989).

3.5.2 Anatomical Location of the Recording Electrodes

The first major study on positioning the cerebral electrodes for investigating brain activity was performed by Jasper (1958). The locations of the electrodes were based on percentage measurements using the bony landmarks of the skull as reference points. The system was named the 10-20 system based on the fact that electrode positioning was either 10% or 20% of defined distances on the scalp, see fig 3.6. After the positions were established anatomical studies were carried out to determine the cortical areas lying underneath the electrodes. Cadaver skulls were X-rayed and the electrode positions were drilled through before removing the brain. Only the location of the central and rolandic fissures with respect to the electrode placements were commented on, with C3 and C4 lying over or precentral to the rolandic fissure and the sylvian fissure running between T4 and F8 and T3 and F7.

The method used in positioning the recordings points of the EEG is based on the percentage system of Jasper where the head circumference and the nasion to inion distances are measured. This system therefore allows for variations in head size across the population.

There is however considerable variation, in the population, in the position of the cerebral cortex beneath the skull which leads to variations in the distribution of evoked responses. CT scanning has been employed to compare the scalp markers of the 10-20 system with the underlying anatomy.(Homan et al 1987). A precentral location for C3/C4 was reported in most of the 12 adults studied. Twelve instances of quadrant asymmetries of 10% or greater were also recorded, in four subjects the right posterior quadrant was larger than the left. Electrode pairs

were found to mostly occupy the same Brodmann area in both hemispheres. Any deviation from the primary location was not solely or even primarily dependent on circumferential asymmetry. Variation in O1 and O2 did however result in some of the markers falling outside of the predominant location in Brodmanns area 17, see table 3.1.

Electrode Position	Brodmann Location	Cortical Location
P3,4	7	Superior parietal lobule near intra-parietal sulcus, superior to posterior portion of supramarginal gyrus.
T5,6	T5-37	Left- middle temporal gyrus caudal to termination of sylvian fissure.
	T6-19,37,39	Right overlapping superior temporal sulcus, with rostro-caudal location even with termination of sylvian fissure.
O1,2	17	Occipital lobe, lateral and superior to occipital pole, overlapping calcarine fissure.

Table 3.1. Primary cortical location of scalp electrodes. Table adapted from Homan, Herman and Purdy.1987.)

Homans work was continued by Myslobodsky and Bar-Ziv (1989) who aimed to investigate the accuracy of bilateral occipital electrode placement and examine the sources of errors experienced by Homan et al. They performed CT scans on subjects after locating the occipital electrodes of the 10-20 and Queen Square system. The electrodes points marked were Cbz, O1, O2, Pz, Fp1 and Fp2 (10-20 system) and LO, RO, MO and MF, mid frontal (Queen Square system). Two factors contributed to antero-posterior marker dispersion; (i) an imperfect alignment of the endion with the inion and (ii) a variance of the distance of the endion from the occipital pole. The occipital pole was located from 11 to 33mm over the endion. In one third of the sample the occipital falx deviated from the midline, mostly to the right, markers were therefore often seen as skewed to the left with respect to the longitudinal fissure. The more rostrally located elctrodes were placed somewhat more accurately with respect to the longitudinal fissure, this was observed in the reference electrode (12cm above the nasion) used for the Queen Square system which was seldom off the longitudinal fissure. In 11 of the 12 subjects the left intraparietal sulcus was located about 0.5cm more medially than the right one. In 37% of the subjects the inion could not be located with confidence.

The nasion to inion distance ranged from 31-38 cm with a mean of 34cm. The lateral markers were seldom over symmetrical hemisphere sites and O1 and O2 could not be safely assumed to lie over homotopic sites. They quoted, that it was possible that VEP variance along the sagittal line may be misinterpreted as a result of subtle physiological differences between the projection of the lower and upper visual fields on the visual cortex. The major origin of the horizontal and perhaps the sagittal marker dispersion is variance in the normal anatomy of the occipital bone. In conclusion they stated that none of the assumptions used by the 10-20 system should be taken for granted when bilateral measurements are planned.

The topography of the underlying cortex within the 10-20 system was further investigated by Steinmetz, Furst and Meyer (1989) using Magnetic Resonance Imaging (MRI). The absolute variation of the calcarine sulcus with respect to the inion was found to be 4cm. The level of the occipital electrodes corresponded approximately to the midline of this band. The lateral endpoints of the central sulci lay approximately 1cm superior to the cortical representation of C3/C4, this corresponded with the findings of Jasper that C3/C4 may overlay the precentral or postcentral cortex. The variation zone of the calcarine sulcus was surprisingly large this was attributed to the unreliability of the inion as an accurate cranial landmark for the visual cortex, see fig 3.7.

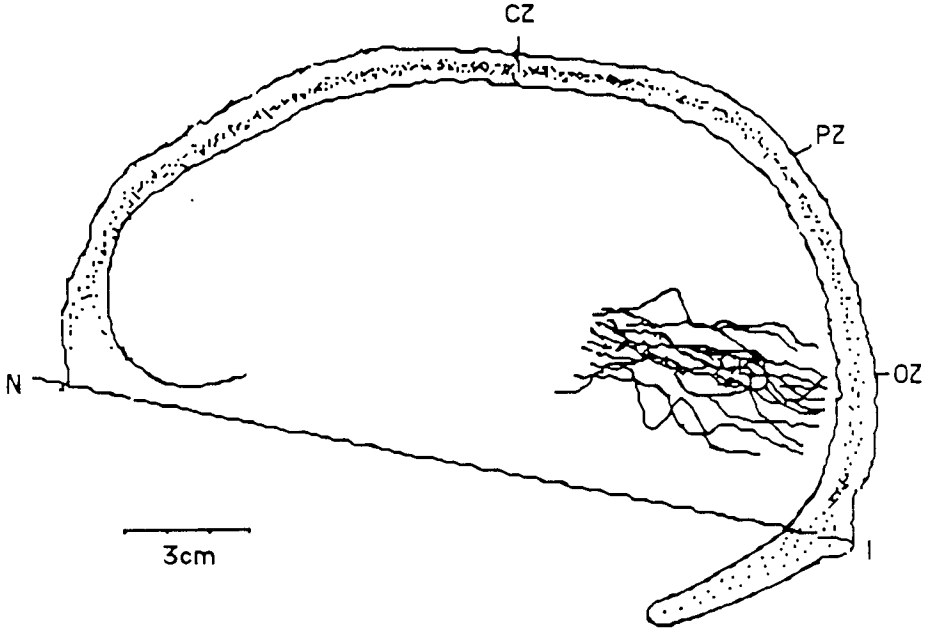

Fig 3.7. Variation zone for the calcarine fissure within the 10-20 system as derived from magnetic resonance imaging in 16 left and 16 right brain hemispheres . N = nasion; I = inion; N-I = nasion-inion line. The diagram was constructed by superimposition of 32 proportionally magnified overlays on a standard skull; all inion points coincided. The variation zone measures 4cm. (After Steinmetz, Furst and Meyer 1989.)

Occipital lobe morphology was further investigated with the use of MRI scans (Myslobodsky et al 1991). The right calcarine sulcus occupied a higher position above the inion and the left sulcus appeared to be steeper (left 67.8+/-8.69 vs right 73.1+/-4.29°, angle with a line perpendicular to the nasion to inion line) these were both however, insignificant observations. In addition the parieto-occipital sulcus was shown to be located slightly more rostrally on the right compared with the left side. Brain asymmetry was shown to be greatest at the occipital poles. Asymmetries in the occipital lobes were found to change within a space separated by several cuts and different asymmetry values for the ventral and dorsal aspects of the brain may be observed. The areas of the ventral and dorsal halves were therefore assessed separately on each of six consecutive cuts through the occipital lobe. There was a strong predominance of the left occiput in the most caudal ventral and to a lesser extent dorsal aspect of the lobe. In the transaxial plane, a consistent left predominance was seen only in the ventricular and subventricular series of cuts. More rostrally there was a gradual reduction in the asymmetry indices with reversal toward positive values dorsally. The calcarine variation zone was calculated to be between 2-4cm from the inion, similar to that found by Steinmetz et al (1989).

In addition wide variation in the projection of area 17 on the cortex has been demonstrated (Brindley 1972). Plaster casts were made of the posterior poles of normal human brains. The brains were sliced coronally and the striate cortex was identified and marked with black ink. Large inter and intra-individual variation was observed, see fig 3.8 and 3.9.

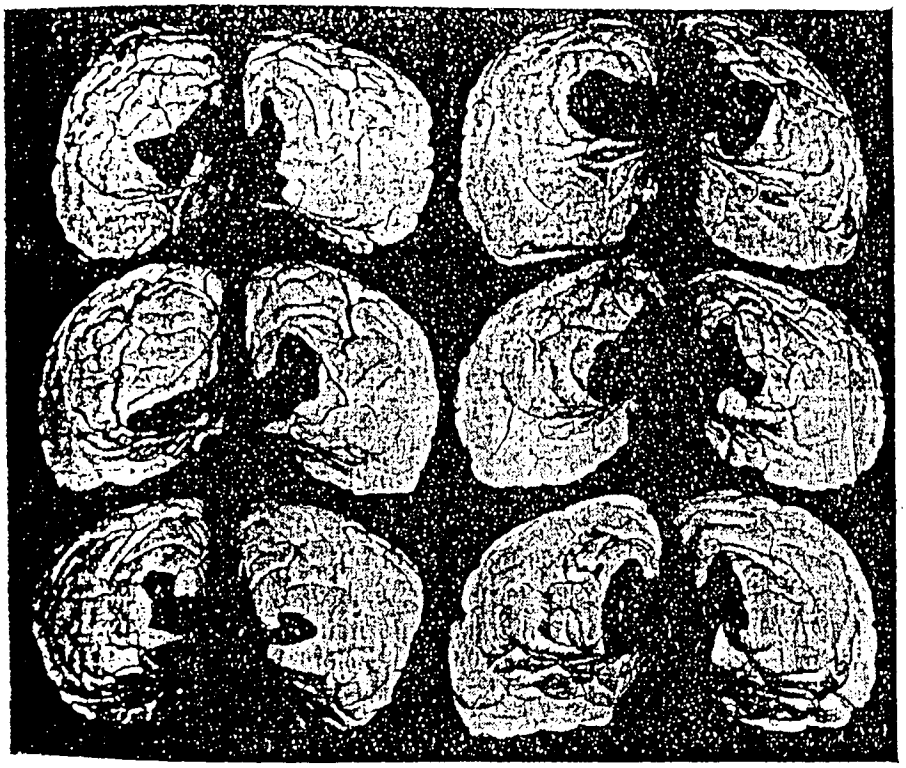

Fig 3.8. Posterior aspects of six pairs of marked plaster casts illustrating the variation of the representation of the striate cortex on the occipital lobe. (After Brindley 1972)

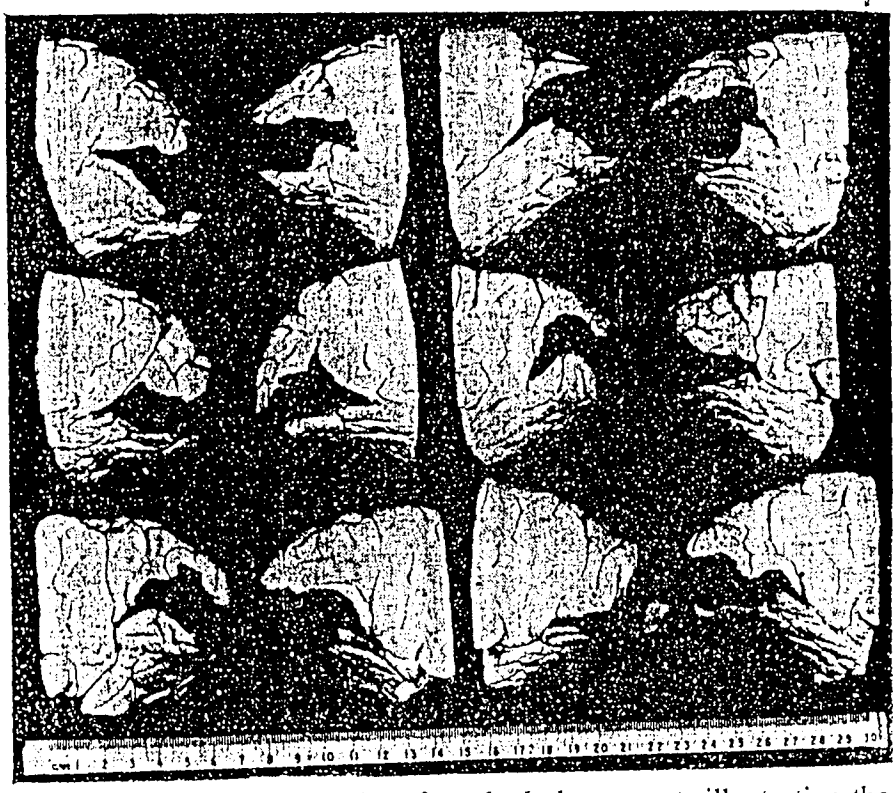

Fig 3.9. Medial aspects of six pairs of marked plaster casts illustrating the variation of the representation of the striate cortex on the occipital lobe. (After Brindley 1972.)

3.5.3 Referential Recordings

Differential amplification is used in evoked potential (EP) work, this rejects common mode interference. Differential amplification is installed between two inputs, if these inputs change by the same voltage with respect to the ground the change will not appear at the amplifier output. For evoked potential recording one electrode is connected to input one and a second electrode is connected to input two.

In referential recordings one site may be chosen as lead 2 for the amplifier, this is constant for all the electrodes recorded. The site chosen is presumed to be inactive and is usually located at some distance from the areas generating the evoked potential. Various cephalic sites have been chosen by different investigators including a mid frontal reference, the nose, the chin and linked ears. Whichever site is chosen none can be presumed to be inactive for all source configurations.

The amplifiers ability to discriminate signals is governed by the common mode rejection ratio. The signals are either a) in phase at the two inputs i.e. artefacts that affect both electrodes or b) out of phase at the two inputs. High common mode rejection is essential in most EP recording e.g. to remove mains interference. The amplifiers also increase the amplitude of the discriminated potentials and if artefacts do not appear with equal amplitude on the electrodes these will also be amplified.

3.5.4 Choice of Reference

3.5.4.i Average Reference (AR)

Offner (1950) proposed the use of the AR based on the assumption that the EEG is generated by a large number of randomly orientated current dipoles, the average value of the potentials recorded should be near zero. This assumption does not hold so well for evoked potentials as they are not random signals. If a large potential is recorded on one channel it will appear on all the remaining channels with reversed polarity and with an amplitude a fraction of the potential dependent on the number of recording channels. Bertrand (1985) showed that for the average value to approach zero the electrodes must be distributed over both hemispheres, at least.

When recording from restricted areas of the scalp the AR is not the most ideal reference to use. In the case of tangential sources channels distributed over the

scalp will pick up both positive and negative potentials which average to zero, whereas with radial sources the channels distributed over the area will either record positive or negative potentials and will not average to zero. Thickbroom et al (1984) have reported that AR slightly accentuates the pattern reversal VEP response.

3.5.4.ii Balanced Non-Cephalic Reference (BNCR)

This reference was designed by Stephenson and Gibbs (1951) to overcome the problems of active cephalic references. Two electrodes are used, one is placed on the sterno-clavicular junction and the other on the tip of the seventh cervical vertebra. A variable resistor in each lead is adjusted until the Electrocardiogram (ECG) is eliminated. For the reference to be totally inactive the patient must be very relaxed and preferably in a supine position, this makes the recording of pattern VEPs difficult.

The BNCR can introduce some low frequency artefacts into the recording and also more technical difficulties are experienced resulting in longer recording sessions (Lehtonnen and Koivikko 1971).

3.5.4.iii Bipolar Reference

This is most commonly used in EEG recordings. The technique uses a chain of electrodes, all electrodes are considered active and each electrode is referred to its neighbour i.e. first is referred to the second, second is referred to the third etc. A focus of activity will be recorded on two channels as a phase reversal. Bipolar recordings were used by Harding et al (1969) as an aid to determining the origin of visual field defects. A phase reversal indicated which hemisphere the signal was originating from.

3.5.4.iv Common Reference

In this form of reference all active electrodes are placed over the area of interest e.g. the occiput and these are referred to the same cephalic electrode placed on an 'inactive' area. The common references used are:

3.5.4.v Fz

One of the most frequently used 'common' reference is Fz, this has been used by many groups (Barrett et al (1976), Blumhardt et al(1977), Michaels et al (1971), Flanagan and Harding (1985) and Edwards and Drasdo (1987)). The problem

with this reference is that a frontal negative occurs in this region at approximately the same latency as the P100 and if the two coincide an exaggeration of the P100 results or a P100 may be recorded that is not actually present (Hobley 1989).

3.5.4.vi Linked Ears

With monocular full field stimulation a low amplitude positive peak can sometimes be recorded occuring at around 100ms and can lead to attenuation of the P100 (Shih 1988), this is therefore not a satisfactory inactive reference for use in VEP studies.

3.5.4.vii Chin and Mastoid

The use of this reference can induce muscle artefact into the recordings and so making it unsatisfactory as regards inactivity. Differences in early activity were observed when chin and BNCR were compared to flash stimulation (Lehtonnen and Koivikko 1971)

3.5.5 Topographic Mapping Displays

This method of presentation displays the amplitudes of the evoked response at a certain latency recorded from a number of electrodes sites over the scalp. The major drawback of this is that the recording is multidimensional and is being transferred onto two dimensional paper. As the recording points do not cover all the scalp area the amplitudes between these recording sites must be interpolated and may not actually be present. The sampling of the recording sites must therefore be such as not to produce aliasing of the response.

The technique gives a clear presentation of the surface distribution of potentials recorded from the scalp. The potentials recorded from a certain number of electrodes are used to compute isopotential gradient maps over the scalp surface. In 1951 Walter et al developed a 'new toposcopic display system' in which twelve individual cathode ray tubes were used to display the information initially by radial but later by helicon scan. The display was not however, related to the amplitude of the response but the frequency. This relation leads to difficulties in interpretation and as a consequence this technique has not gained much recognition in VEP studies.

Remond (1964) first produced a method to display potentials which were presented as contour maps of potential versus time. This technique however produced maps

that were quite complex and only represented the responses in a single direction, a complete topographical picture was therefore not obtained. They did however have the advantage that the map contained a temporal sequence.

Early maps were plots of isopotential lines joining the electrode recording points on the scalp (Lehmann 1969). Methods had to be developed to calculate the potential at each point on the scalp surface that was not directly recorded from. Ragot and Remond (1978) using a second order interpolation method involving both space and time displayed maps with isopotential lines plotted at 2μV intervals. Forty eight electrodes were recorded from and were attached to a plastic shell shaped from a plaster mould of the subject's shaven head. An interelectrode spacing of 4cm was used. Maps were produced to pattern onset stimulation, from the distribution each component appeared to be of a saltatory nature each one rising, culminating and declining on the same spot.

Duffy (1979) developed a system for the topographic mapping and computerised display of scalp recorded signals, this was referred to as brain electrical activity mapping (BEAM). The maps were computed using 3D interpolation with a 3 nearest neighbours technique, from these maps data analysis could be performed, in addition other features such as cartooning through data could be incorporated. Significance probability mapping (SPM) could also be performed on the data and two types are available.

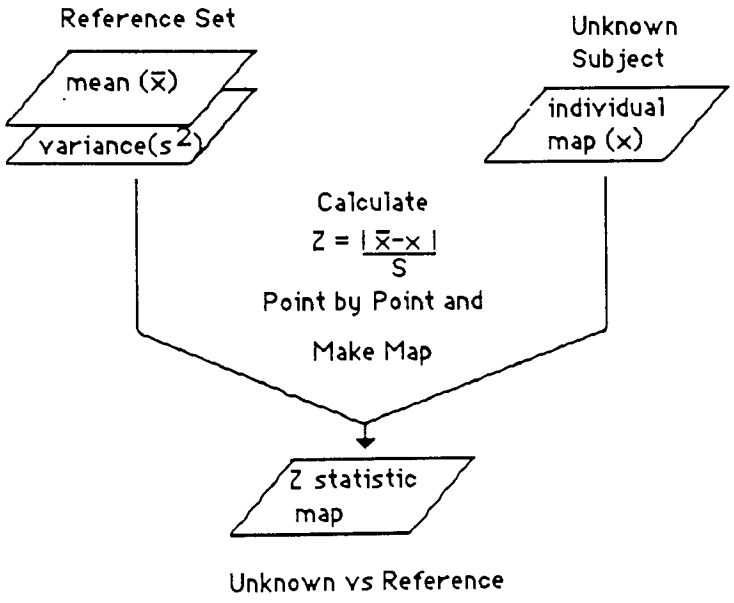

Fig 3.10. Formation of significance probability map by Z transform. (After F.H.Duffy, P.H.Bartels and J.L.Burchfield 1981.)

One process is based on the Students t test statistic, this is used to highlight areas of difference between two groups of subjects. The other is based on the Z transform statistic is used to highlight areas in which the brain's electrical activity differs statistically from that of a reference population. Grid sector analysis (GSA) can then be implemented to discriminate between a SPM showing a large focal abnormality and an SPM showing a diffuse abnormality. The procedure for the significance mapping is illustrated in fig. 3.10 and 3.11.

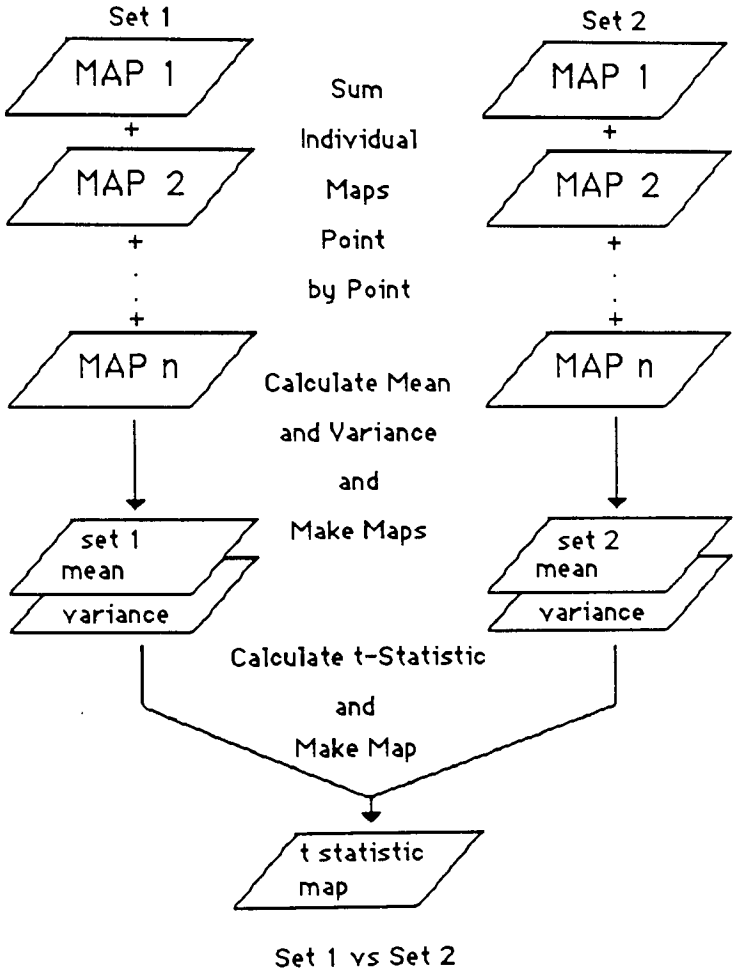

Fig 3.11. Formation of significance probability map by Student's t test. (After F.H.Duffy, P.H.Bartels and J.L.Burchfield 1981.)

Thickbroom et al (1984) and Buchsbaum et al (1982) have used a four nearest neighbours method of interpolation to produce topographic distributions of the evoked potential. The Biologic Brain Atlas and the Nicolet Pathfinder II mapping systems used in this thesis both compute their maps by four electrode linear interpolation.

The linear four nearest neighbours interpolation is calculated by first identifying the four neighbours by standard analytical geometry. Weights are then calculated where each weight is in inverse linear proportion to the distance of the particular picture element from each of the four electrodes. The weights are scaled to be four decimal fractions totalling 1.00. The computation is described by Buchsbaum et al (1982) and is shown as follows;

$$T=\sum_{i=1}^{i=4} D_i$$

$$S=\sum_{i=1}^{i=4} T/D_i$$

$$W_i=T/D_i \times 1/S$$

Where i=1....4, are the four nearest neighbours, d= the distance from the point to be interpolated to the ith electrode; then W_i= the weight assigned to the ith electrode. The value for each picture element is then computed as the sum of the weighted contributions from the four nearest neighbours.

A method has also been described by Perrin et al (1987) using surface spline interpolation. This method gave a better estimate of locations of electrical extrema, which were not always located at an electrode site as they are with the four nearest neighbours linear interpolation. The disadvantage of this system however, was the longer computational time required.

Duffy (1981) has recommended the placing of at least four artifact electrodes to aid in the detection and elmination, or reduction, of eye blink, eye movement and muscle activity in the temporal and occipital regions. Topographic maps highlight the spatial structure of underlying data, which can make both real and artifactual deviations from normal more visible. The reduction of artifact is therefore very important in brain mapping and more stringent procedures to recognise and reduce artifact are required than may be used for normal EEG and EP recordings. Colour scales should be bidirectional i.e zero to plus maximum and zero to negative maximum and the colour sequence should be chosen so that sequential contour line crossings are associated with the appearance of equally distinct colour steps. It is the opinion that colour adds a great deal to the topographic image. In mapping it is important that each electrode is properly positioned by measurement spot placement and all electrodes must have comparable low electrode impedence. They should also remain securely attached and be free from motion effects. Reference is a

problem in the EP, the use of Laplacian can increase the signal but may also increase the amplitude of the noise. Duffy has found that it produces more complex, more confusing and less intuitive maps than those of the raw data.

Coburn and Moreno (1988) however disputed this statement, proposing that the use of the Hjorth-Laplacian reference for source localisation suppresses much of the volume conducted activity and results in a clearer picture of the underlying electrocortical events. The distribution of the recorded data does not accurately reflect the cortical distribution of neuronal activity subadjacent to the recording electrode and due to the dipolar nature of the sources the potentials can project via volume conduction to distant recording sites. Thus the positive or negative recorded at a specific electrode (ignoring the issues of a truly inactive reference) does not necessarily reflect the electrical state of the immediate subadjacent cortical tissue. It is also important that the map should be placed in context, this can be achieved by either presenting serial maps of the data or presenting the time series waveform. At present time there seems to be no substitute for the raw waveforms in the accurate interpretation of the mapped data.

It has been proposed that optimised EP mapping should negotiate pratical solutions on the basis of several requirements (Desmedt et al 1987). First, the number of channels should not exceed a manageable set (e.g.21), otherwise the time taken to set up and maintain adequate recording conditions becomes excessive. Second both hemispheres should be recorded concomitantly to image EP fields that extend across the midline (Desmedt and Bourguet 1985) and recording only one hemisphere at a time is not sufficient (Coppola et al 1982; Giard et al 1985). For imaging the peak values of any potential field, an electrode must be near the field culmination, electrodes around that focal site only record potentials of lower amplitudes. This requires either using many electrodes or optimising the recording position. Finally the mapping algorithm should not impose restrictions. Colour of the scale is rather arbitary but there are arguments to suggest the use of red as negative and blue as positive. This is due to the fact that neuronal excitation involves a negative shift in the extracellular space and since all EPs are extracellular potentials it would therefore seem justified to depict the activaton with a red colour. It can not be said however that scalp positivities reflect reduced excitation as the geometry of the dipoar source has to be taken into consideration. Mapping displays the rapidly evolving brain potential fields over distinct scalp locations with adequate time resolution. This is invaluable for analysing the sequential actunation of the distinct neural generators that involve different cortical areas over time and

would be impossible to achieve by mere inspection of the raw data. This was stated as maybe being more pertinent to the mapping of somatosensory EPs. Each map should include 4000 pixels and the value of the pixels should be determined by interpolation between the four nearest neighbours with third power exponent of the distance. Linear interpolation is less satisfactory and is not in line with the volume conductor model.

3.5.6 Averaging

This process is used to enhance evoked potentials that are produced by a stimulus and are recorded within the background EEG. The background EEG has a greater amplitude when compared with evoked potentials and therefore if only one sweep is recorded the signal would be lost. Averaging increases the signal to noise (S/N) ratio, and improves with the value of $\sqrt{N}$. All methods based on averaging presume that the sources are stationary, i.e. that after each stimulus presentation the activity is in the same position and occurs at the same latency. However, if the stimulus also evokes non stationary activity, not just EEG, this may be averaged out and the resulting distribution will be much simpler than the true response (Nunez 1988). In addition to this there may be differences in the attention and fatigue level of the patient during averaging and sensory adaptation may occur. The averaged evoked potential may not therefore give an accurate representation of any single trial response.

3.5.7 Time Domain Averaging

This type of averaging acts as a comb filter and emphasizes the components of the potentials that occur at a frequency of F, 2F, 3FHz etc where F is the frequency of the trigger. The frequencies of the subharmonics i.e. F/2 and any frequency not related to the trigger frequency do not appear in the average (Regan 1989).

3.5.8 Filtering

Filters are used in all evoked potential work to reduce the noise in the recordings and also reduce the number of averages that are required to give a clean signal. Most filters are used before the recording is digitised and are therefore said to be analog. Although the action of filtering does in some way resemble the effect of averaging it does have serious effects on both the amplitude and morphology of the response, these are not seen with averaging alone. Filtering of the high frequency components is required to remove components that are above the limit set by the sampling rate. If the sampling rate is too low aliasing will occur and the resultant

wave will not resemble the wave that was initially collected. The minimum sampling rate is set by the Nyquist criterion and must be at least twice the highest frequency present in the evoked potential. A notch filter can be used in most evoked potential recording but should not be used routinely as it can lead to severe distortion of the potential. The notch filter removes just one frequency from the recording e.g. 50Hz, mains. The rate at which the filter acts can vary, e.g. in a high frequency filter a roll off of 6dB per octave indicates that the signal amplitude will reduce by 50% with every doubling of the signal frequency. The term 3dB down point is often used, this is the frequency at which the amplitude has been reduced by 30%. The low frequency filter may be expressed as a time constant. In this respect it is defined as the time taken for the callibration signal to fall to 37% of its initial value.

3.5.8.i Effects of filtering on the waveform;

High filter attenuation; when a square wave is passed through a high frequency filter (a low pass filter) and the filter level is reduced the corners of the wave become increasingly smoothed. The effect on the evoked potential is to increase the latency of the signal e.g. when the filters are changed from 0.6-100Hz to 0.6-15Hz a positive component that occurs at 107ms with the former filter will occur at 117ms with the latter (Regan 1989).

Low filter attenuation; if a square wave is passed through a low frequency filter (a high pass filter) distortion of the wave occurs as the DC levels can not be indefinitely maintained. The effect on the evoked potential is to enhance the negative deflections and reduce the positive deflections, there is also an effect on the latency such that the positive peaks occur earlier and the negative peaks occur later (Regan 1989). It is therefore possible to obtain spurious peaks if the low frequency filtering is too extreme.

3.5.9 Baseline of the Recording

When an amplitude of a component is quoted it has to be from the peak of that component to a known point, this is usually the baseline of the response. The baseline can be adjusted and can be placed anywhere in the record, this will not affect the morphology but it will affect the amplitude of the waveform, if the topography of the response is of interest this will also be affected. It is popular to place the baseline along the average of the first portion of the trace before the stimulus was activated however, the prestimulus may be too variable and may

show activity left over from the preceding stimulus. This is also not possible if the evoked potential is only recorded when the system is triggered.

3.5.10 Analysis of the Wave

3.5.10.i Peak Analysis

The peak is defined as the most positive or negative voltage recorded at a specified latency. This analysis is unsatisfactory where activity from different generators may overlap leading to a complex waveform. A single peak may not only be due to the activation of one source and one source may contribute to more than one peak. In this instance principal component analysis may serve to highlight the number of components responsible for the peak.

3.5.10.ii Area Analysis

Using this procedure the area underneath the waveform is measured, to perform this the baseline of the waveform must be defined.

3.5.10.iii Power Analysis

The component is defined as the occurence of the maximal power in the recording, thus giving a totally objective approach to identifying the components of the waveform. This method was used by Lehmann to give the hilliness of the waveform and calculates the mean of the absolute voltage deviation from the average reference. The r.m.s field power is then calculated between all the electrode pairs possible (Lehmann 1985).

3.5.11 Principle Component Analysis

The total variance of the evoked potential is calculated using a statistical procedure. The basic assumption of this technique is that the evoked potential is the linear sum of the activities of a number of neural generators whose currents are conducted to the recording electrode by volume conduction (Regan 1989). Several workers have implemented this technique to investigate the generators of the VEP (Shibasaki, Nakamura and Nishida 1987, Maier et al 1987, Van Dijk and Spekreijse 1990, Ossenblok and Spekreijse 1991).

3.5.12 Pattern Stimulators

The pattern can be generated by various methods including television screens and projector systems. The problem encountered with TV stimulators are that each frame of the picture is produced by a raster which starts at the top left hand corner. Each frame is repeated at 20ms intervals, to give a clean pattern reversal response the reversal should be locked to the frame rate, if not, reversal will take place at a variable point in the frame and a transient horizontal line will be seen at the instant of reversal. This will affect the latencies and amplitudes of the principle peaks. The latency and amplitude of the evoked potential are increased by locking the reversal rate to the frame rate, due to the fact that the centre of the visual field is not reversing until 10ms after the top left hand corner. Unfortunately this has been reported to increase the noise recorded in the responses (Van Lith, Marle and Van Dok-Mak 1978). When the pattern reversal is independent of the frame rate the centre of the field will reverse early in a proportion of the presentations and hence result in earlier latencies. Van Lith, Marle and Vijfvinkel-Bruinenga (1979) also recorded what they termed 'visual hum' from the use of TV stimulators, a recording of 50Hz interference was made only when the subject could see the stimulator, if the stimulator although still on was occluded the interference was extinguished. The visual hum increased in amplitude with an increase in the luminance of the stimulator. The response was a result of the frame rate of 50Hz. Visual hum can be reduced by lowering the stimulus luminance and increasing the frame frequency of the stimulator.

3.6 Recording The Magnetic Field

The first measurements of a magnetic field was recorded from that associated with an electrical potential in the human heart (Baule and McFee 1963). In 1968 Cohen demonstrated the magnetic field produced by brain activity and in 1972 Cohen went onto record the first magnetoencephalogram (MEG). The magnetic field evoked from brain activity is very small compared with that of the Earth's magnetic field and urban noise, see table 3.2.

Biomagnetic Activity	Amplitude (pT)	Bandwidth (Hz)
Magnetocardiogram	50	0.05 ÷ 1000
High resolution magnetocardiogram	0.2	0.05 ÷ 300
Fetal magnetocardiogram	1	0.05 ÷ 100
Magnetoencephalogram(MEG)	1	0.5 ÷ 30
Evoked fields (VEF, SEF, AEF)	0.1	d.c. ÷ 60
Magnetomyogram (MMG)	10	d.c. ÷ 2000
Magneto-oculgram (MOG)	10	d.c.
Magnetoretinogram (MRG)	0.1	0.1 ÷ 30

Table 3.2. Amplitudes and spectra of some biomagnetic signals. Some of the strongest biomagnetic fields can disturb the aquisition of the weakest. This is one of the sources of noise. (After Duret and Karp 1983.)

A specialised piece of equipment is therefore required to isolate the field due to brain activity. The instrument used is called a Magnetometer (fig 3.12), this consists of three components;

1.Flux transformer.

2.SQUID (Superconducting QUantum Interference Device) and electronics

3.Cryogenic vessel (Dewar).

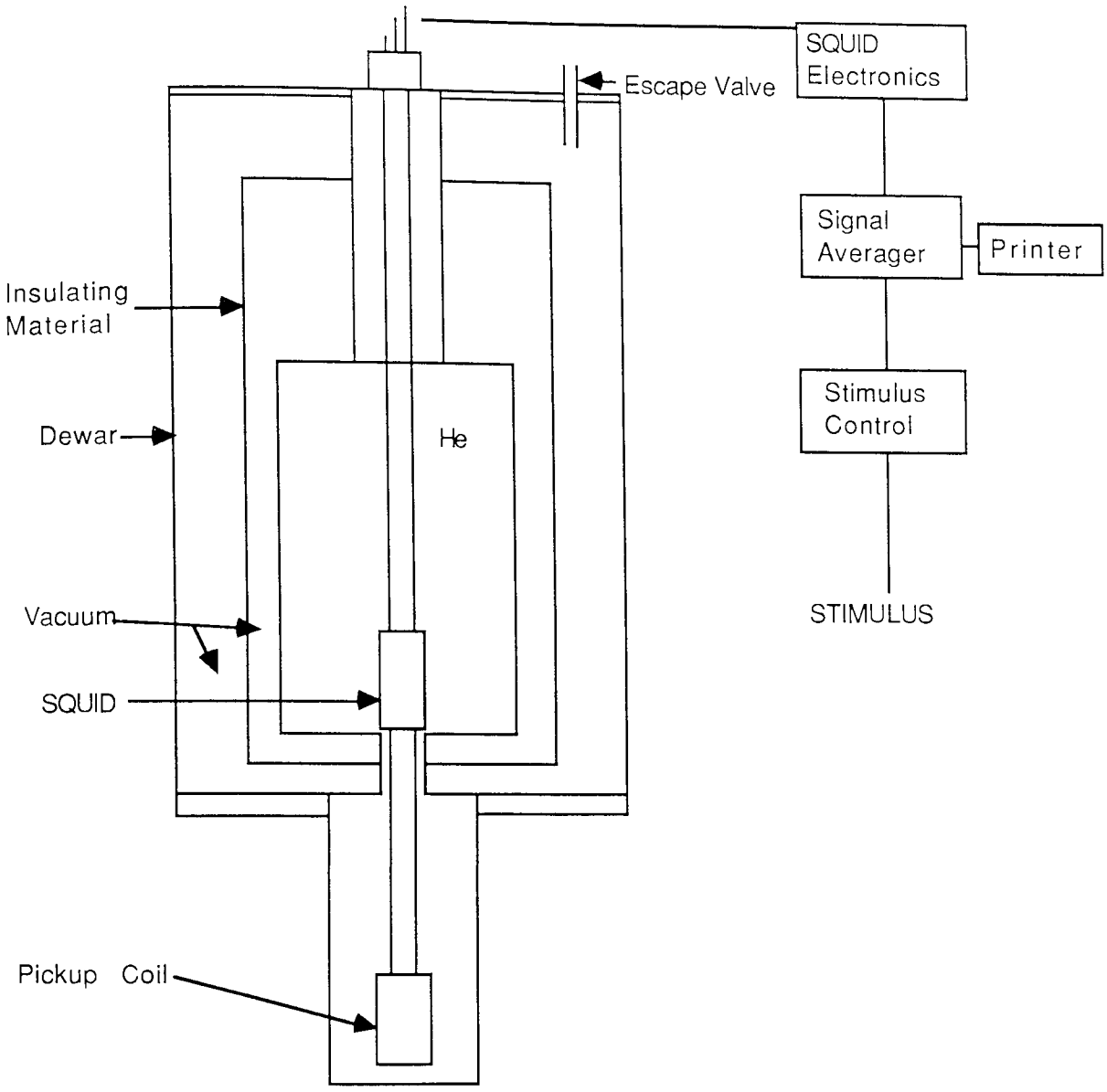

Fig 3.11. Schematic Diagram of the Magnetometer.

The SQUID is immersed in liquid Helium (temperature of 4.2°K) and housed in a Dewar. The SQUID does not sense the magnetic field directly but is connected to the outside world via the detection and input coils, these make up the flux transformer. The coils are made up of superconducting material and a magnetic field placed in close proximity to the pickup coils sets up a current which flows to the input coil. The current flowing in the input coil has a magnetic field associated with it and this is impressed onto the SQUID. The SQUID used for all the experimental work in this thesis was a DC SQUID. When a current is set up in a superconducting material it will circulate indefinitely. When a magnetic flux is applied to the detection coils a current Ii circulates around the transformer to maintain the total flux in the circuit constant. The current is given by

$$Ii = \frac{\text{field applied}}{Ld+Li+Le}$$

Ld= inductance in the detection coil
Li= inductance in the input coil
Le= inductance in the lead coil

The current flowing in the flux transformer is proportional to the magnetic field sensed by the detection/pickup coil. A SQUID is used as a method to accurately measure the current flowing in the flux transformer. To measure the value of current there must be a resistor and a potential, if however a resistor was placed into a superconducting loop it would no longer be superconducting. A resistor is therefore not installed in the flux transformer as this would reduce the value of the current we are trying to measure. The SQUID consists of 'loop' of superconducting material with two breaks called Josephson junctions. The junctions are produced by the imposition of a narrow insulating barrier and are characterised by a critical current, Ic and a capacitance Cj. A DC current flows around the SQUID (therefore called a DC SQUID), whose maximum value Imax is equal to the value of 2Ic. Another type of SQUID system is manufactured called rf SQUID this does not have a circulating DC current. The Josephson junctions utilise the ac Josephson effect whereby if a small voltage is applied to the junction an ac current is produced across the junction given by the equation;

$$Ic=Is.\sin wt$$

This Josephson current is modulated by the applied flux which varies at the signal frequency fs and this in turn modulates the junction voltage Vj

$$fj=\frac{2eVj}{h}$$

The junction acts as a parametric amplifier (energy is transferred from the junction and amplification of the signal is achieved) ideal amplification is predicted by the ratio fj/fs. When a flux is applied to the ring Imax initially decreases due to interference between the wave functions in the two arms of the SQUID. The voltage difference across the two junctions is recorded as the output of the SQUID.

The SQUID provides a voltage output proportional to the magnetic field variation inductively sensed by the detection coils (Romani and Rossini 1988). A negative feedback arrangement is used to establish a flux locked loop and provide a linearised voltage output which is proportional to the flux applied to the SQUID.

3.6.1 Flux Transformer

A flux transformer is used to couple the flux source and the SQUID ring. The flux transformer is made up of superconducting material and consists of the pickup/detection coil and the input coil. The external magnetic field induces a current in the circuit which flows from the detection to the input coil and this shielding current thus set up becomes the input to the SQUID. The SQUID does not sense the field directly.

Advantages of using a flux transformer (Tinkham 1975):

1. The SQUID is not affected by the external temperature and magnetic field in the recording lab.

2. The sensitivity of the SQUID can be adjusted by introducing a dropping inductor into the flux transformer.

3. A negative feedback can be introduced to convert the magnetometer to a null balancing device.

4. The area of the pickup coil and the number of turns in the flux transformer can be changed to increase the performance of the SQUID.

3.6.2 Gradiometer

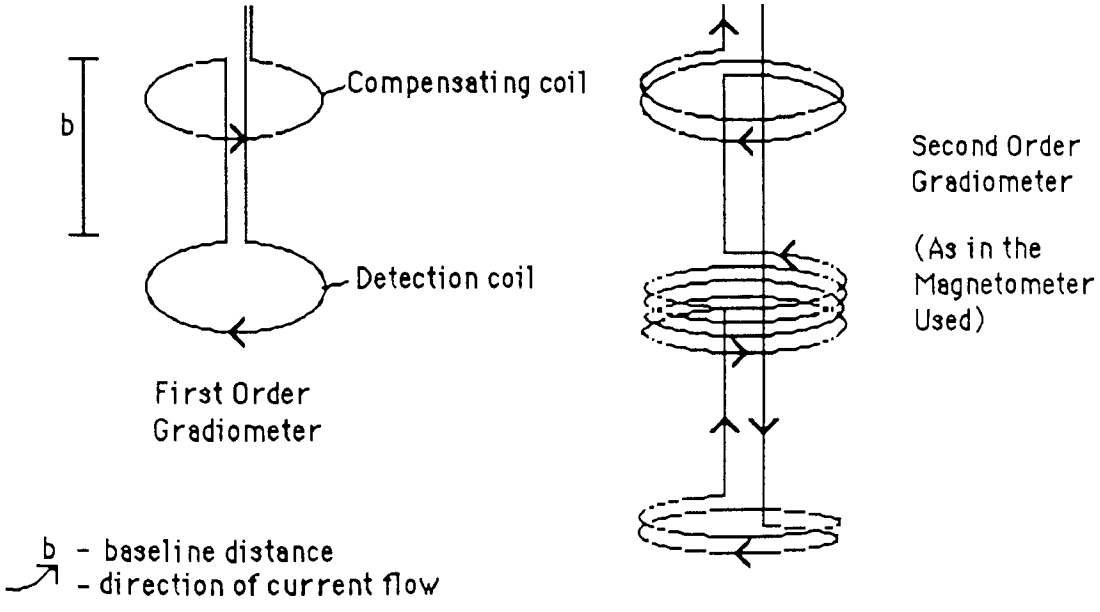

Fig 3.13. Diagram to illustrate a first and second order gradiometer.

In a magnetically unshielded environment the flux transformer can be wound to produce a gradiometer, fig.3.13. If the coil is not wound to produce this effect any magnetic field will be sensed and as the Earth's magnetic field and urban noise are much greater than the evoked brain activity only the magnetic field due to unwanted distant sources would be recorded. To eliminate distant sources the detection and the input coil are wound in opposing directions. In theory a distant source will affect both coils equally, because the current circulating is going in opposite directions the magnetic fields evoked will cancel. In contrast for near sources unequal currents will be induced in both sets of coils and the fields will not cancel. A first order gradiometer consists of a detection and one other coil. A second order gradiometer (as used in the studies in this thesis) possesses another set of coils as shown in fig 3.13. A second order gradiometer should increase cancellation of the distant sources and can therefore be operated successfully in an unshielded environment. The first test of a second order gradiometer in an unscreened lab was performed in 1975 (Brenner et al).

Unfortunately increasing the number of coils reduces the sensitivity of the magnetometer (Hari et al 1988). The effect of increasing source depth on the evoked field amplituderecorded from a magnetometer with a detection coil was compared with a magnetometer with a first order gradiometer and a magnetometer with a second order gradiometer, fig 3.14. For a depth of 20mm the first order gradiometer gave 93% and the second order gradiometer gave 69% of the signal recorded by the detection coil, this effect was even greater with an increase in source depth. The resolution (i.e.resolvable separation between two dipoles) was also dependent on the type of gradiometer used and source depth, being worst for the second order gradiometer and deep sources. At a depth of 20mm the first order gradiometer gave 6% and the second order gradiometer 36% worse resolution than the detection coil and for a 40mm depth the resolution was 84% worse for the second order gradiometer.

It therefore follows that if deep sources are to be investigated there has to be some consideration in the choice of magnetometer. Under optimal conditions separations of just a few mm of superficial sources can be detected.

Third order gradiometers have been successfully used in evoked brain activity to a flash light stimulus (Weinberg et al 1984).

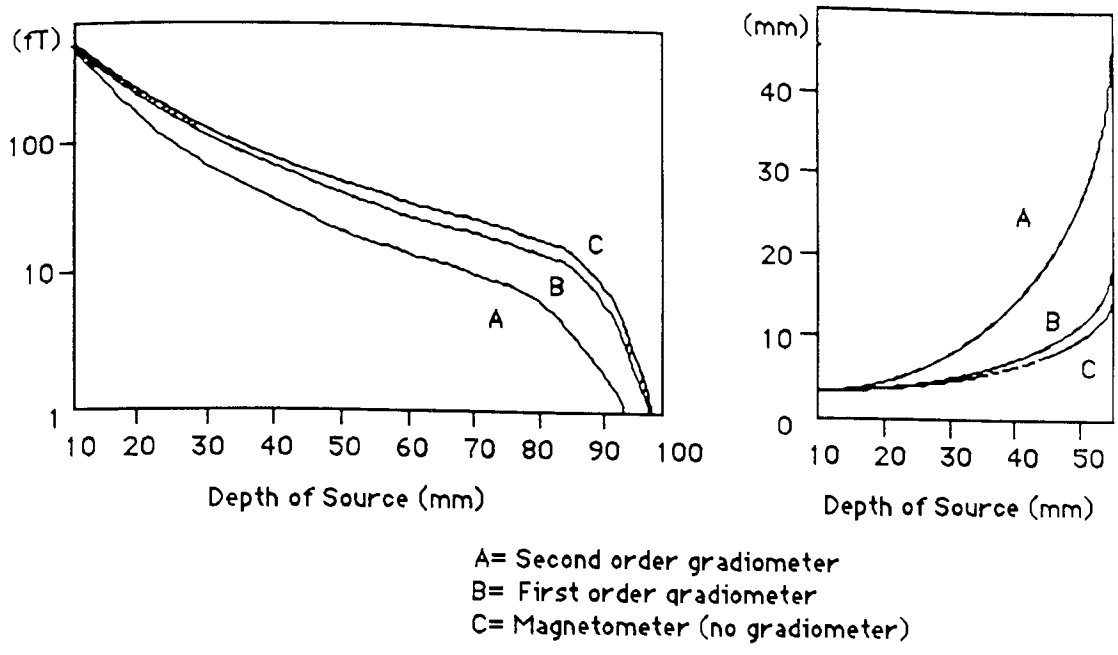

Fig 3.14. Graphs to compare the effect of the source depth on the strength of the signal and the resolution of two dipoles for a second order gradiometer (A), a first order gradiometer (B) and a magnetometer (C). (After Hari et al 1988.)

The pickup coil must be kept at a constant distance from the head when recording. If the distance is altered then the spatial distribution and relative amplitude of the response at the recording sites will be affected and the reliability in dipole estimation will reduce (Romani and Leoni 1984).

3.6.3 Baseline

The distance between the coils is the baseline distance. The distance between the source and the pickup coil should be less than the baseline distance. As the distance between the source and the pickup coil increases the source will begin to have a more equal effect on both the pickup coil and other detection coils, which leads to an attenuation of the input signal, the cortical source is now acting as a distant source (Kaufman et al 1981). The choice of the baseline is dictated by the nature of the source under investigation and also the conditions of the ambient noise levels, an improved rejection of distant sources is achieved with a shorter baseline (Romani et al 1982). The baseline distance also has an effect on the separation of the maxima thus affecting depth calculations, this affect is however quite small compared with the affect on the signal strength.

3.6.4 Pickup Coil Diameter

The optimal resolving power between the sources can be achieved by choosing a coil diameter of the order of the minimum distance between the proximal coil and the source (Duret and Karp 1984). A coil radius greater than or equal to the depth of the dipole displaces the maxima further, therefore increasing the observed span of the maxima. This results in the approximation of a deeper source. A finite coil size will reduce the maximum strength of the recorded magnetic field below the true value. A conversion curve for both dipole depth and strength must be used (Romani et al 1982). The corrections for finite radius and baseline are substantial and tend to cancel when calculating the true depth of the dipole but reinforce when calculating the source strength. The choice of radius size may be compromised by the desire to achieve the greatest field sensitivity, the larger the diameter the greater is the sensitivity to weaker fields (Kaufman et al 1981).

Wikswo and Roth (1988) compared the ability of two magnetometers in determining the spatial extent of a current source. The normal component of the magnetic field was measured and an homogeneous volume conductor model was used to model the electrical activity. Homogeneity was assumed as the depth of the source was small compared with the radius of curvature of the skull. The model was formulated in terms of spatial frequency and represented only the transmembrane potential. Two magnetometers were compared, one termed large had a flat noise spectrum of 20fT$\sqrt{Hz}$, a 30mm diameter coil and a 30mm spacing between the coil and the dendrite. The second had a flat noise spectrum of 50fT$\sqrt{Hz}$, a 3mm diameter coil and a 3mm spacing between the coil and the dendrite. They attempted to calculate the spatial distribution of the transmembrane potential from the magnetic field. It was impossible to calculate accurately the spatial extent from the large magnetometer whereas with the smaller magnetometer the spatial extent could be calculated to within approximately 1mm. It was concluded that "whenever the coil diameter and the coil to dendrite distance are much larger than the dimensions of the source the inverse calculation will be difficult if not impossible, and the achievable spatial resolution will be severely limited".

3.6.5 The Dewar

The SQUID is housed in a cryogenic vessel (Dewar). For the SQUID and the flux transformer to be superconducting they must be kept at a low temperature (9.2°K

for Niobium) (Romani et al 1982). The low temperature is achieved by immersing them in liquid Helium at 4.2°K. The dewar is normally made out of epoxy glass composites and plastics, which give it strength and are good insulators, they also have a low content of paramagnetic impurities. To reduce the heat transfer in the walls of the dewar there is a vacuum space containing multiple layers of material with high reflectivity e.g. aluminised Mylar. The dewar is vapour cooled by gaseous Helium which flows in the chamber surrounding the liquid Helium. This cools copper strips which run in this outer chamber and connect to the superinsulating material at various points. The superinsulating section is at a minimum around the probe. The outer chamber is a vacuum in which there are pellets of a molecular sieve to absorb any gaseous Helium that may escape. The Helium is only kept in the tail by gravity and so the dewar can not be tipped through an angle of greater than 45°. The most widely used Dewar holds five litres of liquid Helium (Duret and Karp 1983).

An advance over dewars, which have to be periodically filled with Helium (every three days) because of evaporation, is the use of refrigeration technology which is capable of keeping the instruments at liquid Helium temperatures while using gaseous Helium. The technology was developed by Little (1978) using the Joule-Thompson effect. The Helium is continually recycled. The probe may also be used in angles greater than 45°.

Zimmerman et al (1978) also developed multiple stage Stirling cycle using a piston and displacer mechanism where cooling is achieved by gaseous expansion. The weakness of this technique is temperature variation which can alter the performance of the SQUID. The technique must be used in a shielded room or where the dc field and gradients are reduced to low levels.

3.6.6 Balancing

The effective area of the coils are varied to make the coils as identical as possible, this is achieved by positioning small superconducting tabs near the coil. Second order gradiometers can also be balanced against field gradients, the baseline of the upper first order gradiometer is adjusted to match the lower one.

The ambient field varies in all directions and so the gradiometer must reduce the noise to a minimum in all directions, the axial direction and two orthogonal directions. To achieve the best rejection the product of the area and number of turns of individual coils must be balanced. This is achieved by placing small

for Niobium) (Romani et al 1982). The low temperature is achieved by immersing them in liquid Helium at 4.2°K. The dewar is normally made out of epoxy glass composites and plastics, which give it strength and are good insulators, they also have a low content of paramagnetic impurities. To reduce the heat transfer in the walls of the dewar there is a vacuum space containing multiple layers of material with high reflectivity e.g. aluminised Mylar. The dewar is vapour cooled by gaseous Helium which flows in the chamber surrounding the liquid Helium. This cools copper strips which run in this outer chamber and connect to the superinsulating material at various points. The superinsulating section is at a minimum around the probe. The outer chamber is a vacuum in which there are pellets of a molecular sieve to absorb any gaseous Helium that may escape. The Helium is only kept in the tail by gravity and so the dewar can not be tipped through an angle of greater than 45°. The most widely used Dewar holds five litres of liquid Helium (Duret and Karp 1983).

An advance over dewars, which have to be periodically filled with Helium (every three days) because of evaporation, is the use of refrigeration technology which is capable of keeping the instruments at liquid Helium temperatures while using gaseous Helium. The technology was developed by Little (1978) using the Joule-Thompson effect. The Helium is continually recycled. The probe may also be used in angles greater than 45°.

Zimmerman et al (1978) also developed multiple stage Stirling cycle using a piston and displacer mechanism where cooling is achieved by gaseous expansion. The weakness of this technique is temperature variation which can alter the performance of the SQUID. The technique must be used in a shielded room or where the dc field and gradients are reduced to low levels.

3.6.6 Balancing

The effective area of the coils are varied to make the coils as identical as possible, this is achieved by positioning small superconducting tabs near the coil. Second order gradiometers can also be balanced against field gradients, the baseline of the upper first order gradiometer is adjusted to match the lower one.

The ambient field varies in all directions and so the gradiometer must reduce the noise to a minimum in all directions, the axial direction and two orthogonal directions. To achieve the best rejection the product of the area and number of turns of individual coils must be balanced. This is achieved by placing small

amount of unwanted fields recorded. A shielded environment should reduce the presence of unwanted fields.

Various levels of shielding are available.

1) Light shielding reduces the eddy currents and so increases the amplitude and the reproducibility of the response (Romani and Narici 1986). Even when second order gradiometers are used the measurements are still limited by fluctuations in the level of the ambient field. The shielding is frequency dependent, above the cutoff frequency the shielding is proportional to the frequency. The cutoff frequency is inversely proportional to the thickness of the shield, its linear dimensions and its conductivity, as shown:

$$f_c = \frac{2}{\pi \mu a t Ó}$$

f_c=cutoff frequency
a=side length
μ=vacuum permittivity
Ó=metal conductivity
t=metal thickness

Zimmerman (1977) designed an eddy current shield using aluminium plates. This resulted in better shielding for the horizontal component of the ambient field. The noise at 10Hz was approximately 100fT/$\sqrt{}$Hz.

2) Ferromagnetic shielding: the most efficient construction for this is in the shape of a sphere but most are constructed in the form of a cube. Attenuation is not frequency dependent, at low frequencies it is proportional to the metal permittivity and thickness and inversely proportional to the diameter of the room. Most of the rooms are constructed from 2, 3 or 6 layers of mu metal. Noise level in the best is less than 10fT/$\sqrt{}$Hz at 10 Hz.

3) Active shielding: mostly used with ferromagnetic (if at all), this can provide some improvement at low frequencies.

The first room successfully used was constructed in 1971 by Cohen. It consisted of three layers of high permeability material with the inner two layers being attached to aluminium plates. This gave both magnetic and eddy current shielding. The shape approximated a sphere, it had 26 sides. The room was mounted on pneumatic suspension to reduce vibrations. Copper coils were attached to the walls

to give an ac field, these could be 'shaken' to reduce any trapped fields and increase the permeability.

Shielding efficiency depends on the permeability of the material, the shape, the size of the housing and the thickness of the wall. The shielding effect is not constant inside a cube, the shielding factor is lower in the centre than near the walls (the shielding factor is given by the ratio between external interference field strength and residual field strength in the interior). AC fields generally result in an increase in the shielding factor in metallic materials due to the inducement of eddy currents in the material. Los Alamos tested their shielded room made out of Aluminium shielding and an inner high permeable metal. The noise spectra had an increasing slope between 10 and 100 $fT/\sqrt{Hz}$ for the frequency range of 100-0.5 Hz. The shielding factor peaked at 1500 for a frequency of 10Hz.

Openings in the shielding are inevitable e.g. doors. The external field can therefore enter the room in two ways; a) through the wall or b) through the opening. The field through the opening drops exponentially with the distance from the surface of the opening. The magnetometer should therefore be positioned away from these openings. Openings for ventilation can be shielded by mounting chimneys or lattices around the aperture.

3.7 The Effect of Stimulus Parameters on the Evoked Field and Evoked Potential

3.7.1 Evoked Potential Studies

3.7.1.i Choice of Stimulus: Gratings Compared with Checks

In a sine wave grating stimulus all the power of the stimulus is in one spatial frequency and in one orientation see fig 3.15. The amplitude spectrum of the checkerboard is however orientated with the fundamental along the 45° diagonals. A checkerboard pattern can be made up from a vertical and horizontal square wave grating but it is the mathematical product of the two and not the sum (DeValois 1988) in addition a checkerboard cannot be synthesized by the superimposition of many sine wave gratings (Regan 1989). Although the stimulus is complex it is not complex enough to be broadband i.e. it does not have equal power at all

frequencies.

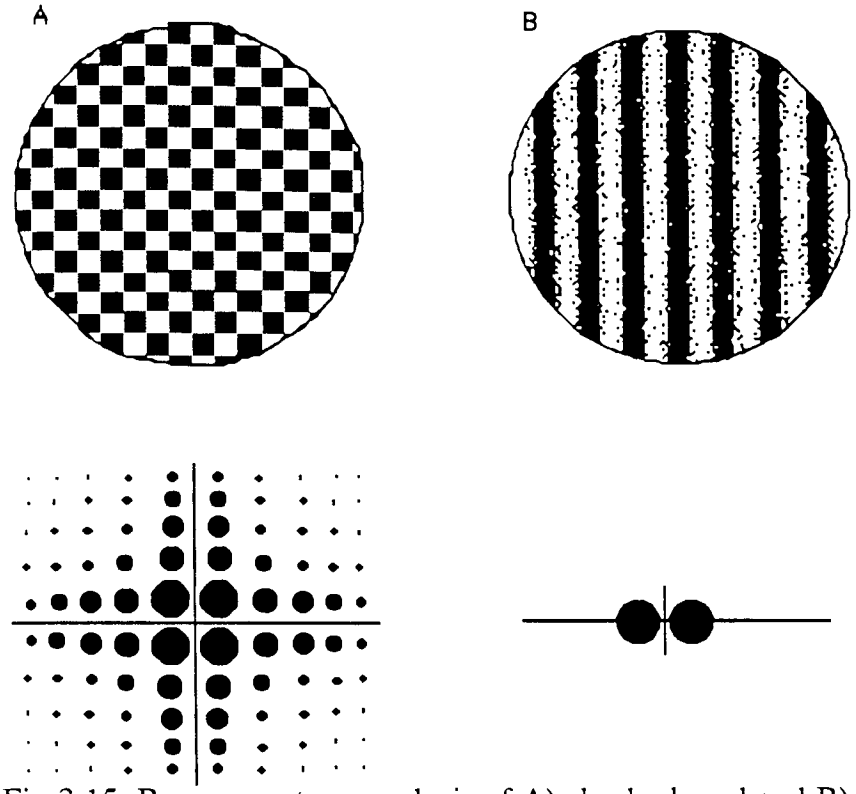

Fig 3.15. Power spectrum analysis of A) checkerboard and B) sinusoidal gratings. All the power of the sinusoidal grating is in one spatial frequency and one direction. The checkerboard stimulus contains power in higher spatial frequencies as well as the peak spatial frequency. When the checkerboard is aligned vertically and horizontally all the power is concentrated in the oblique directions. After Bodis-Wollner, Brannan, Ghilardi and Mylin. (1990).

When a check is modulated by a sine or square wave whose frequency is FHz, the pattern reversal VEP is found to have a fundamental frequency of 2FHz, the averaged waveform is made up of even harmonics of frequencies 2F, 4F, 6F, 8F and so on with zero power at the local flicker frequency of FHz (Regan 1989). The fundamental of a check pattern can be expressed as (Bodis-Wollner, Brannan, Ghilardi and Mylin 1990);

$$f = 60/1.4w$$

w = the width of the check
f = cycles per degree

3.7.1.ii Effect of Reversal Rate.

When the stimulation rate is less than 3.5Hz (7 reversals a second) the response is said to be transient and the latency and amplitudes of the major components can be measured (Bodis-Wollner, Ghilardi and Mylin 1986), see fig.3.16.

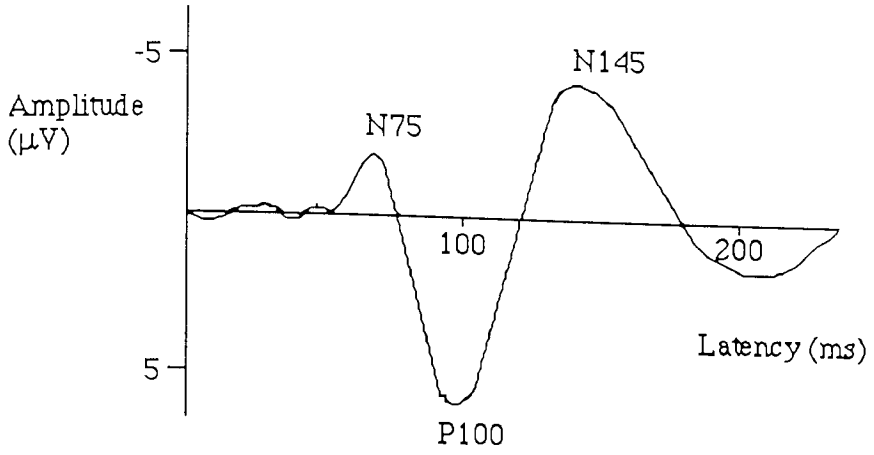

Fig. 3.16. Waveform Morphology of the pattern reversal transient response, illustrating the major peak components with their polarity and approximate latency.

Regan (1977) showed that small (12') checks responded best to reversal rates of 6-7 Hz and gave a weak response at 10Hz. An unpatterned field gave the strongest response at 10Hz and large checks (40') gave strong reponses at 3-7Hz as well as 10Hz. This fits with the proposal that VEPs to large checks are due to pattern specific and flicker responses, see later in this chapter.

3.7.1.iii Effect of Spatial Frequency

Plant, Zimmern and Durden (1983) compared the effect of varying the spatial frequency of sinusoidal gratings on the pattern onset and pattern reversal response. The latency of the early positive was found to increase with increasing frequency above 2cpd (cycles per degree). Below 2cpd the responses were more variable and the latencies tended to increase. The early components appeared similar for both pattern reversal and pattern onset when the spatial frequency was below 1cpd and in some subjects the positive component possessed two peaks. This supported work by Jones and Keck (1978) that VEPs to low spatial frequency gratings have two early positive waves. It was proposed that one of the peaks may be a related to peripheral stimulation. The earlier wave should be identified with the major positive wave at higher spatial frequencies. Peak to peak amplitudes were recorded, all the components showed spatial selectivity apart from the P2 (occurring at around 200ms) of the pattern reversal response. Above 2cpd the amplitudes were higher for the pattern onset stimulus and peaked at a higher spatial frequency.

Reports have also been made of an increase in the latency of the response with checks as well as grating stimuli (Sokol and Moskowitz 1981, Edwards 1989, Pike and Polish 1988). Edwards (1989) observed that the ipsilateral channel after

pattern reversal half foveal stimulation tended to produce a response with a double peak, the first peak having approximately the same latency as the contralateral P100. With an increase in check size the amplitude of the second peak tended to dominate the response. Plant et al (1983) speculated that the response to a checkerboard is dominated by cells with spatial selectivity of 4cpd whether this is a fundamental Fourier component of a pattern of smaller checks or a higher harmonic of a pattern of larger checks. This is a result of the peak amplitude response occuring at 4 cpd with a 20° field. The maximum of the positive tended to be at higher spatial frequencies as the field size was reduced, 2cpd at 20°, 4cpd at 10°, 8cpd at 5°.

Plant et al (1983) proceeded to investigate the effect of field size on the amplitude (baseline to peak) of the response. The spatial tuning of the major positive was similar for both pattern onset and pattern reversal. The overall amplitude was also similar except for the 20° field, where the amplitude for the pattern reversal positivity tended to be lower than that to a 10° field. They attributed this to inhibition by the peripheral contrast reversal response on the foveal response. For any given spatial frequency the amplitude of the VEP increased as the field size increased. This response showed saturation and did so at a smaller field size with higher spatial frequencies.

Foveal sensitivity peaks to stimulus sizes of 10-14' (Bodis-Wollner, Ghilardi and Mylin 1986), the optimum spatial frequency however increases as stimulus eccentricity is increased (Harter and White 1970, Meredith and Celesia 1982, Edwards 1989). This is presumably the result of an increase in average receptive field size with eccentricity (Dow et al 1984). Harter and White (1970) found the optimum check size to be 7.5-30' for a central field of 3° and 30-60'for a peripheral field of 4.5-7.5°. It is estimated that the centre of the largest human foveal ganglion cell is smaller than 28' (Bodis-Wollner, Brannan, Ghilardi and Mylin 1990), the fovea will therefore be stimulated by checks of less than or equal to 28' (Bodis-Wollner, Ghilardi and Mylin 1986). A vague spatial tuning effect with pattern reversal checkerboard stimuli has been demonstrated (Edwards 1989), however the peak of the amplitude versus spatial frequency curve varied between subjects. Kurita-Tashima et al (1991) demonstrated modulation of the P100 and N145 components of the pattern reversal by the log of the check size producing a significant curvilinear U shaped relationship, the minimum P100 latency occured with check sizes of 34.3'.

The effect of orientation and spatial frequency of a grating pattern was investigated by Adachi-Usami (1988) using steady state pattern reversal. The response was recorded from one electrode at Oz and referred to the right earlobe. The grating response was also compared with the response to a checkerboard stimulus. A circular field of 4° was used, the response amplitude was always lower for the gratings and peaked at higher spatial frequencies. The maximum response for the checks was obtained with a check size of 14', whereas the maximum for the gratings was at 4.4 cpd (equivalent to 7'). A decrease in the amplitude with high spatial frequencies was observed when the orientation was oblique. The amplitude to checkerboard stimulation peaked with a field size of 6°, while with gratings the saturation level was dependent on the spatial frequency. With an increase in field size the peak of the amplitude versus element size curve shifted towards larger element sizes and greater amplitudes. The response to equal area stimulation concentric to the macula was also recorded. The amplitude reduced as the retinal site stimulated shifted towards the periphery, this was clearly related to the check size used. For full field stimulation the check size giving the maximum response was 17.4' whereas when a central scotoma of 8° was used, and the periphery was stimulated by an area equal to a full field of 8° the maximum response was recorded with a 34.8' check.

An increase in the latency of the response when both the check and field size were reduced has also been demonstrated (Flanagan 1987). The field and check sizes were matched for cortical magnification, the latency increased from 95.6ms to 110.3ms when the field size was reduced from 30° to 3°.

3.7.1.iv Chromatic Stimulation

Regan (1973) investigated the chromatic response using both check and bar patterns. Each check or bar emitted a mixture of both red and green colours, the colour and luminance was varied by independently changing the red and green luminance. Pattern reversal stimulation was produced by interchanging the luminance of the red and green but the net red and green luminance in each check did not change. Luminance contrast was produced by using bright and dim checks of the same colour. In 3° full field stimulation with an 11' check the greatest amplitude was found with a reversal rate of 6-8Hz. The luminance contrast response had a similar optimal frequency however some subjects showed a difference between red and green.

Murray et al (1986) compared responses to the onset of chromatic and achromatic gratings, and also those of pattern reversal. Responses were recorded from electrodes positioned over In, Oz, POz and Pz to a range of spatial frequencies and stimulus sizes. The field stimulated for most of the responses was postioned mainly in the lower half stimulating the lower central 0-9° and upper 0-1°. For chromatic onset stimulation the response was dominated by a negative wave at approximately 120-140ms, whereas the achromatic response was dominated by a positive response around the same latency. These responses were maximal for gratings of 2-6cpd and over the Oz electrode. At 8cpd the chromatic response was of very small amplitude, whereas at 1cpd the responses were very similar. The negative response was present providing the factor G/R+G was within 6% of the isoluminance value. When the response was recorded to pattern reversal of a 2cpd grating reversing in 2.5° of the lower half field there was little or no difference between the responses from the chromatic and achromatic stimuli. In contrast to this Thompson and Drasdo (1991) observed a negative peak in the reversal chromatic response. The negative peak was observed at a latency of approximately 165ms i.e. delayed and of opposite polarity to the luminance contrast response, the distribution was however the same as the luminance response. If 10% luminance contrast was introduced on top of the chromatic contrast a negative was still observed but this was preceded by a luminance positive peak. Both abrupt and slow onset resulted in a larger and slightly delayed negative (CII), this being largest with slow onset. Again the distributions of the two responses, chromatic and achromatic, were the same.

The responses to luminance and chromatic contrast have also been investigated in the rhesus monkey (Previc 1986), fig.3.17. The effect of spatial and temporal frequency was observed. The luminance potential peaked at 4cpd whereas the chromatic response amplitude declined significantly beyond 1cpd, i.e. displaying low pass filtering. The response to the red and green grating was seen to increase remarkably with a slight imbalance in the luminance, although a slight imbalance should not prevent a largely chromatic contrast VEP from being recorded (Thompson and Drasdo 1991). No difference in the effect of temporal frequency was observed. This led to the conclusion that chromatic VEPs show lowpass tuning in spatial and temporal domains but luminance VEPs show lowpass tuning in only the temporal domain. These findings supported the view that the pattern reversal response originates in area 17 and that this area processed both types of responses.

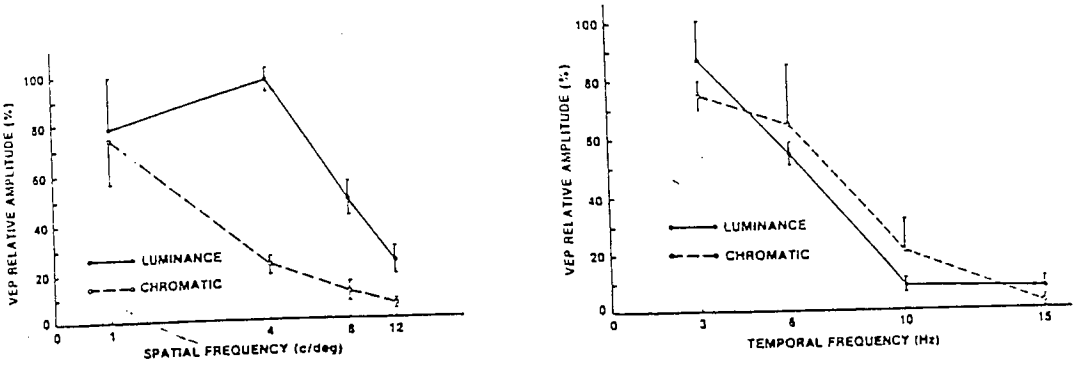

Fig 3.17. Left graph shows VEP relative amplitude, based on Fourier power averaged across all eight electrodes,.to luminance and chromatic contrast as a function of spatial frequency, using 3 Hz modulation. Right graph shows VEP relative amplitude to luminance and chromatic contrast as a function of temporal frequency, using a 1c/deg grating. After F.H.Previc. (1986).

3.7.1.v The Effect of Luminance and Contrast.

Luminance has a minimal effect on the amplitude of the reversal VEP (Halliday 1977). With a reduction of the retinal luminance by 1 log unit there was an increase in the latency of the pattern reversal response by 15msec.

Contrast is defined by Michaelson equation as Lmax - Lmin / Lmax + Lmin. This is normally set up as monochromatic luminance contrast in the form of black and white checks or bars. Low and high contrast VEPs may represent the response of different groups of neurons, low contrast preferentially stimulating Y cells which project to the magnocellular layers of the LGN.

The amplitude of the steady state reversal VEP has been shown to be proportional to the log of the suprathreshold contrast of the stimulus. Extrapolation of the line to zero gives a prediction of the psychophysical contrast threshold (Campbell and Maffei 1970, Campbell and Kulikowski 1972, Wright and Johnston 1982). Below 3 cpd the results were best fitted by two regression lines due to the gradient of the line reducing with a reduction in contrast (Campbell and Maffei 1970). Murray and Kulikowski (1983) postulated that these two branches of the contrast versus amplitude response were the result of separate pattern and movement detecting mechanisms. The upper branch of the curve was the result of movement detecting mechanisms and extrapolated to give the movement threshold and the lower branch was the result of pattern detecting mechanisms and extrapolated to give the pattern

threshold. Pattern detection depends on the standing contrast and movement is a function of the contrast change. The pattern reversal VEP was considered to be generated mainly by movement detectors. At low spatial frequencies pattern onset/offset stimuli activate movement detectors and the on, off and reversal VEP were indistinguishable. When the spatial frequency was increased the waveform changed and was no longer symmetrical, the on being greater than the off response. If the pattern reversal response was subtracted from the onset response, a close indication of the pattern threshold was obtained suggesting this may be a pattern related VEP.

3.7.1.vi Modes of Stimulation and Their Relationship.

The visual system can be activated by both pattern and uniform light stimulation. Pattern stimuli can be presented as either pattern reversal or onset/offset. The response following pattern onset stimulation is characterised by three major peaks termed CI, CII and CIII, the respective latencies are 65-80ms, 90-110ms and longer than 130ms, depending on the stimulus parameters (Jeffreys 1968). Various workers have hypothesised as to the relationship between pattern onset, offset and reversal. By changing contrast a progression from a pattern onset to a pattern reversal stimulus can be obtained (Estevez and Spekreijse 1974). It was concluded that the pattern reversal response was produced by interaction between the pattern onset and offset response, although the majority of it was the result of the offset response. As the offset response is thought to be sensitive to a reduction in contrast, the reversal response was presumed to originate by the same mechanism. Jeffreys (1977, 1980) proposed that the pattern reversal response was due to the supersition of two positive peaks with different scalp distributions, these related to CI of the pattern onset response and the pattern offset response.

Different scalp distributions have been reported for both pattern reversal and pattern offset with upper and lower half field stimulation (Skrandies, Richter and Lehmann 1980). For lower half field stimulation the off response peaked closest to the inion, in contrast the reversal response peaked more anteriorly, the reverse was true for upper half field stimulation. It was concluded that these two components were not related. Other workers have however demonstrated that the distribution of the pattern offset and pattern reversal responses are similar whereas the onset response gave different latencies and distributions (Kriss and Halliday 1980). With gratings of spatial frequencies less than 1cpd the pattern reversal and patten onset response appear very similar (Plant et al 1983, Kulikowski 1977).

3.7.1.vii The Mechanism Generating The Pattern Reversal Response.

Van der Tweel and Spekreijse (1968) suggested that the pattern reversal VEP to large checks was the result of two components related to the sharply focused edges and the local luminance in each individual check. The local flicker component being more prominent with larger checks. If the edges were obstructed by fine lines the VEP was abolished only when the check size was small. Other workers have shown results consistent with the proposal that high spatial frequency grating responses are a contrast response and low spatial frequencies responses are the result of local flicker (Bodis-Wollner, Hendley and Kulikowski 1972) . Regan (1977) also compared the responses to flicker with those to large checks and small checks, see reversal rate.

Kulikowski (1977) proposed that the pattern reversal response was a result of both contrast and motion mechanisms. It has been suggested that pattern reversal can best be described in terms of motion onset and offset (Spekreijse et al 1985). Reducing the inter stimulus interval between motion onset and offset resulted in an interaction between the components producing a pattern reversal P100. Motion onset had a rather symmetrical topographical distribution whereas the motion offset had a contralateral distribution, these distributions were replicated in the early and late components of the reversal VEP respectively. In addition adaptation to a steady velocity before displacement affected the response, the displacement response is therefore generated by a motion sensitive mechanism. This effect depended on the axes of the adaptive motion and displacement. Their data implied that motion VEPs are determined by a mechanism sensitive to omnidirectional motion rather than by a mechanism sensitive to unidirectional motion.

The responses to abrupt displacement of less than one check were also investigated, this is not equivalent to contrast reversal and is experienced as motion. As the displacement was increased the displacement VEP progressively grew into the reversal VEP. There was no qualitative distinction between the reversal VEPs and those due to displacement. Fenwick and Turner (1977) demonstrated a linear increase in the amplitude of the VEP with an increase in the displacement of the checks, up to a displacement of one check. This increase in amplitude with check displacement was verified by Spekreijse et al (1985). The amplitude of the VEP may therefore be related to the number of visual elements stimulated, which is in turn proportional to the area covered by increasing the displacement of the checks. A significant increase in the latency of full square

displacement compared with 0.25, 0.50 and 0.75 displacements was also demonstrated.

Dagnelie et al (1986) investigated the contrast and motion responses of the Macaque. The stimuli used were checkerboard pattern reversal, checkerboard pattern appearance and disappearance and checkerboard pattern motion on-off, all with 12' checks and 20% contrast. Subdural electrodes were implanted into the foveal and peripheral regions of area 17. In the periphery the pattern reversal response was very different to the pattern appearance response, in contrast from the fovea these responses were both similar. These foveal responses were also very similar to the peripheral appearance response. The response to motion from the periphery showed a positive and negative deflection at the onset and offset of motion respectively, from these a synthesised reversal response could be produced. A response to motion in the fovea was only observed with velocities greater than 2.5deg/sec. The motion onset and offset responses resembled the pattern disappearance and appearance responses respectively. A pure contrast response could be recorded, with pattern appearance/disappearance stimuli at both the fovea and the periphery. The results infer that a motion mechanism exists in the periphery and parafovea and the pattern reversal response can be fully explained in terms of a motion on-off response. The foveal motion offset could be fully explained in terms of an appearance response and the same for motion onset and pattern disappearance therefore, in the foveal region of the macaque area 17 responses to pattern motion stimuli could be attributed to a contrast sensitive mechanism. A response to both motion and contrast was found in the periphery and parafovea whereas for foveal stimulation both motion and pattern reversal elicited contrast responses. These results supported both contrast and motion contributions to the pattern reversal response. It was concluded that as 'the pattern reversal stimulus can activate both contrast and motion mechanisms it is an ambiguous stimulus to use'.

3.7.1.viii Cell Physiology and the Source of the Pattern Reversal VEP.

The retinal ganglion cells mediating foveal vision may be broadly classified in the cat into two groups X and Y cells. The X cells are circular antagonistic with the centre and surround in complete opposition. In the Y cells however the centre and the surround will never completely cancel (Bodis-Wollner, Ghilardi and Mylin 1986). The Y cells also exhibit a frequency doubling response, if both an X cell and a Y cell are stimulated with a spot of light modulated at 4Hz the response from the X cell will be at 4Hz whereas responses from the Y cells will be at both 4 and 8

Hz. In the primate large bodied cells (M) are similar to those of the cat Y cells, and many but not all of the small cells are similar to the X cells, termed P cells (Bodis-Wollner, Brannan, Ghilardi and Mylin 1990).

The magnocellular system is phasic and responds best to low contrast, low spatial detail with a high temporal profile. In contrast to this the parvocellular system is tonic and responds best to high contrast, high spatial detail at low temporal rates. Parvocellular neurons have small receptive fields which could explain a reduction observed in chromatic high frequency resolution in the temporal but not the spatial domain (Previc 1986). Recently both tonic opponent cells and those found in or projecting to the magnocellular layers (i.e.phasic neurons) have been found to respond to both luminance and chromatic contrast, although it is not clear as to which of these is more critically involved in coding purely chromatic contrast in the absence of any luminance variations. It has been hypothesised that a colour opponent parvocellular cell may respond best to chromatic contrast at low spatial frequencies and to luminance contrast at high spatial frequencies (Previc 1986).

It is therefore evident that by selecting the appropriate stimulus characteristics it should be possible to investigate the responses from different sets of neurons. High contrast stimuli should preferentially stimulate the parvocellular neurons whereas low contrast will stimulate magnocellular pathways, medium contrast will affect both. By implementing this it is possible to study certain disease mechanisms which preferentially affect different cell types. For example, in glaucoma the site of damage is predominantly in the large cells.(Atkin et al 1979, Quigley and Hendrickson 1984). Orientation specific losses in medium spatial frequencies are observed (Kupersmith et al 1983) and low contrast VEPs are diagnostically useful in the study of Multiple Sclerosis (Bodis-Wollner, Brannan, Ghilardi and Mylin 1990). Parkinsonian patients exhibit a loss in spatial frequency tuning i.e they fail to show an increase in sensitivity for medium spatial frequencies. It is therefore important to select the correct spatial frequency to show an effect (Bodis-Wollner et al 1987). In maculopathy patients a VEP loss may only become evident when 14' or 7' checks are used (Papakostopoulos et al 1984).

3.8 Evoked Field Single Point Recordings

Brenner et al (1975) recorded the pattern onset VEF using a single channel magnetometer. A large repeatable response was recorded at approximately 50ms about 5cm above the inion which was found to reverse in phase at a position less than 5cm from the midline on the left. Thus indicating that the response produced

activation of a cortical area which resulted in field being directed out of the head near the midline and into the scalp to the left.

3.8.1 Effect of Flash Intensity

Early workers, using single channel magnetometers, were more interested in the effect of stimulus parameters on the VEF than in the absolute location of the activity in the cortex. Teyler et al (1975) looked at the effect of flash intensity on the amplitude and latency of the VEF and the VEP, recorded simultaneously. The VEP was recorded from Oz and the VEF was recorded from a position midway between the inion and the ear. As the flash intensity increased the amplitude of the VEP increased and the latency reduced, in contrast to an increase in amplitude but no change in latency. They postulated that as both the amplitudes increase with intensity both methods reflect different aspects of the same source.

3.8.2 Consequence of Variations in Spatial and Temporal Frequency

After locating the position of a field extrema the variation in the flux density as a function of spatial and temporal frequency was investigated by Okada et al (1982). The stimulus was a grating presented in the right half of the visual field at a steady state reversal rate. The amplitude of the second harmonic was found to be highest from a grating of intermediate spatial frequency (1-4cpd). However, as the temporal frequency increased from 3.5-11.5 Hz the spatial frequency that gave the maximum response reduced from 3 to 1 cpd. The latency of the response has been found to increase with an increase in spatial frequency (Williamson et al 1978, Okada et al 1982).

3.8.3 Effect of Luminance

Okada and Storch in collaboration with Williamson and Kaufman studied the effects of average luminance on the visual evoked field. The stimulus was a 1cpd grating presented to the right half field. The luminances used were 50, 5 and 0.5 cd/m^2 with the contrast remaining constant. The change in mean luminance resulted in a change in the field orientation, although the depth did not change systematically, and an increase in latency with a reduction in the meanluminance.

3.8.4 Effect of Contrast

The VEP and VEF responses were compared after stimulation with a grating whose contrast varied from near threshold to near saturation. The phase lags agreed for

the low spatial frequency stimuli indicating from the signs of the VEP and the VEF that the current flow was in opposite directions. There was however, a deviation of the phase for high spatial frequencies thus indicating that more than one source may be responding and separately generating the two responses. The latency of the response has also been found to be dependent on the contrast of the stimulus with an increase in contrast resulting in a decrease in the response latency (Okada et al 1982). A linear relationship was found between voltage and field amplitude but the proportionality factor varied with the spatial frequency. This may be the result of a change in the direction of the dominant intracellular current or may be a result of the spatial frequency channels active in the visual system. It was also shown that for spatial frequencies of greater than 6cpd the VEP lags the VEF, this may again infer that more than one source is active at that instance.

3.8.5 Effect of Reversal Rate and Spatial Frequency

The slope of the function relating phase and reversal rate has been shown to increase monotonically with the spatial frequency of the pattern (Brenner et al 1981).

a) b)

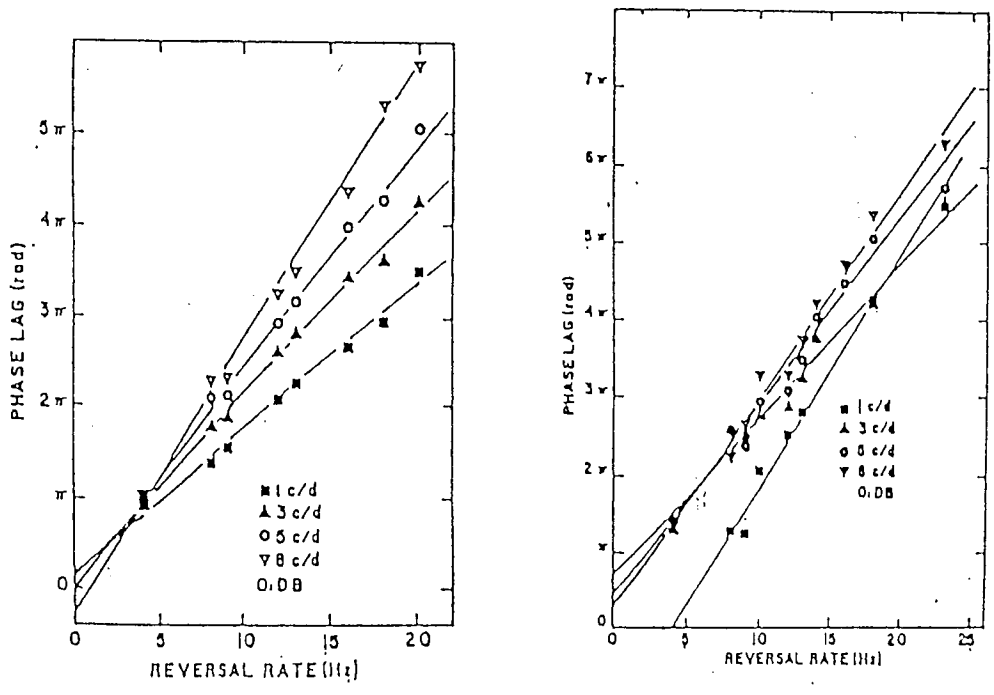

Fig 3.18. Graphs to show the phase of the response versus the stimulus reversal rate for stimuli at various spatial frequencies measured at a) a point on the midline of the scalp and 4cm above the inion and b) on the midline and 9cm above the inion. After D.Brenner, Y.Okada, S.J.Williamson and L.Kaufman (1981).

The reponse was recorded from two positions on the midline to reversal rates from 8 to 20 Hz with spatial frequencies of 1, 3, 5 and 8 cycles per degree (cpd). The higher recording position in one subject gave an increase in latency with an increase in the reversal rate for all spatial frequencies except for the 1cpd stimulus. The latencies of the response were statistically different for the 1 and 3 cpd stimuli at the two recording positions, fig.3.18. This, they proposed was the result of activation of two separate sets of cells. The full field response recorded from between 30 and 49 points over the occiput, was shown to be approximately equal to the vector sum of the responses from the lateral half fields.

3.8.6 Effect of Field Stimulus Location

The maximum magnetic field strength to quadrant stimulation was recorded after stimulation in the lower temporal quadrant (Schmidt and Blum 1984). This was suggested to be due to the projection of this area being situated in the upper cortex and therefore closer to the pickup coil thus, they concluded, the response was following the retinotopic mapping of the visual field on the cortex. The response was recorded from four points over the upper right and left and lower right and left occipital area and the stimulus used was a square wave grating of spatial frequencies varying from 0.34 to 5cpd in a field of 6.3 x 5°. Peripheral quadrant stimulation was also performed by moving the fixation point away from the TV monitor. This displacement was performed in a stepwise fashion and the response was recorded until the amplitude reduced to noise level. The furthest displacement that gave a recordable signal was 1.75°. With half field stimulation the maximum response was recorded over the contralateral hemisphere with the dipole directed towards the midline. No source dipole fitting procedure was attempted, the dipole was fitted by eye.

CHAPTER 4

Generator Studies of the Source of Evoked Potentials

4.1 Introduction

Many studies have attempted to locate the areas of visual cortex activated after visual stimulation. A variety of methods can be implemented to confirm the areas activated. Activity can be observed using positron emission tomography (PET), PET scans can then be compared to either CT (computed tomography) or MRI (Magnetic Resonance Imaging) scans to identify the anatomical location of the activation. Low temporal resolution however hinders this method. A greater temporal resolution can be obtained when the evoked potential is recorded this is, however gained at the expense of spatial resolution. To improve the spatial resolution the magnetic field of the evoked response can be recorded. The distribution of both the evoked potential and evoked magnetic field can be used to compute the location of hypothetical dipoles representing the position of the evoked activity.

4.2 PET Localisation of Evoked Activity

PET produces an image of the distribution of a previously administered radionuclide in any area of the body. This technique has been used in humans to measure brain blood flow, blood volume, metabolism of glucose and oxygen, acid-base inbalance, receptor pharmacology and transmitter metabolism (Raichle 1990). An increase in neuronal activity in a specific area will be accompanied by an increase in glucose metabolism and oxygen consumption so resulting in an increase in blood flow. Any of these three changes can be used by PET imaging. The least sensitive is the increase in oxygen consumption and is therefore rarely used. Although a direct relationship exists between increased functional activity and increased glucose metabolism (Phelps et al 1981, Celesia et al 1982) the measurement takes 45 minutes to complete, it is therefore difficult to repeat. Patient fatigue as well as adaptive changes in the brain may also cause problems. To study rCBF (regional cerebral blood flow) and LCMRGlc (local cerebral metabolic rate for glucose) a tracer has to be either inhaled (rCBF) or injected (LCMRGlc). The tracers most widely used are [^{18}F]fluoromethane for rCBF and [^{18}F]2-fluoro-2-deoxyglucose ([^{18}F]DG) for LCMRGlc. Measurement of the rCBF following the intravenous

injection of ^{15}O-water using an adaptation of the classic Kety tissue autoradigraphic technique is fast (40 seconds for a single measurement), sensitive and easily repeatable (Raichle 1990).

The spatial resolution of PET devices defined as the full width at half maximum (FWHM) is of the order of 10-20mm. An increase in the spatial resolution of the images can be produced by subtracting the activated state from a control state. Raichle (1990) has improved resolution to 1-2mm by using an averaging procedure whereby after subtraction the responses from individual subjects are summed and scaled to account for the differences in brain dimensions. It is virtually impossible for PET to reveal the underlying neuronal elements participating in the functional changes however, the localisation information gained from PET can be implemented by other techiques to ascertain the exact nature of the processes. It must be noted that the blood flow and metabolism changes occur in the cell processes rather than the cell bodies, the cell bodies can often be located a distance from the site of observed changes.

4.3 Methods of Anatomical Localisation of the Evoked Activity

4.3.1 X-ray Computed Tomography (CT)

CT images are computer generated images of the tissue density produced by tomographically measuring the attenuation of tissue to X rays passed through the body at many different angles. The data is analysed to produce high quality images of the brain in various orientations and depths. The major contribution of the CT image is the ability to provide highly accurate data on the location of specific lesions of the brain.

4.3.2 Magnetic Resonance Imaging (MRI)

This technique is based on the phenomenon of nucleur magnetism. Most atomic nuclei have a magnetic moment which when exposed to a strong static magnetic field becomes aligned with the field. Only certain states of orientation are possible, for the proton these states are parallel and anti-parallel. Irradiation with radiofrequency energy causes changes in the orientation from these fixed states. After excitation the nuclei will realign with the magnetic field, this does not happen instantaneously but with some time constant, T1, this process is called the relaxation time. This recovery produces weak radio frequency signals, the longer T1 the less recovery and the lower the signal. The signal intentsity depends on the structure of

the region, the signal intensity increases as follows fat > white matter > gray matter > cerebro spinal fluid (CSF). T1 weighted contrast scans are used for the location of anatomical structures. The signal strength decays with another time constant which is also tissue specific, this is called T2 or the tranverse relaxation time. The longer T2 is the more signal is available, the CSF now has the highest intensity and fat the lowest. The strength of the signal from a particular nuclei is the product of its magnetic moment, its abundance in nature and its concentration in the tissue. This technique therefore affords an excellent way to obtain *in vivo* anatomical information of the human brain. Most imaging of the human brain makes use of the strong signal obtained from the hydrogen nuclei although other nuclei can be studied e.g. ^{31}P, ^{23}Na and ^{13}C, this technique is termed magnetic resonance spectroscopy.

4.3.3 Stereotaxic Imaging

This procedure has been developed by Fox, Perimutter and Raichle (1986) for use with PET scans of functional processes. This approach determines the anatomical location of a PET region of interest with the coordinate system of atlases for stereotaxic noeurological surgery (Raichle 1986, 1990). Measurements made from a lateral skull radiograph and from a tomographic transmission scan form the basis of this method. Regions defined by this procedure can easily be compared among subjects in a study and among different subject populations with in a laboratory.

4.4 PET Scan Studies of the Visual Cortex

Both the primary (PVC, Brodmann's area 17) and association visual cortex (AVC, Brodmann's area 18 and 19) were investigated by Phelps et al (1981a, 1981b). Using PET they studied the area of activation in normals as well as patients with homonymous hemianopias, blindness and visual aura. The activity in PVC and AVC increased by 2.4 and 4.5X respectively with pattern reversal stimulation and by 4 and 10X after viewing a complex scene when compared to flash. The activity in PVC and AVC after white light stimulation only increased by 12% and 6% respectively, compared with no stimulation. They hypothesised that this small increase was a result of the simplicity of the stimulus and also the fact that the majority of the processing of white light had already occured in the LGN and the Superior Colliculus. It was concluded that a greater involvement of higher order processing was required for pattern recognition. No asymmetry was observed between the hemispheres with full field stimulation to one eye, both eyes or in the unstimulated state, each hemisphere was therefore stimulated equally by the

pathways from one eye. The pattern reversal VEP was recorded simultaneously with the metabolic rate to correlate any changes in the amplitude with changes in the area of activation. No significant relation between the metabolic rate and the amplitude of the N75-P100 complex in the VEP was found. Responses to monocular and binocular stimulation were also compared, an increase in the PVC and AVC activity of 37% and 18% respectively was observed after binocular stimulation. This was not corroborated in the VEP, where two out of the three subjects tested showed an increase in the VEP amplitude on monocular stimulation. All the hemianopic subjects tested showed a reduction in activity of both the PVC and AVC on the side contralateral to the field defect.

An increase in the rCBF in areas 17, 18, and 19 was observed by Celesia et al (1982) for both pattern reversal stimulation and flash. They could not demonstrate an increase in the activity of the mesial surface of the occipital lobe for pattern stimulation to explain paradoxical lateralisation. Flash and pattern VEPs were also recorded in patients with hemianopsia, in one patient with a left hemianopia the distribution of the flash response was maximal over the left hemisphere whereas the pattern response was maximal over the right hemisphere. The distribution of the surface recorded VEP to flash and pattern were presumed to reflect the complex interaction within at least three cortical areas, rather than the sole transmission of striate dipoles. Celesia (1980) has demonstrated recordable visual evoked potentials in a patient with a bilateral infarcts of the occipital lobe, this may be the result of preservation of a small area of the striate cortex. Meredith and Celesia (1982) demonstrated that only a small amount of the striate cortex (approximately $7mm^2$) had to be intact for a VEP to be recordable. A recordable VEP has also been shown with bilateral destruction of areas 18 and 19 (Bodis-Wollner 1977).

Schwartz, Christman and Wolf (1984) investigated the activation of the primary visual cortex using PEtransaxialT. The pattern onset stimulus was projected to the lateral half fields and stimulated the central upper and peripheral lower visual field. After activation they observed an asymmetry between left and right, as would be expected this being greatest for a peripheral stimulus. The peripheral stimulus was also shown in one subject to activate a more anterior area of the visual cortex.

Activation of macular and peripheral areas were further investigated by Fox et al (1986) who, using PET and rCBF, located the activity in the visual cortex. The stimulus was a 10Hz reversing checkerboard annuli, increasing check size with eccentricity. Macular responses were maximal posteriorly and inferiorly at the

occipital pole whereas peripheral responses were maximal superiorly on the medial occipital surface. Perimacular activity was located between the two, in agreement with the retinotopic mapping of the visual field. This work was continued by Bassem et al (1989) with the inclusion of MRI scans. The response to full altitudinal half field, peripheral and macular stimulation was recorded. The lower field responses were centred in the upper bank of the calcarine sulcus and the upper field responses were centred in the lower bank. Activation of the extrastriate cortex was also demonstrated including the temporal occipital parietal pit (TOPP), which may correspond to the MT, and the posterior thalamus.

Kushner et al (1988) also employed central and peripheral half field presentation with a reversing pattern of a 3° check. Fourteen different brain regions were analysed using CMR (cerebral metabolic rate) and PET. A significant increase in the CMR was shown in the posterior contralateral striate cortex with central stimulation. An increase was also shown in the anterior contralateral striate cortex with peripheral stimulation, although this failed to reach significance. In the lateral occipital, inferior parietal, superior frontal, superior temporal, anterior parietal and prefrontal cortex a greater activity was seen on the right side compared with the left. There was an increase in activity of the right peristriate only for right peripheral left central stimulation. They postulated this confirmed animal studies of an occipito-tempero-frontal pathway involved in object recognition and an occipito-parieto-frontal pathway involved in spatial vision.

4.5 Intra Cortical Recordings

Intracerebral and scalp evoked potentials to pattern reversal and flash stimulation have been recorded by Ducati, Fava and Motti (1988) in eight patients. The electrode was passed through the visual cortex, traversing the white matter under area 18 in the first 1.5-2cm and then through the white matter and possibly the gray matter of area 17. The response from the cortical surface was found to be clearer and of a larger amplitude than the scalp potential. A polarity reversal in the response signified that the electrode had passed the wave origin. The PRVEP inverted when the electrode crossed the cortex and therefore the generators of N75-P100 were proposed to be located in area 17 and the parastriate cortex. The largest response was 20-40mm from the scalp surface, the response was not present 60mm from the scalp. Flash stimulus activated the whole of the striate cortex. They concluded that the pattern reversal response appears to behave like the long latency flash response,

this response was thought to be generated in the superficial layers (layer II pyramidal cells) of the striate cortex.

4.6 Current Source Density Analysis

The physical origin of recorded evoked potentials are current sinks and sources in the extracellular space. A number of workers have therefore looked at current sources and sinks in the visual cortex, this is achieved by analysis of the recorded electrical potential produced after stimulation of the cortex. The second spatial derivative of the field potential yields the source/sink distribution in the extracellular space. Formulation of the current source density (CSD) can be easily accepted because, according to Ohm's law, the steeper the potential fall off, the more current flows. Changes in the potential gradient therefore imply changes in the amount of current flowing. CSD analysis may therefore disclose and localise the generators of the evoked potentials (Mitzdorf 1986).

Kraut, Arezzo and Vaughan (1985) investigated the current source sink configuraton for the flash response in the monkey. The results indicated that the flash stimulus activated the parvocellular thalamorecipient laminae. The alterations in the motor unit activity were principally found in layers IV, synchronous depolarisation of the thalamorecipient afferent terminals would yield the observed current sink within the region of the terminals with a deeper current source. It was concluded that sequential depolarisation and hyperpolarisation of stellate cells within layer IVCb generated the prominent N40 and P65 components of the flash response. The N40 and P65 were proposed to be equivalent to the N70 and P100 of the human flash response. The P100 response may therefore be a manifestation of inhibitory reponse within the thalamorecipient layers analogous to those that generate the P65 in the monkey.

Mitzdorf analysed the responses of electrical and visual stimulation from areas 17 and 18 of the cat visual cortex. The dominant cause of the sinks and sources was thought to be excitatory synaptic activity, no discrete CSD components were found as a result of inhibitory synaptic activation. The visual stimuli consisted of flashes of light, a Ganzfeld change in luminance, appearance and disappearance or reversal of a grating, moving gratings and moving bars. These were presented both monocularly and binocularly in a wide area of the visual field and also in restricted central and peripheral areas. Electrical stimulation of the optic radiation resulted in a dipolar sink/source in layers IV/III followed by two further dipoles in layers III/II. Symmetrical source/sink/source distributions were apparent with the sink in the

lower layer IV, in layer V and in layer VI. The dipolar sink/source distribution produced far field potentials whereas the symmetrical source/sink/source distibutions caused local (closed field) contributions to the potential. The onset latencies of all components in area 18 were found to be slightly shorter than in area 17, confirming that area 18 may be activated essentially by Y type afferents. Monosynaptic sinks demonstrated that the afferent fibres terminated in layer IV and VI. In layer IV the Y type of afferents terminated above the X type and then proceeded to contact cells in layer III. X type afferents mainly contact cells that do not extend into layer III. Polysynaptic sinks demonstrated three pathways along which the afferent information is processed in the cortex. In the first pathway afferent Y type of activity was projected to the supra granular layers. Layer III pyramidal cells were activated disynaptically within layer III. The same cell type was activated trisynaptically at the peripheral dendrites within layer II via local and long distance connections. In the second pathway afferent activity was projected down to layer V, in area 17 the X type of activity is relayed along this pathway, mainly layer VI pyramidal cells were activated. The third pathway also consisted of Y type afferents and possessed one relay in layer VI which subsequently projected to layer III. Three different types of Y afferents were also proposed. One class of fast conducting afferents activated area 18, a second class consisted of slower conducting fibres that projected to layer IVa and the supra granular layers. A third class of very fast conducting Y afferents produced intracortical evoked inhibition. In area 17 the dominant concern was the processing of X type afferents within the infragranular layers. All the different types of the visual stimuli activated the three main pathways, altering the stimulus however produced slight changes in the sequence of the sinks and sources and in the speed of activation of the sequence. The responses to contour rich stimuli had longer response latencies and reduced amplitudes compared with those to stimuli with few or no contours. The early sink in layer VI was delayed more than the early sink in layer IV and less afferent activity was projected from the input layer IV to the supragranular layers. The responses to whole field stimulation were smaller than those restricted stimulation, this was thought to be the result of lateral inhibition. Responses to retinotopically non corresponding stimuli were found to be slightly delayed compared with responses to retinotopically corresponding stimuli. They suggested that the responses to retinotopically non corresponding stimuli disperse laterally in the cortex and then at terminal sites activate the same pathways as the corresponding stimuli.

Current source density analysis has also been performed on evoked potentials recorded from the primary visual cortex of the rat and cat (Bode-Gruel, Singer and

Aldenhoff 1987). The extracellular field potentials were recorded after square wave stimulation. The earliest postsynaptic response was a sink with a peak in layer IV, this was followed by a larger sink in layer III. A well defined sink occurred with an onset latency of 2.5ms in the superficial part of layer V, and was followed by a second prolonged sink. In layer VI another short latency sink was observed whose latency decreased with increasing depth. This deep sink was split in two, probably by a source associated with the early sink in layer V. Sinks in layer III were delayed compared with those from layer IV suggesting they resulted from afferents originating in layer IV. The apical dendrites of layer III pyramidal cells were the most likely targets of the pathway from layer IV to layer III. The sources corresponding to the sinks in layer II were mainly located in layer III. A disynaptic excitatory input was suggested to exist from layer IV to layer V. The profiles generating the layer V sinks were most likely to be layer VI pyramidal cells.

Schreoder et al (1988,1990,1991) have investigated the cortical generators of evoked activity in the monkey (M.fáscicularis) striate cortex with VEPs, CSD and multiunit activity. The cortex was stimulated with white light flashes, a reversing square wave grating (1991) and a chromatic and achromatic grating (1988). The pattern VEP recorded consisted of four components; an early negative, N50, then P60, N80 and P125. The Monkey N50 is thought to correspond to the human N70, the monkey P60 to the human P100, the monkey N80 to the negativity following the P100 and P125 may correspond at least in part to the second positive component. The N50 represented activation of the stellate cell ensembles in the thalamorecepient layer IVC. The P60 arose from activation of the supragranular neurons, presumably the pyramidal cells. A large extrastriate contribution to the N80 component was observed. P125 appeared to originate in area 17 with a significant contribution from extrastriate areas. Pattern responses, when compared with the flash responses, had a later onset and were more weighted towards the supragranular laminae. These differences were more accentuated with chromatic pattern stimulation (Schroeder et al 1990).

Schroeder et al (1990) specifically looked at the later responses, presumably of extrastriate origin, by recording activity in areas V2 and V4. The N80 component produced a clear polarity inversion in the middle of V4. The initial portion of the P125 had a polarity inversion accompanied by a large current source in superficial V2, whereas the later portions of P125 inverted in the middle of V4. No evidence of any contribution from these areas was seen to the early pattern reversal response

but there may be some evidence of a small contribution from the middle of V2 and V4 to the initial portions of the flash VEP.

4.7 Visual Evoked Field Studies

4.7.1 Source Localisation Methods

When the distribution of the evoked response has been established, the data is often used to estimate the location of the area of cortex whose activation has given rise to the recorded distribution. The approach most widely used is the forward method, in which the distribution from a known dipole is calculated and compared with the recorded response. The dimensions, orientation and strength of the dipole can all be modified until a good match is achieved, the dipole giving this distribution is then said to represent the source of the response. The inverse method calculates the source of the response only from the data collected. This is open to inaccuracies as the response may be generated by more than one source configuration.

Wienberg et al (1985) positioned single and multiple current dipoles in a human skull filled with an electrically conducting medium. Both the electric and magnetic field were recorded. The dipoles were arranged to fit along the sides of an equilateral triangle and each dipole could be activated independently. A least squares estimate of the five parameters defining location, orientation and magnitude of a tangential dipole were computed from the recorded field values. For the calculations the head was modelled as a sphere. This procedure accurately located the dipoles within 2mm and 4 degrees although the magnitude of the dipole was underestimated by 15%. When two dipoles were activated together and the current was flowing to form a 'V' the field pattern was virtually indistinguishable from that of a single dipole. In contrast when the current was flowing in the form of a current pathway the distribution could be fitted with two seperate dipoles.

Nunez (1986) illustrated the effects of multiple primary sources on the estimation of the source location, and showed the depth errors resulting from the assumption of a single diole see fig 4.1. The depth of an assumed single dipole from the pattern of two dipoles in the same direction and separated in the tangential direction appeared to be overerestimated. In contrast the depth of two dipoles oriented in opposite directions and at different depths appeared to be underestimated. The dipole locations were not estimated by comparing experimental with theoretical field patterns as is now widely used, although it was noted that this method does not take into account any interaction that may occur from secondary sources.

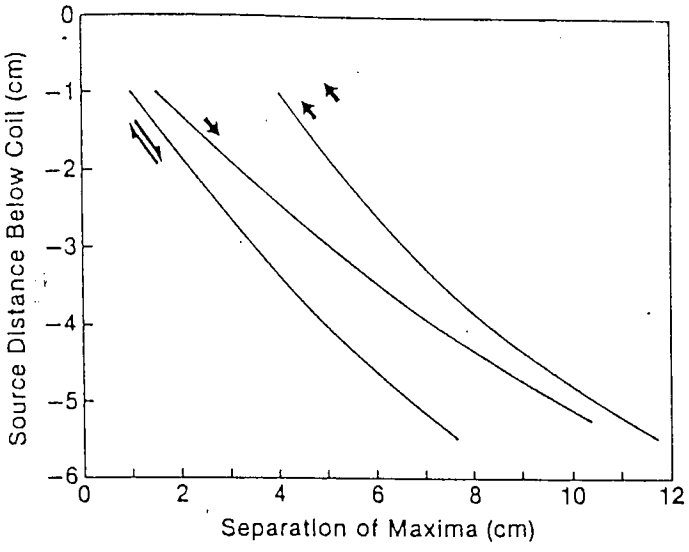

Fig 4.1 The theoretical separation distance of maximum and minimum radial magnetic fields for three dipole configurations are plotted versus the source distance below the contiguous SQUID coil at r=10cm (assumed to be the effective point of measurement of the field). No correction is made for the nonzero coil diameter. In the case of the oppositely directed dipoles the source depth refers to a radial location halfway between the dipoles. After Nunez (1986).

4.7.2 Equivalent Dipole Source Localisation From Magnetic Field Measurements.

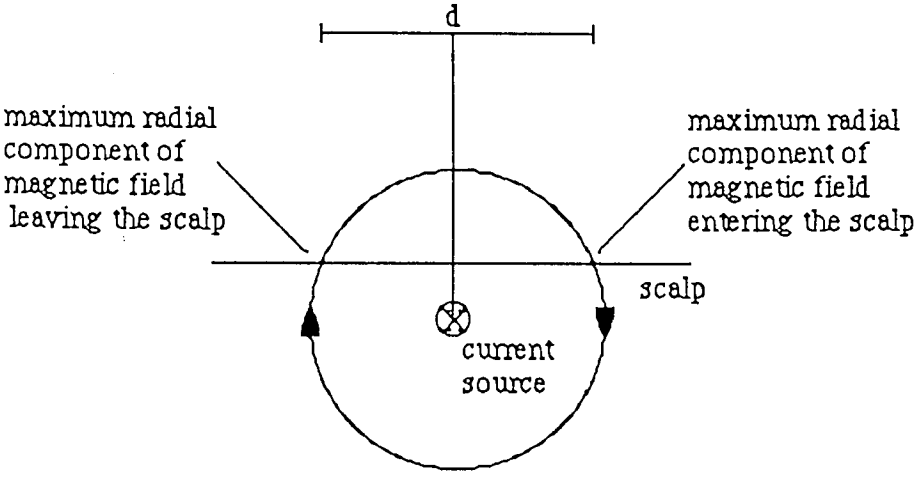

Fig 4.2 Diagram to illustrate the magnetic field encircling an equivalent current dipole located beneath a surface.

$$D = \frac{d}{\sqrt{2}}$$

D= depth of the dipole
d=distance between the maxima

If the magnetic field is recorded on a flat plane the depth of the dipole can be calculated from the above equation see fig 4.2. The direction of the dipole can be derived by using Fleming's right hand grip rule. If however the dipole is located in spherical body then the depth calculation must also take into account the radius of the sphere.

The field distribution must be recorded to achieve an accurate representation of the source. Five parameters of the dipole must be derived from the distribution:

1. Three parameters of location.

2. One parameter of direction.

3. One parameter of moment or strength.

To be detected a dipole must be oriented in a direction tangential to the scalp or have a tangential component. The surface of the cortex is very convoluted being made up of fissures (valleys) and gyri (hills) so, to achieve a tangentially oriented dipole, it must be located in or on the edge of a fissure not on a gyrus (Rose et al 1987).

Cuffin (1985) investigated the effects of the introduction of fissures using a head model on the recorded magnetic field. The introduction had moderate effects on the spatial MEG patterns the greatest effect was, however seen on the amplitude. Source depth estimates were affected by approximately 0.75cm and the orientation by approximately 18° however the amplitude estimates were affected by as much as 28%. It was therefore concluded that, with the exception of sources near the interhemispheric fissure the effects of fissures are relatively small. For a radial dipole and a tangential dipole pointing toward the fissure the introduction of a fissure increased the field amplitude. The introduction of a fissure with a radial dipole produced volume currents acting as though they originated from a dipole pointing towards the fissure, thus resulting in a tight field map. In contrast, for a tangential dipole positioned parallel to the fissure the introduction of a fissure reduced the field strength, except for points over or adjacent to the fissure.

The field pattern produced by a single dipole has been found to be statistically indistinguishable from that produced by multiple generators and extended sources in

a wide variety of conditions Okada (1984). A linear source was located along an arc or radial line and was represented by a set of dipoles parallel to one another, perpendicular to the source axis and tangential to the volume conductor surface. At a depth of 2cm and angular extent of 30° (3cm) the field was indistinguishable from that of a single current dipole. With increased depth the source became increasingly more indistinguishable. A sheet dipole had to be greater than 18° (18mm) wide (tangential) and 20° (radial) at a depth of 2cm to be distinguishable from a point source. When two dipolar sources were activated the angular orientation between the dipoles had to be greater than 40° for a separation of 1cm. The field is, however distinguishable for all orientations when the dipoles had a separation greater than 2cm.

ECDs (Equivalent Current Dipole) were also estimated from the computed field patterns for the various sources. For a line source the inaccuracy in depth approximation increased with the angular extent and reduced with the depth of the source (the ECD was always estimated as being deeper than the real source). For sheet sources the inaccuracy also increased with extent however the ECD was estimated as being shallower in the radial case and deeper in the tangential case. The depth estimation for the two dipoles was only affected by the separation of the dipoles and not by their orientation.

It was therefore demonstrated that only under certain circumstances can the field evoked by multiple generators be distinguished from a single current source.

4.7.3 Head Modelling

The most simple model for the head is a sphere, as a result this model has been used extensively in the localisation of the sources of electrical activity. The head is not however, accurately modelled by a single sphere because of; i) changes in curvature e.g. when moving from the occipital to the temporal area and ii) the skull is not complete, apertures for the eye sockets and nasal cavity etc, result in changes in the resistivity. In addition the cerebral cortex is very convoluted producing regions of varying conductivity. To achieve maximum accuracy in the approximation of the current dipole the head should be modelled as accurately as possible. Barth et al (1986) examined the accuracy of locating a dipolar source in the right anterior temporal region of a cranium using a spherical model. They found an overestimation of depth for superficial sources and an underestimation for deep sources, the sphere giving the most accurate results was located closest to the centre of the cranial space. The use of simulated field matching and calculating the

location, distance and orientation of the gradiometer coils with respect to centre of a sphere placed in the cranium for each recording point significantly increased the accuracy of source localisation. The effects of a craniotomy were also investigated, gross changes in the conductivity were found to have little effect, consequently it was proposed that areas such as the eye sockets should have little effect on the recorded field. Much of the distortion in the field patterns was due to the non sphericity of the field recording matrix, resulting in the tangential component of the magnetic field being recorded.

Hamalainen and Sarvas (1988) compared three models for the conductivity structure of the head, a sphere model, a realistically shaped multilayer model and a realistically shaped homogeneous model. The magnetic field due to deep sources and those located in the frontal areas could not be accurately computed using the sphere model. A realistically shaped homogeneous model was found to be adequate when the sphere model was not, i.e for deep sources (Menninghaus et al 1991). Spherical models have been shown to be better at locating sources under a horizontal plane through the centre of a sphere, being within 3mm of those based on a four compartmental model representing the brain, cerebro-spinal fluid, skull and scalp (Meijs and Peters 1988). Whereas models with realistically shaped boundaries were better at locating sources above this plane, being within 3mm of those based on the four compartmental model, this was postulated to be the result of the lack of a conducting neck. Superficial sources performed better with all head models.

Problems of source modelling may also relate to the source model chosen. Four types of source model have been proposed (Nunez 1988) activation of these different types may have a significant effect on the accuracy of source localisation. The types described are as follows; Type 1, localised and stationary, in this case the scalp distribution approximates a single dipole and the sources are confined to less than $1cm^2$ of the cortical surface. The dipole does not change location with the passage of time i.e. it is in the same position for each stimulus presentation. Type 2 is localised and nonstationary, this will produce a distribution similar to that from a single dipole, however the location is not fixed with time. Type 3 is stationary but distributed, the sources occupy a large area of the cortex and dipole approximation is not possible. Type 4 is distributed and nonstationary, most EEG and evoked potentials fall into this category. In some cases however the sources can be modelled by types 1, 2, or 3 so that a solution for the probable position of the activity can be estimated. Modelling the source as a current dipole is the most

extensively used approach to locate the signal generator (Gloor 1985). The fact that signal averaging is required to improve the S/N implies that either the source is small or the potential across a hypothetical large dipole layer acting as the source is very low, the former is usually the case. Procedures have been developed to estimate a spatial temporal ensemble of sources that can be used as the starting point for multiple dipole fitting procedures (Mosher et al 1990, George et al 1991).

4.8 Evoked Potential Studies

4.8.1 Source Density Analysis

Source density analysis produces a reference free distribution of the sources and sinks of the evoked potential calculated from the evoked potential distribution. The method gives an indication of the local activity and discriminates against distant generators. Regions of high cortical activity are those in which the density of the dipole source is the greatest, the regions of lower electrical activity act as a sink and accept the current flow back into the scalp. The source derivation calculation is based on a Laplacian equation The divergence of the scalp current density (J) must be calculated in order to determine whether the point is acting as a source or a sink.

$$\text{div } \vec{J} = \frac{\delta Jx}{\delta x} + \frac{\delta Jy}{\delta y}$$ where x and y are surface coordinates

The potential distribution on the scalp using Ohm's law is given by;

$$J = \sigma \vec{E}$$

the definition of the potential, ϕ, in terms of the electric field (ΔE) is;

$$\Delta E = -\vec{\nabla}\phi$$

From substitution in these equations, a term is produced which is proportional to the Laplacian and gives the two dimensional divergence of the current density. The three dimensional divergence equates to zero due to charge conservation.

The scalp current density as evaluated by Nunez (1981) is given by;

$$I = -\approx \frac{\delta^2 V}{\delta x^2} + \frac{\delta^2 V}{\delta y^2}$$

I is proportional to the radial component of the current flow and may also be referred to as the radial current estimate. Large local radial skull currents should indicate the presence of local sources. The radial current density (SCD) is

unfortunately influenced by the conductivity and resistance of the skull and will not therefore be improved until the development of better volume conductor models of the head. Cross channel correlation measures are normalised to be amplitude independent (the cross correlation coefficient is a function of time lag in the case of evoked potentials) and may be more realistic (Nunez 1988).

SCD is a scalar quantity and since it is related to the second derivative of the potential it is independent of the reference electrode. SCD can be calculated either by computing the sums and differences of the signals recorded from bipolar derivations of the 10-20 system (Hjorth 1975), see below, or from a specific multielectrode array (Srebro 1985, Srebro and Purdy 1990).

Hjorth (1975) developed a simplfied version of source derivation, this can be calculated from the following equation;

$$C3(source)=(C3-Cz) + (C3-F3) + (C3-T3) + (C3-P3)$$

The source at C3 is calculated by taking a derivation of the potential difference of the centre electrode and a weighted average of the potentials at the surrounding electrodes.

Hjorth also introduced a correction factor for the electrodes on the edge of the montage, incorporating a three point operator. As long as the conductivity of the scalp under investigation varies uniformly the source distribution calculated from the above equations should coincide with the distribution at a level under the scalp. The Hjorth method of source derivation does however have its limitations; it assumes that the electrodes are equally spaced and positioned at right angles to each other, this is obviously not a realistic assumption if the curvature of the head and it's asymmetry are taken into consideration (Myslobodsky et al 1990).

The principle of source derivation has been applied to topographic mapping of the pattern reversal visual evoked potential (Thickbroom et al 1984). The potential was transformed using their own equations not those of Hjorth (1975). Thirty electrodes were placed over the whole of the scalp, twenty positions were based on the 10-20 system with the remaining evenly interspersed between. The results obtained with a balanced non cephalic reference (BNCR), a common average reference (CAR) and source derivation (SD) distribution were compared. The BNCR accentuated the VEP whereas the CAR gave a similar distribution to the SD

with only slight accentuation of the VEP. They found that the lateral spread of the potential was reduced with SD and concluded that as the SD provides a measure of the current flow into and out of the scalp it is a truer indicator of the electrical events at any one electrode site.

The second spatial derivative or Laplacian derivation has also been calculated to localise the foci in the scalp field when using half field pattern reversal stimulation, this involved the calculation of the bipolar of a bipolar from a single reference recording (Clement, Flanagan and Harding 1985, Flanagan and Harding 1986). When the lateral half fields were stimulated the source was found to be stationary at Oz with the sink being contralateral to the half field stimulated. For upper and lower half field stimulation the responses were more variable with the source being located in the same place for 11/18 of the subjects, 5/18 produced a more anterior lower half field source and 2/18 gave a more anterior upper half field source. Due to this variability no significant difference in the reponse location between upper and lower half fields could be demonstrated.

Pattern onset and pattern reversal half field source derivations have been compared (Biersdorf 1987). The source for the pattern onset was found to be located contralateral to the stimulus whereas the source for the pattern reversal was found to be more variable. The pattern reversal response appeared to be composed of two components, the first with a source contralateral and the second with a source ipsilateral, this was observed with both 56'and 106' checks.

Perrin et al (1987) computed the spatial derivatives of the interpolated values of the potential data recorded from electrodes having an arbitrary distribution, this work was later continued by Pernier et al (1988) who investigated the topography and amplitudes for SCDs (scalp current density) from a point current dipole source located in a spherical head model. The head model was a three shell model representing the neural tissue, skull and scalp. The computed topography of the potential distribution was compared with that of the SCD and the radial component of the magnetic field generated by the same dipoles at different depths under the scalp. The angular distance between the extrema for a tangential dipole was less for the SCD than for the magnetic field. This is demonstrated in the graph,see fig 4.3, illustrating a reduction in the distance between the extrema with a decrease in source depth. The effect of tilting the dipole in a radial direction was also shown, the generator location was more easily identified using the SCD map than the potential map. The effect of tilting could be demonstrated on the SCD map, in contrast it did

not show up on the magnetic map which only records the tangential component. Two dipoles were then placed in the skull at different depths and rotations. The potential map was influenced to a greater extent by the deep source whereas the SCD map mainly showed the contributions from the shallower dipole, this is shown on the graph which demonstrates the attenuation of the signal with a reduction in dipole depth, see fig 4.4. Increasing the depth above a certain depth had no effect on the amplitude of the potential field. The magnetic field preferentially showed the contribution of the deeper dipole. The fact that the SCD is tighter than the potential allows it to localise generators with greater accuracy. As the SCD emphasises generators near the scalp, the electrode spacing must be close enough to obtain a true indication of the source distribution. Srebro (1990) quoted a sampling rate of 1cm for the occiput to give a spatial resolution of sources of 1.4 - 0.4cm.

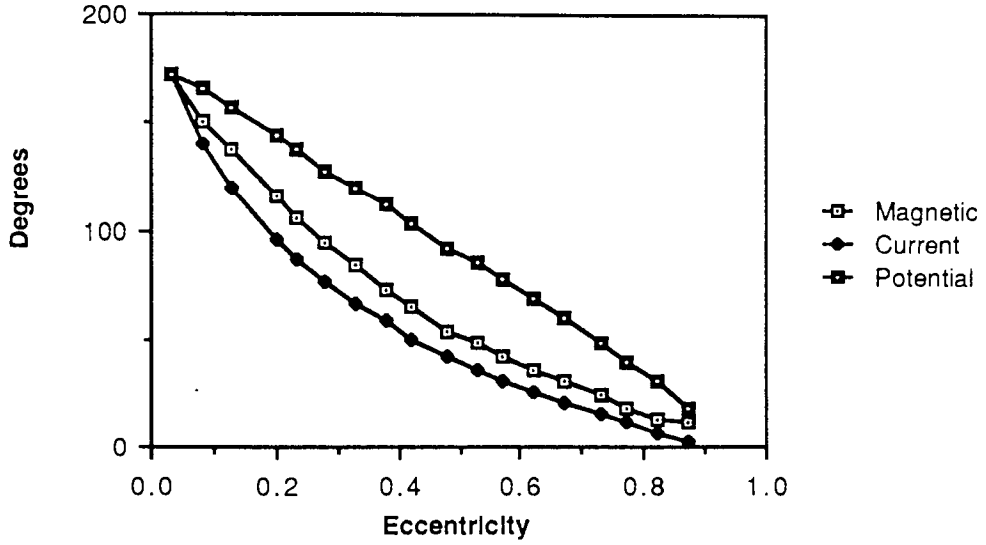

Fig 4.3 Plot of the angular distance on the scalp between the peak and trough of the potential, SCD and magnetic field generated by a tangential dipole according to the eccentricity of the dipole.

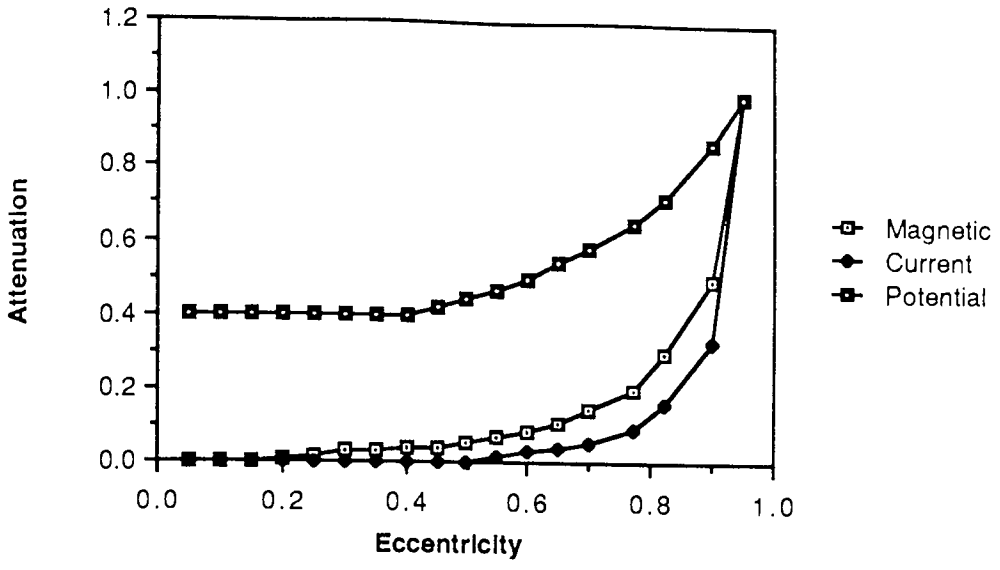

Fig 4.4 Plot of the maximum value of the peak generated by a tangential dipole (normalised with respect to the dipole of eccentricity 0.87) according to the eccentricity of the dipole. Both plots after Pernier, Perrin and Bertrand (1988).

Source derivation of the cortical activity to pattern onset stimulation has been extensively studied by Srebro (1985, 1990). The source derivation was first recorded from fourteen electrode locations, transversely from Pz to the inion and medially from T5 to T6 (Srebro 1985). The source derivation procedure was stated to be relatively insensitive to dipoles located in a tangential orientation. The stimulus used was located in octants and the annuli of octants. Lower half field stimuli activated cortex on the convexity of the occipital lobe contralateral to the stimuli. The more peripheral the stimulus the more rostral was the location of the active cortex, see fig 4.5. Upper half field stimuli evoked activity on the extreme caudal pole, the amplitude being weaker than that from the lower half field, this was presumed to be due to the dipole being located more tangentially.

Posterior pole and/or inferior temporal lobe activity was frequently recorded. This activity often predominated in the upper half field responses, and did not lateralise in relation to the stimulus position. For 7/10 subjects recorded with upper half field stimulation activity was seen from the left or right parietal lobe, for the remaining, activity was derived from activation in the left or right temporal lobe. The responses appeared to be more laterally located for upper central as opposed to upper peripheral stimulation. The figure shows the location of the activity after pattern onset stimulation of central and peripheral octants of a 12° field.

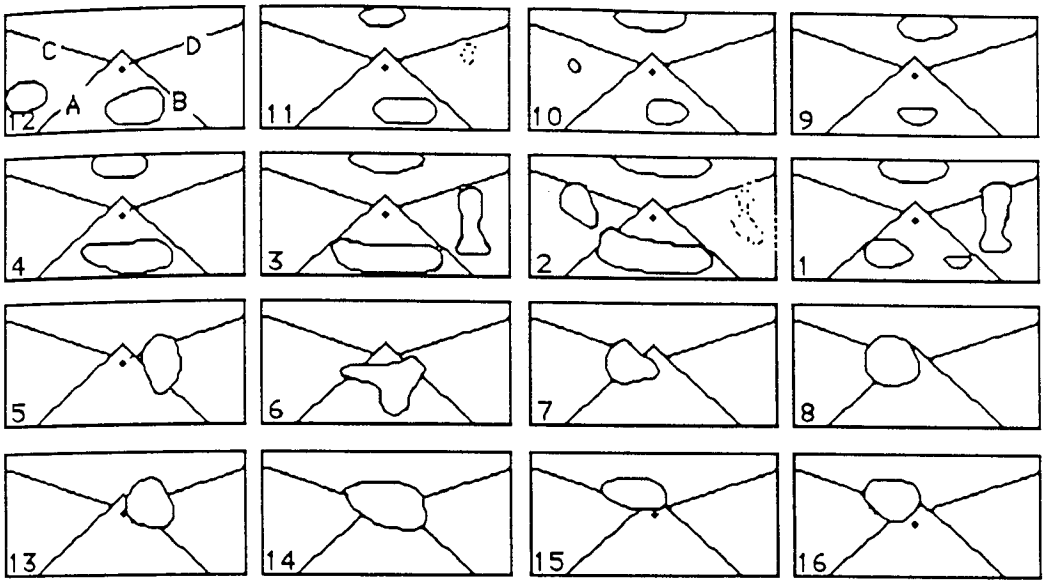

Fig 4.5 The areas of maximum cortical activity after stimulation of various parts of the visual field. The numbers correspond position of the octant starting foveally in the left upper horizontal and rotating anticlockwise. Each map is a Mercator projection with the equator through the cross. The vertical extent of each map is 10.9cm and the horizontal extent at the equator is 20.6cm. Cortical landmarks (accuracy +/- 1cm): A, left occipital-temporal lobe border; B, right occipital-temporal lobe border; C, left temporal-parietal lobe border; D, right temporal-parietal lobe border. After Srebro (1985).

Srebro and Purdy (1990) placed 98 electrodes over the occipital area, with an interelectrode spacing of 2 cm, to achieve good resolution. From these a Laplacian derivation of 44 electrode points was calculated. The stimulus reported on was a central semicircle of 0-1° radius presented in the left and right half fields. The VEP information was correlated with information obtained from CT and MRI scan of the two subjects involved. The first subject gave contralateral activity near the occipital pole for the RHF and bilateral activity for the LHF stimulation, the reverse was observed for the second subject. The evoked potential activity was again observed in the superior parietal lobule for one subject, and the middle and superior temporal lobule for both. The active regions found in the CT and MRI appeared to be too large to just represent the striate cortex, however spread due to passive electrical deconvolution could not be ruled out. The Laplacian derivation may still not localise sufficiently for accurate source positioning.

4.8.2 Global Field Power

Global field power is computed as the root mean square of the potential differences between all possible electrode pairs. This value objectively indicates the overall level of the scalp activity as a functon of time. The principal is to consider all possible potential differences in the montage with equal weight and thus compute the reference free mean potential difference at each moment in time.by using the equation:

$$GFP(\text{reference free}) = \sqrt{(1/2n)} * \sum_{i=1}^{n} \sum_{j=1}^{n} (u_i - u_j)$$

where n = the number of electrodes measuring the potentials e_i and e_j; i, j = 1....n, the observed voltages are $u_i = e_i - e_{\text{common reference}}$.

The meaningful computation of the electric field power is based on electrodes approximately equidistantly spaced over a reasonably large area of the scalp. The maxima of the field power reflects the time during which the scalp field had pronounced peaks and troughs and the minima indicate times during which the scalp field had a generally flat appearance, showing only a few field lines and shallow gradients. The maxima of the field power has been proposed to represent the maximal activity of the neural populations. When the latency of the maximal field power has been computed then the distribution of the potential at that latency gives the location of the source. In each map there is a maximal and minimal field value and the neural generator will have a net orientation along a line which connects these two points. Different distributions are caused by different sources but identical fields may or maynot be the result of the same source.

4.8.3 Principal Component Analysis

Principal component analysis (PCA) computes the number of components that are necessary to account for the recorded distribution. The number of principal components active gives a good indication of the number of active dipoles. PCA in itself does not neccesarily produce physiologically meaningful components however, because the components are by definition uncorrelated. To transform the orthogonal principal components into meaningful physiological components the

hypothesis that the sources are the result of a single current dipole is implemented (Maier et al 1987).

Skrandies and Lehmann (1982) computed the global field power from stimulation of the lateral,13° and 26°, and upper and lower, 13°, half fields. Forty five channels were recorded from and principal component analysis (PCA) was then performed on the global field data. The field power defined two components with a mean latency of 105.8ms (+/-4.1) and 145.1ms (+/-11.3). PCA at these latencies revealed three underlying spatial principal components. Component one showed antero-posterior scalp distribution differences with extreme values over the occiput surrounded by steep gradients. The second component mainly displayed lateral differences and the third component had a concentric distribution with a maximum at parietal sites. The scores of the various components defined their contribution to the observed distribution of the potential field. Component two was identified as a lateralisation component. This component displayed a significant interaction between size and retinal location of the stimulus with large stimuli showing a more pronounced lateralisation over the hemisphere ipsilateral to the half field stimulated. Stimulating the central 2° and an annuli of 2-4° with flash, pattern onset, pattern reversal, motion and a grid pattern Maier et al (1987) investigated the location of the principal components of the response. Twenty four electrode were placed over the occipital area. To locate the dipole sources a model of a current dipole source, in a three shell model head, was developed, dipole approximation was performed after principal component analysis (PCA). For luminance high frequency flicker stimuli sources were located in the striate area, for both central and peripheral stimulation see table 4.1. Pattern onset was then investigated, with both central and peripheral stimuli in the left half field. The check size used varied with the area stimulated; for central stimulation they were 12' and for the periphery they were 32'. PCA gave two components for pattern onset, PC1 consisted of a positive peak (CI) and was followed 30ms later by a negative peak. When moving from central to peripheral these components were still present. The apparent contralateral maximum of PC1 shifted about 3cm upward when changing from central to peripheral stimulation. The equipotential maps of PC2 matched those of the luminance maps. The components were located in the striate area for PC2 and in area 18 for PC1. Pattern disappearance yielded a larger PC2 but apart from this was, in many ways similar to the pattern onset response, see table 4.1.

	≈	Ø	*f*	rad%	tan%	∂	amp	err%
Area 17 centre								
Luminance Flicker	0.0	1.9	.67	43	57	-112.8	0.16	5
Pattern onset PC2	14.9	-7.8	0.69	35	65	-125.2	3.6	2
Grid onset	33.5	-13.7	0.37	23	77	-145.8	4.3	1
Pattern offset	-1.9	-6.1	0.42	83	17	-126.6	2.1	2
Reversal	12.5	-2.2	0.59	47	53	-162.5	1.7	7
Motion onset	6.7	-20.9	0.36	60	40	154.4	2.7	1
Area 17 periphery								
Luminance Flicker	-5.8	1.3	0.61	14	86	-159.6	0.07	3
Pattern onset	-12.0	5.2	0.76	9	91	-154.5	1.9	10
Area 18 centre								
Pattern onset	38.4	8.2	0.57	30	70	-97.2	4.3	2
Pattern offset	37.3	-2.2	0.69	79	21	159.4	1.4	3
Reversal	30.0	1.0	0.79	36	64	-5.5	0.8	3
Area 18 periphery								
Pattern onset PC1	24.1	3.8	0.68	82	18	-27.7	3.0	2

Table 4.1. Positions (≈,Ø and depth *f*), orientations (radial and tangential percentages, rad% and tan % and the tangential direction ∂) and the amplitudes (in μVcm^2) of the dipoles computed from the equipotential maps of the prinicipal components. The last column gives the error of the fit, as calculated from the sum of the squares of the normalised differences between measured and computed potentials in the 24 electrodes. After Maier, Dagnelie, Skekreijse and Van Dijk (1987).

Pattern reversal central stimulation gave a similar picture with a large area 17 component (PC2) and a much weaker PC1. The location of the maximum for PC1 was more lateral over the contralateral hemisphere, and slightly higher than PC2. PC2 for pattern reversal was maximal around the midline. A single component was found to account for the activity after stimulation with a grid pattern, resembling the PC2 found in the onset response. One component could also describe the map to the motion stimuli and this was also found to have a clear area 17 origin.

Ossenblok and Spekreijse (1991) have also investigated the cortical origins of the pattern onset response. For large check stimuli two components were required to account for the variance in the response. The two components did overlap but the first was found to dominate the peak CI and the second the third peak CIII. Each component corresponded to a dipolar source and both were found to originate in the extrastriate visual cortex. Table 4.2 describes the dipole positions for the two

principal components after various field stimulation. Lower quadrant dipoles of C1 were mainly radial and dominated the half field response, in contrast the upper quadrant source was mainly tangential.

Position of Field Stimulated	Dipole positions for Component one	Dipole positions for Component three
Lateral half fields	Dipole mainly radial and located contralaterally. Potential distribution maximum positive contralateral.	Dipole mainly tangential and located contralaterally, not as deep as C1. Potential distribution positive ipsilateral and negative contralateral.
Quarter fields	Lower quadrant dipole shifted further from the midline compared with the half field but still mainly radial. Upper dipole mainly tangential, closer to the midline, deeper and lower.	Similar position and orientation for both upper and lower quadrants. All located contralaterally and at same depth, slightly deeper than lower quadrant C1 but shallower than upper quadrant C1 and half field C1.
Octants	Stimuli near the horizontal meridian did not reverse in polarity. Lower octants mainly radial and upper octants mainly tangential. Orientations of dipoles from vertical octants were similar, both directed inferiorly. Horizontal octants gave dipoles directed away from the midline toward the contralateral side. Upper octants' dipoles were located deeper in the model, the upper horizontal giving the deepest source.	All octants resulted in similar dipole positions, mainly tangential and clearly contralateral. No change in dipole direction or potential distribution with changes in stimulus position. Dipoles were directed away from the midline toward the contralateral side. Lower octants' dipoles located slightly deeper, lower horizontal gave the deepest dipole.

Table 4.2. The location of the equivalent dipole sources of the principal components found after stimulation of different regions of the visual field with a pattern onset stimulus. After Ossenblok and Spekreijse (1991).

The early dipole is suggested to originate from activation of area 18 as the dipole position from octant stimulation appeared to follow the spherical surface of the extrastriate cortex. Upper quadrant and octant stimulation were shown to result from deeper dipoles, this is in contrast to results of Ahlfors et al (1991) who, recording magnetic fields showed that deeper dipolar sources accounted for the lower octant responses. The dipole sources for C3 appeared to remain stationary with different field stimuli, the source was therefore presumed to be located in area 19 as each area within this area represents the whole hemiretinal projections.

Without dipole location procedures, Drasdo (1980) postulated that the early wave, CI from pattern onset originated in area 18 and 19 when large checks were used and moved towards the striate area when very small checks were used. The disappearance of CI on the midline with large target stimulation was suggested to be due to the overlap of CI by an earlier component, CO. With patterns of fine lines and checks the wave CII appeared to coincide with a generator in the striate area. In addition Lesevre and Joseph, (1979) without dipole location procedures, hypothesised that the generators for P90 (CI) could be located in area 19. The succeeding two peaks CII and CIII were thought to originate in area 18.

4.8.4 Dipole Source Localisation of Evoked Potential Activity

The sources of the flash evoked potential have been investigated by computing the dipole that gave a best fit topographical distribution to that recorded over the scalp (Henderson, Butler and Glass 1975). The head was modelled by a homogeneous conducting sphere. The dipole calculated from the recorded potential at 128ms was consistent with a generator located in the striate cortex, the depth of the dipole was calculated to be approximately 3.8cm.

Evoked potential data to pattern onset stimulation has also been modelled with a single dipole located in homogeneous sphere (Sencaj and Aunon 1982, Darcey 1980, 1981, Butler et al 1985). All authors have investigated the response to half and quadrant fields. Sencaj and Aunon (1982) recorded the potential from six channels over the occipital cortex, referred to linked ears. The dipoles were calculated from the potentials recorded at latencies of 80, 100 and 120ms. Dipole locations were compared from single and averaged evoked potentials, single sweep data appeared to produce dipoles that were not as lateral or anterior. The averaged data after upper and lower half field stimulation resulted in dipoles that were located in approximately the same area but with a polarity reversal. Left upper and lower quadrant dipoles were located in the same area however the dipoles for right upper and lower quadrants were more displaced with respect to one another. The upper right quadrant gave a lower, more laterally placed dipole.

The pattern onset response, to a red checkerboard, has been investigated by Darcey (1980, 1981). The stimulus was located in central 10° area, stimulation consisted of full field and the constituent half and quadrant fields. The distribution was recorded from 40 channels located from an equiangular matrix and referred to an average reference. The matrix covered an area from 15° below the inion to 135° above, and

from 75° to the left and right of the midline. The components of the response were located at the occurence of maximum field power. The dipoles were calculated for two components, one occuring at 92 +/-4 ms and the other between 120-160ms. The evoked potential distributions of the half and full field appeared to be predictable from superimposition of the distribution from the constituent areas. The dipole locations were calculated using the forward method, see fig.4.6. The first component gave sources in the occipital area near the midline, the dipoles appeared to be quite lateralised, more so for upper than lower quadrant stimulation. The second components' dipoles were contralateral and bilateral when predicted and were, in most cases located in the same location as the first component but rotated through 180°.

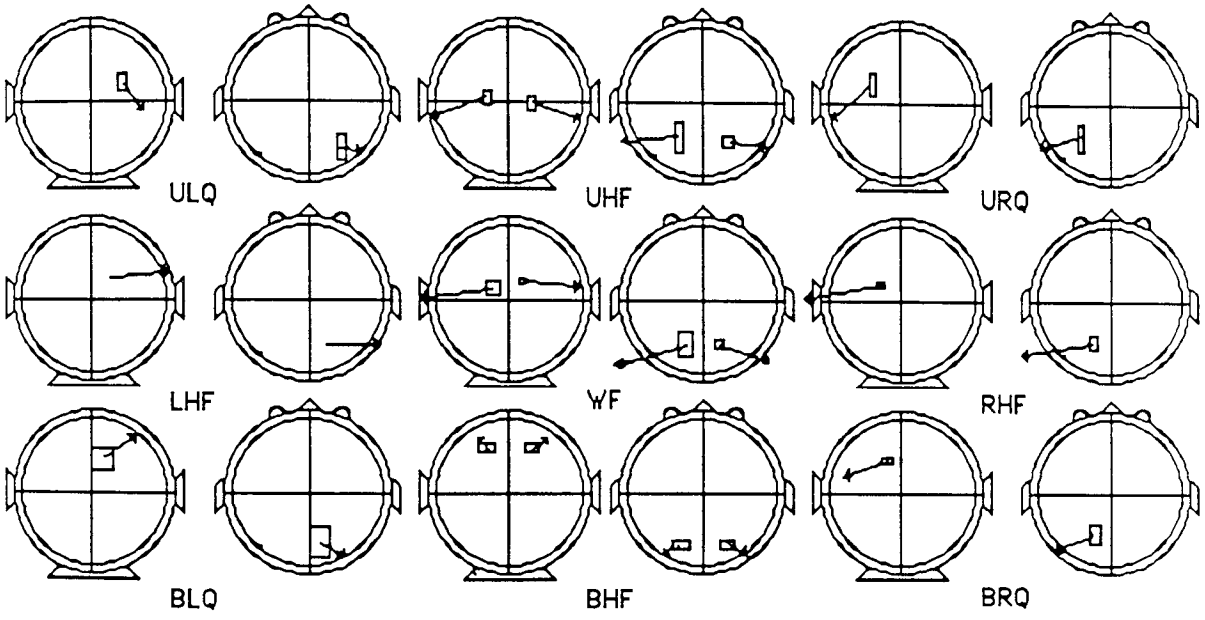

Fig 4.6 The positions of the calculated dipoles after pattern onset stimulation of various fields. ULQ; upper left quadrant, UHF; upper half field, URQ; upper right quadrant, LHF; left half field, WF; whole field, RHF; right half field, BLQ; bottom left quadrant, BHF; bottom half field, BRQ; bottom right quadrant. The left views show the source as seen from above and the right views show the source as viewed from the vertex. The inner circle denotes the inner surface of the model skull. After Darcey, Ary and Fender (1980).

Butler et al (1985) using the forward method of dipole localisation investigated the sources of the pattern onset response to stimulation of foveal quadrants, half fields and peripheral octants. The dipole orientation was found to rotate through 135° when upper and lower field stimulation were compared. The orientations of the dipoles to peripheral stimulation would predict that generation of the potential is by surface negative cortex. The foveal sources elicited dipoles situated lateral to the midline and contralateral to the field of stimulation. In foveal quadrant stimulation there was a tendency for the dipole to be located lower for the upper field

stimulation, as would be predicted. Jeffreys and Axford (1972) observed that the amplitude of the pattern onset initial negative was mainly dependent on stimulation of the peripheral section of each quadrant.

Early investigations, as to the proposed site of generation of the pattern onset and pattern reversal response, postulated that the PR response was generated by surface positive cortex in the extrastriate areas (Halliday and Michael 1977) and the PO response was generated by surface negative cortex in the striate cortex. The major problem with the generation of the PO in surface negative cortex was experienced with foveal stimulation where the initial component, CI, was positive (Butler et al 1987, Drasdo 1980).

Lehmann, Darcey and Skrandies (1982) recorded the pattern reversal response from 45 channels over the occipital area. Stimuli were located in the left, right, upper and lower half fields. The total field sizes used were 13° and 26°, the dipoles for the 13° field were oriented more radially than those from the 26° targets, see fig.4.7. The upper and lower dipoles appeared to be located along the midline with the upper field dipole being located more posteriorly.

Intracerebral recordings were also performed on two subjects. Left and right half field stimulation supported the concept of an occipital generator process for the dominant positive component. Lower and upper half field stimulation gave current densities above and below the level of the calcarine fissure respectively. They suggested the extrastriate area as the generator for the reversal response as this could explain the component distribution from upper and lower as well as lateral half fields.

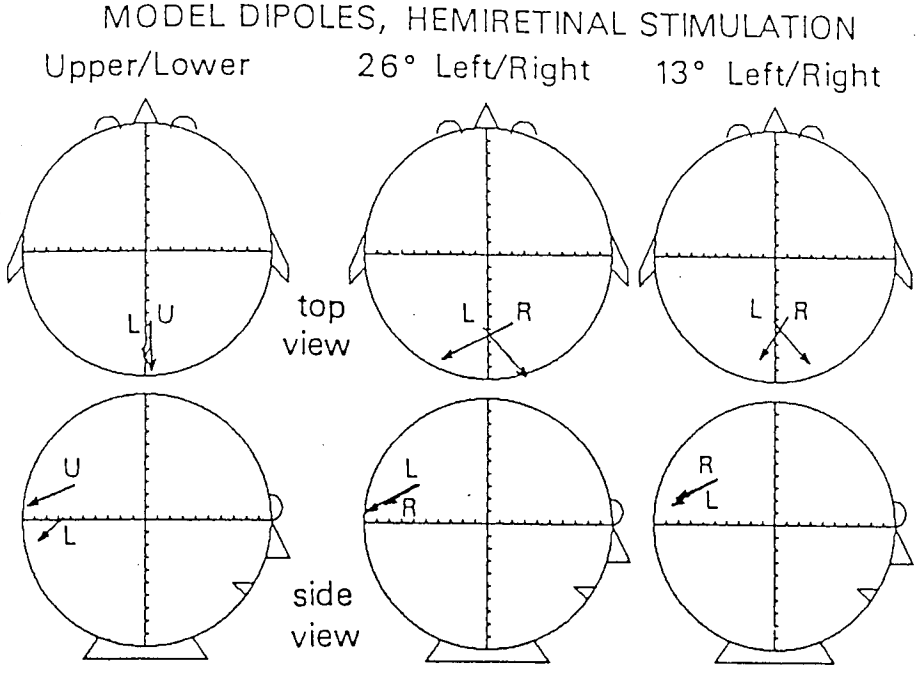

Fig.4.7 Equivalent dipole model generators (arrows) computed for the best fit at times of maximal field power of the upper, lower, left and right half retinae.Origins of the arrows give the locations of the dipoles; lengths of the arrows indicate dipole magnitudes, arrowheads indicate the positive side of the dipoles. After Lehmann, Darcey and Skrandies (1982).

4.8.5 Spatial Deconvolution

This combines information about the estimated volume conductive properties of the head with multichannel surface potential data to obtain the estimates of either cortical source activity or cortical surface potential (Nunez 1988). It is well known that there is no unique source distribution for any given surface potential distribution however, it is not quite so well appreciated that a unique relationship does exist between scalp potential and cortical surface potential, provided that there are no sources between the surfaces. The principle spatial deconvolution is based on the latter relationship. The theoretical potential difference between two locations on the surface of a three sphere model due to N radial dipoles sources in the inner sphere (cortex) can be calculated. There is still uncertainty in the sensitivity of the method because of the use of the volume conductor model of the head which does not take into account local variations due to skull thickness and changes in conductivity (Nunez 1988).

CHAPTER 5

Investigation of the Distribution of the Pattern Reversal Response to Various Field Locations.

5.1 Introduction

Previous research has investigated the distribution of the evoked response to various field locations however, most work has looked at the distribution of the pattern onset response, limited work with brain mapping and a pattern reversal stimulus has been attempted. The most likely origin of the response in the visual cortex has been postulated following the aquisition of the response distribution. Methods have also been developed to highlight the sources e.g. source derivation and principal component analysis (Hjorth 1975, Ossenblok and Spekreijse 1991).

Edwards (1989) investigated the pattern reversal response to M scaled targets in the left half foveal/parafoveal field. The stimuli were developed to activate just $1cm^2$ of the surface of a single gyri, if only the surface of the gyri is stimulated then the response should be of large amplitude and well localised. The response distributions were found to vary greatly between the subjects, this was thought to be due to the generator lying either in a fissure or on a gyral surface.

5.2 Method

The distribution of the pattern reversal response is localised over the occiput, a close array of electrodes over the occipital area was therefore selected. Various montages have previously been employed for the location of closely spaced electrodes. Inappropriately large interelectrode spacing may lead to significant errors of localisation and erroneous measurements of amplitudes due to aliasing (Spitzer et al 1989). The optimal electrode spacing can be computed using the Nyquist limit theorum. The Nyquist distance will vary for different cerebral evoked potentials however, Spitzer et al determined the minimum distance for SEPs to be less than 3cm. A grid spacing of 2-3 cm has also been advised for EEG localisation (Van Dijk and Spekreijse 1990).

Many groups have used a cm spacing with no consideration of the size of the subjects head (Srebro 1985, Kuriowa, Celesia and Tohgi 1987, Abe and Kuriowa

1989, Celesia, Meredith and Pluff 1983, Cobb and Morton 1970, Hoeppner, Bergen and Morell 1984, Yiannakis and Walsh 1983, Lehmann, Kavanagh and Fender 1979) whereas other groups have advocated placing the electrodes between the standard electrode positions of the 10-20 system (Thickbroom, Mastaglia and Carroll 1984) or displacing some of the 10-20 positions posteriorly (Butler et al 1987). Other reports have used a chain of electrodes in either a cm spacing (Halliday and coworkers, Haimovic and Pedley 1982, Fukui, Kato and Kuriowa 1986, Adachi-Usami and Lehmann 1983) or a percentage system (Flanagan 1985, 1986, Haimovic and Pedley 1982, Shagass, Amadeo and Roemer 1976, Rugg et al 1985, Harding, Smith and Smith 1980). The Queens square system advocated by Halliday and co-workers has been shown to produce more variance in the location of the electrodes with respect to the cortical structures than the 10-20 system (Myslobodsky 1990). The 10-20 system developed by Jasper (1958) locates the electrodes with a spacing of 10 and 20 percent of the nasion-inion distance and the half head circumference. Equiangular spacing conforming to the sphere best fitting the posterior two thirds of the subjects head (Darcey, Ary and Fender 1980) , and percentage systems not based on the 10-20 system have also been employed (Edwards 1989). Lehmann and Skrandies (1977, 1982) have looked extensively at the distribution of the pattern reversal visual evoked potential. For detailed mapping studies 45 electrodes were symmetrically positioned over the scalp from 30% of the nasion-inion distance above the nasion to 3.5cm below the inion and covered 70% of the distance between the two meati acousti externi with "roughly equidistant electrode spacing". It is not clear as to whether a percentage system has been used.

5.2.1 Montage Selection

Initially a montage based on the 10-20 system was adopted this used the electrode positions of O1, Oz, O2, Pz, P3, P4. The remaining electrode points were positioned in between the standard placements. Difficulties arose in the location of the posterior electrode points over the inion and neck line as the standard placements were sparse. In addition due to the fact that positions P3 and P4 were required the whole 10-20 montage had to be marked. This lead to an increase in the preparation time, which was already long. This montage was compared to a coordinate system of Drasdo and Furlong (1988),the percentage sytem method of marking electrode positions proved to be much easier and faster than the previous described montage, this was therefore employed for the rest of the study.

The coordinate system developed by Drasdo and Furlong (1988) takes into consideration the curvature of the scalp (fig.5.1). It is a percentage system, and for visual studies a projection with a vertical polar axis is used, the vertex defined by the 10-20 system is the pole. This position is first marked on the scalp, a baseplane containing the inion and the nasion is then visualised. The nasion to inion distance, through the vertex, and the half head circumference are measured. The centre of the montage lies along the vertex to the inion, the spacing to the left and right was 10% of the half head circumference and the spacing in the vertical direction was 10% of the nasion to inion distance. Some distortion was evident at increasing distances from the inion, but this did not exceed +/-10% of the montage and was only experienced in the horizontal direction. Any point on the montage can be given a grid reference if desired.

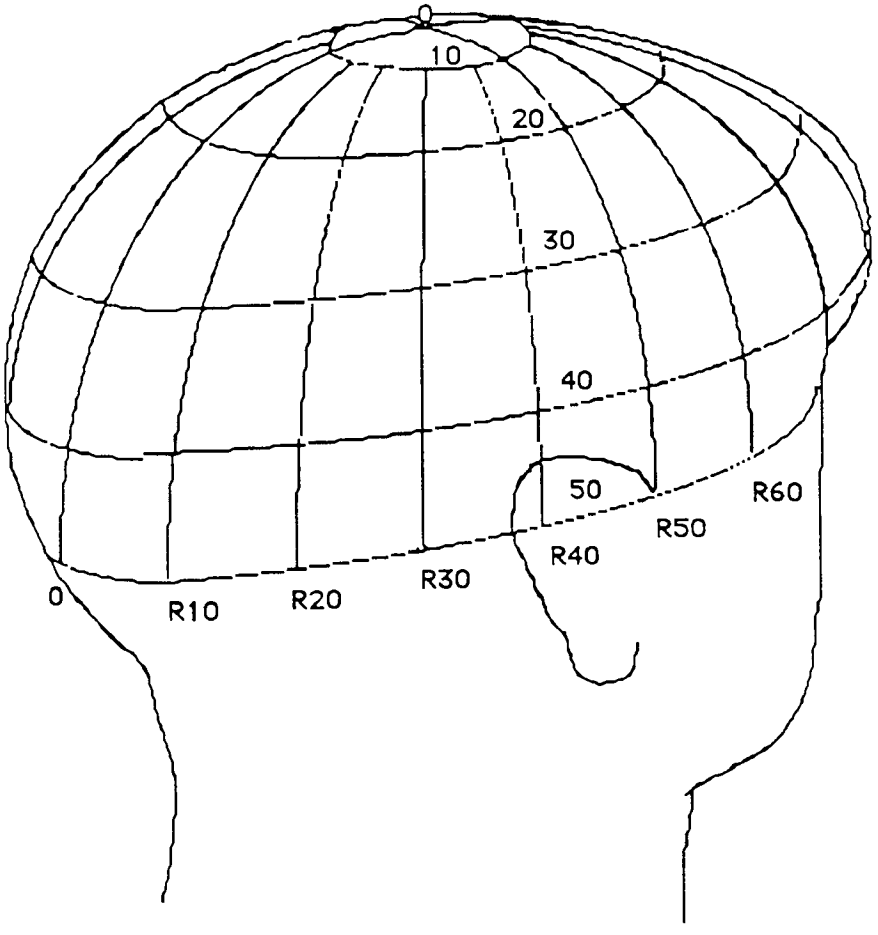

Fig 5.1. The coordinate system mapped by a cylindrical projection providing a rectangular graticule with minimal distortion for the occipital cortex. The grid reference system is illustrated. After Drasdo and Furlong (1988).

It was decided to use the percentage grid centred around the Oz electrode. An advantage of using a percentage system is that group maps can be computed as the recording electrodes should be positioned over the same relative region for all the subjects.

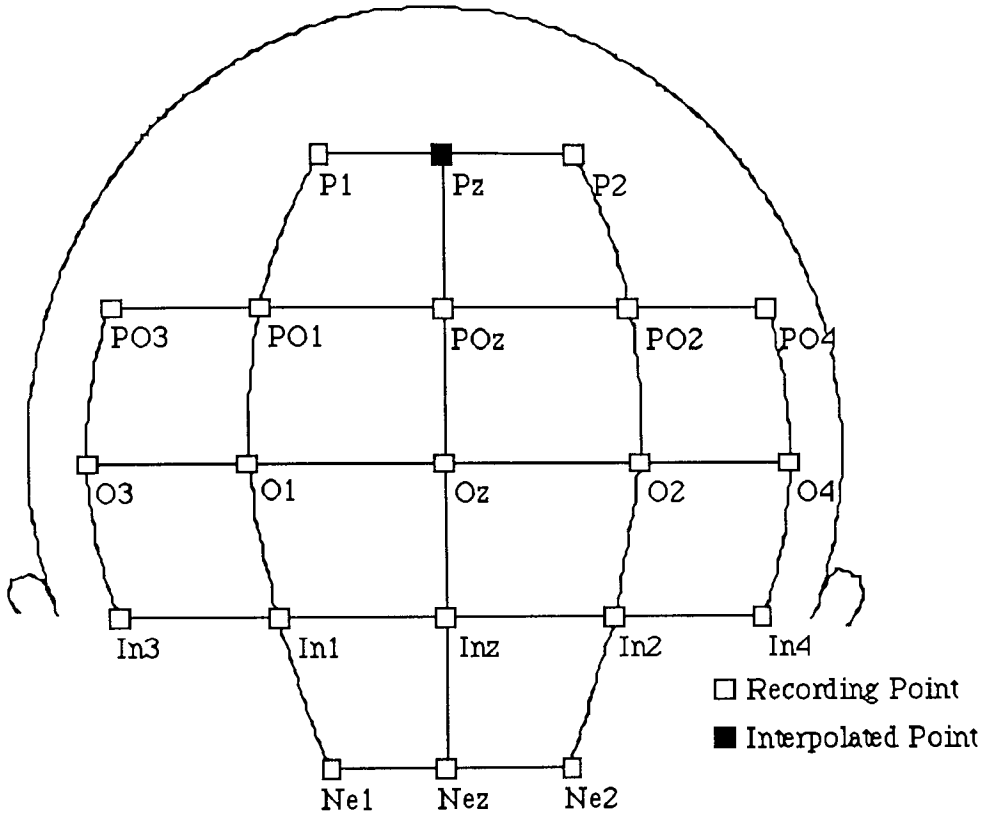

Fig 5.2 Montage of electrode placement used in the study.

An Fz reference was chosen as this has been most widely used in previous studies of this type (Edwards 1989, Flanagan 1987, Halliday and co-workers 1970, 1977, 1979). Non cephalic references rely on the patient being as supine as possible, so making pattern stimulation impractical (Hobley 1987). Average reference although useful for whole head recordings is impractical for electrodes located in a tightly spaced array over a limited area of the cortex as all the responses may not sum to zero. Other references such as linked ears lead to ambiguities when looking at lateralisation of the response (Nunez 1981).

Twenty one silver-silver chloride electrodes were placed over the occipital area. Before the electrodes were positioned the scalp surface was gently abraded with

Omniprep™. The electrodes were then attached with blenderm™ tape, or glue if required and the electrode impedence was maintained below 5KΩ.

Responses were recorded on a Biologic Brain Atlas III mapping system. The amplifiers were set to a gain of 30,000, the filters used were high pass 1Hz and low pass 30Hz (3dB down point and 12dB/octave roll off). The time window was set at 512ms and the response was recorded with 256 data points, giving a sampling rate of 2ms The sampling rate must be high enough to faithfully record fast transients in the waveform but must also be low enough to avoid saturating the storage capacity of the computer. Aliasing may arise if a signal containing high frequencies is sampled at too low a rate, the high frequencies will then generate spurious low frequency signals. A good general rule of thumb is that the sampling rate should be at least three times the high frequency end of the bandpass (Coburn and Moreno 1988). An internal callibration had to be performed before recording could commence; a 100μV square wave signal was passed through each amplifier and a measurement of the issuing voltage and DC offset were shown, this procedure could be repeated until the amplifiers were all similar. Fifty responses were recorded for each stimulus presentation, and each stimulus was presented at least twice. Once the response had been recorded it was stored on disc for subsequent analysis.

The data is presented as equipotential maps, the values of the potential between the recording positions is interpolated by a four nearest neighbours linear interpolation procedure. The Biologic Brain Atlas III mapping system has an inkjet printer but for presentation in this thesis thermal printouts from a Nicolet Pathfinder II™ have been used. The voltage amplitudes (peak to baseline) were inputed into the Pathfinder II™ mapping software and maps were calculated employing the same linear interpolation procedure as the Biologic Brain Atlas III mapping system.

Group responses can be presented as either mean maps or mean waveform maps. A group mean map is the average of the maps of the maximum reponse of each subject at a specific latency whereas the group mean waveform maps are maps taken from the average waveform of the whole 512ms for all the subjects. The distribution of the group mean waveform map may be affected by peak latency variation between subjects.

Monocular stimulation was chosen due to the fact that if employed clinically and one eye is defective the normal eye can act as control. Monocular right eye stimulation was chosen for all the studies unless otherwise stated.

The check size used was fixed at 27' for all the stimuli and is used clinically in the department, the overall luminance was 1050 cd/m^2 and the contrast was 80%. Field sizes used were full field 20° and lateral half fields of 0-10°. Central scotomata of 4° and 7°s and full fields of 4° and 7°s were also used. The area covered by 4° is approximately 15cm^2, the area covered by 7° is 3X this and that covered by the 20° full field is 25X. A 7° scotoma was chosen so that a response should still be present but, mostly due to the stimulation of the area surrounding the fovea. It has been shown that the P100 is increasingly attenuated and eventually abolished with increasing central scotoma sizes of upto 10° (Halliday 1979).

The potential distribution is presented as maps at the position of the major peaks in the response. Group mean waveform maps and group mean maps were constructed from the data from 12 subjects with an age range 22-55 years, all with 6/6 acuity wearing corrections if necessary.

5.3 Results

5.3.1 Group Mean Maps Compared With Group Mean Waveform Maps.

Group mean waveforms were computed for all subjects and stimuli, see fig 5.3 - 5.5, 5.10-5.13, and from these, maps of the topogaphical distributions at the latencies of the major peak components were constructed. Group mean maps were also computed from all subjects that showed a specific component with the stimuli. As a result group mean maps were not necessarily composed of maps from all subjects. Both the group mean maps and group mean waveforms are discussed.

Figure 5.3. Group mean waveform of the response following full field pattern reversal stimulation. The position of the recording electrode is indicated to the left of the waveform. The maximum positive peak is cursored.

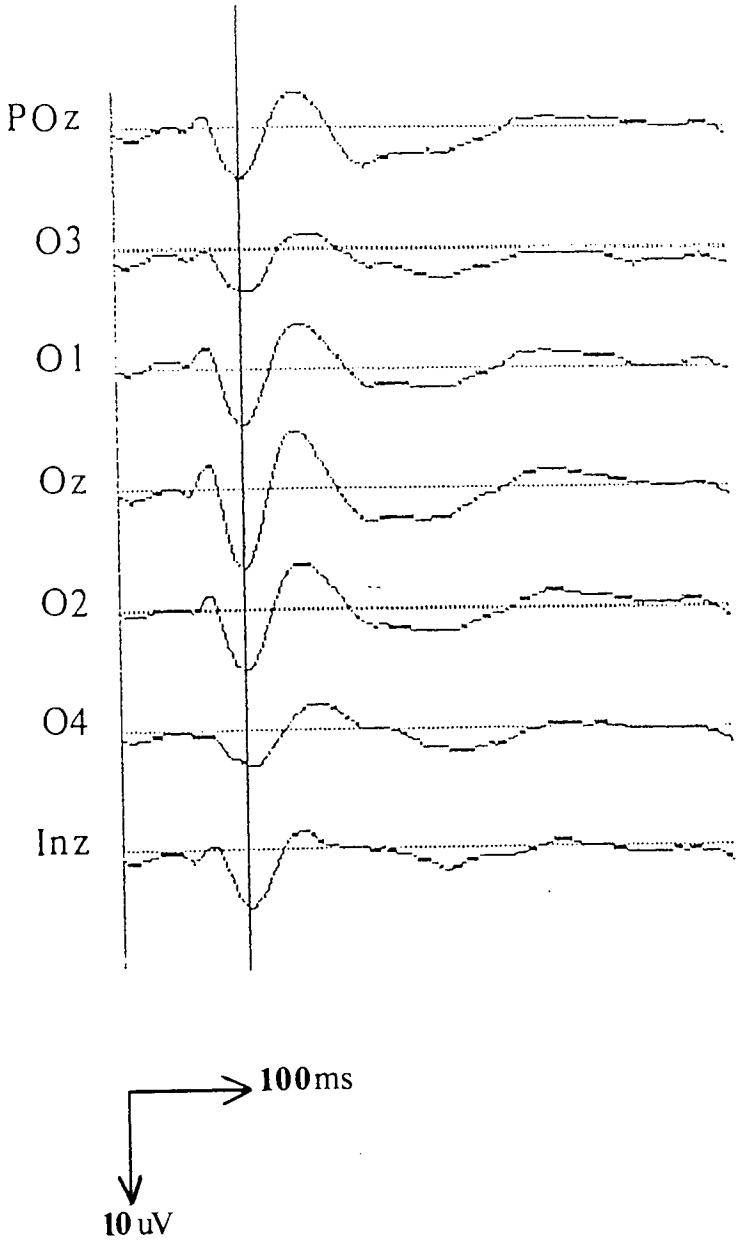
POz
O3
O1
Oz
O2
O4
Inz
100ms
10uV

Figure 5.4. Group mean waveform of the response following right half field pattern reversal stimulation. The position of the recording electrode is indicated to the left of the waveform. The maximum positive peak is cursored.

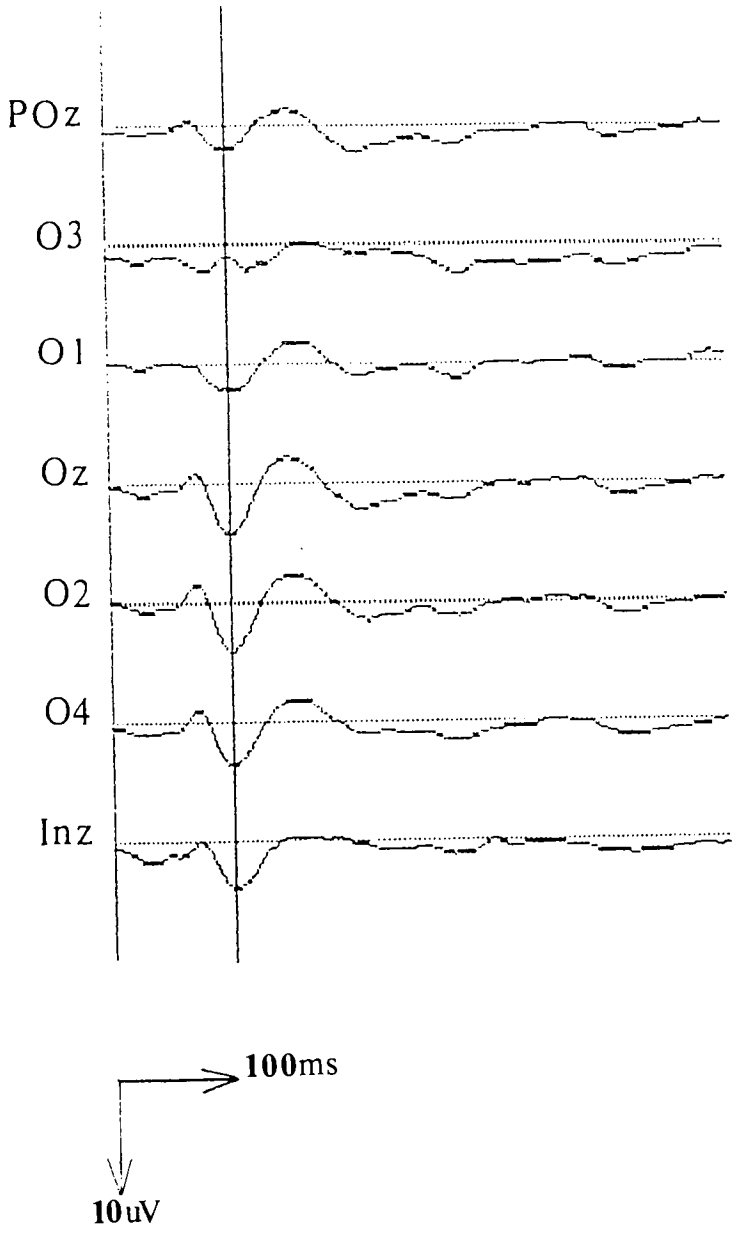
POz
O3
O1
Oz
O2
O4
Inz
100ms
10uV

Figure 5.5. Group mean waveform of the response following left half field pattern reversal stimulation. The position of the recording electrode is indicated to the left of the waveform. The maximum positive peak is cursored.

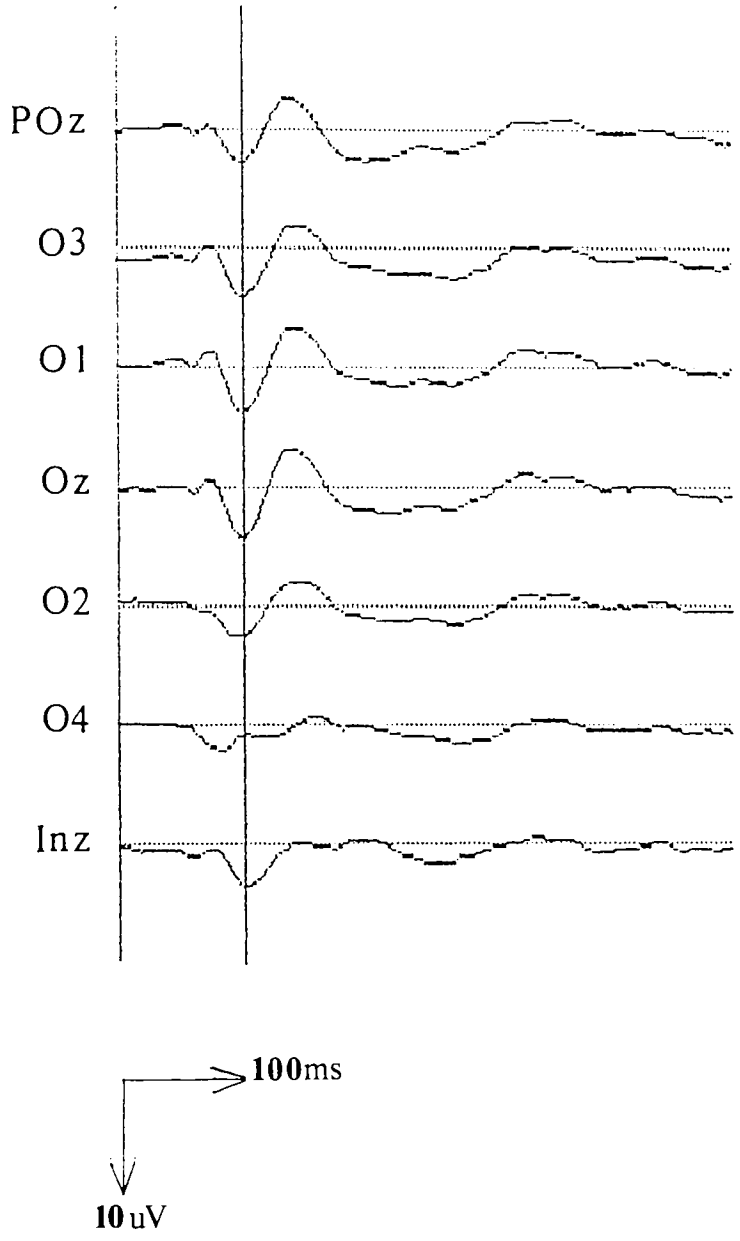
POz
O3
O1
Oz
O2
O4
Inz
100ms
10uV

Field	N75	P80	P100	N105	P120	N145
FF	12subjects	----------	12subjects	----------	3 subjects	12subjects
RHF	12subjects	5 subjects	12subjects	2 subjects	4 subjects	12subjects
LHF	12subjects	7 subjects	12subjects	4 subjects	5 subjects	12subjects
FF4°	10subjects	----------	12subjects	----------	1 subject	12subjects
FF7°	10subjects	3 subjects	12subjects	----------	3 subjects	12subjects
CS4°	10subjects	5 subjects	12subjects	----------	7 subjects	12subjects
CS7°	11subjects	5 subjects	12subjects	----------	7 subjects	12subjects

Table 5.1 The Number of Subjects Producing the Different Components of the Pattern Reversal Response to Various Stimuli.

Field	N75	P80	P100	N105	P120	N145
FF	CE	----------	CE	----------	CE	CE
RHF		C	I	C	C	I
LHF	I	C	I	C	C	I
FF4°	P over L	----------	CE	----------	P, CE	CE
FF7°	CE	----------	CE	----------	Over L	CE
CS4°	CE	----------	CE		CE	CE
CS7°	CE	Over R	CE		Over L	A, CE

Table 5.2 Location of the Maximum Potential From Group Mean Maps for the Individual Components. Legend; A=anterior, P=posterior, I=ipsilateral, C=contralateral, L=left, R=right, CE=central.

Field	Full	Right Half	Left Half
N75	76.17(3.01)	73.8(2.89)	77.4 (3.91)
P80		79.83(5.81)	82.89(4.59)
P100	103.5(6.56)	104 (7.77)	102.33(7.23)
N105		104.4(6.23)	103.43(4.58)
P120	116.0(2.0)	122.5(11.2)	122.(8.0)
N145	144.8(11.52)	149.5(15.0)	145.2(7.31)

Table 5.3 Group Mean and Standard Deviation, in Brackets, of the Peak Latencies (ms) Following Full and Lateral Half Field Stimulation.

Field	Full	Right Half	Left Half
N75 (ms)	-2.74(3.02)	-2.53(1.95)	-1.48(1.37)
P80		3.87(1.34)	3.54(1.41)
P100	8.98(2.11)	6.03(1.89)	5.99(1.92)
N105		-0.39(2.27)	-1.82(1.12)
P120	4.86(2.50)	3.39(1.85)	3.69(0.95)
N145	-6.84(3.02)	-4.66(2.25)	-4.22(1.95)

Table 5.4 Group Mean and Standard Deviation, in brackets, of the Peak to Baseline Amplitudes (μV) Following Full and Lateral Half Field Stimulation.

5.3.2 Morphology and Topographical Distributions of the Waveforms

5.3.2.i Full Field; Topographic Distribution from Group Mean Waveform

The initial peak was a negativity with a central slightly left lateralised response, a low amplitude positivity can be observed over the extremes of the montage, see fig

Figure 5.6. Topographic distribution of the major peaks in the group mean waveforms following full (FF) stimulation. Amplitude values are shown in the scale to the right of the maps (μV). Note the individual amplitude scale values for each map.

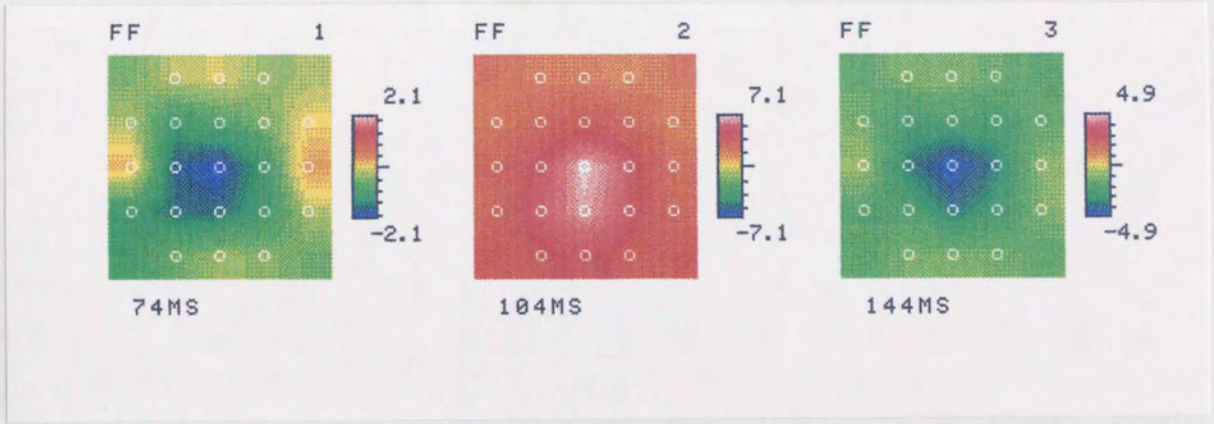
FF 1
2.1
-2.1
74MS
FF 2
7.1
-7.1
104MS
FF 3
4.9
-4.9
144MS

Figure 5.7. Topographic distribution of the major peaks of the group mean maps following full field (FF) stimulation. Key; EARLYN = early negativity, EARLYP = early positivity, LATEP = late positivity and LATEN = late negativity. Amplitude values are shown in the scale to the right of the maps (μV). Note the individual amplitude scale values for each map.

FF
1
2.1
-2.1
EARLYN
FF
2
8.3
-8.3
P100
FF
3
6.1
-6.1
LATEP
FF
4
6.3
-6.3
LATEN

5.6. The major positive deflection, P100, was maximal over the Oz line, this location is presumed to be over the middle of the band of intersubject variation of the level of the extension of the calcarine fissure, the intersubject variation extended from the inion to Oz, no-one produced a maximum higher than the Oz line. The succeeding negative component was also seen to be centrally distributed on the group mean waveform maps.

5.3.2.ii Morphological Variations Between Subjects

All subjects demonstrated an initial negativity with a mean latency of 76.4 +/-3.24ms. The next peak P100 showed a mean latency of 103.4 +/-6.67ms and was again present in all subjects. A later positivity was recorded in three subjects, this possessed a mean latency of 116 +/-2ms and was not evident in the group mean waveform maps. A group mean map of this component from the three subjects showed a positivity maximal over the central area of the montage, with a slightly more diffuse distribution than the preceeding P100, see fig 5.7. This was followed by a negativity recorded in all subjects with a mean latency of 143.6 +/-10.7ms. Individual latency and amplitude values are found in appendix table A.1.

5.3.2.iii Lateral Half Field Stimulation; Topographic Distribution from Group Mean Waveform

The first component was again a negativity distributed ipsilaterally with a contralateral positivity, see fig 5.8. The contralateral positivity reached its peak slightly later than the negativity. This was followed by the P100, being ipsilaterally distributed with no contralateral negativity visible on the map. In previous studies it was demonstrated that to produce nonparadoxical lateralisation the field size must be 0-2.5° i.e. the area of cortex stimulated must be located over the postero-lateral region (Harding, Smith and Smith 1980). As more of the periphery is stimulated the response tends to be located over the ipsilateral hemisphere. The sequence was completed by a late ipsilateral negativity present in all subjects. Individual latency and amplitude values are found in appendix table A.1.

5.3.2.iv Morphological Variations Between Subjects

5.3.2.iva Right Half Field

The initial component was a negativity present in 90% of the subjects with a mean peak latency of 74.22+/-2.90ms, this was maximally distributed ipsilaterally with a

Figure 5.8. Topographic distribution of the major peaks in the group mean waveforms following right (RHF) and left half field (LHF) stimulation. Amplitude values are shown in the scale to the right of the maps (μV). Note the individual amplitude scale values for each map.

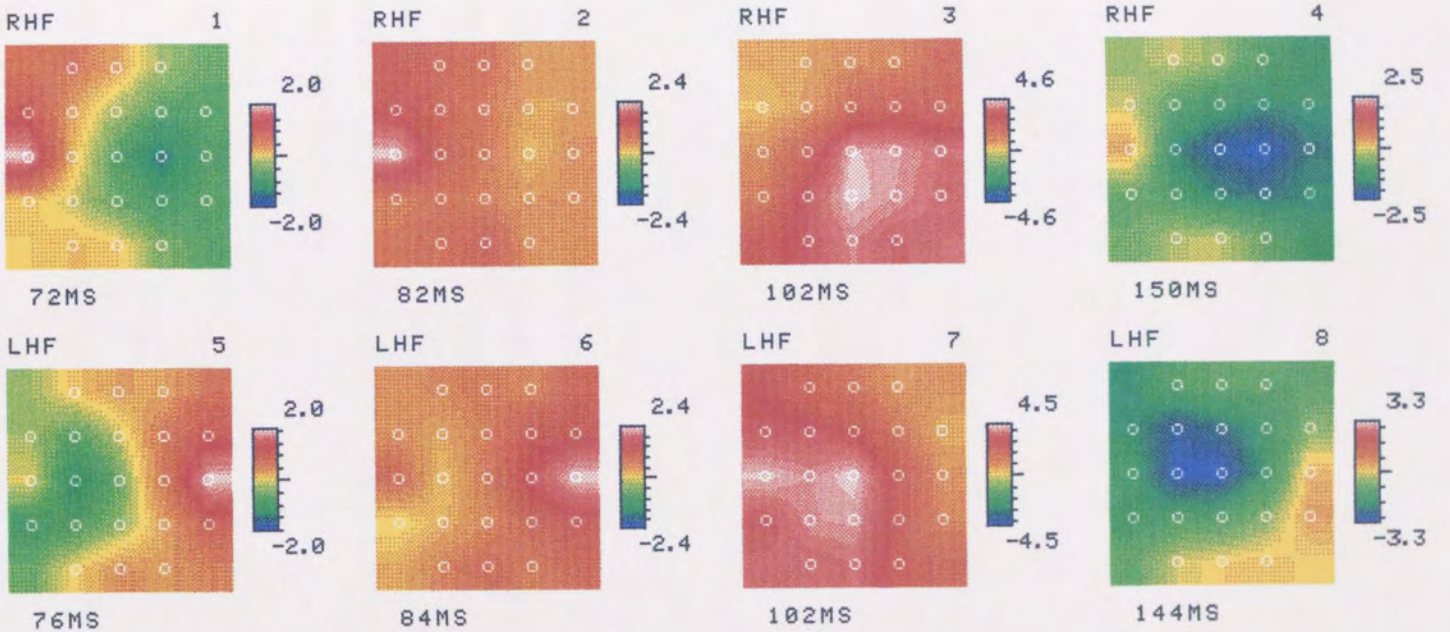
RHF 1
2.0
-2.0
72MS
RHF 2
2.4
-2.4
82MS
RHF 3
4.6
-4.6
102MS
RHF 4
2.5
-2.5
150MS
LHF 5
2.0
-2.0
76MS
LHF 6
2.4
-2.4
84MS
LHF 7
4.5
-4.5
102MS
LHF 8
3.3
-3.3
144MS

Figure 5.9. Topographic distribution of the major peaks of the group mean maps following right (RHF) and left half field (LHF) stimulation. Key; EARLYN = early negativity, EARLYP = early positivity, LATEP = late positivity and LATEN = late negativity. Amplitude values are shown in the scale to the right of the maps (μV). Note the individual amplitude scale values for each map.

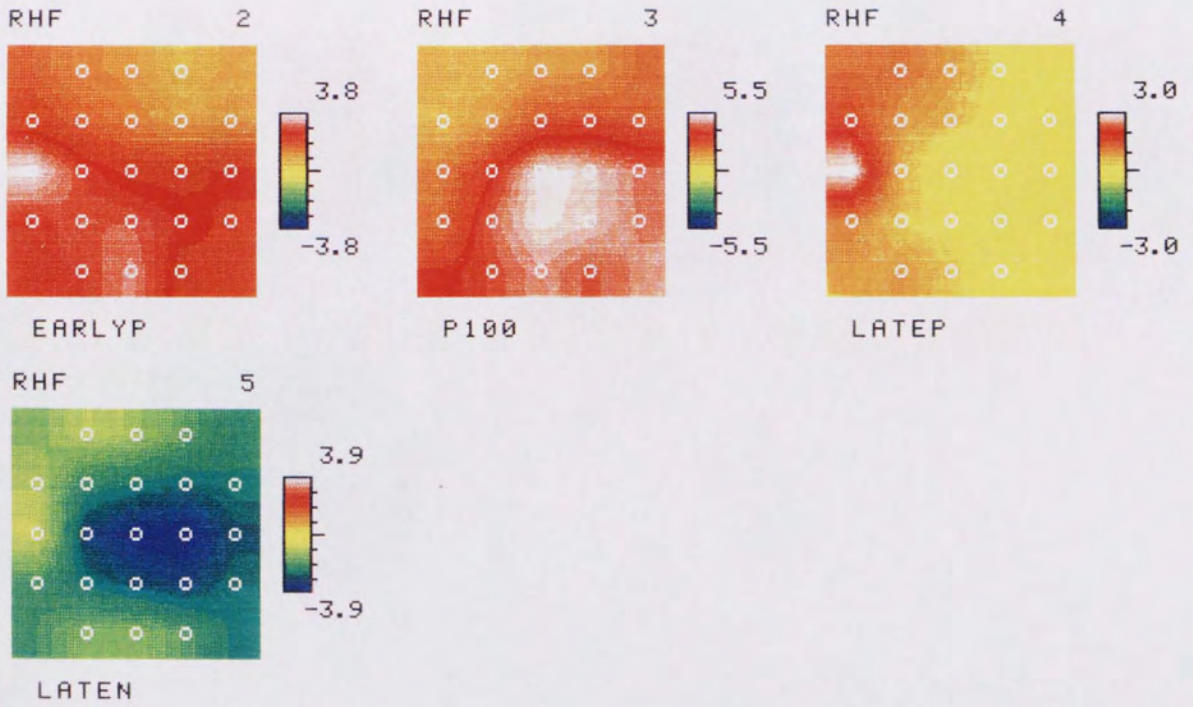
RHF 2
3.8
-3.8
EARLYP
RHF 3
5.5
-5.5
P100
RHF 4
3.0
-3.0
LATEP
RHF 5
3.9
-3.9
LATEN

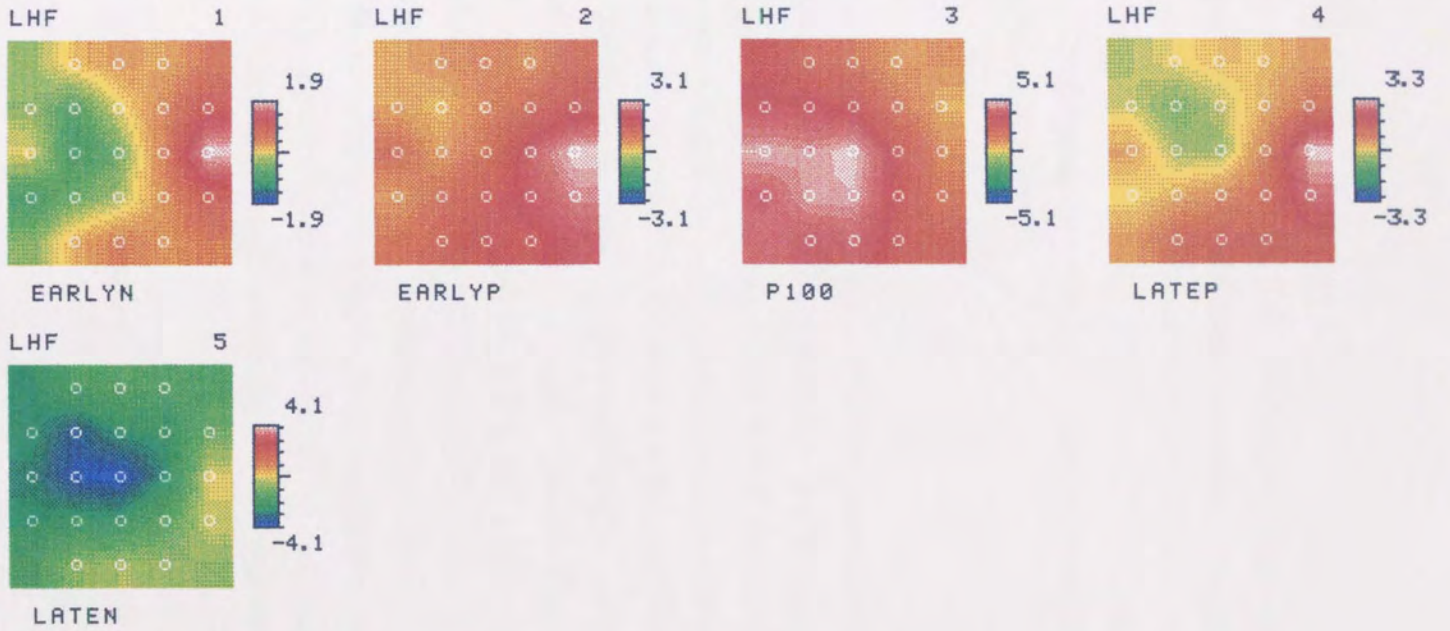
LHF 1
1.9
-1.9
EARLYN
LHF 2
3.1
-3.1
EARLYP
LHF 3
5.1
-5.1
P100
LHF 4
3.3
-3.3
LATEP
LHF 5
4.1
-4.1
LATEN

contralateral positivity, see fig 5.9. The contralateral positivity reached its peak about 6msec later than the ipsilateral negativity. The subsequent peak was the P100, this was ipsilaterally distributed. In 80% of the subjects there was a contralateral negativity which was of low amplitude in 20%, this was maximal over O3 and PO3. Following this was a contralateral positivity present in 40% of the subjects and maximal over O3.

5.3.2.ivb Left Half Field

The sequence of components in left half field stimulation was equivalent to right half field stimulation however the peak latencies and amplitudes did vary. The first component was the ipsilateral negativity present in all subjects, this was maximal over electrodes O3 and IN3. The contralateral components appeared in some subjects to be more prominent with left as opposed to right half field stimulation. In only one subject were none of the contralateral components observed. The contralateral positivity peaked 7msec later than the negativity and was present in 60% of the subjects. The next peak, the ipsilateral P100 was observed in all subjects and was maximal over Oz, O1 and O3. In two subjects this was maximal over the Pz line (KR and CD). The following contralateral negativity was observed in 60% of the subjects and preceeded the contralateral positivity present in 90%. The contralateral positivity was maximal over the extremes of the montage i.e. O4, In4 and PO4. The last repeatable response was the ipsilateral negativity occuring in all subjects.

5.3.3 Central Scotomata and Central Stimulation

Field	Full 4°	Full 7°	Central Scot 4	Central Scot 7
N75	74.6(6.19)	76.36(8.98)	73.5(3.51)	74.0(2.98)
P80			87.6(2.19)	90.8(3.35)
P100	105.8(6.18)	104.83(7.21)	101.0(6.29)	101.83(7.60)
P120		119.6(5.18)	116.86(7.01)	127.0(11.01)
N145	143.0(12.78)	144.0(11.94)	142.17(13.09)	146.91(16.38)

Table 5.5 The group mean and standard deviation, in brackets, of the peak latencies (ms) following central and peripheral stimulation..

Figure 5.10. Group mean waveform of the response following central 7° field pattern reversal stimulation. The position of the recording electrode is indicated to the left of the waveform. The maximum positive peak is cursored.

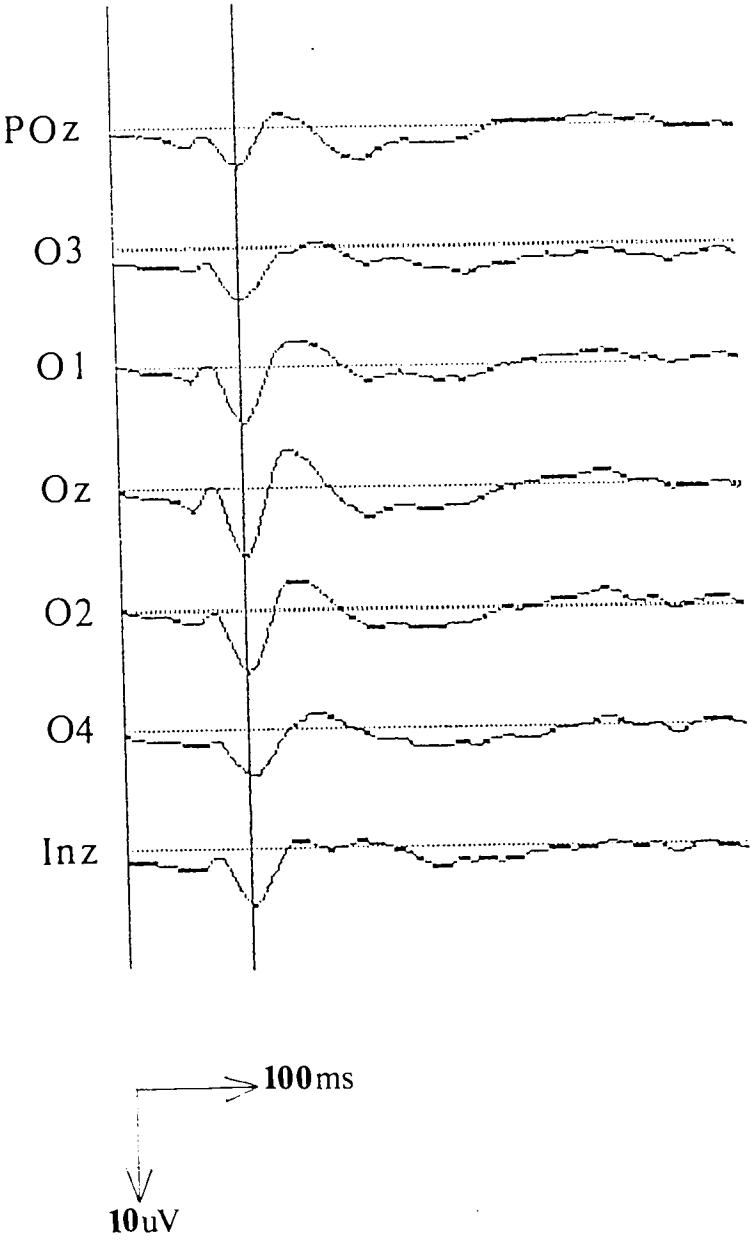
POz
O3
O1
Oz
O2
O4
Inz
100ms
10uV

Figure 5.11. Group mean waveform of the response following central 4° field pattern reversal stimulation. The position of the recording electrode is indicated to the left of the waveform. The maximum positive peak is cursored.

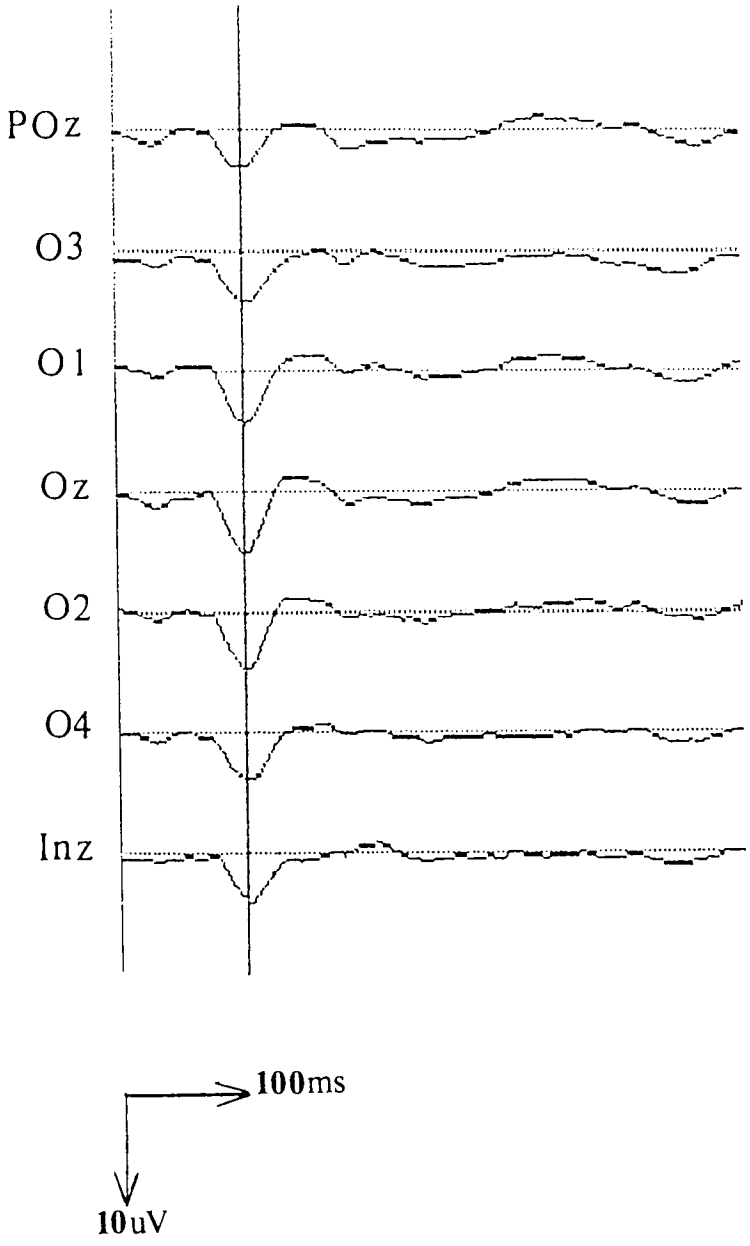
POz
O3
O1
Oz
O2
O4
Inz
100ms
10uV

Figure 5.12. Group mean waveform of the pattern reversal response following central 4° occlusion. The position of the recording electrode is indicated to the left of the waveform. The maximum positive peak is cursored.

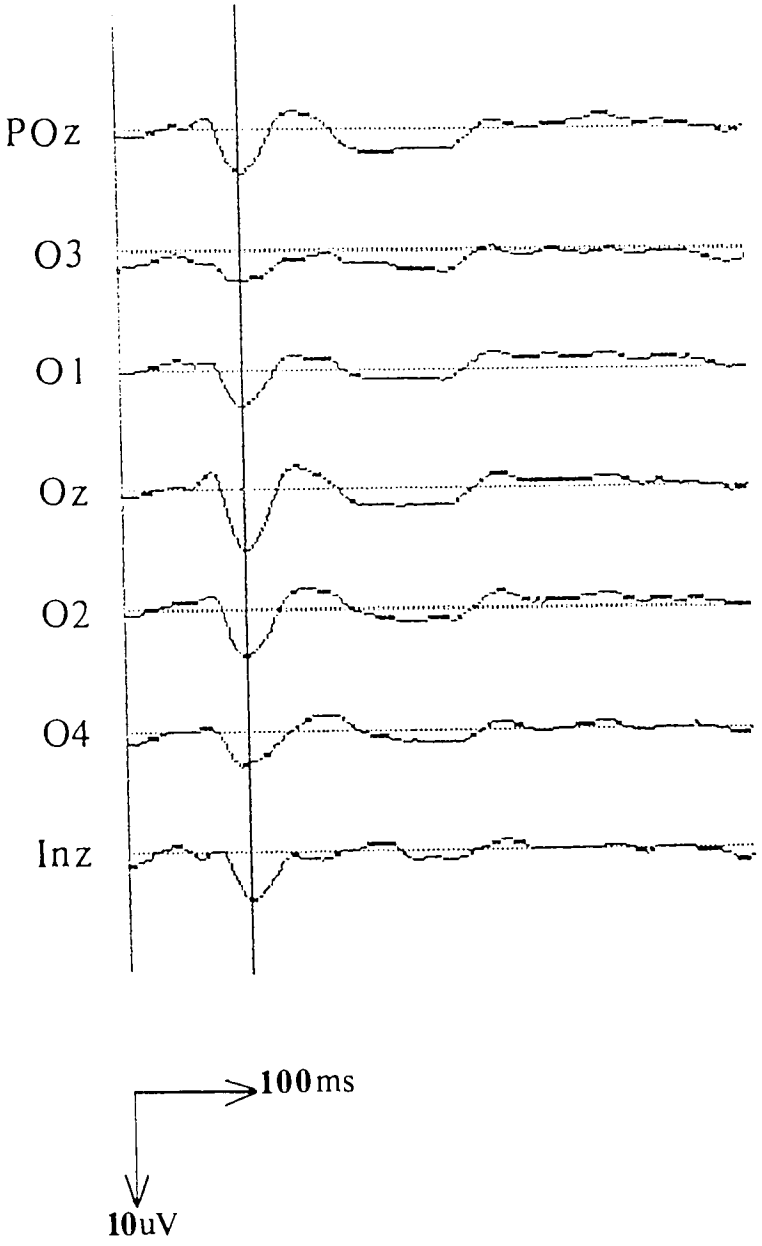
POz
O3
O1
Oz
O2
O4
Inz
100ms
10uV

Figure 5.13. Group mean waveform of the pattern reversal response following central 7° occlusion. The position of the recording electrode is indicated to the left of the waveform. The maximum positive peak is cursored.

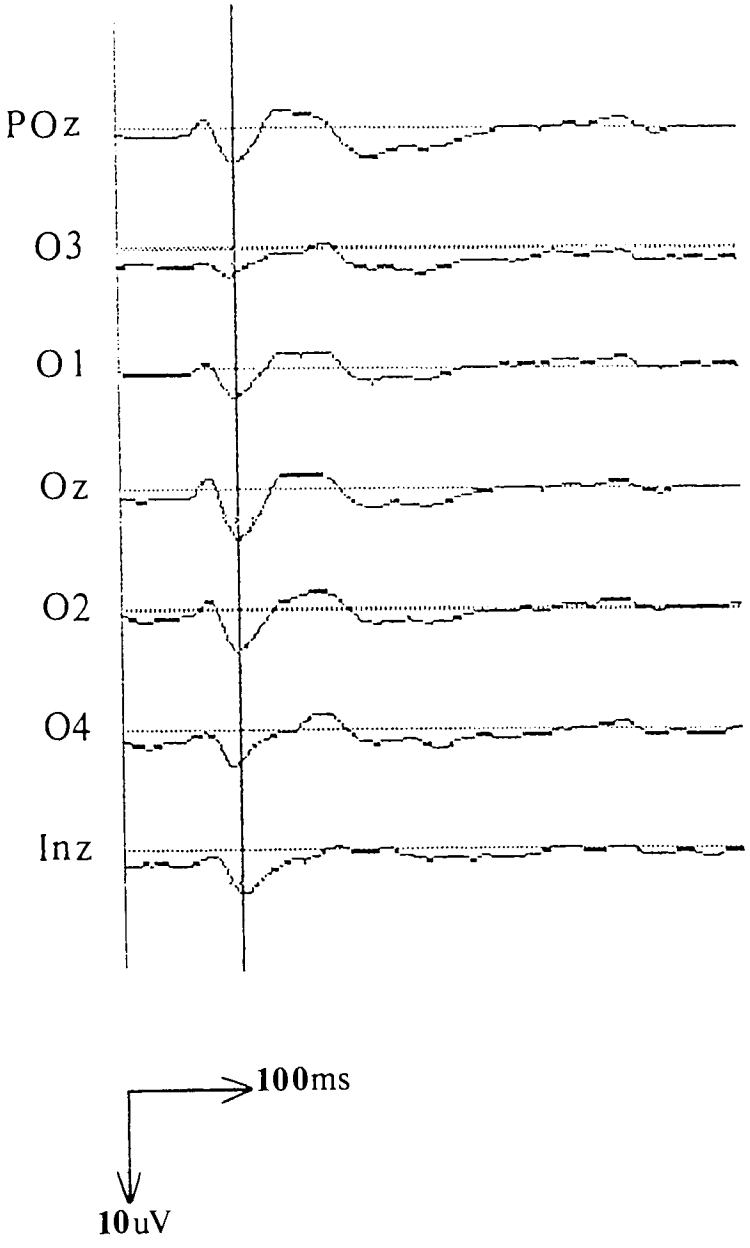
POz
O3
O1
Oz
O2
O4
Inz
100ms
10uV

Field	Full 4°	Full 7°	Central Scot 4	Central Scot 7
N75	-2.33(1.18)	-1.79(1.44)	-1.97(2.12)	-2.09(0.81)
P80			3.86(1.08)	3.15(1.98)
P100	6.13(2.09)	6.53(2.69)	6.79(1.76)	4.81(1.87)
P120	5.81 1 subj	6.05(1.86)	4.93(1.89)	3.31(0.76)
N145	-3.13(2.05)	-4.73(2.94)	-3.57(1.38)	-3.61(1.38)

Table 5.6 The group mean and standard deviation, in brackets, of the peak to baseline amplitudes (μV).of the major peaks responses following central and peripheral stimulation.

5.3.3.i Central Stimulation; Topographic Distribution from Group Mean Waveform

A low amplitude early negativity was recorded from FF7° with a distribution over O1 and Oz, no early negativity was shown with FF4° stimulation, see fig 5.14. The distribution of the positivity, P100 was not as localised as that from full field 20° stimulation, more spread was apparent over O1 and O2, the amplitude was also reduced. The late negativity was distributed maximally over Oz for all stimuli however it was observed that a positivity over the extremes of the montage increased in amplitude with a reduction in field size.

5.3.3.ii Morphological Variations Between Subjects

The early negativity was not observed in 2 subjects with 7° central field and in 4 subjects with a 4° central field. In four subjects the negativity was either of low amplitude or just present as a negative deflection with the 4° field, lower amplitude negativity was also seen in four subjects after central 7° stimulation. The topographical distribution of the group mean responses are shown in fig 5.15. This resulted in only 2 subjects producing a definite initial negativity with central 4° stimulation as compared with 4 subjects for 7° stimulation. The late negative was present as a deflection in one subject for 4° stimulation and was of low amplitude on 7° stimulation.

Figure 5.14. Topographic distribution of the major peaks in the group mean waveforms following central 4° (FF4) and 7° (FF7) stimulation. Amplitude values are shown in the scale to the right of the maps (μV). Note the individual amplitude scale values for each map.

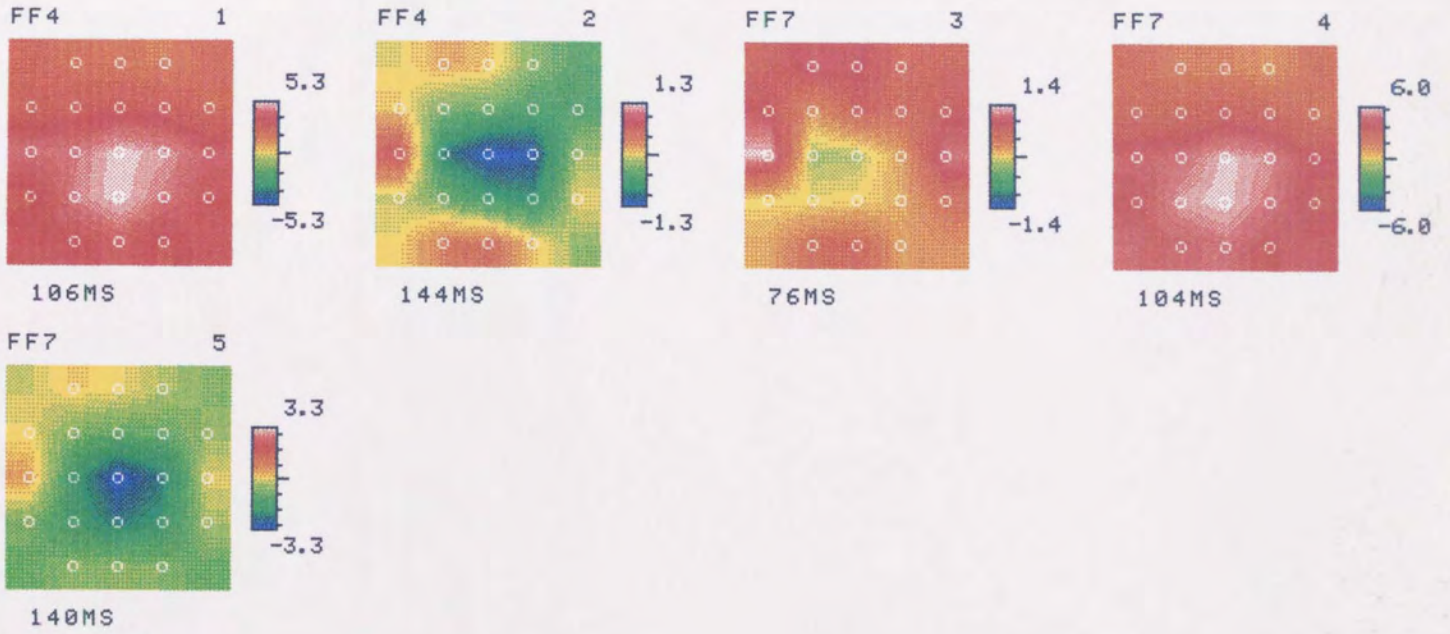
FF4
1
5.3
-5.3
106MS
FF4
2
1.3
-1.3
144MS
FF7
3
1.4
-1.4
76MS
FF7
4
6.0
-6.0
104MS
FF7
5
3.3
-3.3
140MS

Figure 5.15. Topographic distribution of the major peaks of the group mean maps following central 4° (FF4) and 7° (FF7) stimulation. Key; EARLYN = early negativity, EARLYP = early positivity, LATEP = late positivity and LATEN = late negativity. Amplitude values are shown in the scale to the right of the maps (μV). Note the individual amplitude scale values for each map.

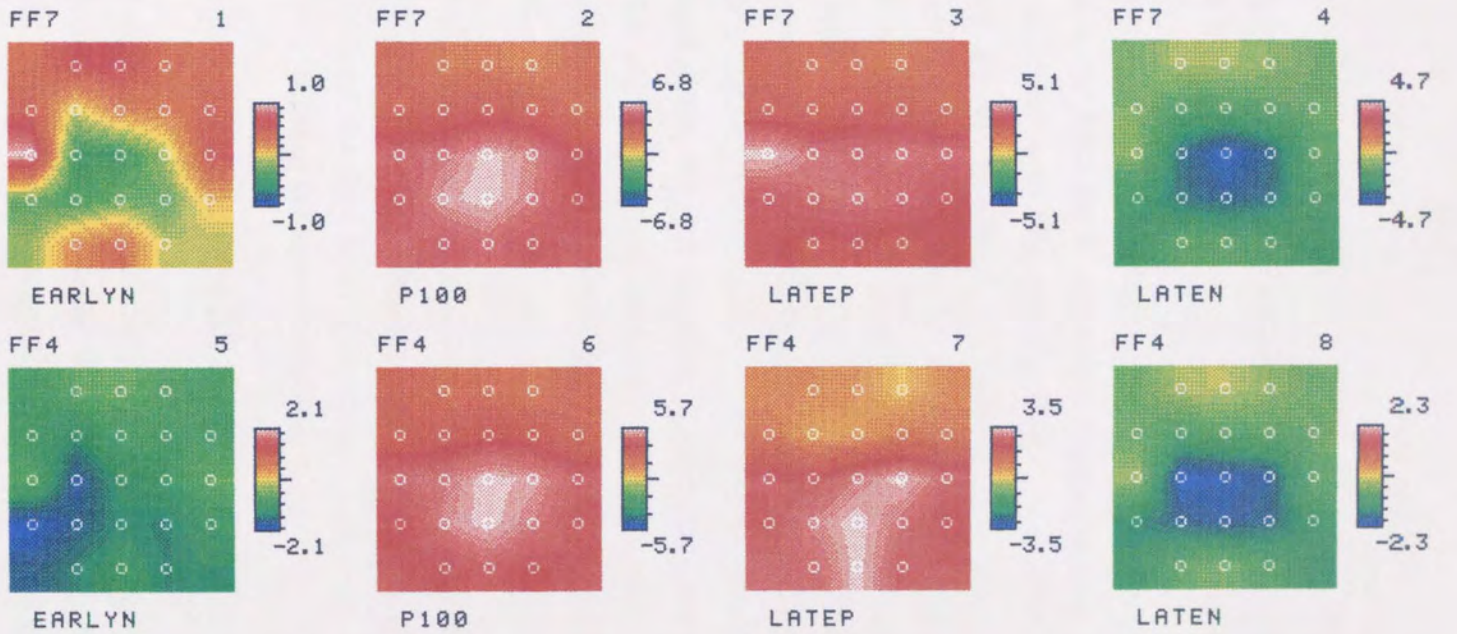
FF7 1
1.0
-1.0
EARLYN
FF7 2
6.8
-6.8
P100
FF7 3
5.1
-5.1
LATEP
FF7 4
4.7
-4.7
LATEN
FF4 5
2.1
-2.1
EARLYN
FF4 6
5.7
-5.7
P100
FF4 7
3.5
-3.5
LATEP
FF4 8
2.3
-2.3
LATEN

5.3.3.iii Peripheral Stimulation (Central Scotomata); Topographic Distribution from Group Mean Waveform

An early negativity was recorded with both occlusions. The amplitude of this response was lower from the 7° occlusion, the distribution was however similar for both being maximal over Oz, see fig 5.16. A positivity was simultaneously recorded over the left border of the montage, the amplitude of which was not affected by an increase in the size of occlusion. The P100 was then recorded from the central 4° occlusion this was maximal over the right/centre of the montage and migrated to become maximal over Oz. Seven degree occlusion produced a response over Oz, Pz and INz, this was a central localised band of positivity. The amplitude reduced with increasing scotoma size. Two later negativities were recorded from both of the occlusions, the first occuring around 134-142ms was maximal over the anterior region with a positivity over the posterior region. The late negativity was more lateralised from the 4° occlusion, for the 7° occlusion the distribution was more bilateral.

In a number of subjects peripheral stimulation produced a maximum over electrodes along the POz line, as though the peripheral generator was located more anteriorly on the cortex than the full field generator. This may be due to the stimulus preferentially stimulating the lower periphery.

5.3.3.iv Morphological Variations Between Subjects

Ten percent of the subjects produced no initial negativity with the 4° scotoma, this increased to twenty percent with the 7° scotoma. The early negative was of a low amplitude in 50% of the subjects for the 4° scotoma and in 30% with the 7° scotoma. This early negative was larger in amplitude than the negativity recorded on full field stimulation in 20% of the subjects for the 7° scotoma and in 30% with the 4° scotoma. No significant difference was however demonstrated between the amplitudes following 4 and 7° occlusion. The P100 was recorded in all subjects, it was of low amplitude for one subject with both scotoma sizes.

The late negative was not present in one subject with a central scotoma of 7° and was of low amplitude with 1 subject for both scotomas. Over the extremes of the montage i.e. over O3, O4, PO3, PO4, IN3 and IN4, in 90% of the subjects with 4° occlusion and 70% with 7° occlusion there appeared to be components similar to those observed contralaterally in half field stimulation, see fig 5.17. These consisted of an early positivity with a negative deflection and a later positivity.

Figure 5.16. Topographic distribution of the major peaks in the group mean waveforms following occlusion of the central 4° (CS4) and 7° (CS7). Amplitude values are shown in the scale to the right of the maps (μV). Note the individual amplitude scale values for each map.

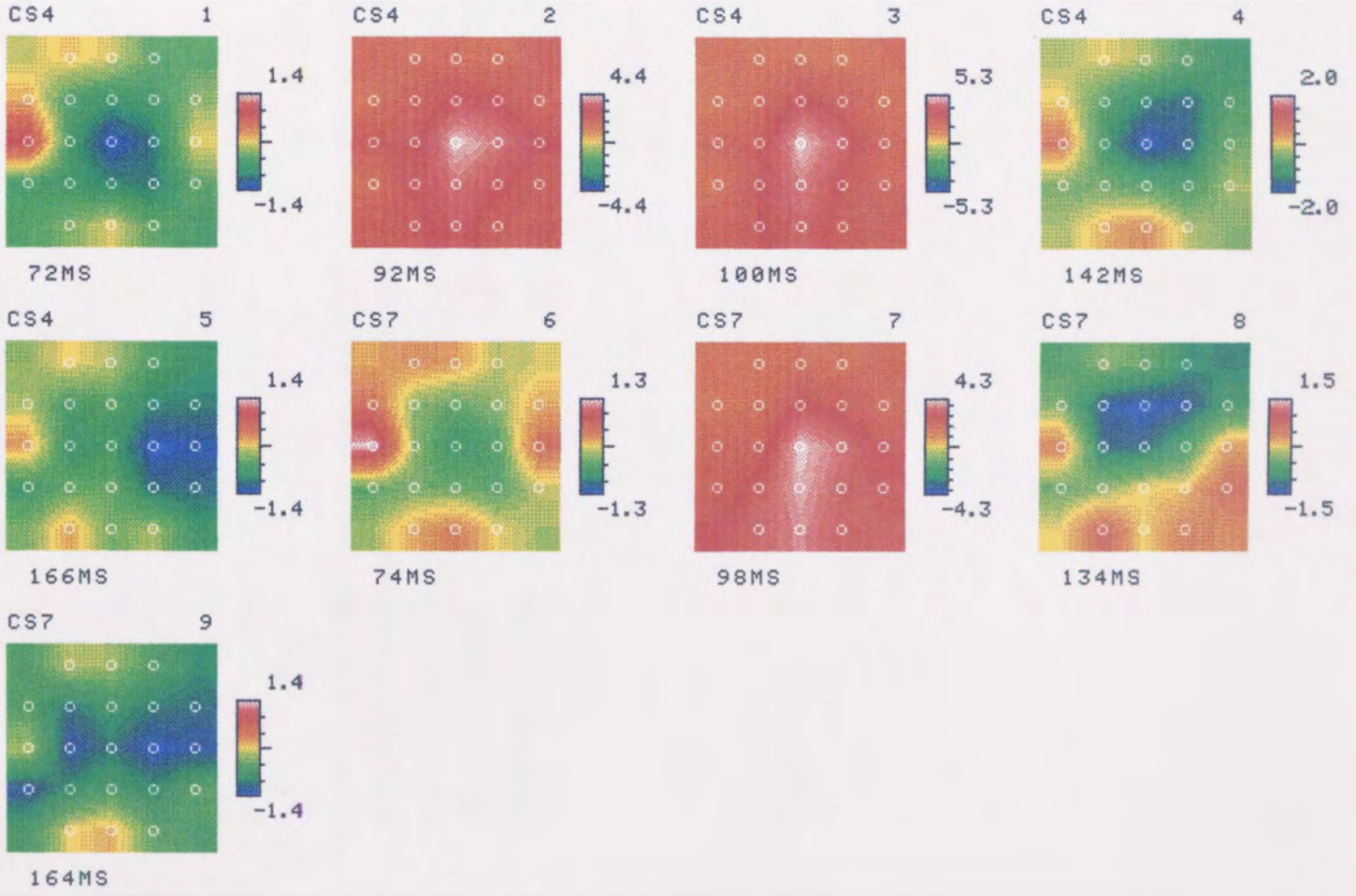
CS4 1
1.4
-1.4
72MS
CS4 2
4.4
-4.4
92MS
CS4 3
5.3
-5.3
100MS
CS4 4
2.0
-2.0
142MS
CS4 5
1.4
-1.4
166MS
CS7 6
1.3
-1.3
74MS
CS7 7
4.3
-4.3
98MS
CS7 8
1.5
-1.5
134MS
CS7 9
1.4
-1.4
164MS

Figure 5.17. Topographic distribution of the major peaks of the group mean maps following central 4° (CS4) and 7° (CS7) occlusion. Key; EARLYN = early negativity, EARLYP = early positivity, LATEP = late positivity and LATEN = late negativity. Amplitude values are shown in the scale to the right of the maps (μV). Note the individual amplitude scale values for each map.

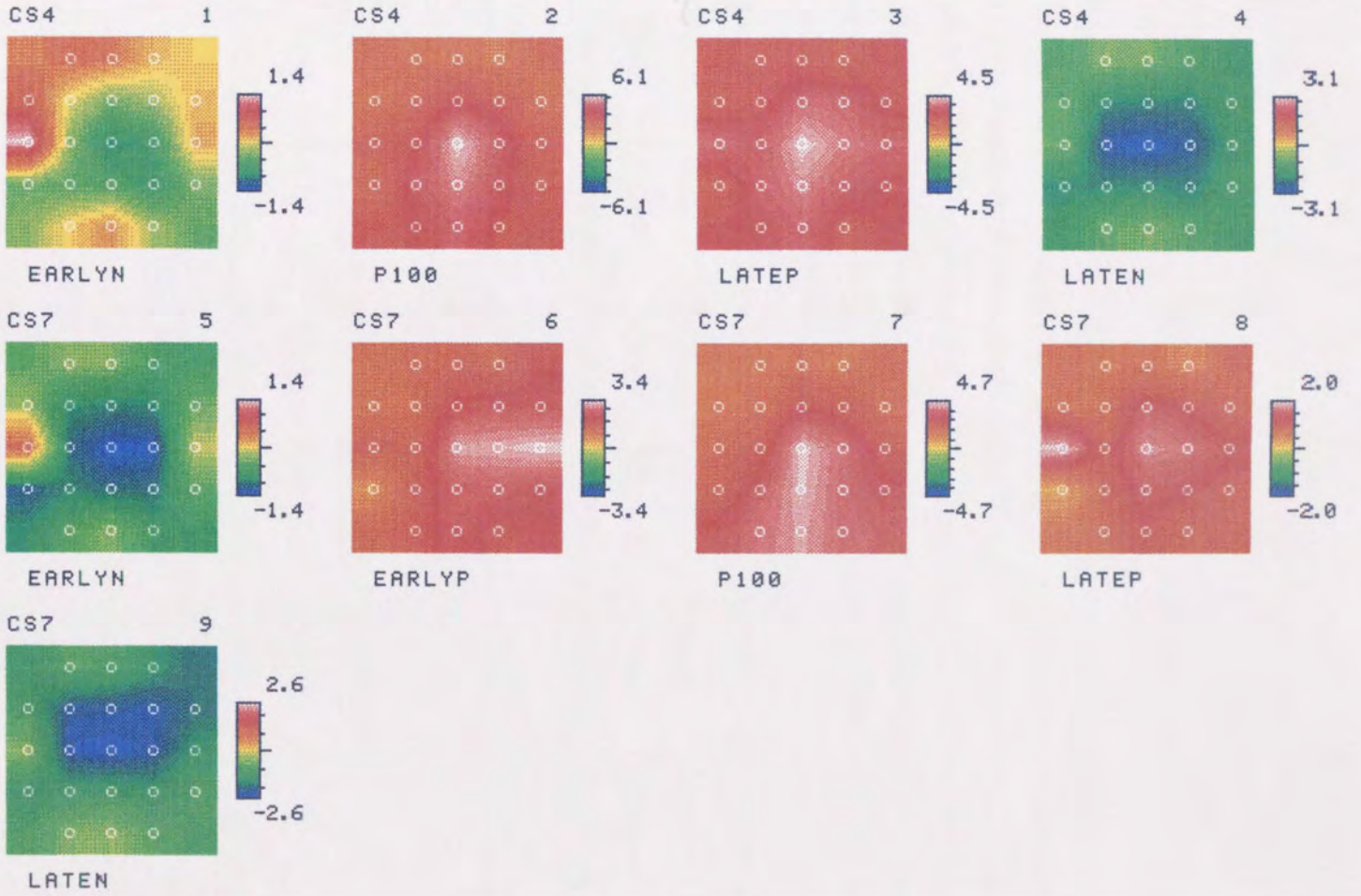
CS4 1
1.4
-1.4
EARLYN
CS4 2
6.1
-6.1
P100
CS4 3
4.5
-4.5
LATEP
CS4 4
3.1
-3.1
LATEN
CS7 5
1.4
-1.4
EARLYN
CS7 6
3.4
-3.4
EARLYP
CS7 7
4.7
-4.7
P100
CS7 8
2.0
-2.0
LATEP
CS7 9
2.6
-2.6
LATEN

5.4 Global Field Power Analysis of the Group Averaged Waveforms

Global field power calculates the root mean square of the potential differences between all possible electrode pairs. It is used to objectively distinguish the level of scalp activity as a function of time, the peak of the global field power plot then implies the latency of maximal scalp activity. The maxima of the global field power plots can therefore indicate the latency at which the map contains the largest simultaneous peaks and troughs. The position of the neural geneator will then lie along a line joining the two maxima in the map.

Stimulus Location	Field Power Latency	Field Power Amplitude	Field Power Latency	Field Power Amplitude	Field Power Latency	Field Power Amplitude
Full Field	76ms	0.71	**104ms**	**1.45**	142ms	1.09
Left Half Field	76ms	0.79	**104ms**	**1.20**	140ms	0.80
Right Half Field	74ms	0.81	**102ms**	**1.38**	140ms	0.80
Central 4° Scotoma	72ms	0.53	**102ms**	**0.95**	142ms	0.69
Central 7° Scotoma	72ms	0.49	**102ms**	**0.87**	130ms	0.78
Full Field 4°			**108ms**	**1.05**	140ms	0.55
Full Field 7°	76ms	0.44	**106ms**	**1.33**	140ms	0.95

Table 5.7 Latencies and amplitudes of the maximal field power following various stimulus field locations. Highlighted values indicate maximal power in the sweep.

Global field power analysis was performed on the group mean waveforms, the distribution was then compared with the distribution at the peak latencies for all

stimuli. The components listed are the peaks of the global field plot for each stimulus location observed between 70 and 150msec from the group mean waveforms. The amplitudes and latencies highlighted are the maximal values in the designated time range. The initial component is of low amplitude and maximally positive over the contralateral hemisphere for lateral half field stimulation. With full field stimulation this initial component is negative and maximal over the centre of the montage. Both the second and third peaks of the half field maps show a maximum over the ipsilateral hemisphere, positive for the earlier peak, negative for the later.

Full field stimulation peaks all possess a central distribution, the first peak has a slight left lateralisation, the distribution is composed of a negative, positive, negative sequence.

The field power around 100msec was shown to reduce with an increase in the size of central occlusion. The distribution of the later peak also tends to move more anterior with the larger scotoma. The distribution of the maximal field power becomes more medial as the scotoma increases. An initial component was not present in the global field power plot for small field stimulation, this corresponds with a reduction in the amplitude and occurence of N75. The amplitude of the potential is very low for the initial peak in the 7° field. The later component of the 7° field has the same distribution as the later component of the full field response although the amplitude of the response is lower. The distribution of the second peak is slightly more lateralised than the full 20° and of lower amplitude.

The latencies of the maximal global field power corresponded closely with the latencies of the major peaks in the group mean waveform, as a result the topopgraphical distributions at the greatest field strength are similar to those at the peak latency.

5.5 Discussion

5.5.1 Early Negativity (N75)

Recent work suggests that the human N75 corresponds to the monkey N50. The N50 component in the monkey represents activation of the stellate cell ensembles in the thalamorecepient layer IVC. As a consequence it has been proposed that N75 provides the most direct index of the integrity of the subcortical visual pathways (Schroeder et al 1990).

This component was present in the group mean maps for all fields except for right half field stimulation where only a negative deflection was present.

On full 20° stimulation N75 is maximal over Oz with a low amplitude positivity over O3 and O4. With reduction in the field size the negativity is prominant in a smaller number of subjects and was only clearly demonstrated in two subjects with central 4° stimulation. Statistical analysis, using the Student t test, indicated a significant reduction in the amplitude of N75 with a reduction in field size (20° compared with 7° $p<0.001$, 20° compared with 4° $p<0.05$). This confirms results of Mauguiere et al (1985) who observed an attenuation of N75 when stimulating the central 2°18' compared with the peripheral field (12°x16° field with the central 2°18' occluded), with no effect on the topographical distribution. Onofrj et al (1990, 1991) have however demonstrated the presence of this early negativity with central half field stimulation and have shown an amplitude increase with an increase in the stimulating spatial frequency. The discrepancies between this and the present study are probably related to the size of the stimulating element.

From the group mean maps of half field stimulation N75 is maximal over the ipsilateral hemisphere for left half field stimulation, on right half field stimulation a negativity was not observed this may be a result of a wide variation in the location of the response between subjects. Independent of stimulus size N75 to half field has been shown to have a larger amplitude than N75 recorded with full field stimulation (Onofrj 1990).

With peripheral stimulation the negativity remains maximal over Oz, as with full field stimulation however, with a central scotoma of 7° the amplitude was reduced or absent in five subjects. Statistical analysis, using the Student t test, showed no significant effect on the amplitude with the introduction of a 4° scotoma in contrast the response was significantly reduced with a 7° scotoma ($p<0.05$). This may be due to the area of generation becoming more anterior resulting in increased cancellation effects along the longitudinal fissure.

5.5.2 Early Positivity (P85)

This component was not present with any of the full field stimuli. With lateral half field stimuli however,the positivity was maximal over the contralateral extremes of the montage, over O4 for the left half field and over O3 for the right half field. An early positivity was present over O4 with a 7° central scotoma.

5.5.3 Major Positivity (P100).

It is thought that corresponding to the P100 in humans is the monkey P60. When investigated in monkeys this component inverted in laminar III, the major CSD correlate of this being a current source/sink configuration in layer III, with higher resolution this resolved into several supragranular source/sink configurations. P60 therefore arose from di and trisynaptic activation of the supragranular neurons, presumably the pyramidal cells. The recorded waveform thus reflected a primary contribution from superficial current sources representing passive current return to active current sinks, i.e. net EPSPs in pyramidal cell ensembles. The P100 was therefore thought to arise from depolarisation of the supragranular layers, presumably layers 2 and 3, i.e. the pyramidal cells and thus the P100 indexes the initial response plus several synaptic stages within the striate cortex (Schroeder et al 1990).

The major positivity was maximal over Oz for full 20° stimulation, as the field size was reduced the response became increasingly more diffuse, being distributed over the Oz line. With lateral half field stimulation the response was maximal ipsilateral to the field. The response became more centrally distributed over Oz and Inz with peripheral stimulation.

Paradoxical lateralisation to left and right half field stimulation has previously been demonstrated (Barrett et al 1976). This was suggested to be a consequence of the cortical generators being located on the medial and posteromedial surface of the visual cortex where the neurones are orientated transversely, if modelled by a current dipole the positive pole would be directed toward the ipsilateral hemisphere. Electrodes positioned on the ipsilateral hemisphere would therefore be optimally placed to record the P100, fig 5.18.

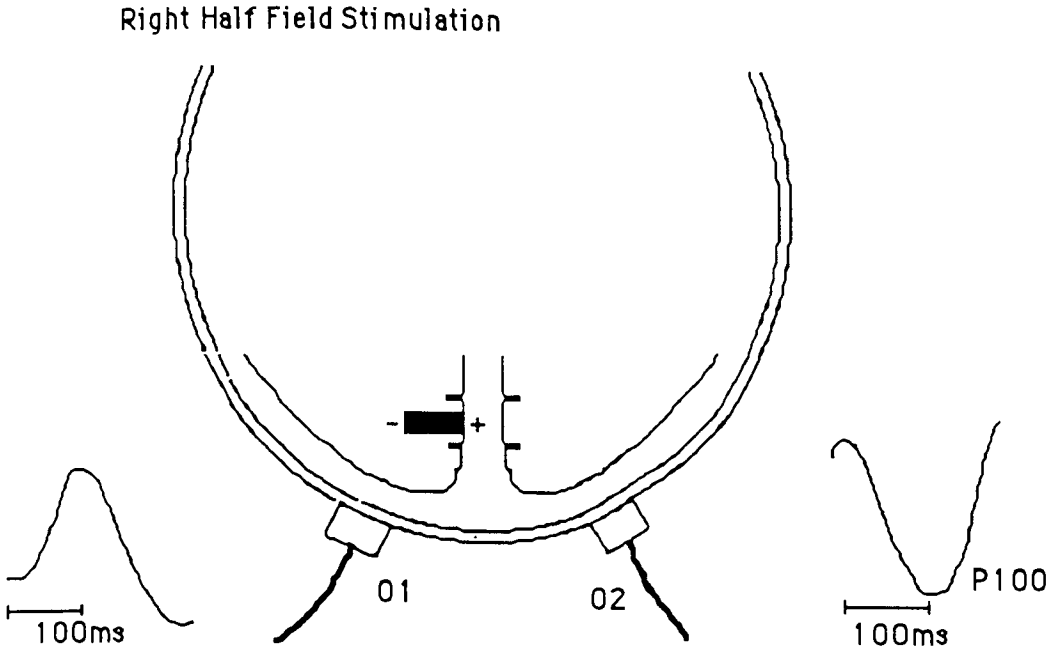

Fig 5.18. Diagrammatic representation of the position of the dipoles from half field stimulation. After Barrett et al (1976)

With a reduction in field size the response becomes less well lateralised, the generators in this case are more posteriorly placed around the occipital pole (Skrandies, Richter and Lehmann 1980, Blumhardt, Barrett and Halliday 1977, Harding, Smith and Smith 1980). Fig 5.19 illustrates the location of the approximate foveal and peripheral generators and the vector sum for various representations of the striate cortex on the occipital pole. Reducing the check size while keeping the field size constant (0-14°), still results in ipsilateral lateralisation (Harding, Smith and Smith 1980). If however, a foveal field (0-2°) is used the trend for the response to be contralateral increases with small check stimulation (Brecelj and Cunningham 1985).

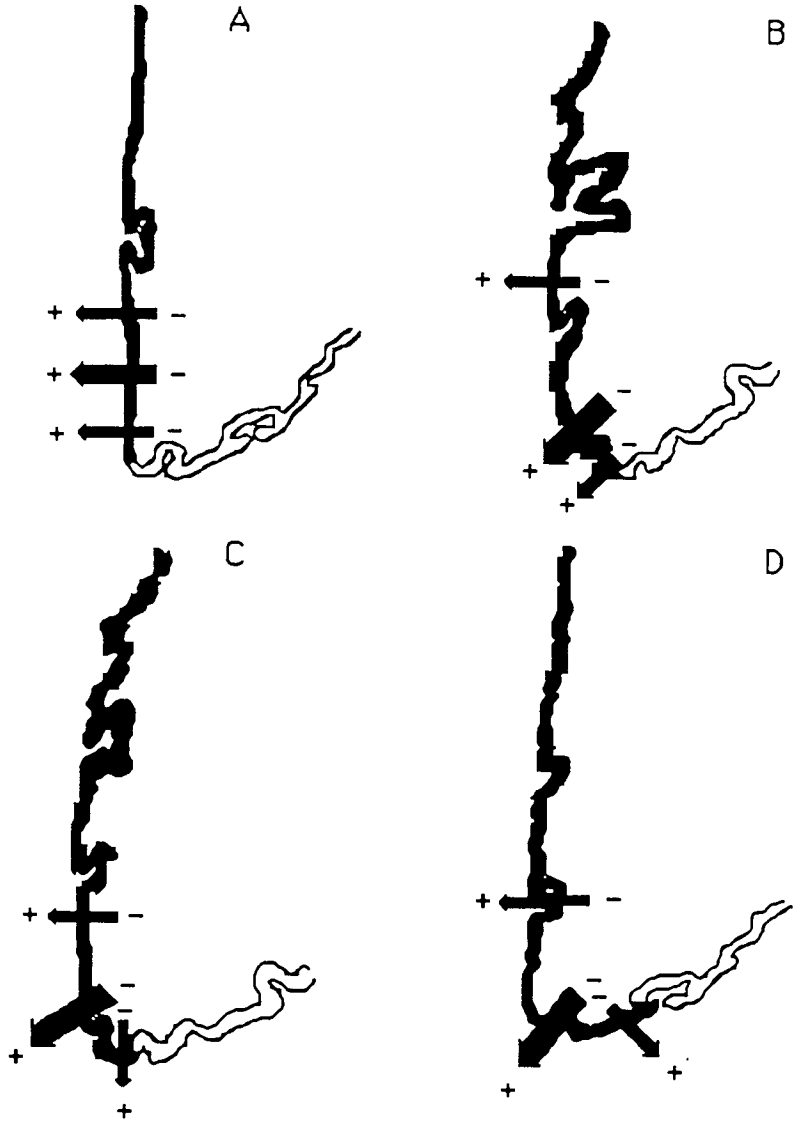

Fig. 5.19 Normal variation in the representation of the striate cortex over the occipital pole. The narrow dipoles represent the foveal and peripheral projections and the large dipole represents the vector sum.After Blumhardt et al (1989).

It has been hypothesised that part of the ipsilateral response could be generated in the ipsilateral hemisphere through the operation of transcollosal connections (Beauchamps 1976, Wildberger 1976), this has, however not been supported by work done by Blumhardt and Halliday (1979) on a patient with a total hemispherectomy. Flanagan and Harding(1987) confirmed the generation of the response in the contralateral hemisphere after investigating the P100 distribution using source derivation. With a transverse electrode montage a source was observed over Oz for both lateral half fields with a sink contralateral to the half field.

Individual variations in the striate cortex position on the occipital pole are thought to account for variations in the P100 lateralisaton between individuals on half field stimulation (Mauguiere et al 1985).

The data from the P100 latency and amplitude was split into two groups to investigate the effect of field size (FF20°, FF4°, FF7°, CS4° and CS7°) and also the effect of field location (FF, HF) on the latency and amplitude of the P100. Two way analysis of variance in randomised blocks was then performed. No significant effect of latency was found in either data set, however there was a significant effect on the amplitude of the P100 with the different field sizes ($F = 3.83$ $p<0.01$ least significant difference (L.S.D.) = 1.33).

No significant difference in the amplitude of the P100 was shown between full field 4°, full field 7° and a central scotoma of 4°. The amplitude after full field 20° stimulation was however significantly greater than all field sizes ($F = 3.83$ $p<0.01$). In addition a central scotoma of 7° reduced the amplitude significantly when compared with full field 4° and 7° and a central scotoma of 4° ($F = 3.83$ $p<0.01$), in agreement with results of Fukui, Kato and Kuriowa (1986), in addition they showed a significant increase in latency of the P100 which was not corroborated in this study. This increase in latency was due to the contralateral components of P75-N105-P135 extending over the central recording points (Blumhardt et al 1977, Fukui, Kato and Kuriowa 1986, Onofrj et al 1991). As the P100 latency reduced the P135 was taken as the major positive and the P100 was said to be delayed.

It is therefore apparent that occluding the central field or reducing the overall field size has a significant effect on the amplitude of the response this could confirm that the response is generated both centrally and peripherally (Haimovic and Pedley 1986). In contrast the latency of the P100 is not significantly affected by central occlusion or a reduction in field size, it could therefore be postulated that both central and peripheral fibres have the same origins and it is only the amount of fibres being activated that determines the response. Increasing the scotoma size appears to have a greater effect than reducing the field size, the P100 may preferentially be the result of central stimulation.

No significant difference was shown between the amplitudes following left or right half field stimulation. This is in contrast to previous reports which have shown a significantly greater amplitude response from right half field stimulation (Kuriowa, Celesia and Tohgi 1987, Pike and Polish 1988 and Abe and Kuriowa 1989).

Dipolar fits to investigate the site of response generation from the distribution of the P100 have been shown however, much of the previous dipole modelling work has concentrated on the pattern onset response.

A striate generator for the pattern reversal response has been proposed (Ducati et al 1982, Maiers et al 1987). Principal component analysis on the response to stimulation of the central 2° revealed two components (Maiers et al 1987), these were located in the striate cortex (C2) and area 18 (C1). Reversal stimulation of this area produced a large C2 and a much weaker C1, the location of the maximum for C1 was more lateral over the contralateral hemisphere and slightly higher than C2. In contrast an extrastriate generator has also been proposed for the pattern reversal response (Halliday and Michael 1977) to account for both the distribution from upper, lower, left and right half field stimulation (Lehmann, Darcey and Skrandies 1982), see fig 5.20.

Results from intracerebral recordings on two subjects also appear to support the concept that the sources are located at some depth below the scalp (Lehmann, Darcey and Skrandies 1982).

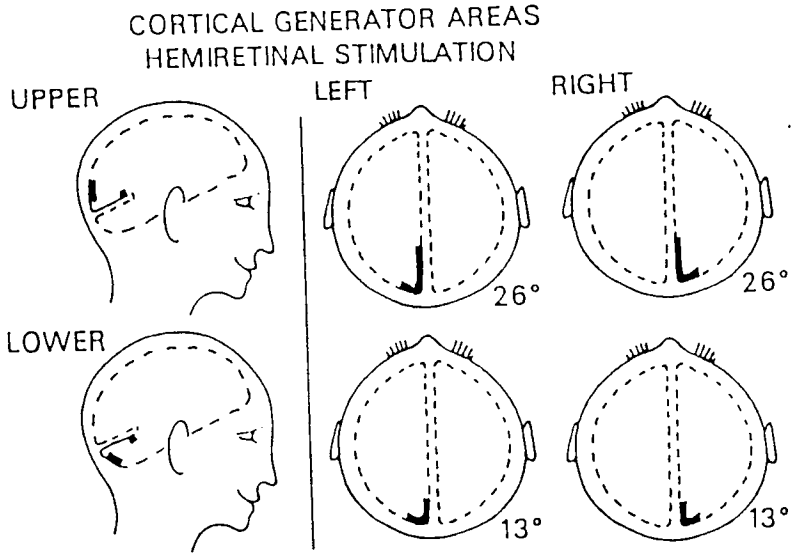

Fig 5.20. A schematic illustration of the geometry of the extrastriate visual cortical areas (highlighted) which are the hypothesised generator areas activated by the various hemiretinal stimuli, as a most plausible model to account for the data recorded. The lines between the highlighted area in the side views indicate striate areas which are less likely to be the generators. The side views are slightly parasagittal cross sections. Top views are cross sections slightly above (or below) the level of the calcarine fissure. After Lehmann, Darcey and Skrandies (1982).

5.5.4 Contralateral Negativity (N105)

A vague negativity was observed in a small number of subjects, due to the low amplitude of this component this was not transposed onto either the group mean maps or group mean waveforms. A prominent contralateral negativity has been reported in previous studies (Blumhardt et al 1977), however a smaller field and check size were used in the present study thus resulting in a more central response.

5.5.5 Late Positivity (P120)

This late positivity was only observed in three subjects after full field stimulation, the group mean map showed a positivity over Oz with a slightly more diffuse distribution than the P100. On lateral half field stimulation the response had a similar distribution to the early positivity i.e. maximal over the contralateral hemisphere. The positivity was therefore contralateral for the lateral half fields. On full field 4° stimulation the positivity was only observed in one subject, with full field 7° the positivity was produced by five subjects and was maximally distributed over the Oz line.

The positivity was also present with central occlusion however, the amplitude and the number of observations reduced with increasing scotoma size. The response was more centrally distributed for the 7° scotoma.

5.5.6 Late Negativity (N145)

The negativity following the P100 is thought to correspond to the N80 in the monkey. A large extrastriate contribution to this component was observed in the monkey with a clear polarity inversion in the middle of V4 (Schroeder et al 1990, 1991). It should therefore follow that the late negativity reflects activity in the exstrastriate regions.

This component was present with the majority of stimulus presentations and in most cases tended to be of a larger amplitude than the earlier negativity. On full field stimulation the maximal of N145 was located over Oz. With right half field stimulation N145 was maximal over the right of the montage but diffused well over the midline onto the ipsilateral hemisphere, on left half field stimulation the maxima was again over the ipsilateral hemisphere however less spread onto the contralateral hemisphere was apparent. N145 therefore appears to be maximal ipsilaterally for lateral half field stimulation. On peripheral stimulation N145 was maximal over Oz

with increasing scotoma size the distribution became more anterior. Reduction of the field size tended to produce an increasingly more diffuse distribution.

From work on the monkey, as previously mentioned it is thought that the P100 is the result of striate generators and the N145 is due to extrastriate activation, it is therefore interesting to note that the distribution of the two responses are very similar with the same lateralities on half field stimulation Two way analysis of variance was performed on the latency and amplitude of the N145 to elicit any effect of field size, complete data sets were only obtained from full 20°, 4° and 7° and both the 4° and 7° scotomas. No significant effect of field size on either the latency or amplitude was found. This is not in agreement with Mauguiere et al (1985) who found the N145 amplitude to be slightly greater for central as opposed to peripheral stimulation. It is however evident that although the distribution of the N145 is similar to that of the P100 the two components do not appear to possess the same properties.

5.5.7 The Contralateral Components after Stimulation with Central Scotomata

The contralateral components have previously been shown to be accentuated and then slightly reduce with an increase in scotoma size, considerable intersubject variablility was however encountered (Blumhardt et al 1978). The reduction in amplitude of the ipsilateral P100 has been shown to be almost linearly related to the increase in scotoma size, P100 was abolished in the majority of subjects with a scotoma of 10° radius (Blumhardt et al 1977). The large amplitude of the contralateral components recorded by Blumhardt et al and Fukui et al 1986 may be due to the large check sizes used, 50', which would preferentially stimulate the periphery, resulting in the orientation of the dipole being more posterior and tangentially orientated.

Onofrj et al (1991) using 3° half fields showed that the ipsilateral and contralateral components could still be recorded, the amplitude was however reduced by approximately 50%. Distributions obtained with 6° half field or 3° central occlusion were only slightly different to those after the full half field. When the central 6° was occluded the response consisted of widespread contralateral activity with a reduction in amplitude of 50%, ipsilateral components were recorded over the temporal and anterior derivations. Lateralisation of the components was enhanced with an increase in the spatial frequency content of the stimulus.

In the present study components resembling the contralateral half field morphology were recorded over the extremes of the montage from 25 % of the subjects with central scotoma of the full field. It would therefore appear that occlusion of the central area results in the source becoming more tangentially orientated, contralateral components which have previously been masked by the central radial source are disclosed. Contralateral components recorded from the extremes of the montage could be the result of the negative pole of one dipolar source being superimposed on the positivity from the other half field. Halliday et al (1977) have described the waveforms from a patient with dense binocular central scotoma, on half field stimulation the contralateral but not ipsilateral components were recorded. The full field response was therefore a PNP type complex maximal over either side of the midline.

5.6 Summary

N75 was present with all stimuli, there was a significant reduction in the amplitude of this peak following a reduction in field size (20° compared with 7° $p<0.001$, 20° compared with 4° $p<0.05$) and the introduction of a 7° central scotoma ($p<0.05$).

An early positivity, P80 was not apparent on full field stimulation, this peak was however present after half field stimulation and central 7° occlusion.

Paradoxical ipsilateral lateralisation of the P100 was demonstrated with left and right half field stimulation. No significant ampltiude or latency difference was shown between the responses from both half fields. A significant reduction in amplitude of P100 was however demonstrated when the field size was reduced to 7° and 4° and when the central 4° of the field was occluded ($F = 3.83$ $p<0.01$). The amplitude was further significantly reduced with the introduciotn of a 7° scotoma when compared with full field 4° and 7° and a central scotoma of 4° ($F = 3.83$ $p<0.01$).

A late positivity was recorded over the posterior region of the montage in three subjects following full field stimulation, this peak was however more prominent on lateral half field stimulation and central occlusion. On lateral half field stimulation P120 was maximal over the contralateral reigon.

The distribution of N145 appears to be similar to that of P100 being maximal over the ipsilateral/central region of the montage on lateral half field stimulation. Although the distributions were similar the same amplitude trends following a

reduction in the size of the stimulating field and inclusion of a central scotoma were not evident.

CHAPTER 6

Comparison of the Distribution of the VEMR and the VEP to half field stimulation.

6.1 Introduction

It is well established that the VEP to half field stimulation exhibits paradoxical ipsilateral lateralisation thus producing a maximal response over the wrong hemisphere (see chapter 5). Blumhardt et al (1978) suggested that this was due to the VEP being relatively more sensitive to radial dipoles. The Visual Evoked Magnetic Response (VEMR), is, however more sensitive to tangential dipoles and should therefore evade the problems of this paradoxical lateralisation.

A comparative study of the distribution of the half field pattern reversal potential and magnetic field has only previously been reported in one subject with right half field stimulation (Janday 1987). Earlier studies comparing the visual evoked potential and visual evoked field have either used a pattern onset stimulus (Stok 1984) or have failed to investigate the topographical distribution of the VEP (Seki 1991). Consequently the topographical distribution of the VEMR half field responses were investigated and compared to the distribution of the VEP half field responses. It is well documented that the VEP and VEMR contain complementary information with respect to the response generators (e.g. Chapman 1991, Spekreijse and van Dijk 1991). The VEP and VEMR combined can predict whether a distribution with two opposite sign maxima is the result of two radial or one tangential dipole source (Wood 1985). The VEP dipole orientations can also be used to predict whether VEMR responses to a stimulus will be detectable (Maclin, Rose and Paulson 1991).

It has also previously been demonstrated that the location of the VEP maxima to lateral half field stimulation may be dependent on the check size of the stimulus (Brecelj and Cunningham 1987, Edwards 1989). If the location of the maxima changes this would imply that there has been an alteration in the orientation of the source resulting in a change in the tangential and radial components of the approximate current dipole. It was therefore additionally decided to investigate the effect of check size on the topographical distribution of the evoked potential and field.

6.2 VEMR Methods

The VEMR was recorded with a single channel dc second order gradiometer BTi SQUID (model 601). The magnetometer has a 2cm diameter pickup coil and a 5cm baseline. The response was filtered at 0.3-30 Hz with a four pole Butterworth filter (24dB/octave roll off) and passed through a 50Hz comb filter before being attenuated and amplified for digital conversion. The white noise level of the whole system was 16.6FT/$\sqrt{Hz}$ at 5Hz. Recordings were made in an unshielded environment. Initial recordings were made on the Datalab processor and 64-128 recordings were averaged after filtering the response between 0.1-30Hz. Subsequent studies have been made with a Biologic traveller which incorporates artifact rejection. The gain was set at 7500-10,000 to achieve a 10% artifact rejection rate. A 500ms baseline was used and the reversal rate was set at 2Hz, fifty responses were averaged. All stimulation was binocular, this being more comfortable and easier for fixation and also producing a more natural viewing situation and larger signals.

6.2.1 Measurement Grid

The simplest method of probe location is to mark the recording positions on the scalp and position the probe directly above these. An increase in the density of the recording locations has been shown to improve the resolution (Hari et al 1988). If the spacing is, however kept constant and the number of recording locations increased the resolution can actually reduce, due to the inclusion of very small fields (Hari et al 1988). Methods other than marking the scalp can be used, for example a grid of wires in the form of a skull cap which carry an AC electrical current can be used (Imperial College). By energising each wire before the recording with a 20Hz sine wave the location of the five channel probe can be calculated.

The great majority of new magnetometers are multichannel systems, more than one channel of information being collected simultaneously. The spacing of the individual probes is fixed and therefore dictates to some extent the rate of spatial sampling (Romani and Rossini 1988). If the distance between the recording points is too small then redundant information may be collected especially if the source being investigated is fairly deep i.e. 3.5cm, as in a cerebral source. The choice of sampling must however be related to the depth of the source under investigation

(Romani and Leoni 1984). A rough estimate for the grid spacing is given by the equation;

$$G=0.7(D+d)$$

D=source depth from the scalp
d=distance between the pickup coil and the scalp

For example if the source depth is 2cm and the pickup coil distance is 1cm then the grid spacing should be in the order of 2.1cm. In addition the overall size of the grid must relate to the source depth, a grid of 14 x 14cm is inadequate for the location of a source 6cm from the pickup coil (Romani and Leoni 1984).

The response was recorded from twenty points marked over the occipital area of the scalp. The interpoint spacing was equal, in both the vertical and horizontal directions, to 10% of the half head circumference, see fig.6.1. A 10% circumference spacing resulted in an interpoint distance of approximately 3cm (range of 2.8-3.0cm). This value was chosen as it gave a correlation with head size. If a fixed value was used, being the same for each subject, there would be no certainty that the probe was positioned over similar cortical areas. A 10% value of the nasion-inion distance for the transverse spacing was not used as this results in a spacing of greater than 3.0cm in all subjects, 3.0cm has been estimated to be the greatest separation that can be used whilst maintaining the accuracy required for localisation procedures (Romani and Rossini 1988), smaller distances may induce inaccuracies in probe location. The total grid dimensions therefore varied from 8.4 x 11.2cm to 9.0 x 12.0cm.

6.2.2 Recording in a Plane, on a Sphere or Normal to the Head

The probe (containing the pickup coil) can be fixed to record the VEMR in a plane above the head, it can be rotated about the centre of a sphere, the dimensions of which should approximate that of the skull and it can also be placed normal to the head and separately located for each recording point. There are disadvantages inherent with each technique (Meijs et al 1987). Meijs et al (1987) have compared the secondary and primary source contribution to the field distribution from tangential and radial dipoles when recording on a plane, following the head contours and on a spherical surface.

When a planar recording strategy was adopted the contribution made by secondary sources was substantial, with a tangential dipole the secondary source contributions counteracted those of the primary source. With a radial dipole neither the primary nor secondary source contributions had recognisable dipolar field patterns. The secondary source contribution from a tangential dipole was found to be less than

10% when recording on a sphere, this contribution however increased as the depth of the dipole increased. When a radial dipole was tested the field recorded from the primary source was small. Secondary sources were also recorded when following the head contours with the probe for a dipole pointing horizontally and lying tangentially, the contribution of these counteracted those of the primary source and distortion of the dipolar pattern was demonstrated. The secondary source contribution again increased with dipole depth. With a dipole in the vertical direction the secondary and primary source contribution summed resulting in some distortion of the field pattern, in a radial direction the primary and secondary sources both produced random distributions.

They suggested that the order of preference for recording was therefore 1) on a sphere, 2) following the head contours and 3) recording on a plane. As the probe is closer to the head when following the contours the response amplitude from the primary source is greater but accompanying this the amplitude from the secondary source is also greater. Using this technique however the probe must be placed normal to the head, if this is not achieved then a proportion of the tangential components of the magnetic field will be recorded, for 10° off normal the tangential component was 20% of the normal component (Meijs et al 1987). As the tangential component is strongly influenced by the secondary source the contribution of the secondary source will therefore increase as the probe moves away from the normal position. This would lead to complicated field plots which may be difficult to interpret in terms of source location. When recording in a sphere the probe can be positioned accurately so it is normal to the scalp so reducing the variation possible from following the contours. Cuffin (1991) used computer modelling to calculate the errors in source localisation when recording from a plane. Realistically shaped head models were used to investigate the localisation accuracy for measurements on a plane and to compare this with measurements from a fixed distance. The MEG was calculated for a source positioned in different head models, the source location was then calculated with a sphere model for the head. For both types of measurement the localisation errors were less than 1cm for tangential sources. A non spherical head shape was found to have the same effect on the inverse solutions calculated from both measurements. Localisation errors and amplitudes increased with both methods for radial sources as the source depth increased. If the tangential component of the magnetic field in the plane recording calculations was included the accuracy of the localisation was reduced by less than 0.6cm. Errors in the tilt of the measurement plane of 10° produced errors in localisation of 1.1cm.

It was decided to record the field with the dewar positioned normal to the scalp. Although this results in a small contribution from the secondary sources it was preferable to recording in a plane. Recording from a sphere was not possible with the gantry set-up used. Recordings were made in a semi-darkened room. Four experienced subjects with an age range of 23-40 were used with no ophthalmological or neurological defects and visual acuities of greater than 6/6 with optical correction if required.

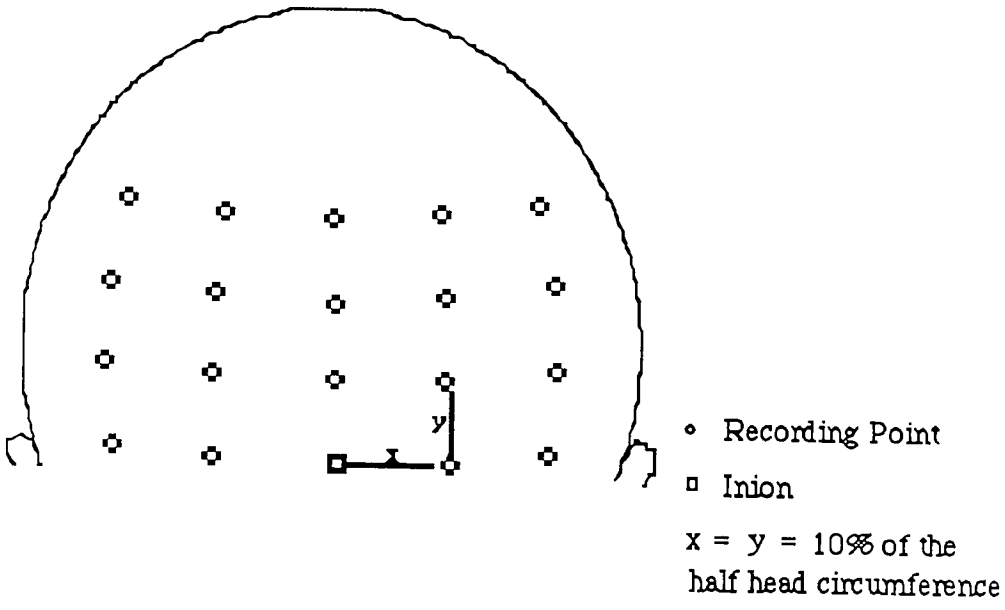

Fig.6.1. Diagram of the recording positions for the VEMR study.

The responses were recorded to pattern reversal stimulation, this was provided by a slide projection system, black and white checkerboard slides being back projected onto a translucent screen. The subjects were instructed to maintain steady fixation on a fixation target placed in the centre of the screen. The response was recorded to 10° full and 0-5° half circular field stimulation. Three check sizes were used in the study; 22', 34' and 70'. The mean luminance of the checks was 975cd/m^2 with a contrast of 80%.

6.2.3 VEMR maps

The value of the maximum field out of the head occuring at around 100ms was measured. This has been shown to be the most consistent component of the pattern reversal response, (Armstrong et al 1990). Fig.6.2 illustrates twenty responses recorded from the montage to a right half field stimulus in subject CD. The amplitude measures were peak to baseline, this was constructed with a line joining the start and finish of the trace. Responses from the twenty points were analysed to assess at what latency the maximum peak occured. When the latency was established the field values for all recording points at this latency were measured. Isofield maps were produced using Pathfinder II™ mapping software and are presented as thermal printouts. The field values between the recording points were calculated using a four nearest neighbours linear interpolation procedure.

6.3 Results

The maps show distributions of in- and outgoing field, red areas represent magnetic field leaving the scalp and blue areas represent magnetic field entering the scalp. If a single source is assumed then it's position can be approximately located under the area of no activity between the two maxima. The direction of the current dipole can be demonstrated by Flemings right hand grip rule.

Care has to be taken interpretating the maps in terms of dipoles since multiple dipoles may be activated and give a distribution similar to a single dipole (Weinberg et al 1985). Only accurate source localisation may have the ability to distinguish these using multiple dipole fitting procedures.

Since a single channel Squid was used the responses had to be recorded sequentially across the grid. A fixed order of recording was used, the first point was the inion, the second to the left and the third to the right, the left and right sequence continued to the last point. Two independently recorded maps from the same stimulus and subject are shown to demonstrate the variability of the recordings, see fig. 6.3.

6.3.1 Topographical Distribution

The topographical distribution of the VEMR for the four subjects is shown in figs. 6.4 - 6.7. The lateral half field maps tend to show maxima located over the contralateral hemisphere, this was more consistent after left half field stimulation.

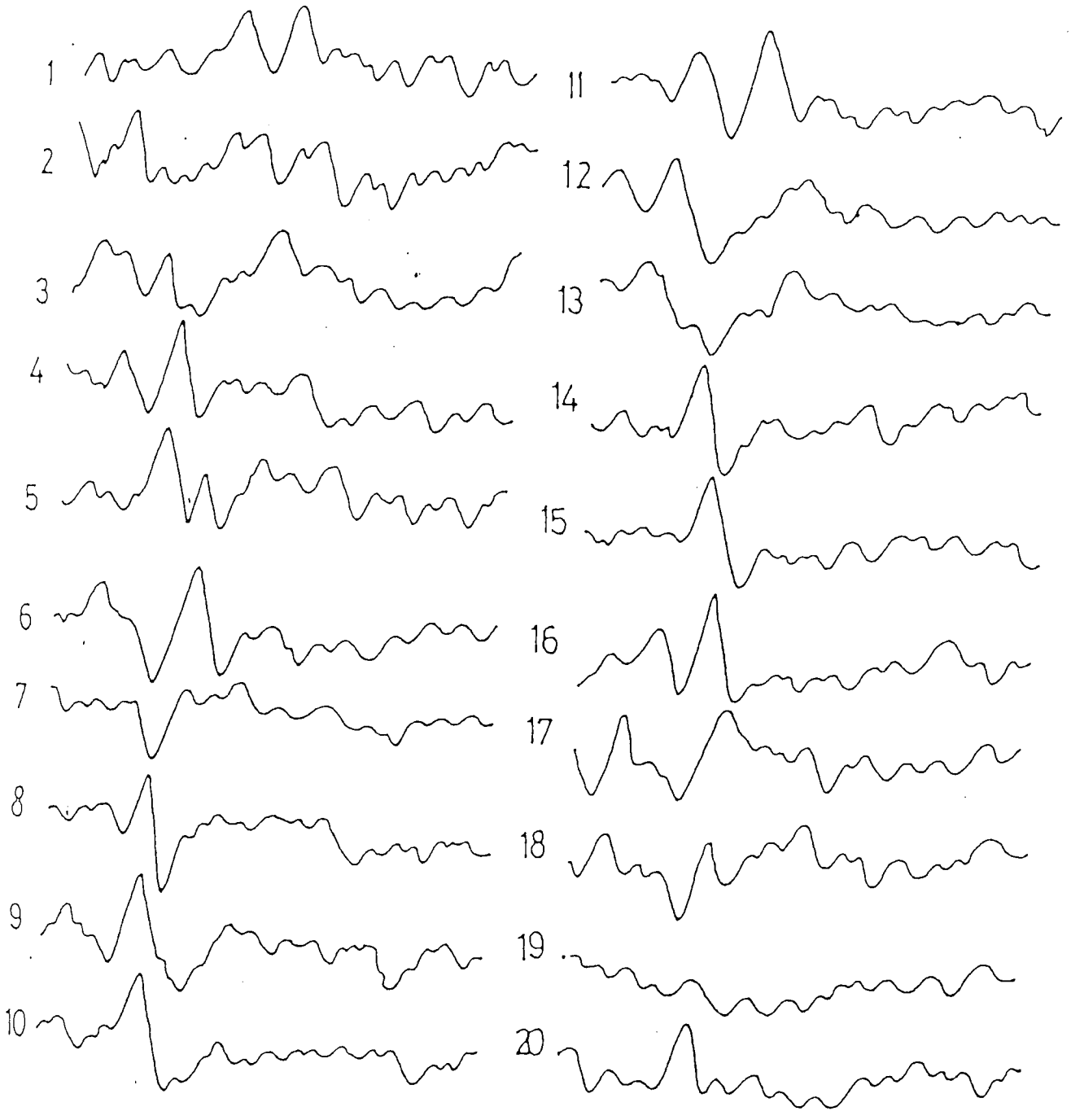

Figure 6.2 VEMR waveform following right half field 22' stimulation. Subject C.D. Waves are numbered 1 to 20 and correspond to the recording positions starting from the top left and running from left to right and top to bottom.

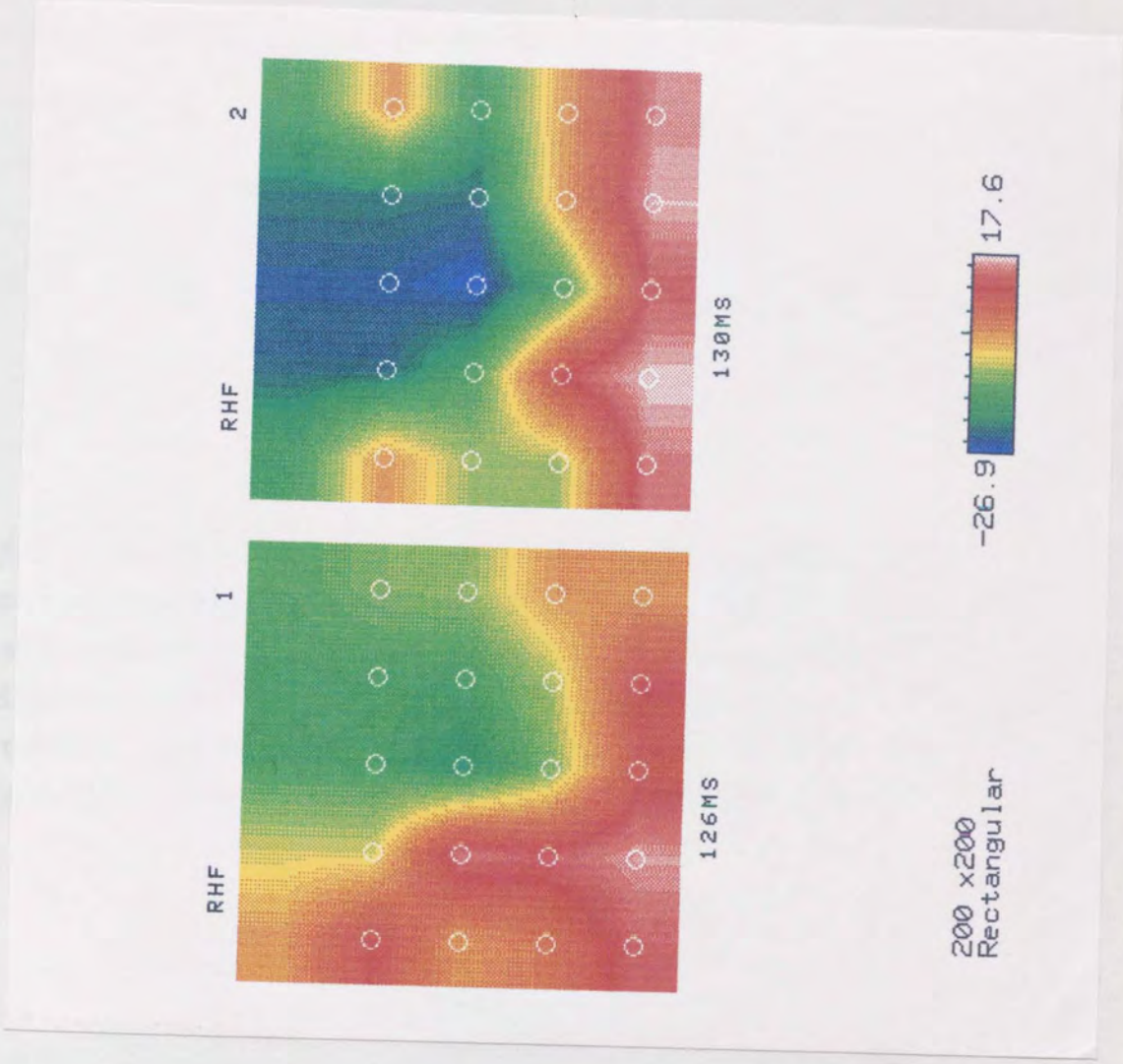

Fig. 6.3. A comparison of the topographical distribution of the VEMR recorded two months apart. 34' check stimulus was positioned in the right half field, subject CN.

Fig. 6.4. Distribution of the major positive (outgoing field) component of the pattern reversal VEMR from 70', 34' and 22' full (FF), left (LHF) and right half field (RHF) stimulation for subject RA. (Top row 70', middle row 34' and bottom row 22' check stimulation). The peak latencies are shown below the maps. Amplitude values are shown in the scale to the right of the maps (μV, 1μV = 8.9fT). Note the different scales used for the separate maps.

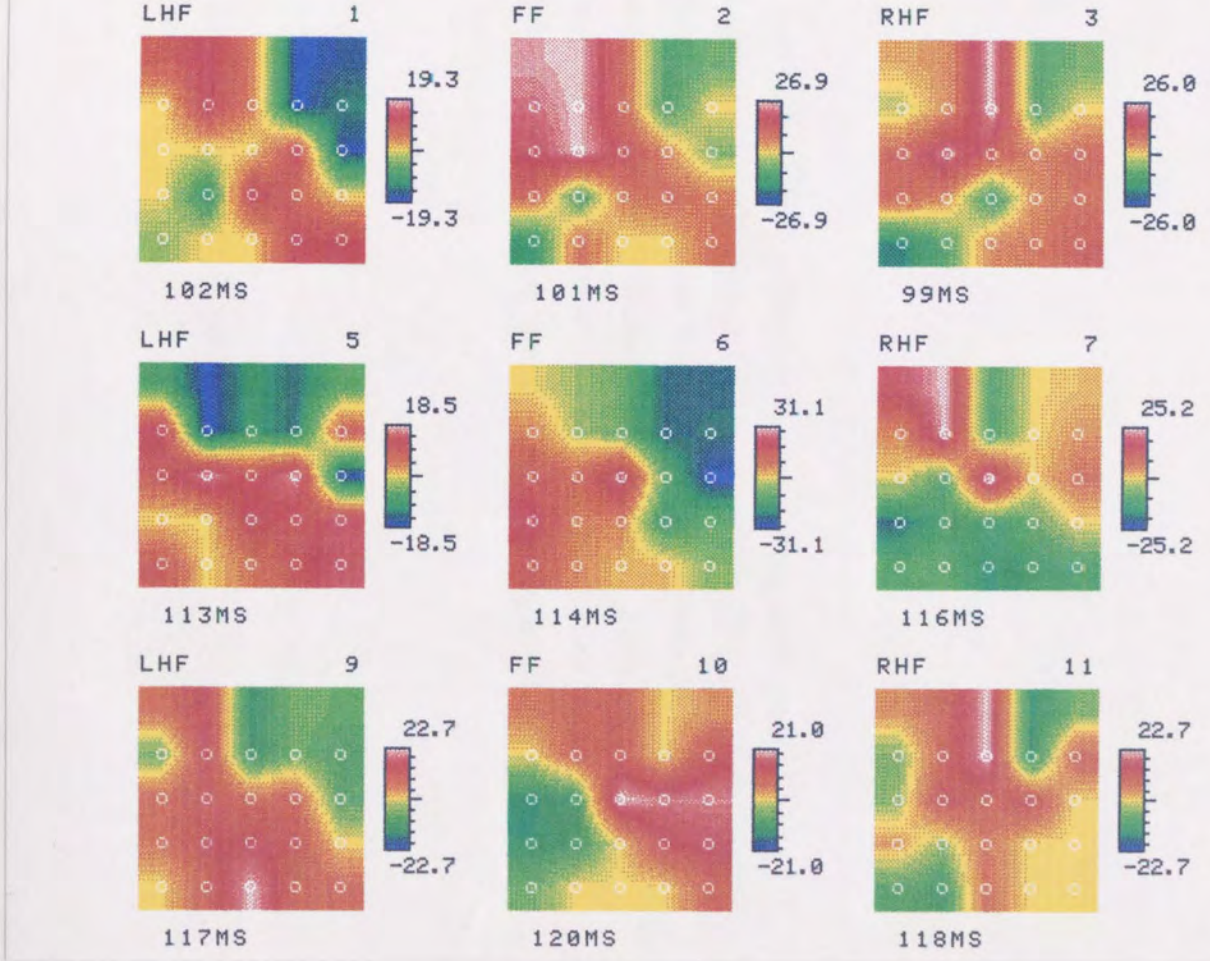
LHF 1
19.3
-19.3
102MS
FF 2
26.9
-26.9
101MS
RHF 3
26.0
-26.0
99MS
LHF 5
18.5
-18.5
113MS
FF 6
31.1
-31.1
114MS
RHF 7
25.2
-25.2
116MS
LHF 9
22.7
-22.7
117MS
FF 10
21.0
-21.0
120MS
RHF 11
22.7
-22.7
118MS

Fig. 6.5. Distribution of the major positive (outgoing field) component of the pattern reversal VEMR from 70', 34' and 22' full (FF), left (LHF) and right half field (RHF) stimulation for subject CD. (Top row 70', middle row 34' and bottom row 22' check stimulation). The peak latencies are shown below the maps. Amplitude values are shown in the scale to the right of the maps (μV, 1μV = 8.9fT). Note the different scales used for the separate maps.

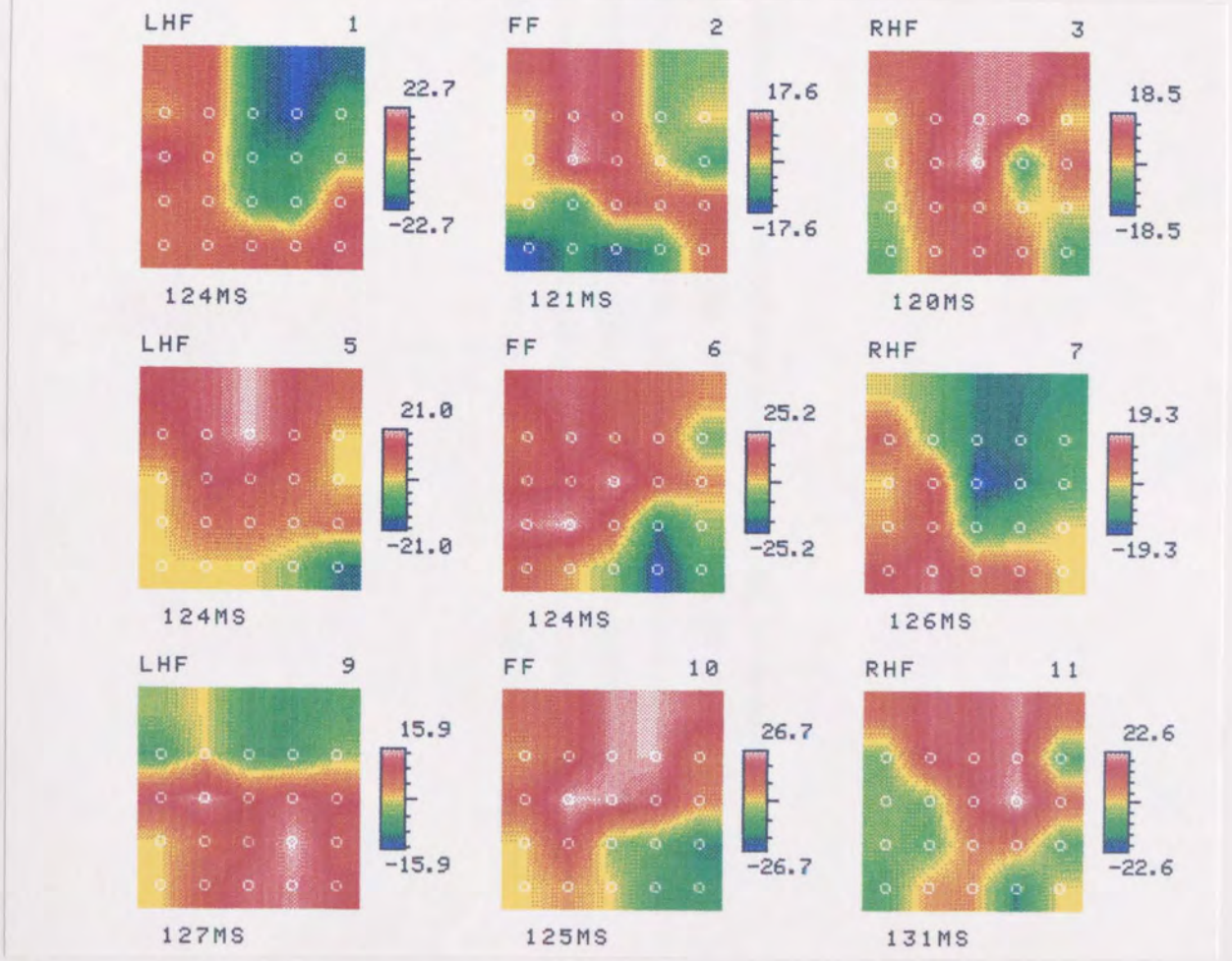
LHF 1
22.7
-22.7
124MS
FF 2
17.6
-17.6
121MS
RHF 3
18.5
-18.5
120MS
LHF 5
21.0
-21.0
124MS
FF 6
25.2
-25.2
124MS
RHF 7
19.3
-19.3
126MS
LHF 9
15.9
-15.9
127MS
FF 10
26.7
-26.7
125MS
RHF 11
22.6
-22.6
131MS

Fig. 6.6. Distribution of the major positive (outgoing field) component of the pattern reversal VEMR from 70', 34' and 22' full (FF), left (LHF) and right half field (RHF) stimulation for subject CN. (Top row 70', middle row 34' and bottom row 22' check stimulation). The peak latencies are shown below the maps. Amplitude values are shown in the scale to the right of the maps (μV, 1μV = 8.9fT). Note the different scales used for the separate maps.

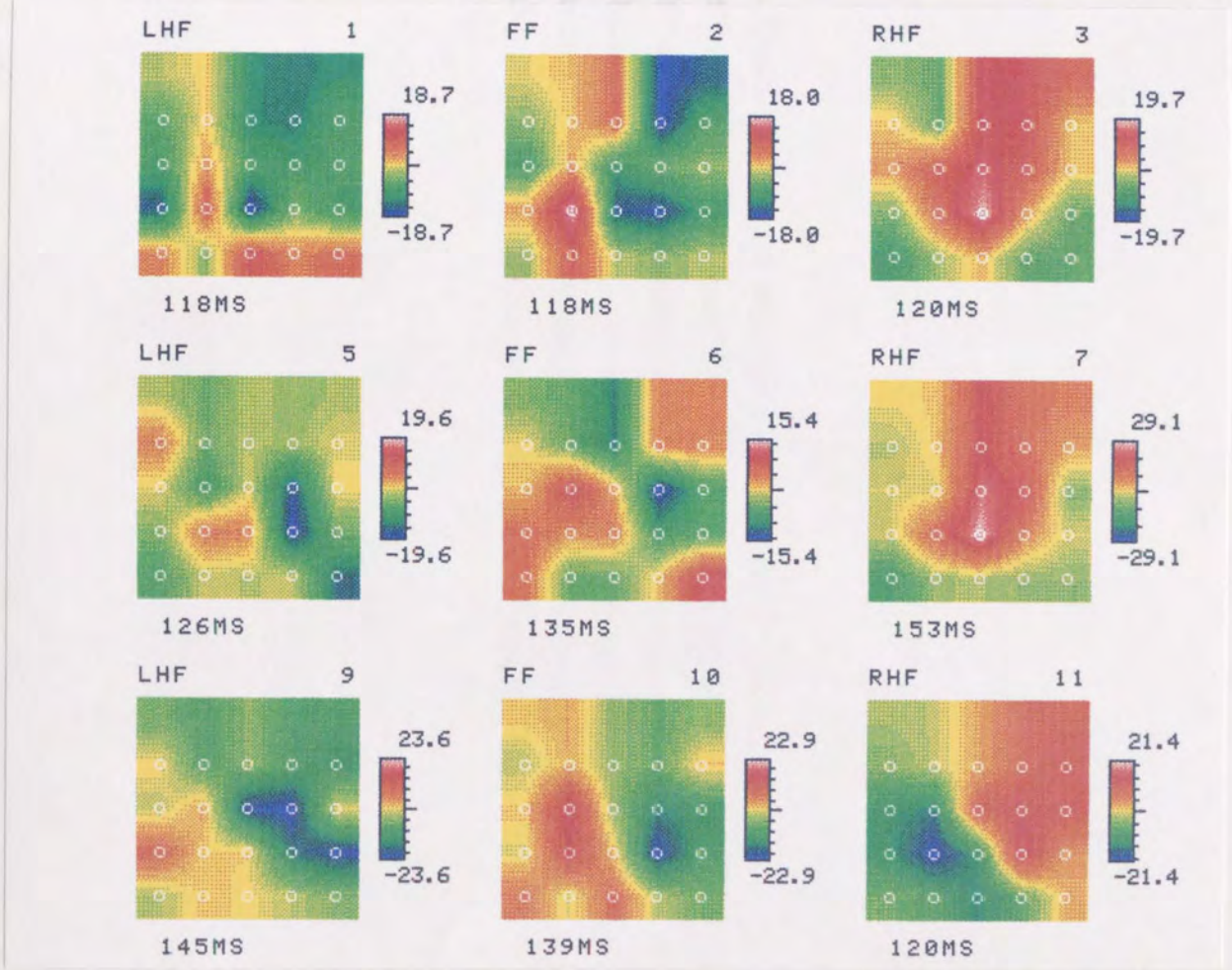
LHF 1
18.7
-18.7
118MS
FF 2
18.0
-18.0
118MS
RHF 3
19.7
-19.7
120MS
LHF 5
19.6
-19.6
126MS
FF 6
15.4
-15.4
135MS
RHF 7
29.1
-29.1
153MS
LHF 9
23.6
-23.6
145MS
FF 10
22.9
-22.9
139MS
RHF 11
21.4
-21.4
120MS

Fig. 6.7. Distribution of the major positive (outgoing field) component of the pattern reversal VEMR from 70', 34' and 22' full (FF), left (LHF) and right half field (RHF) stimulation for subject AS. (Top row 70', middle row 34' and bottom row 22' check stimulation). The peak latencies are shown below the maps. Amplitude values are shown in the scale to the right of the maps (μV, 1μV = 8.9fT). Note the different scales used for the separate maps.

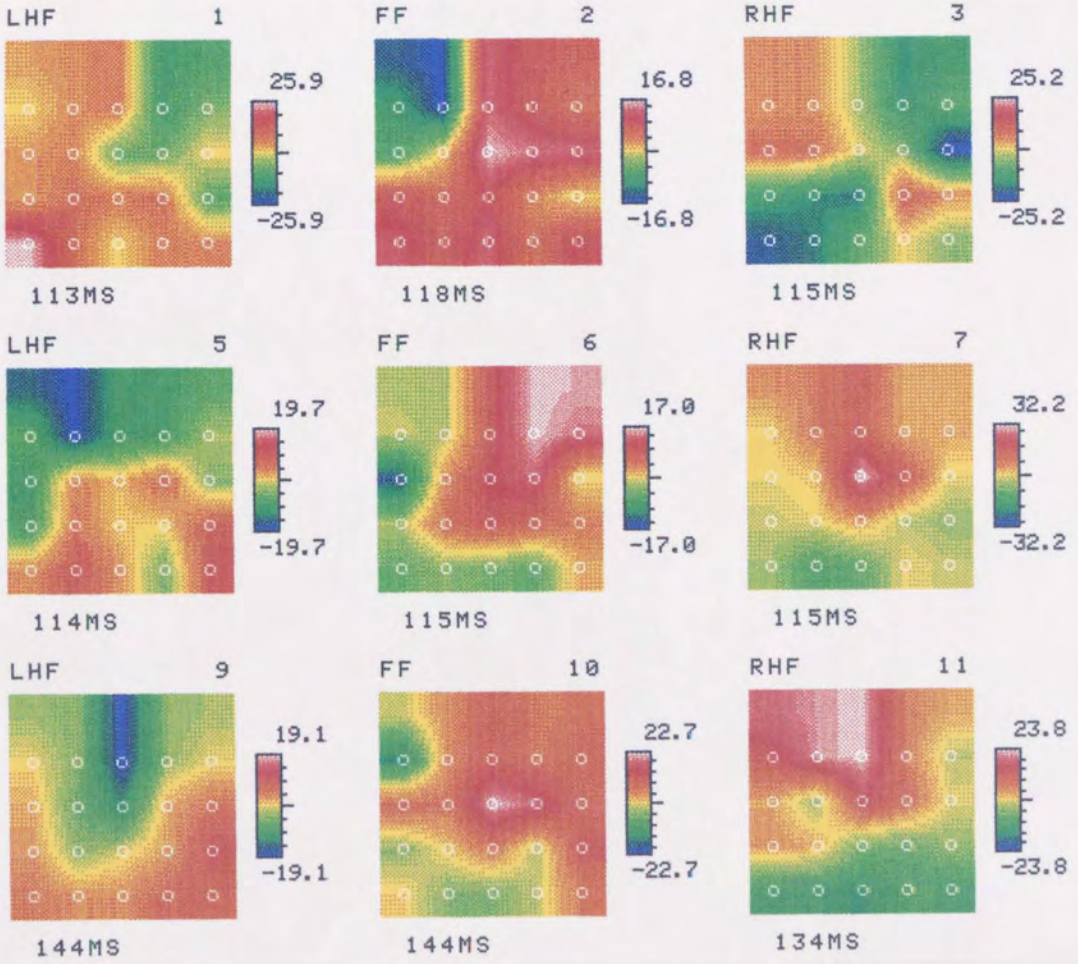
LHF 1
25.9
-25.9
113MS
FF 2
16.8
-16.8
118MS
RHF 3
25.2
-25.2
115MS
LHF 5
19.7
-19.7
114MS
FF 6
17.0
-17.0
115MS
RHF 7
32.2
-32.2
115MS
LHF 9
19.1
-19.1
144MS
FF 10
22.7
-22.7
144MS
RHF 11
23.8
-23.8
134MS

Fig. 6.8. Distribution of the pattern reversal VEMR to full (FF), left (LHF) and right half field (RHF) stimulation for the 70' checks in all subjects. The distributions are from subject RA, on the left, then CD, CN and AS on the right. The peak latencies are shown below the maps. Amplitude values are shown in the scale to the right of the maps (μV, 1μV = 8.9fT). Note the different scales used for the separate maps.

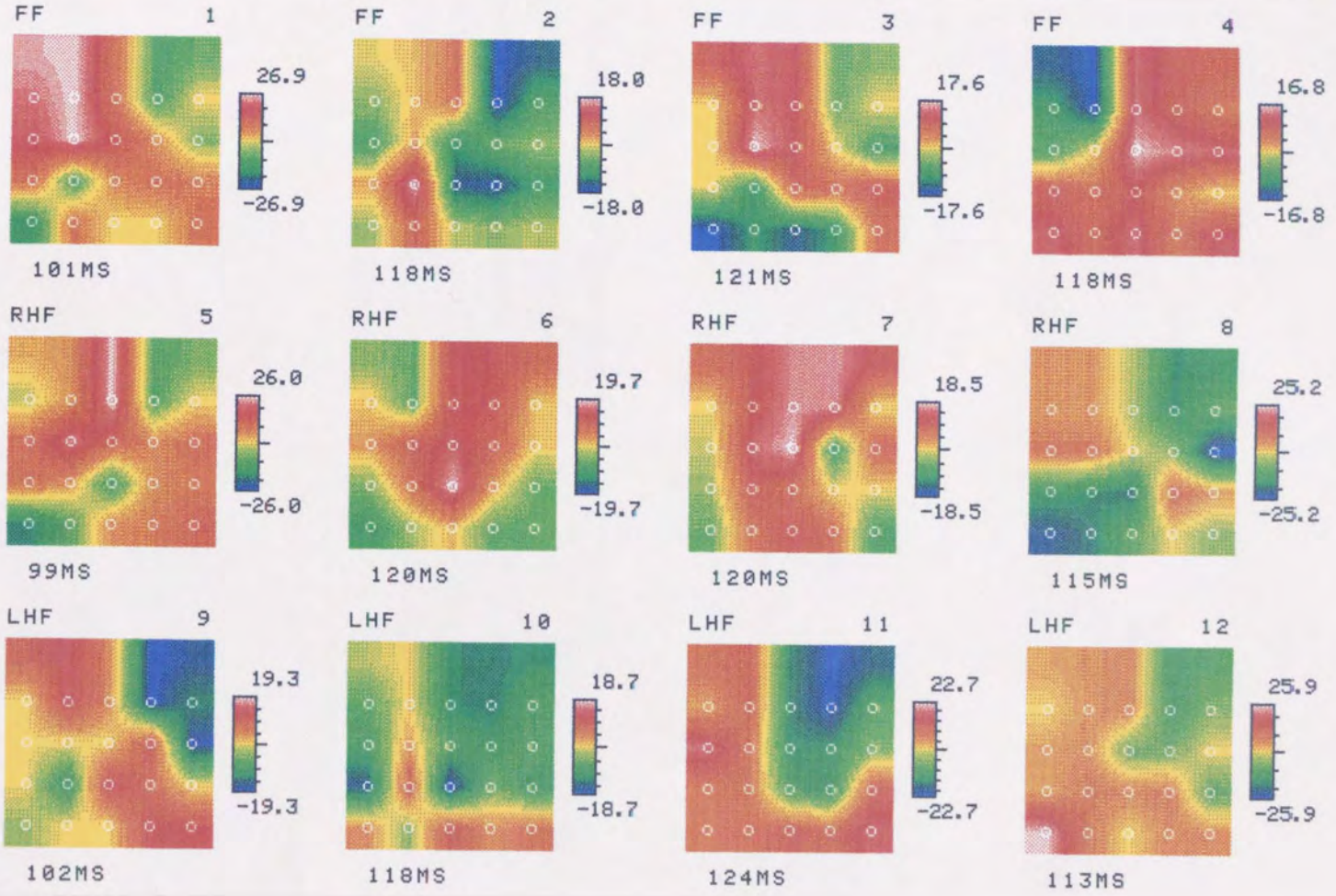
FF 1
26.9
-26.9
101MS
FF 2
18.0
-18.0
118MS
FF 3
17.6
-17.6
121MS
FF 4
16.8
-16.8
118MS
RHF 5
26.0
-26.0
99MS
RHF 6
19.7
-19.7
120MS
RHF 7
18.5
-18.5
120MS
RHF 8
25.2
-25.2
115MS
LHF 9
19.3
-19.3
102MS
LHF 10
18.7
-18.7
118MS
LHF 11
22.7
-22.7
124MS
LHF 12
25.9
-25.9
113MS

Fig. 6.9. Distribution of the pattern reversal VEMR to full (FF), left (LHF) and right half field (RHF) stimulation for the 34' checks in all subjects. The distributions are from subject RA, on the left, then CD, CN and AS on the right. The peak latencies are shown below the maps. Amplitude values are shown in the scale to the right of the maps (μV, 1μV = 8.9fT). Note the different scales used for the separate maps.

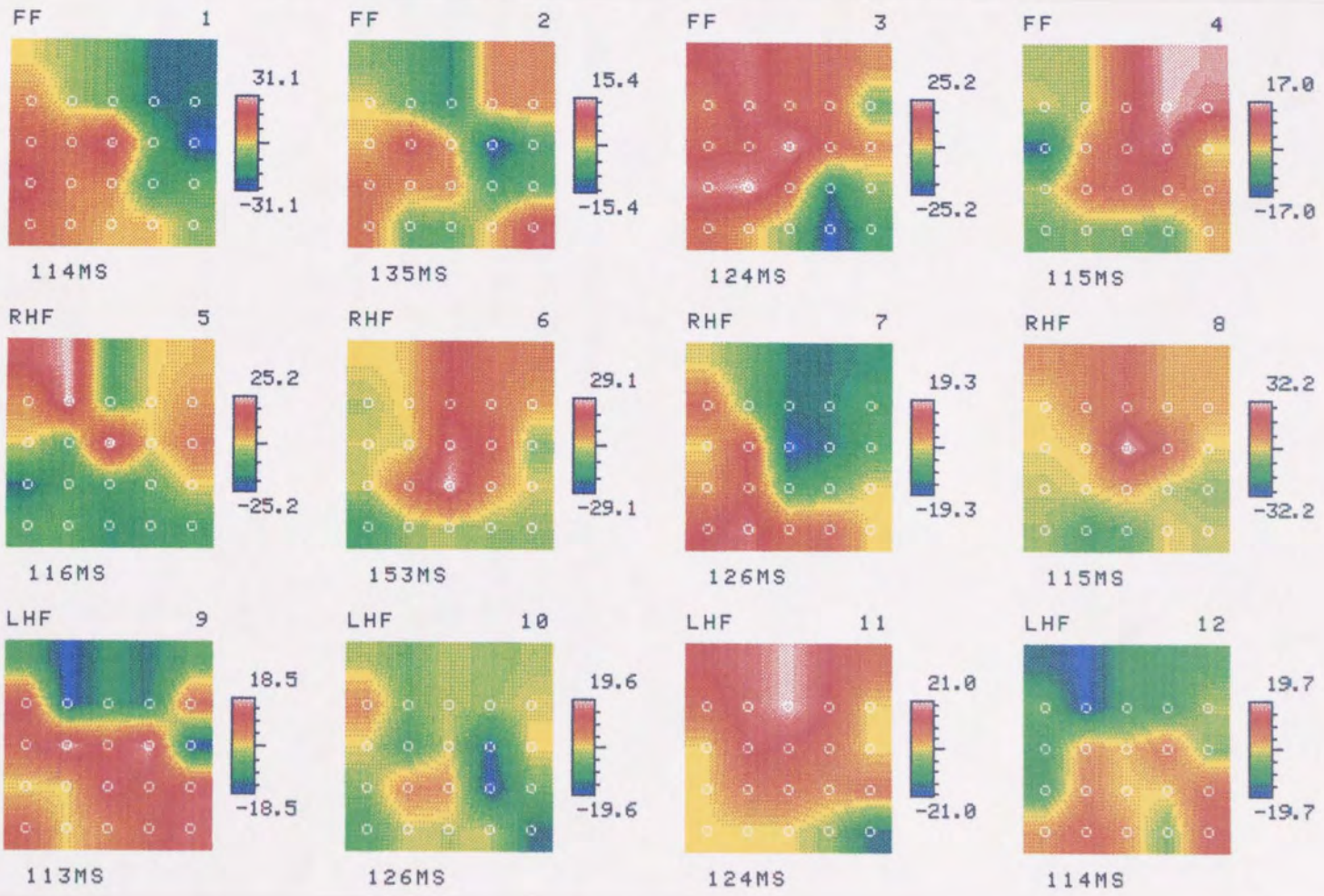
FF 1
31.1
-31.1
114MS
FF 2
15.4
-15.4
135MS
FF 3
25.2
-25.2
124MS
FF 4
17.0
-17.0
115MS
RHF 5
25.2
-25.2
116MS
RHF 6
29.1
-29.1
153MS
RHF 7
19.3
-19.3
126MS
RHF 8
32.2
-32.2
115MS
LHF 9
18.5
-18.5
113MS
LHF 10
19.6
-19.6
126MS
LHF 11
21.0
-21.0
124MS
LHF 12
19.7
-19.7
114MS

Fig. 6.10. Distribution of the pattern reversal VEMR to full (FF), left (LHF) and right half field (RHF) stimulation for the 22' checks in all subjects. The distributions are from subject RA, on the left, then CD, CN and AS on the right. The peak latencies are shown below the maps. Amplitude values are shown in the scale to the right of the maps (μV, 1μV = 8.9fT). Note the different scales used for the separate maps.

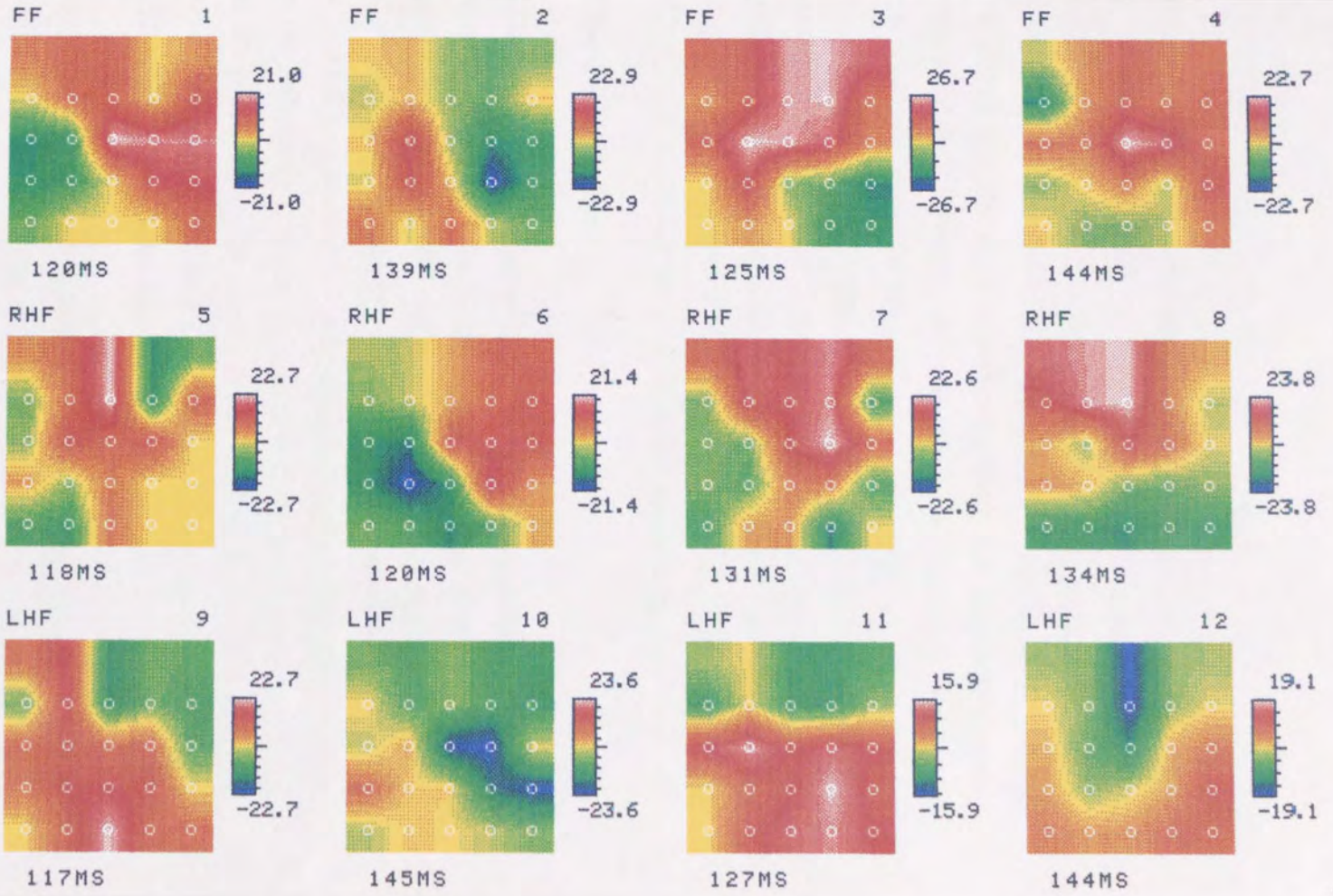
FF 1
21.0
-21.0
120MS
FF 2
22.9
-22.9
139MS
FF 3
26.7
-26.7
125MS
FF 4
22.7
-22.7
144MS
RHF 5
22.7
-22.7
118MS
RHF 6
21.4
-21.4
120MS
RHF 7
22.6
-22.6
131MS
RHF 8
23.8
-23.8
134MS
LHF 9
22.7
-22.7
117MS
LHF 10
23.6
-23.6
145MS
LHF 11
15.9
-15.9
127MS
LHF 12
19.1
-19.1
144MS

6.3.1.i Left Half Field Stimulation

The distribution following 70' check stimulation was the most consistent distribution of all the fields and check sizes. An ingoing field, negativity was recorded over the right anterior region with an outgoing field, positivity over the posterior region, this being maximal over the right posterior region in 2 subjects. With a reduction in check size the right anterior negative and posterior positive distribution was observed in 2 subjects. In one subject a negativity was found over the right and a positivity over the left of the montage, this was apparent for both 34' and 22' checks. In the remaining subject the response after 34' check stimulation was maximal over the right however the polarities were reversed, an anterior positivity and a posterior negativity were recorded. In this subject the negativity was maximal over the centre of the montage on 22' stimulation and the positivity was maximal over the right posterior region of the montage.

6.3.1.ii Right Half Field Stimulation

On right half field stimulation the response was not definitely positioned over the contralateral hemisphere. With 70' checks the maximum positivity was over the midline for 3 subjects the negativity was maximal over the posterior region of the montage, in the other subject the positivity was maximal anteriorly over the left hemisphere. After 34' check stimulation 2 subjects produced maximal positivities over the midline, in the remaining subjects the positivity was maximal over the left anterior for one and the posterior region for the other. On small check stimulation the positivity was maximal anteriorly in 3 subjects, with varying laterality, and maximal over the right central area in the other.

Although the maximal amplitudes were recorded over the contralateral hemisphere some activity was also recorded over the ipsilateral hemisphere. This may have been a result of the recording strategy employed i.e. recording the response following the scalp surface. If a stationary source is assumed that does not change orientation throughout the test time then as the probe moves around the scalp surface sources that are radial to the probe in one region may produce a weak tangential component in another recording position.

The distribution following left half field stimulation appeared to be the most consistent, this may relate to the observation following left half field stimulation in chapter 5 that the contralateral components are most prominent after left half field

stimulation. This may suggest that the source of the left half field response was positioned more tangentially.

The distribution of the responses could be consistent with a source in the contralateral hemisphere. The exact location of the maxima varied between subjects and check sizes, in most cases simple source fitting suggested a source at an oblique angle directed towards the ipsilateral hemisphere. This was apparent for all subjects except subject CN, after 34' stimulation the distribution remained consistent with a source in the contralateral hemisphere however from Flemings right hand rule the current was apparently flowing away from the midline.

6.3.2 Effect of Check Size on the Topographical Distribution

The effect of check size on the distribution of the field for all four subjects is demonstrated in figs.6.8 - 6.10. Reducing the check size appears to have only a minimal effect on the distribution of the half field response, for all subjects except CN. The distribution of CN34' was the inverse of that produced by the other subjects, with the outgoing field being anterior and the ingoing field posterior for left half field stimulation. A preferential effect on the field strength was demonstrated after reduction in check size by subject AS; on right half field stimulation the outgoing field was enhanced with respect to the ingoing field, whereas left half field stimulation enhanced the ingoing field. The ingoing field from subject CN was demonstrated to move from being maximal over the left to being maximal over the right with an increase in check size.

Full field distributions appear to be more variable between subjects. On reduction of the check size the inter subject variability was however found to be low. Only for subject RA was the distribution observed to change substantially, with the distribution from 22' check stimulation being the reverse of that with 34' checks. The distribution of the maxima of subject CD were located consistently more posterior on the montage.

6.3.3 Effect of Check Size on the Response Amplitude

No consistent change in the amplitude was demonstrated with a change in the check size. For full field stimulation the maximum responses from 3/4 subjects (CN,CD,AS) were after small check stimulation whereas for one subject (RA) maxima were demonstrated with large check stimulation. On right half field stimulation the maxima were observed after stimulation with the 34' checks from

2/4 subjects (AS,CD) and with the large and small checks for the remaining (RA and CN respectively). On left half field stimulation two subjects produced maximal responses to small check stimulation (RA,CD) while the remaining showed maximal responses to large check stimulation.

Except for the responses of CN34' and 70' and CD22', the right half field evoked larger amplitude signals. The distribution however appeared to be more consistent between subjects on left half field stimulation (except for CN34' whose response was inconsistent from both left and right half fields).

6.3.4 Effect of Check Size on the Response Latency

The latency of the maximal field was found to increase with an increase in the check size of the stimulus for all subjects, except subject CD after RHF stimulation. Individual latencies are tabulated in the appendix table A.5.

6.4 VEP Methods

For the comparative VEP recordings the response was recorded in a grid with an inter point spacing of 10% of the half head circumference as with the VEMR, the montage was, however, three electrodes on the inion line, then three rows of five electrodes above these and a top row of three electrodes, see fig.6.11. The response was filtered at 1-30 Hz, no 50Hz notch filter was used and the gain was set at 30,000. The VEP was referred to Fz and ground used was Fpz. An Fz reference was used as non cephalic references induced too much artefact when using the stimulus set up employed for the VEMR recording. Average reference was not satisfactory as the electrodes are located over a closely spaced area, the reference will therefore not equate to zero and the reference will artifically reduce the amplitude of the recorded signals.

Before the electrodes were applied the scalp was gently abraded with omniprep™ to reduce the scalp resistance. Silver-silver chloride electrodes were then positioned and held in place by Blenderm tape™. The electrode resistance was maintained below 5KΩ.

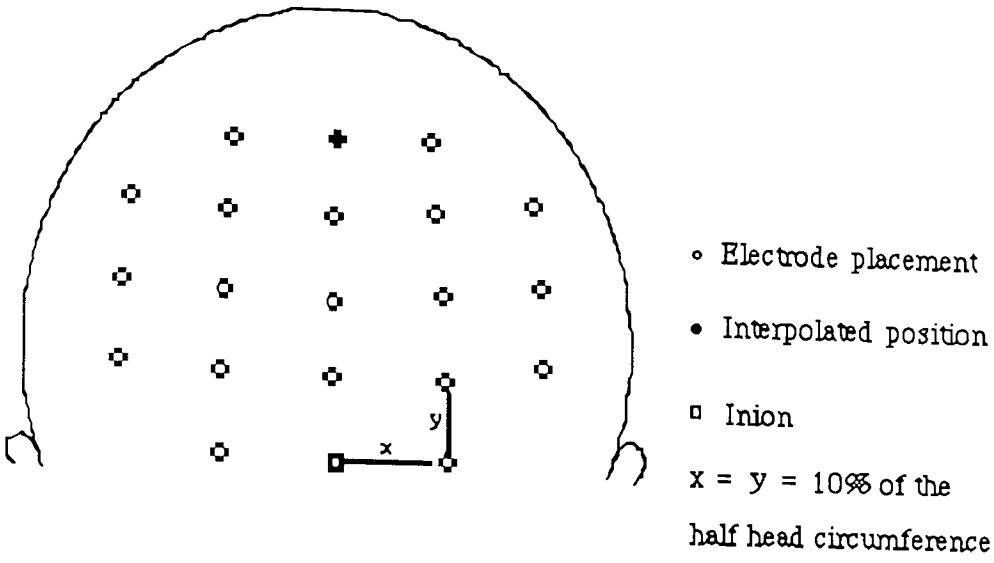

Fig.6.11. Illustration of the electrode positions for the VEP study.

The stimulus parameters were as described in the methods section of the VEMR study. Maps were produced at the latency of the major peaks in the response. The values of the potential were recorded and were transferred onto the Pathfinder II™ mapping software to produce thermal printouts. The potential values between each electrode point were calculated as for the VEMR maps.

6.5 Results

The topograhical distribution of the full and half fields VEP with the range of check sizes for the four subjects are shown in figs. 6.12 - 6.23.

6.5.1 Full Field

The classical response to full field stimulation is a negative-positive-negative response. This type of response was observed in all subjects. The first repeatable component was a negativity, with varying laterality. The component following this was the P100, this also had varying lateralities. In subject CN P100 was consistently maximal over the left of the montage, and in subject RA it was consistently maximal over the right. The P100 was followed by a negative distribution in subjects CD and AS, the latency of this negativity appeared to be earlier in subject AS. A positivity was also observed over the centre of the

Fig 6.12. Distribution of the major components of the pattern reversal VEP from 70' full (FF), left (LHF), and right half field (RHF) stimulation for subject RA, mapped at the peak latency. Latencies of the peak are given below the maps. The peak amplitudes are given in the scale to the right of the maps (μV).
Note the different amplitude scales for each component.

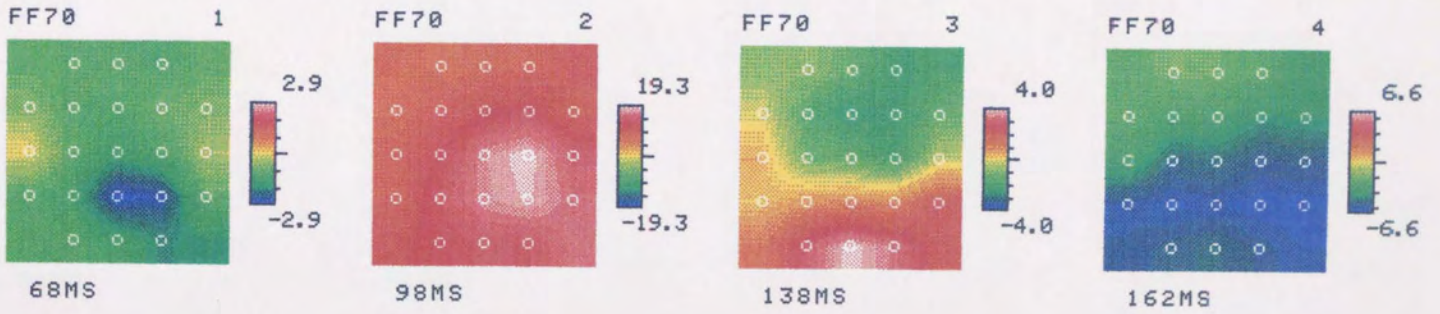
FF70 1
2.9
-2.9
68MS
FF70 2
19.3
-19.3
98MS
FF70 3
4.0
-4.0
138MS
FF70 4
6.6
-6.6
162MS

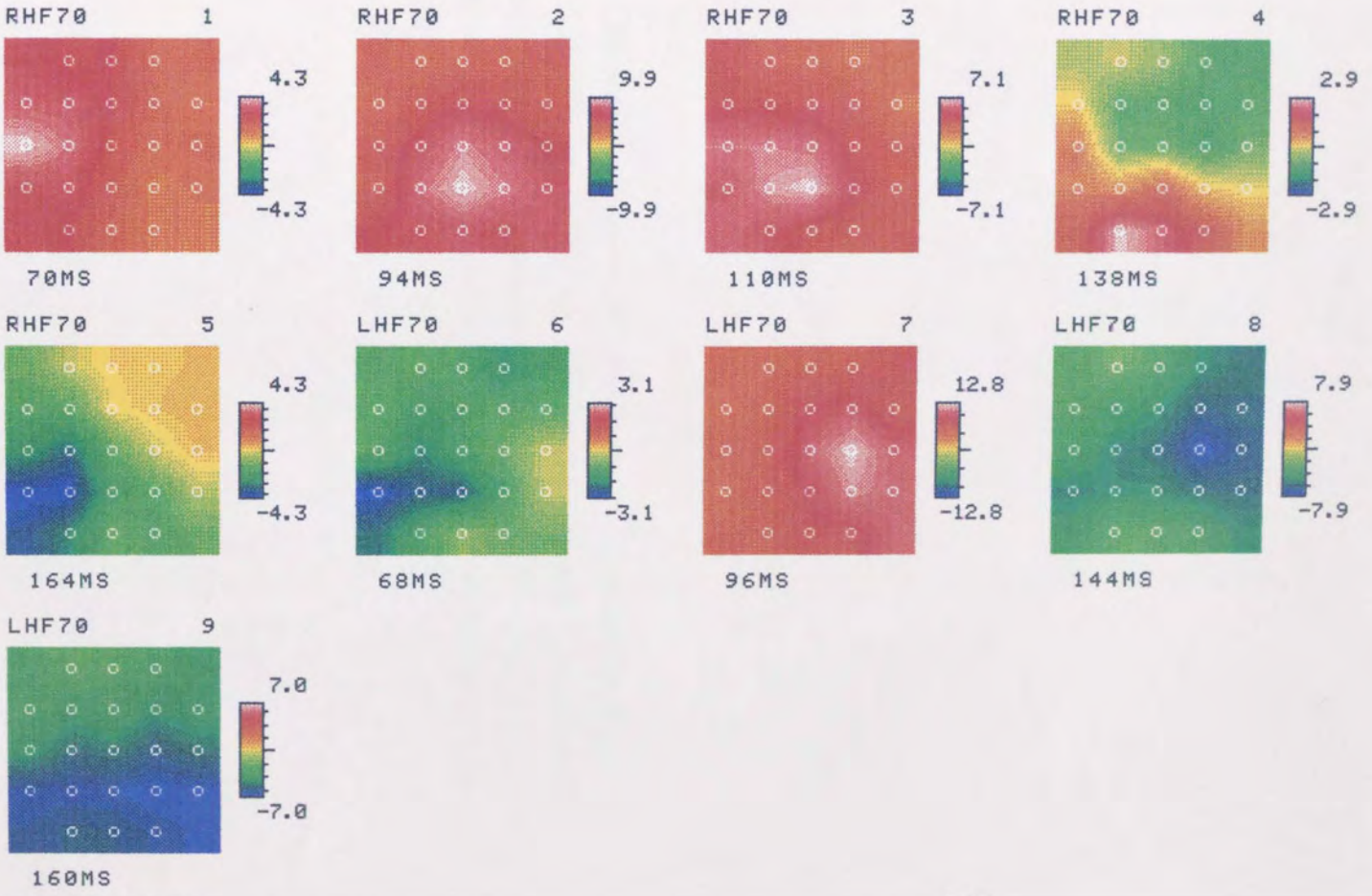
RHF70 1
4.3
-4.3
70MS
RHF70 2
9.9
-9.9
94MS
RHF70 3
7.1
-7.1
110MS
RHF70 4
2.9
-2.9
138MS
RHF70 5
4.3
-4.3
164MS
LHF70 6
3.1
-3.1
68MS
LHF70 7
12.8
-12.8
96MS
LHF70 8
7.9
-7.9
144MS
LHF70 9
7.0
-7.0
160MS

Fig 6.13. Distribution of the major components of the pattern reversal VEP from 34' full (FF), left (LHF), and right half field (RHF) stimulation for subject RA, mapped at the peak latency. Latencies of the peak are given below the maps. The peak amplitudes are given in the scale to the right of the maps (μV).
Note the different amplitude scales for each component.

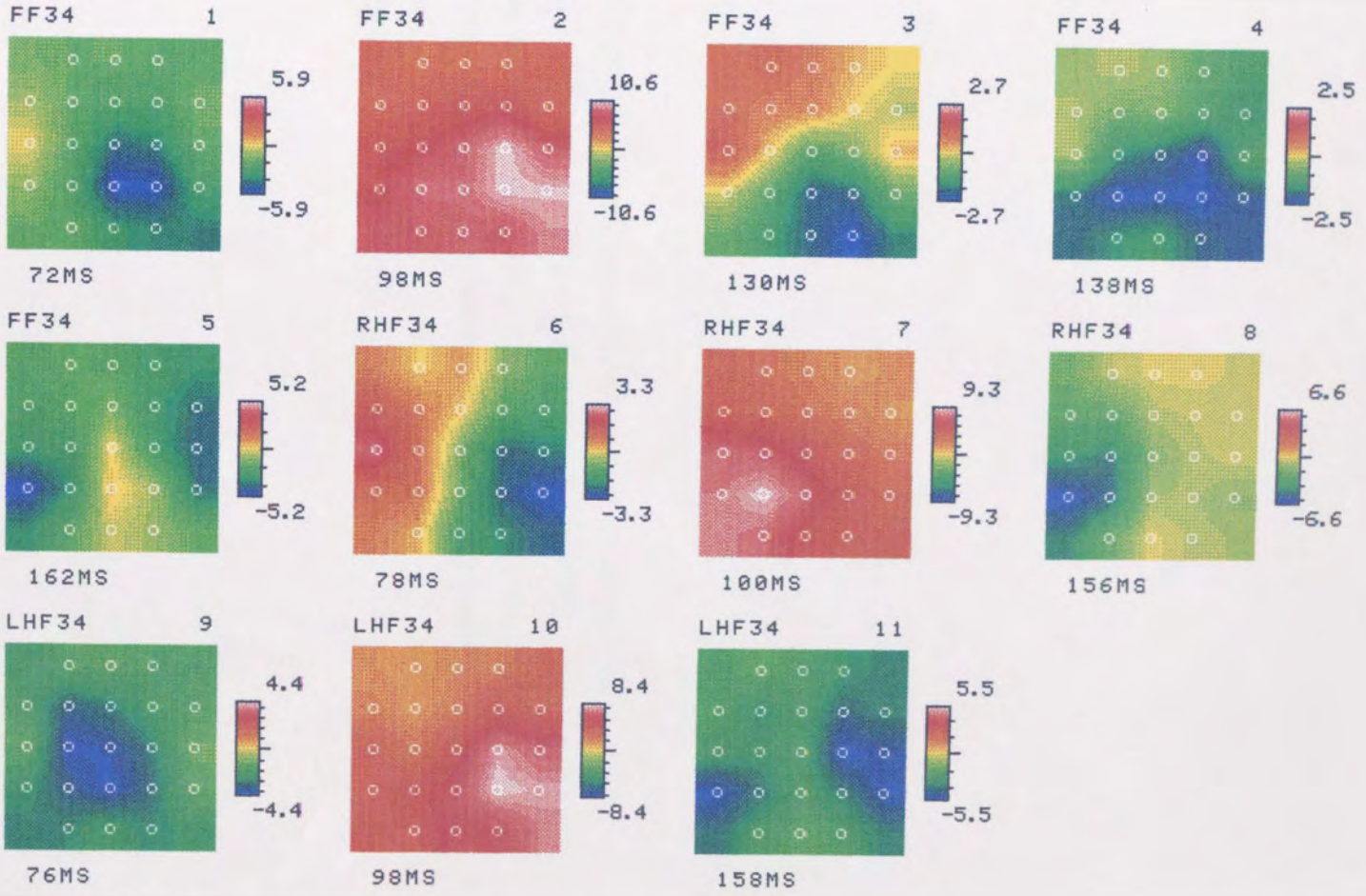
FF34 1
5.9
-5.9
72MS
FF34 2
10.6
-10.6
98MS
FF34 3
2.7
-2.7
130MS
FF34 4
2.5
-2.5
138MS
FF34 5
5.2
-5.2
162MS
RHF34 6
3.3
-3.3
78MS
RHF34 7
9.3
-9.3
100MS
RHF34 8
6.6
-6.6
156MS
LHF34 9
4.4
-4.4
76MS
LHF34 10
8.4
-8.4
98MS
LHF34 11
5.5
-5.5
158MS

Fig 6.14. Distribution of the major components of the pattern reversal VEP from 22' full (FF), left (LHF), and right half field (RHF) stimulation for subject RA, mapped at the peak latency. Latencies of the peak are given below the maps. The peak amplitudes are given in the scale to the right of the maps (μV).
Note the different amplitude scales for each component.

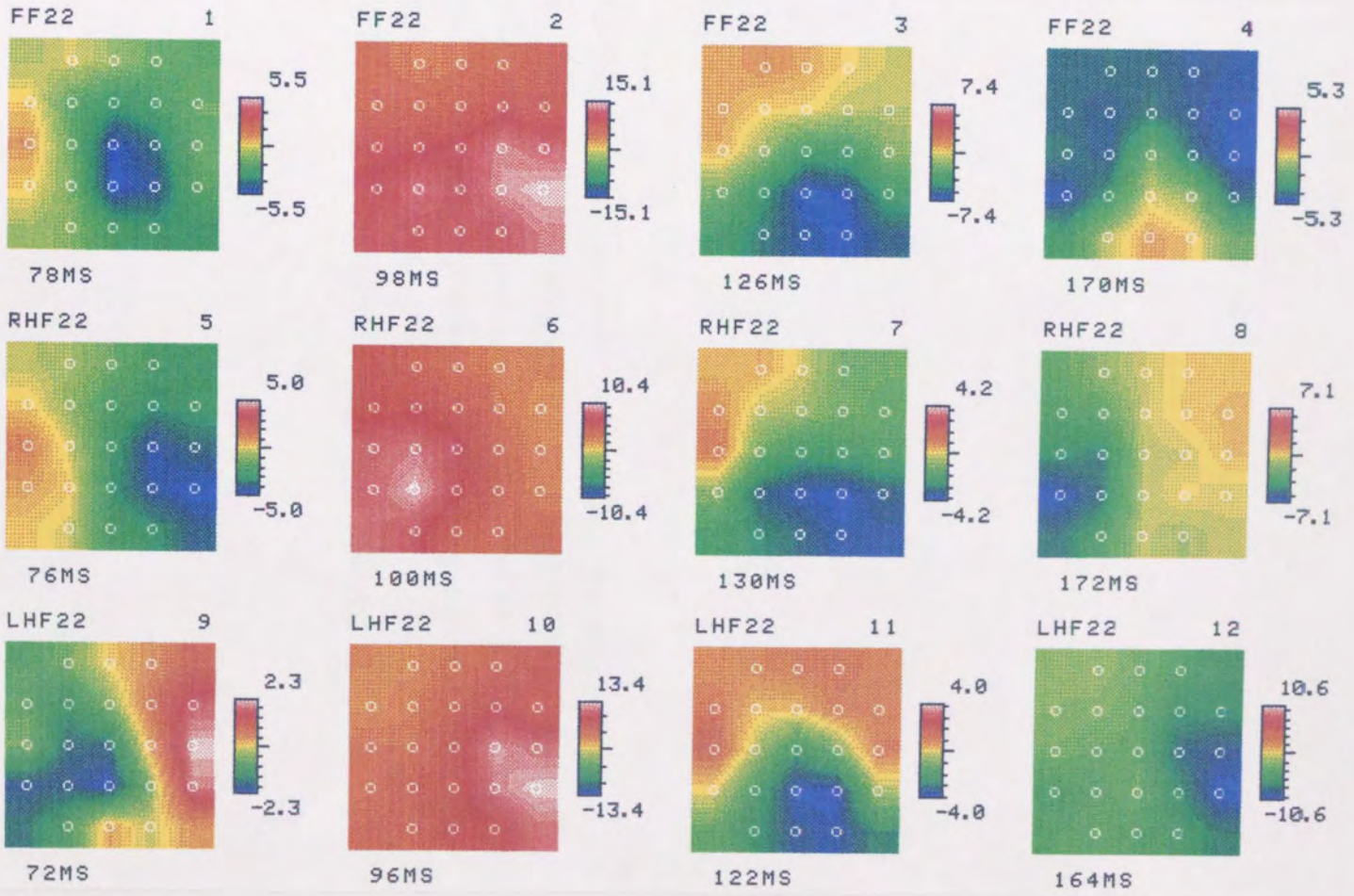
FF22 1
5.5
-5.5
78MS
FF22 2
15.1
-15.1
98MS
FF22 3
7.4
-7.4
126MS
FF22 4
5.3
-5.3
170MS
RHF22 5
5.0
-5.0
76MS
RHF22 6
10.4
-10.4
100MS
RHF22 7
4.2
-4.2
130MS
RHF22 8
7.1
-7.1
172MS
LHF22 9
2.3
-2.3
72MS
LHF22 10
13.4
-13.4
96MS
LHF22 11
4.0
-4.0
122MS
LHF22 12
10.6
-10.6
164MS

Figure 6.15. Distribution of the major components of the pattern reversal VEP from 34' full (FF), left (LHF), and right half field (RHF) stimulation for subject CD, mapped at the peak latency. Latencies of the peak are given below the maps. The peak amplitudes are shown in the scale to the right of the maps (μV).
Note the different amplitude scales used for each component.

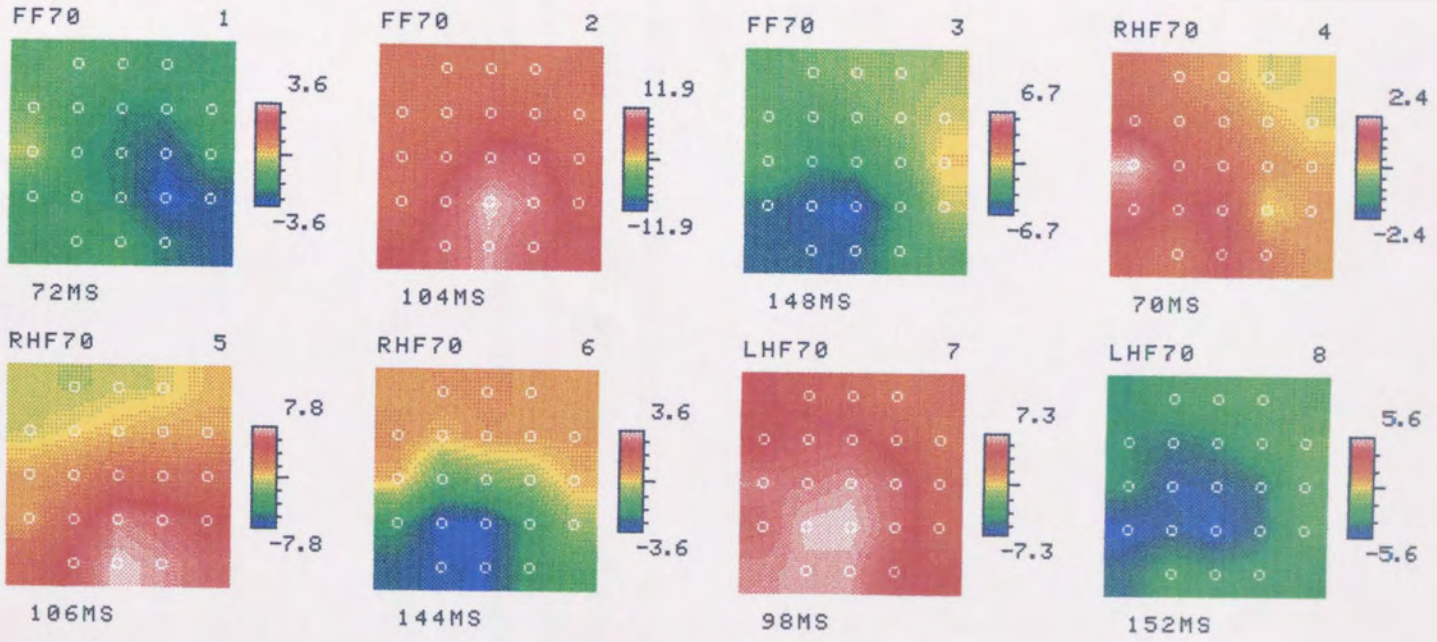
FF70 1
3.6
-3.6
72MS
FF70 2
11.9
-11.9
104MS
FF70 3
6.7
-6.7
148MS
RHF70 4
2.4
-2.4
70MS
RHF70 5
7.8
-7.8
106MS
RHF70 6
3.6
-3.6
144MS
LHF70 7
7.3
-7.3
98MS
LHF70 8
5.6
-5.6
152MS

Fig 6.16. Distribution of the major components of the pattern reversal VEP from 34' full (FF), left (LHF), and right half field (RHF) stimulation for subject CD, mapped at the peak latency. Latencies of the peak are given below the maps. The peak amplitudes are given in the scale to the right of the maps (μV).
Note the different amplitude scales for each component.

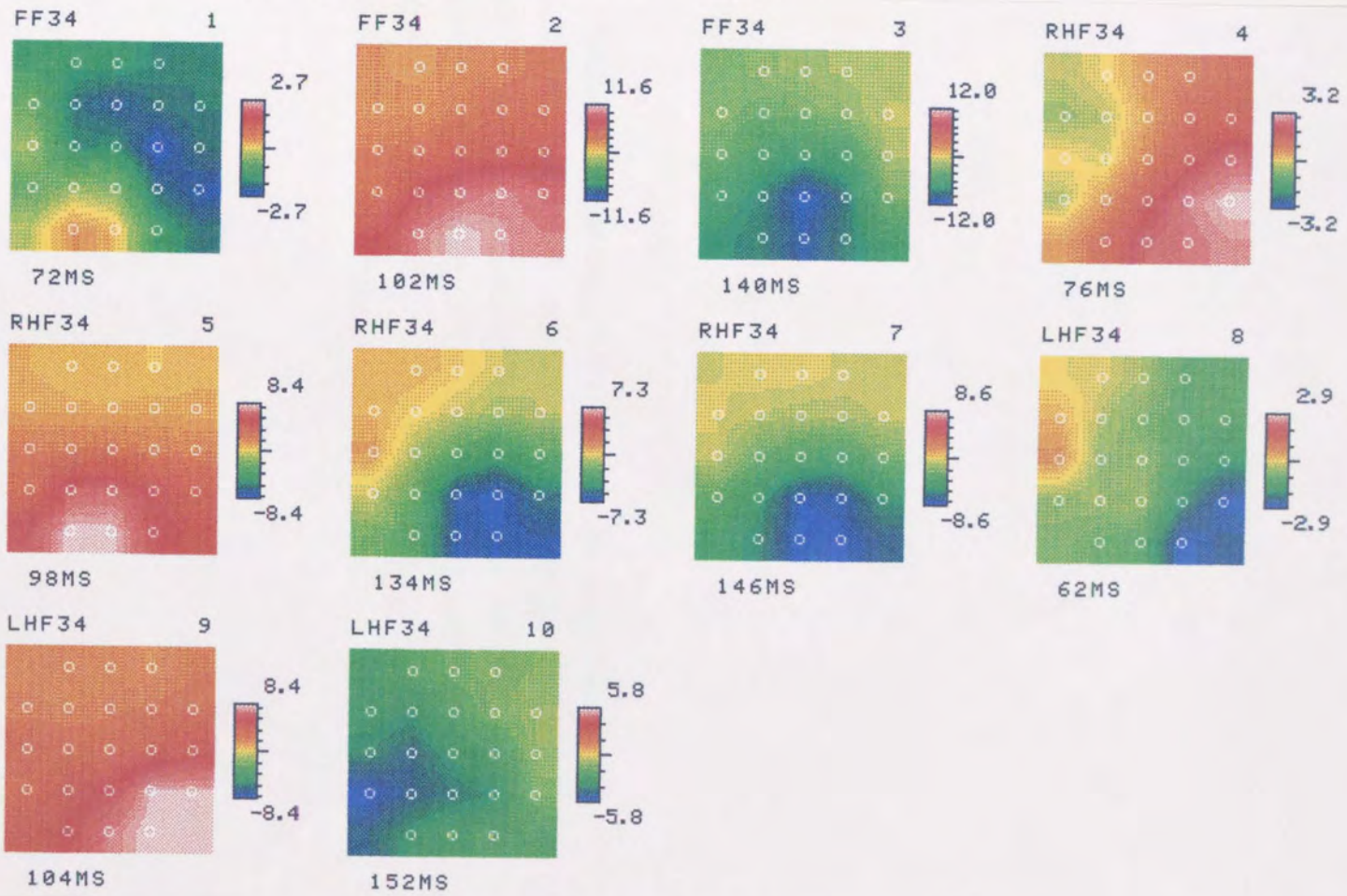
FF34 1
2.7
-2.7
72MS
FF34 2
11.6
-11.6
102MS
FF34 3
12.0
-12.0
140MS
RHF34 4
3.2
-3.2
76MS
RHF34 5
8.4
-8.4
98MS
RHF34 6
7.3
-7.3
134MS
RHF34 7
8.6
-8.6
146MS
LHF34 8
2.9
-2.9
62MS
LHF34 9
8.4
-8.4
104MS
LHF34 10
5.8
-5.8
152MS

Fig 6.17. Distribution of the major components of the pattern reversal VEP from 22' full (FF), left (LHF), and right half field (RHF) stimulation for subject CD, mapped at the peak latency. Latencies of the peak are given below the maps. The peak amplitudes are given in the scale to the right of the maps (μV).
Note the different amplitude scales for each component.

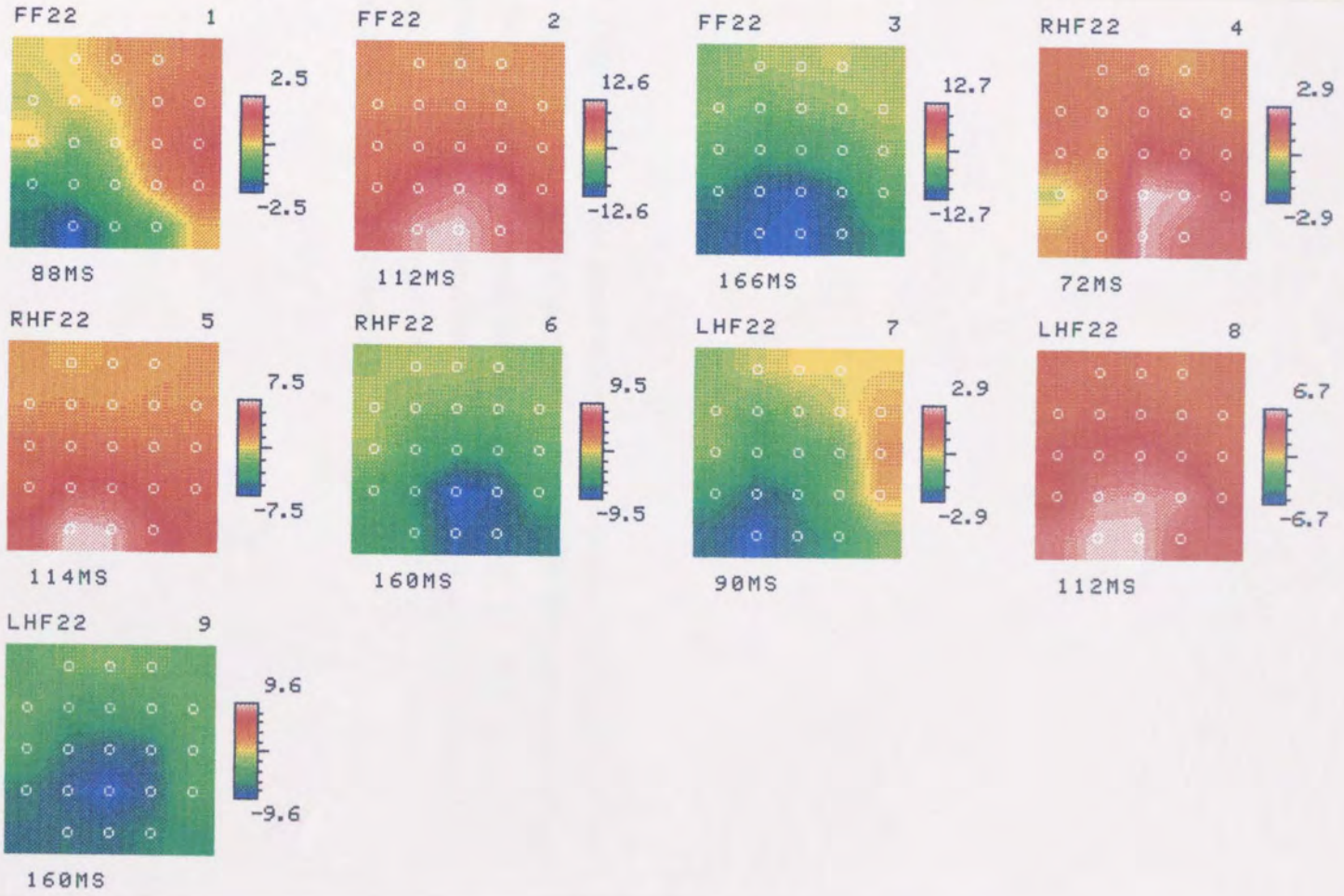
FF22 1
2.5
-2.5
88MS
FF22 2
12.6
-12.6
112MS
FF22 3
12.7
-12.7
166MS
RHF22 4
2.9
-2.9
72MS
RHF22 5
7.5
-7.5
114MS
RHF22 6
9.5
-9.5
160MS
LHF22 7
2.9
-2.9
90MS
LHF22 8
6.7
-6.7
112MS
LHF22 9
9.6
-9.6
160MS

Fig 6.18. Distribution of the major components of the pattern reversal VEP from 70' full (FF), left (LHF), and right half field (RHF) stimulation for subject CN, mapped at the peak latency. Latencies of the peak are given below the maps. The peak amplitudes are given in the scale to the right of the maps (μV).
Note the different amplitude scales for each component.

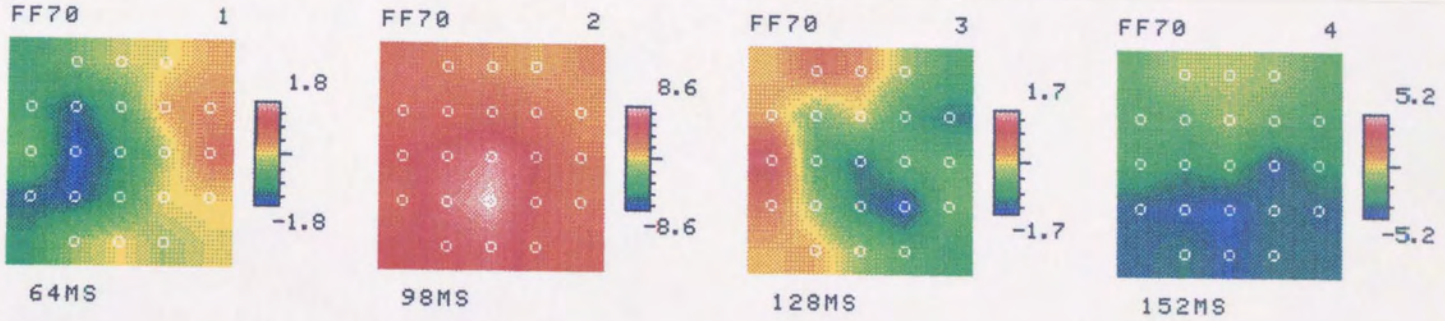
FF70 1
1.8
-1.8
64MS
FF70 2
8.6
-8.6
98MS
FF70 3
1.7
-1.7
128MS
FF70 4
5.2
-5.2
152MS

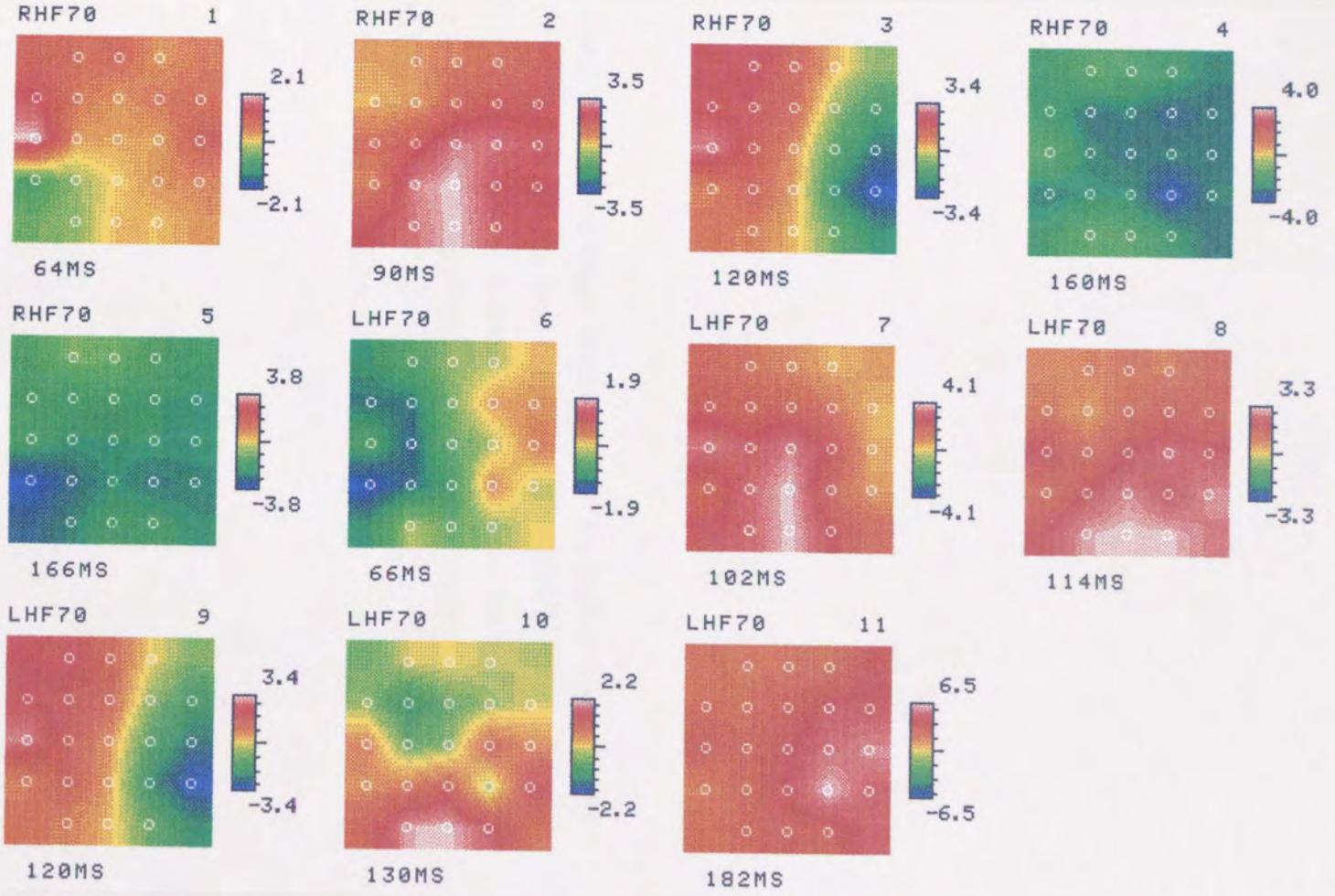
RHF70 1
2.1
-2.1
64MS
RHF70 2
3.5
-3.5
90MS
RHF70 3
3.4
-3.4
120MS
RHF70 4
4.0
-4.0
160MS
RHF70 5
3.8
-3.8
166MS
LHF70 6
1.9
-1.9
66MS
LHF70 7
4.1
-4.1
102MS
LHF70 8
3.3
-3.3
114MS
LHF70 9
3.4
-3.4
120MS
LHF70 10
2.2
-2.2
130MS
LHF70 11
6.5
-6.5
182MS

Fig 6.19. Distribution of the major components of the pattern reversal VEP from 34' full (FF), left (LHF), and right half field (RHF) stimulation for subject CN, mapped at the peak latency. Latencies of the peak are given below the maps. The peak amplitudes are given in the scale to the right of the maps (μV).
Note the different amplitude scales for each component.

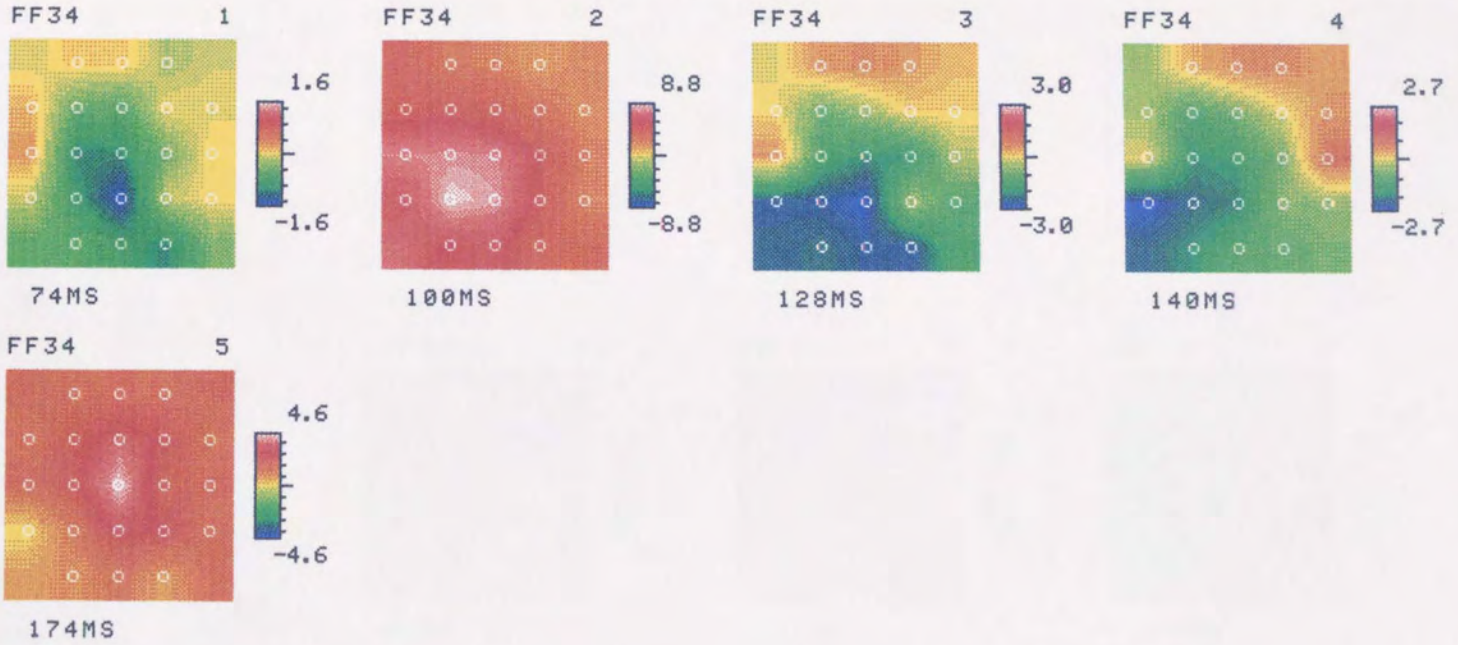
FF34 1
1.6
-1.6
74MS
FF34 2
8.8
-8.8
100MS
FF34 3
3.0
-3.0
128MS
FF34 4
2.7
-2.7
140MS
FF34 5
4.6
-4.6
174MS

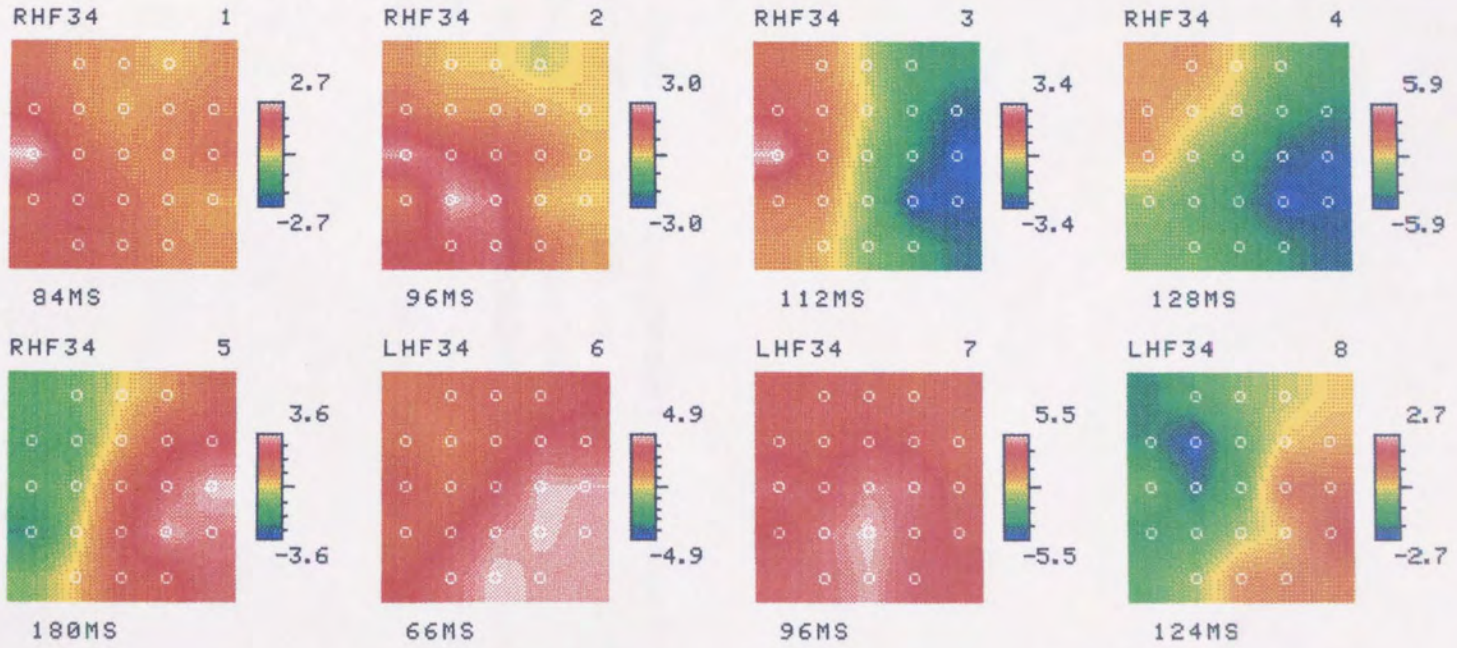
RHF34 1
2.7
-2.7
84MS
RHF34 2
3.0
-3.0
96MS
RHF34 3
3.4
-3.4
112MS
RHF34 4
5.9
-5.9
128MS
RHF34 5
3.6
-3.6
180MS
LHF34 6
4.9
-4.9
66MS
LHF34 7
5.5
-5.5
96MS
LHF34 8
2.7
-2.7
124MS

Fig 6.20. Distribution of the major components of the pattern reversal VEP from 22' full (FF), left (LHF), and right half field (RHF) stimulation for subject CN, mapped at the peak latency. Latencies of the peak are given below the maps. The peak amplitudes are given in the scale to the right of the maps (μV).
Note the different amplitude scales for each component.

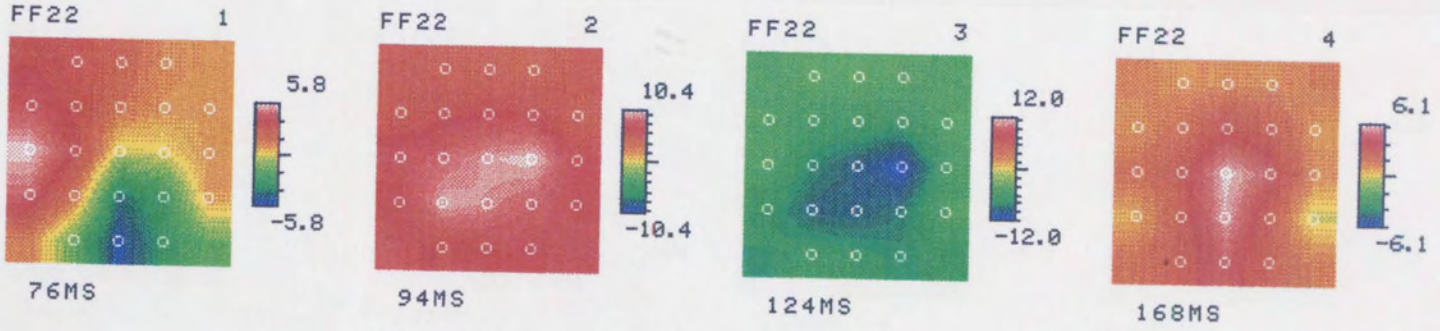
FF22 1
5.8
-5.8
76MS
FF22 2
10.4
-10.4
94MS
FF22 3
12.0
-12.0
124MS
FF22 4
6.1
-6.1
168MS

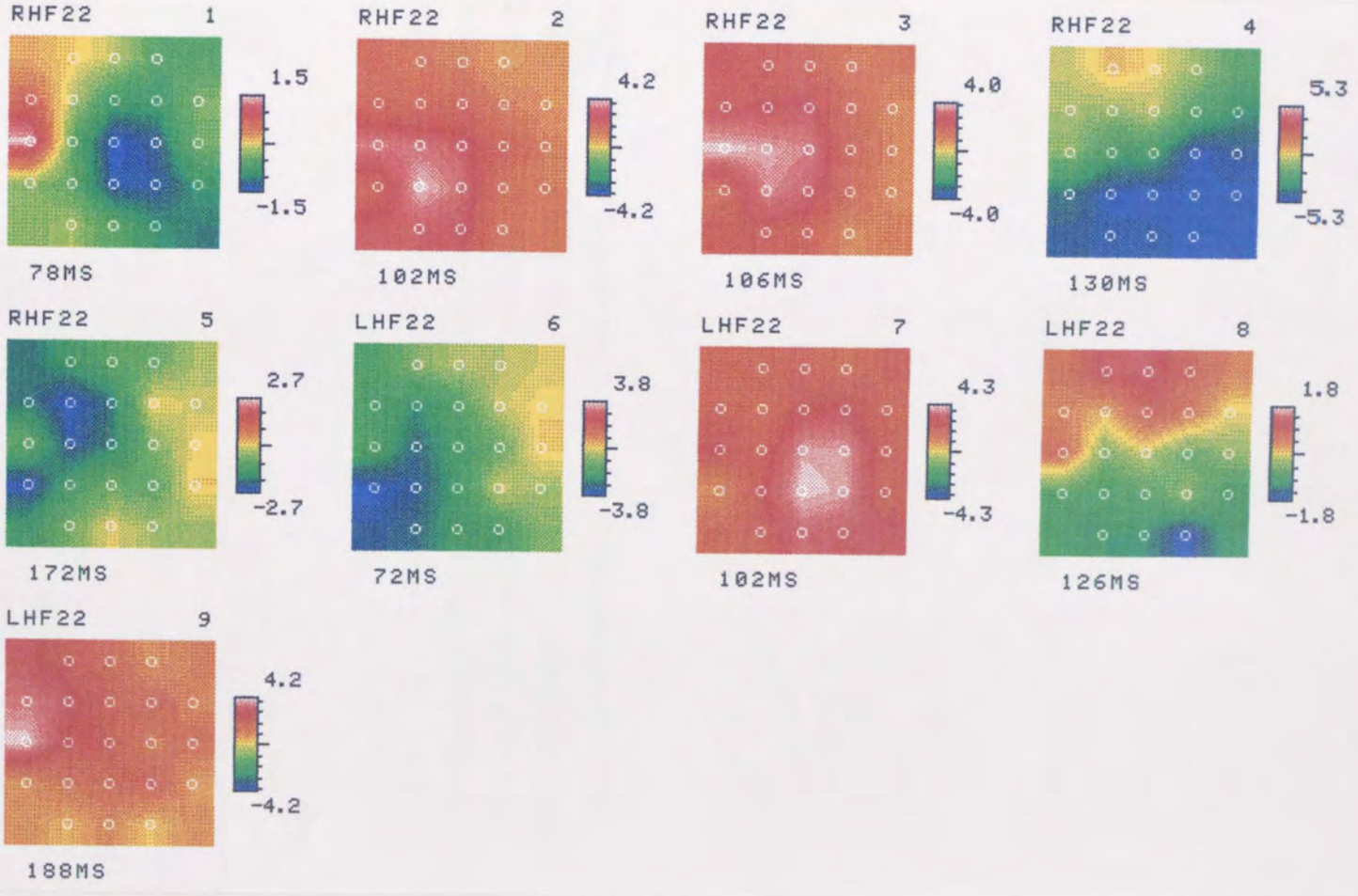
RHF22 1
1.5
-1.5
78MS
RHF22 2
4.2
-4.2
102MS
RHF22 3
4.0
-4.0
106MS
RHF22 4
5.3
-5.3
130MS
RHF22 5
2.7
-2.7
172MS
LHF22 6
3.8
-3.8
72MS
LHF22 7
4.3
-4.3
102MS
LHF22 8
1.8
-1.8
126MS
LHF22 9
4.2
-4.2
188MS

Fig 6.21. Distribution of the major components of the pattern reversal VEP from 70' full (FF), left (LHF), and right half field (RHF) stimulation for subject AS, mapped at the peak latency. Latencies of the peak are given below the maps. The peak amplitudes are given in the scale to the right of the maps (μV).
Note the different amplitude scales for each component.

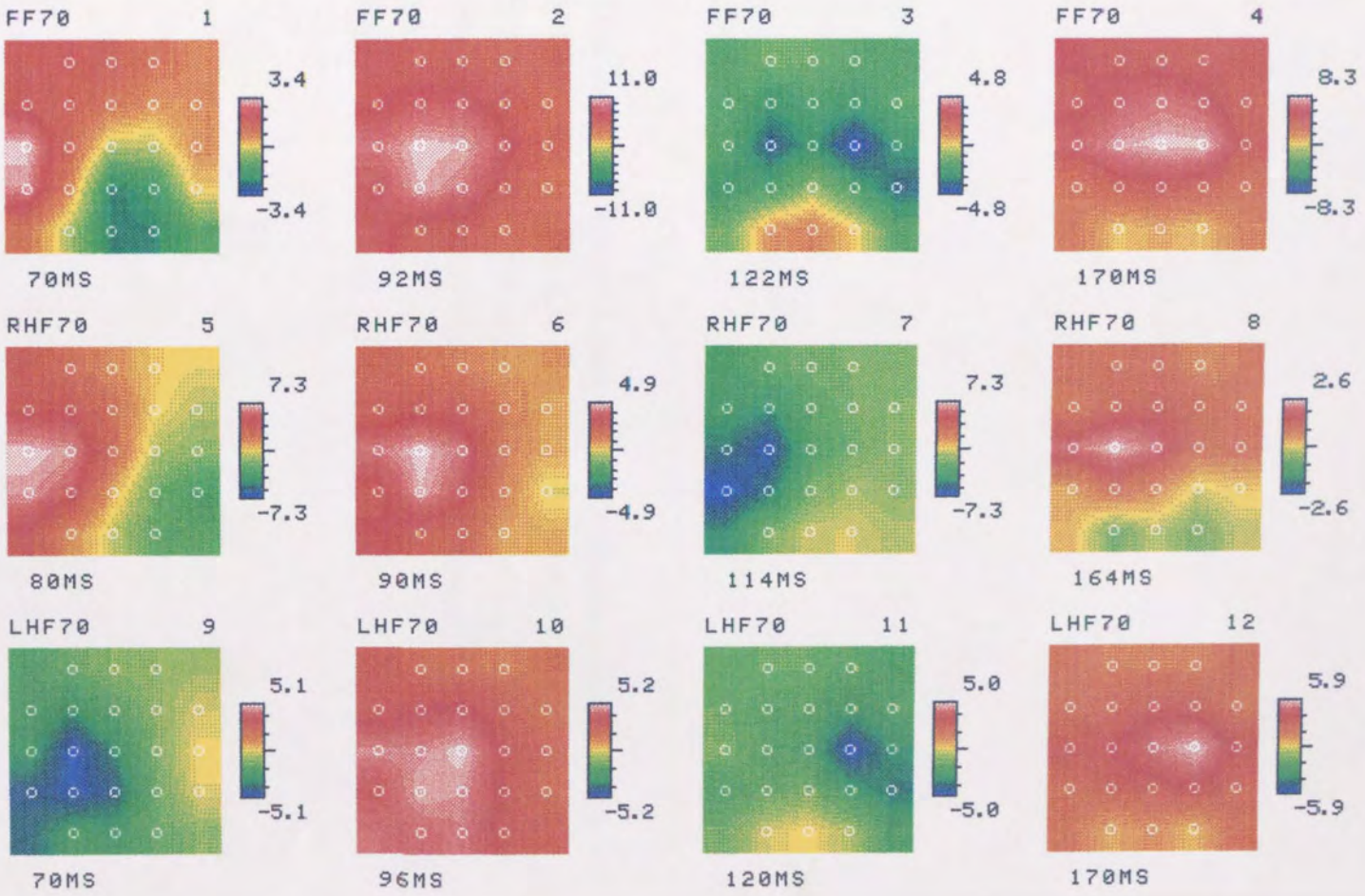
FF70 1
3.4
-3.4
70MS
FF70 2
11.0
-11.0
92MS
FF70 3
4.8
-4.8
122MS
FF70 4
8.3
-8.3
170MS
RHF70 5
7.3
-7.3
80MS
RHF70 6
4.9
-4.9
90MS
RHF70 7
7.3
-7.3
114MS
RHF70 8
2.6
-2.6
164MS
LHF70 9
5.1
-5.1
70MS
LHF70 10
5.2
-5.2
96MS
LHF70 11
5.0
-5.0
120MS
LHF70 12
5.9
-5.9
170MS

Fig 6.22. Distribution of the major components of the pattern reversal VEP from 34' full (FF), left (LHF), and right half field (RHF) stimulation for subject AS, mapped at the peak latency. Latencies of the peak are given below the maps. The peak amplitudes are given in the scale to the right of the maps (μV).
Note the different amplitude scales for each component.

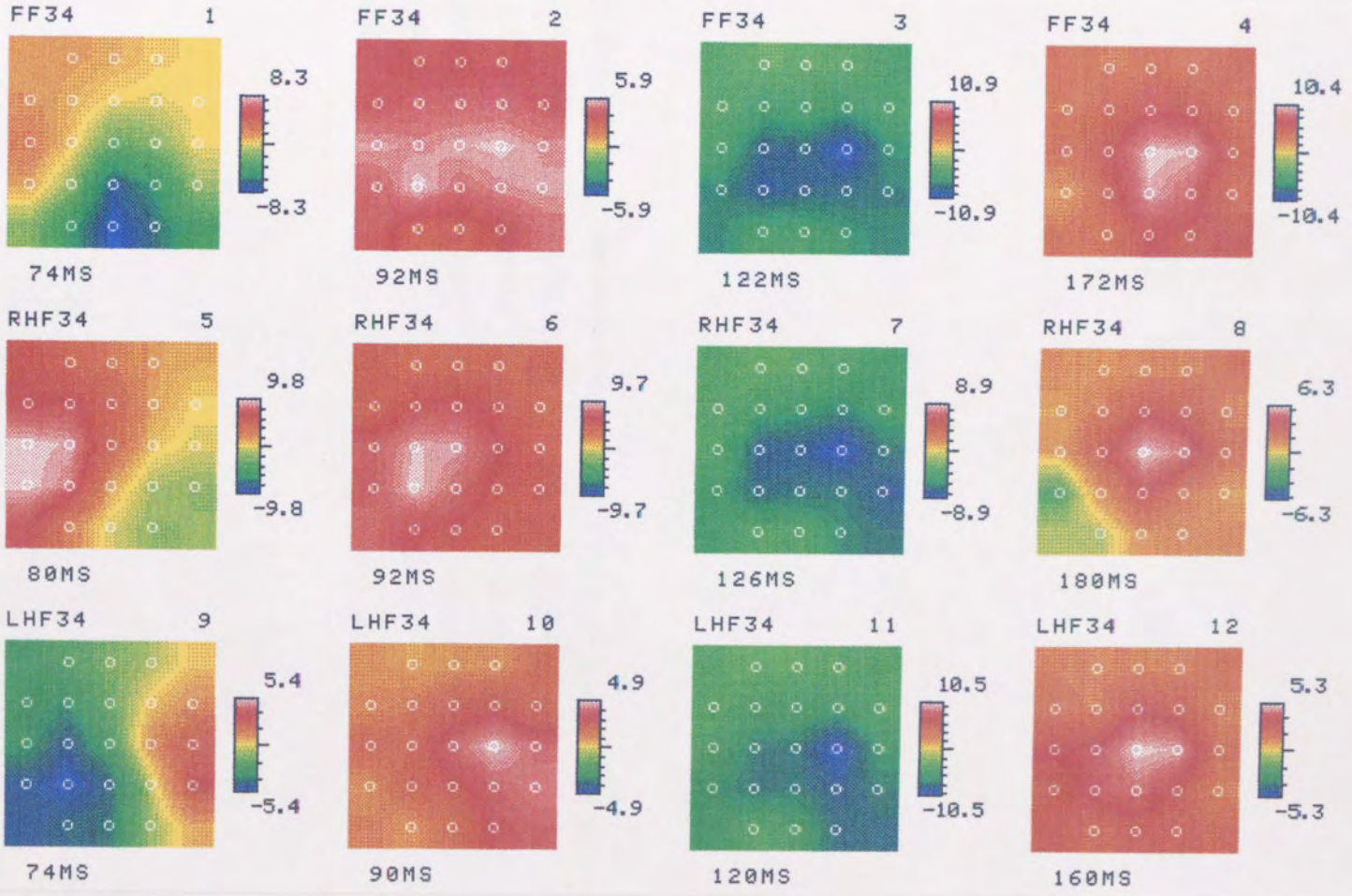
FF34 1
8.3
-8.3
74MS
FF34 2
5.9
-5.9
92MS
FF34 3
10.9
-10.9
122MS
FF34 4
10.4
-10.4
172MS
RHF34 5
9.8
-9.8
80MS
RHF34 6
9.7
-9.7
92MS
RHF34 7
8.9
-8.9
126MS
RHF34 8
6.3
-6.3
180MS
LHF34 9
5.4
-5.4
74MS
LHF34 10
4.9
-4.9
90MS
LHF34 11
10.5
-10.5
120MS
LHF34 12
5.3
-5.3
160MS

Fig 6.23. Distribution of the major components of the pattern reversal VEP from 22' full (FF), left (LHF), and right half field (RHF) stimulation for subject AS, mapped at the peak latency. Latencies of the peak are given below the maps. The peak amplitudes are given in the scale to the right of the maps (μV).
Note the different amplitude scales for each component.

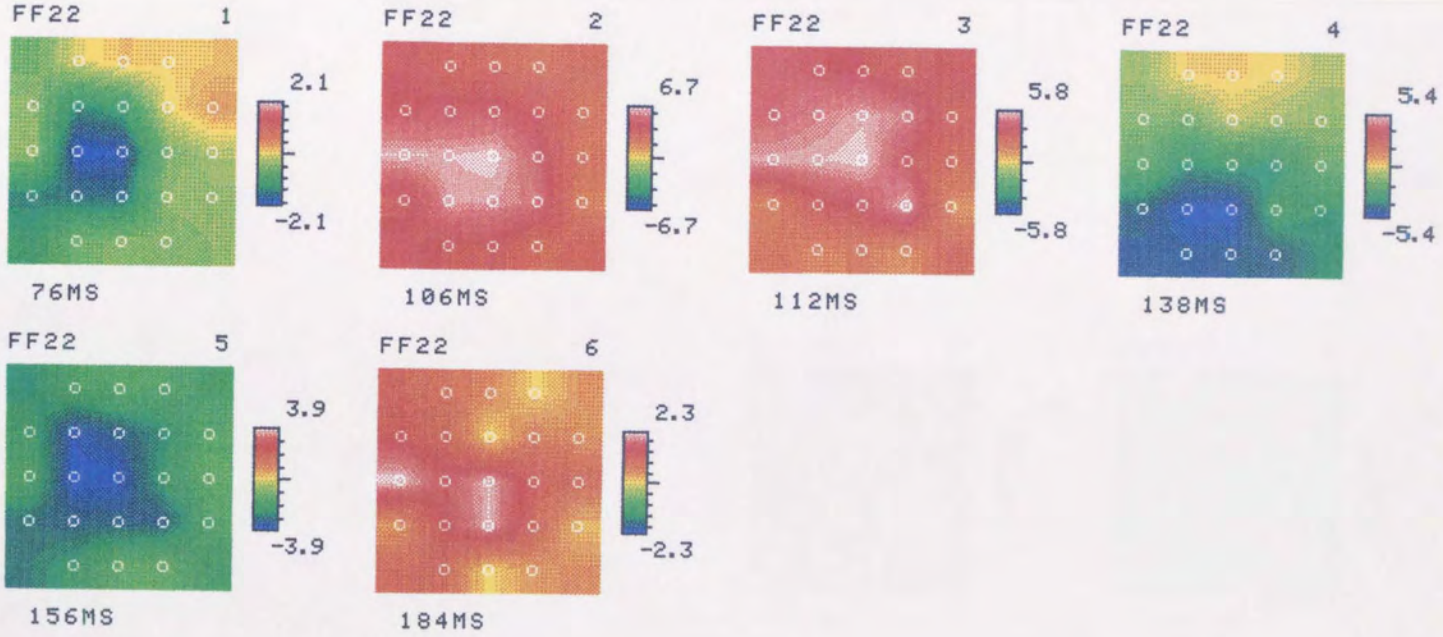
FF22 1
2.1
-2.1
76MS
FF22 2
6.7
-6.7
106MS
FF22 3
5.8
-5.8
112MS
FF22 4
5.4
-5.4
138MS
FF22 5
3.9
-3.9
156MS
FF22 6
2.3
-2.3
184MS

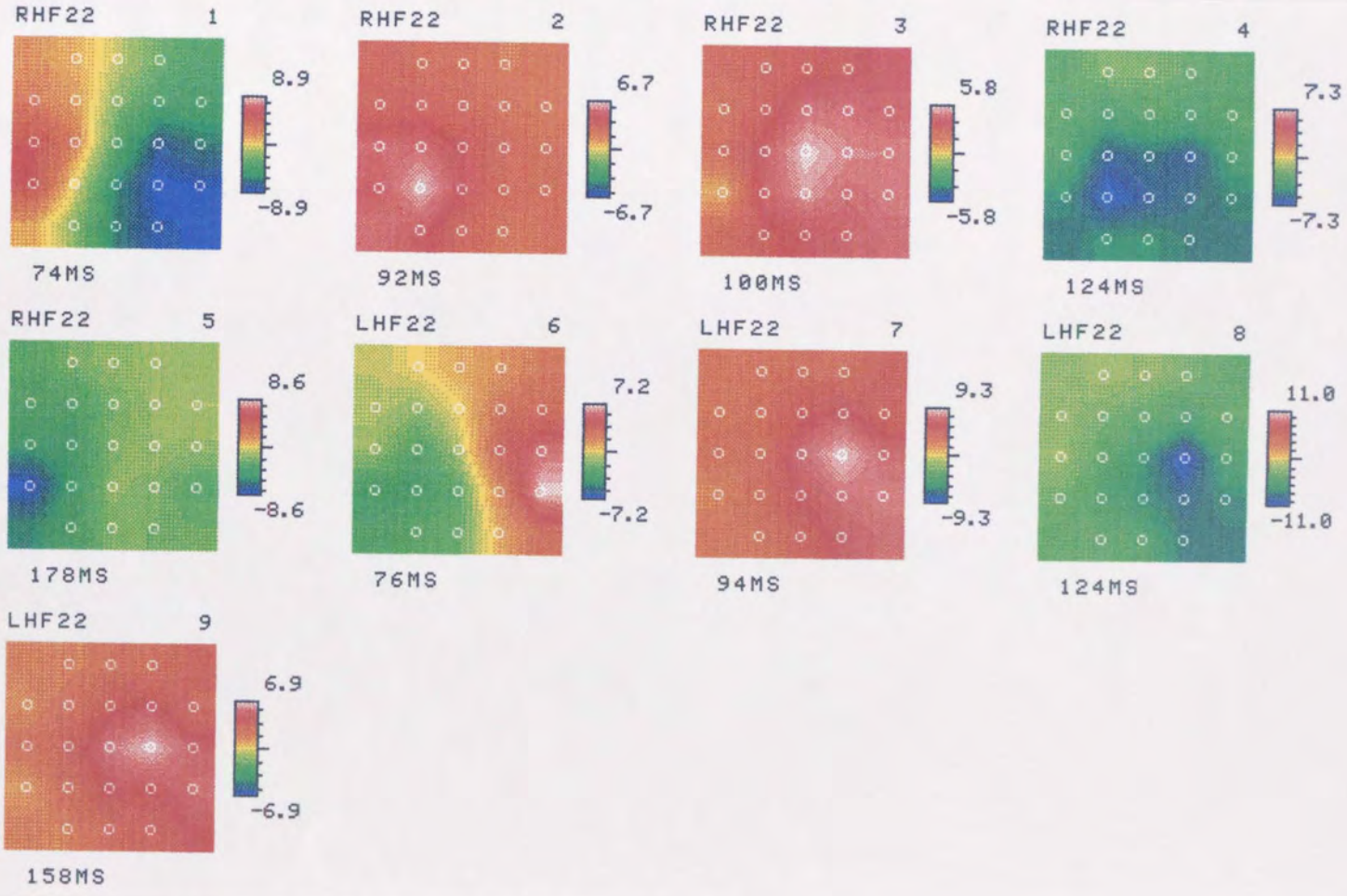
RHF22 1
8.9
-8.9
74MS
RHF22 2
6.7
-6.7
92MS
RHF22 3
5.8
-5.8
100MS
RHF22 4
7.3
-7.3
124MS
RHF22 5
8.6
-8.6
178MS
LHF22 6
7.2
-7.2
76MS
LHF22 7
9.3
-9.3
94MS
LHF22 8
11.0
-11.0
124MS
LHF22 9
6.9
-6.9
158MS

montage following the negativity in subject AS. In subjects CN and RA the P100 was succeeded by a dipolar distribution, the amplitude of the negativity appeared to increase with reducing check size. This was followed by a later negative distribution. The last repeatable response from subject CN was a positivity with the 34' and 22' checks.

6.5.2 Right Half Field

The initial component for the large checks was an ipsilateral negativity followed by a contralateral positivity resulting in a tangential like dipolar field for 2/4 subjects (AS,CN), in the remaining the response was a monopolar contralateral positivity. On 34' check stimulation the response consisted of an early ipsilateral negativity which was followed by a contralateral positivity in all subjects, the latency of the positivity varied between subjects and a dipolar field was observed in three subjects (RA,CD,AS). All distributions possessed a dipolar appearance with the small checks; positive contralateral, negative ipsilateral, the contralateral positivity was again later than the ipsilateral negativity. The polarity of the dipolar distribution was the inverse from one of the subjects (CD) i.e. the positivity was ipsilateral and negativity was contralateral as a result of peak to baseline measurements. In subjects CN and AS the ipsilateral negativity appears to be superimposed onto the contralateral positivity resulting in the positivity appearing as two positive peaks with a negative deflection. This became increasingly apparent as the check size reduced.

The classical distribution of the half field response proposed by Halliday and co workers is separate contralateral and ipsilateral components. The contralateral components consist of a positive-negative-positive complex whereas the ipsilateral components were a negative-positive-negative. The contralateral components being maximally recorded about 10cm from the midline. Note that the montage used in this study did not extend as far out over the lateral hemispheres as this and consequently we may not maximally record the contralateral components. These classical contralateral components were recorded with large check stimulation of subjects AS and CN, see figs 6.26 and 6.27. Subject AS also showed this contralateral distribution with 34' checks. As the check size reduced in subject CN the contralateral components appear to resemble the ipsilateral components. In both subjects CD and RA the contralateral components were more of a positive-negative-positive progression, not all peaks were present simultaneously, see figs 6.24 and 6.25. There appeared to be an independent change in the contralateral

positivity with a change in check size. For subject RA the peak latencies of the contralateral positivity reduced and in subject AS the amplitude appeared to increase with a reduction in check size.

A P100 was recorded for all stimulus presentations, the laterality of this response however appeared to be affected by the check size. The topographic distribution of the P100 on the maps appears to be maximal over the ipsilateral hemisphere with the large checks for 3/4 subjects (RA,CD,CN) and contralateral for all other checks sizes and subjects.

No late contralateral positivity was observed with subjects AS or CD. This component was present with all check sizes for subject CN and with the large checks for subject RA. A negativity was observed following the P100 for subjects CD and AS. This negativity was contralateral with the large checks but became ipsilateral with the small checks. The negativity was posterior with all checks sizes for subject CD. The negativity was followed by a positivity from the 70' and 34' checks and a subsequent negativity for the small checks in subject AS. A negativity followed the positivity in subject CN this was ipsilateral for the larger checks sizes, and contralateral for the 22' checks. A posterior positivity followed the contralateral positivity in subject RA for the large checks this was replaced by a negativity with the 34' checks. Following this was a late negativity which moved from being contralateral with the large checks to anterior with the small checks.

6.5.3 Left Half Field

The classical contralateral components were observed from 3/4 subjects with large check stimulation (CD,CN,AS), as the check size reduced the contralateral components again appeared to resemble the ipsilateral morphology in subjects CN and CD. The latency of the contralateral positivity appeared to shift with changes in the check size so that it virtually matched that of the ipsilateral components. Concurrently the amplitude of the contralateral positivity appeared to exceed that of the ipsilateral positivity and the distribution therefore appeared to shift from being maximal ipsilateral to becoming maximal contralaterally for all subjects except one (CD with the 22' checks) where the ipsilateral positivity was greater than the contralateral positivity, see figs 6.24 - 6.27.

The early negative component was present in all subjects except CD70'. An ipsilateral negativity was recorded with the large checks and a contralateral positivity was also recorded with the small checks. The distribution of the early

Fig. 6.24. The pattern reversal VEP recorded from a row of five electrodes placed above the inion, waveforms from the top to bottom represent the response recorded from electrodes placed from the left to the right of the montage. Responses on the left are to left half field stimulation and those on the right are to right half field stimulation. The top group of responses are following 70', the middle group 34' and the lower 22' check stimulation. Responses are from subject RA.

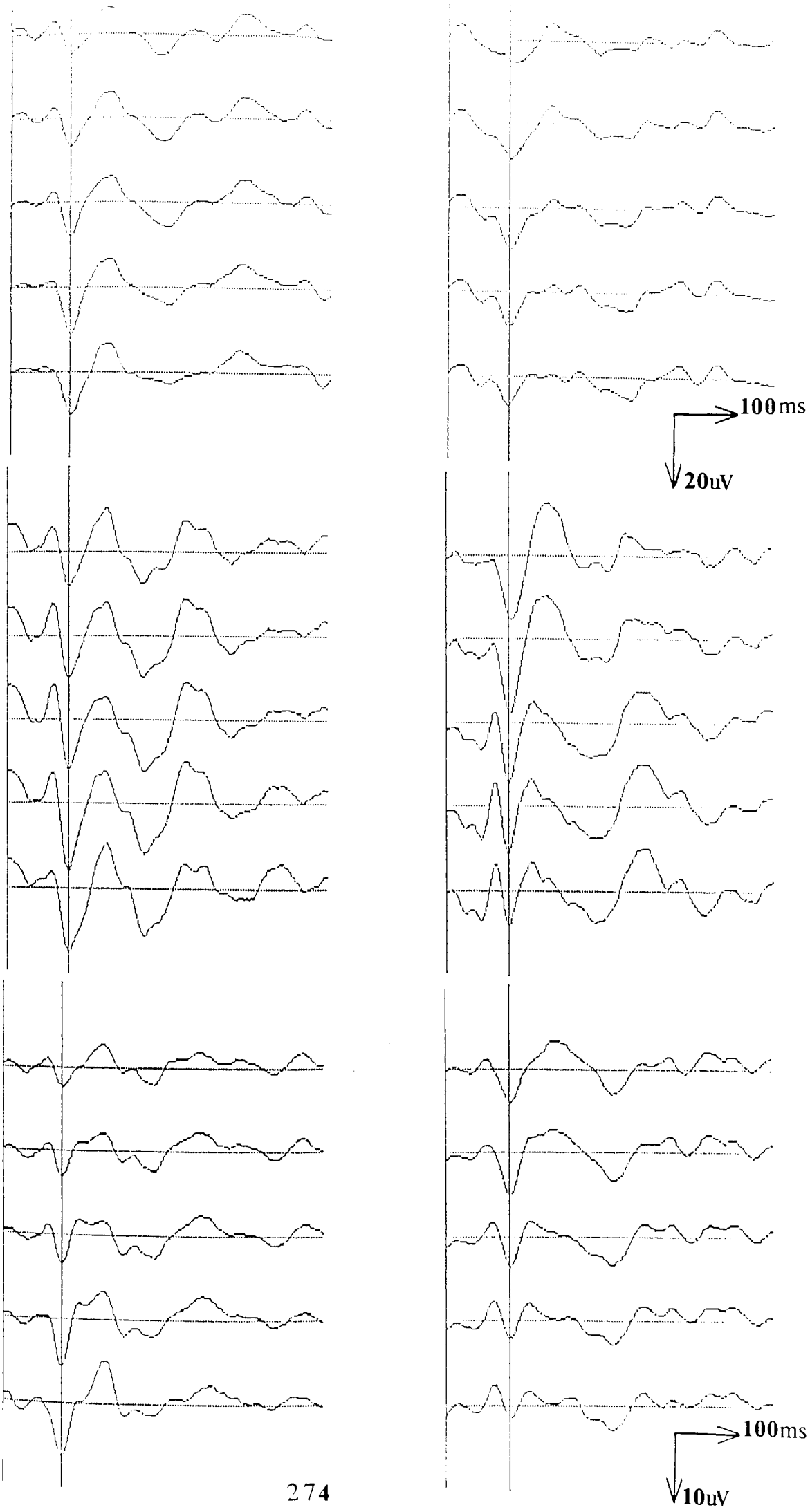
100ms
20uV
100ms
10uV

Fig. 6.25. The pattern reversal VEP recorded from a row of five electrodes placed above the inion, waveforms from the top to bottom represent the response recorded from electrodes placed from the left to the right of the montage. Responses on the left are to left half field stimulation and those on the right are to right half field stimulation. The top group of responses are following 70', the middle group 34' and the lower 22' check stimulation. Responses are from subject CD.

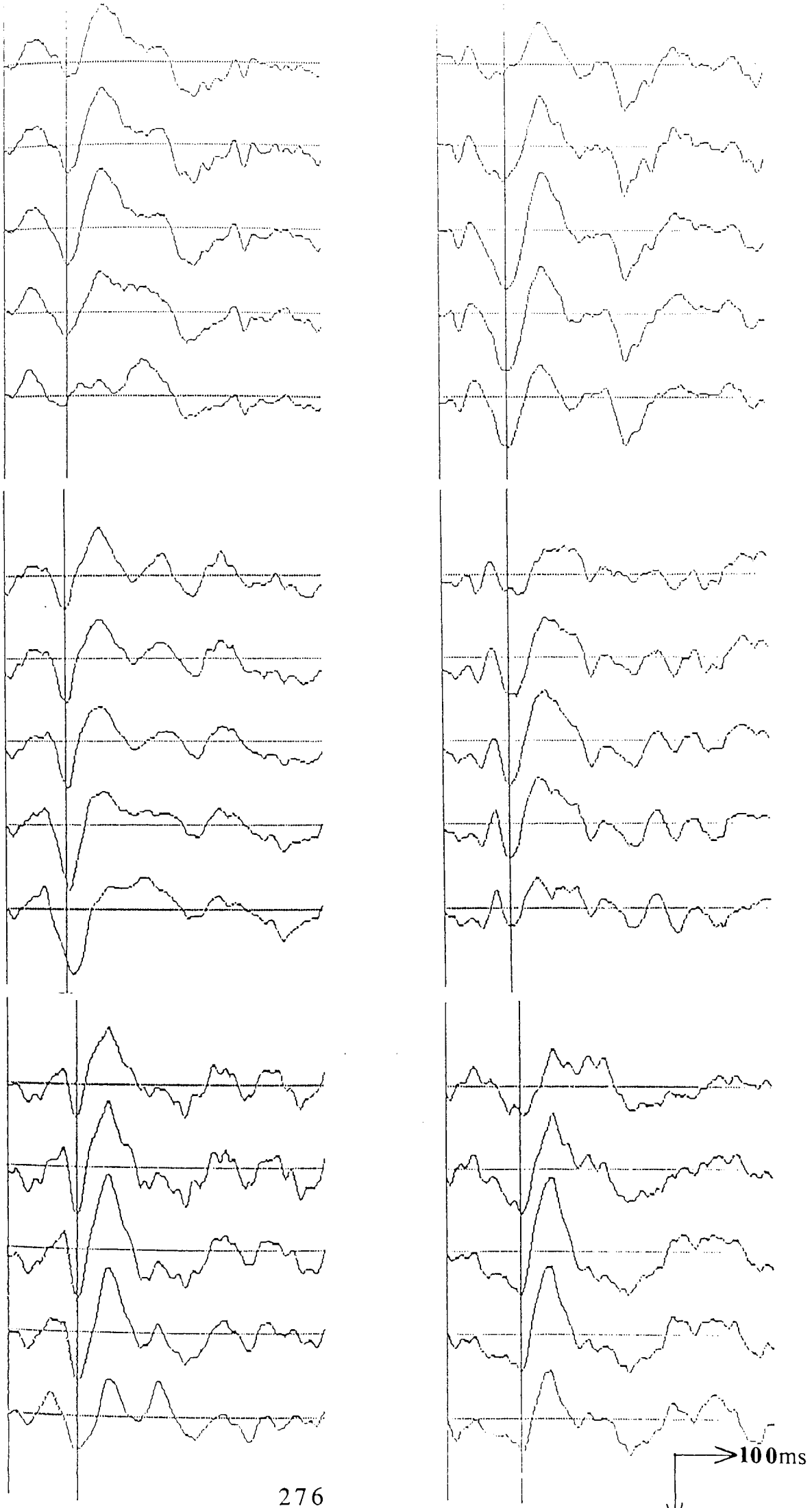
100ms

Fig. 6.26. The pattern reversal VEP recorded from a row of five electrodes placed above the inion, waveforms from the top to bottom represent the response recorded from electrodes placed from the left to the right of the montage. Responses on the left are to left half field stimulation and those on the right are to right half field stimulation. The top group of responses are following 70', the middle group 34' and the lower 22' check stimulation. Responses are from subject CN.

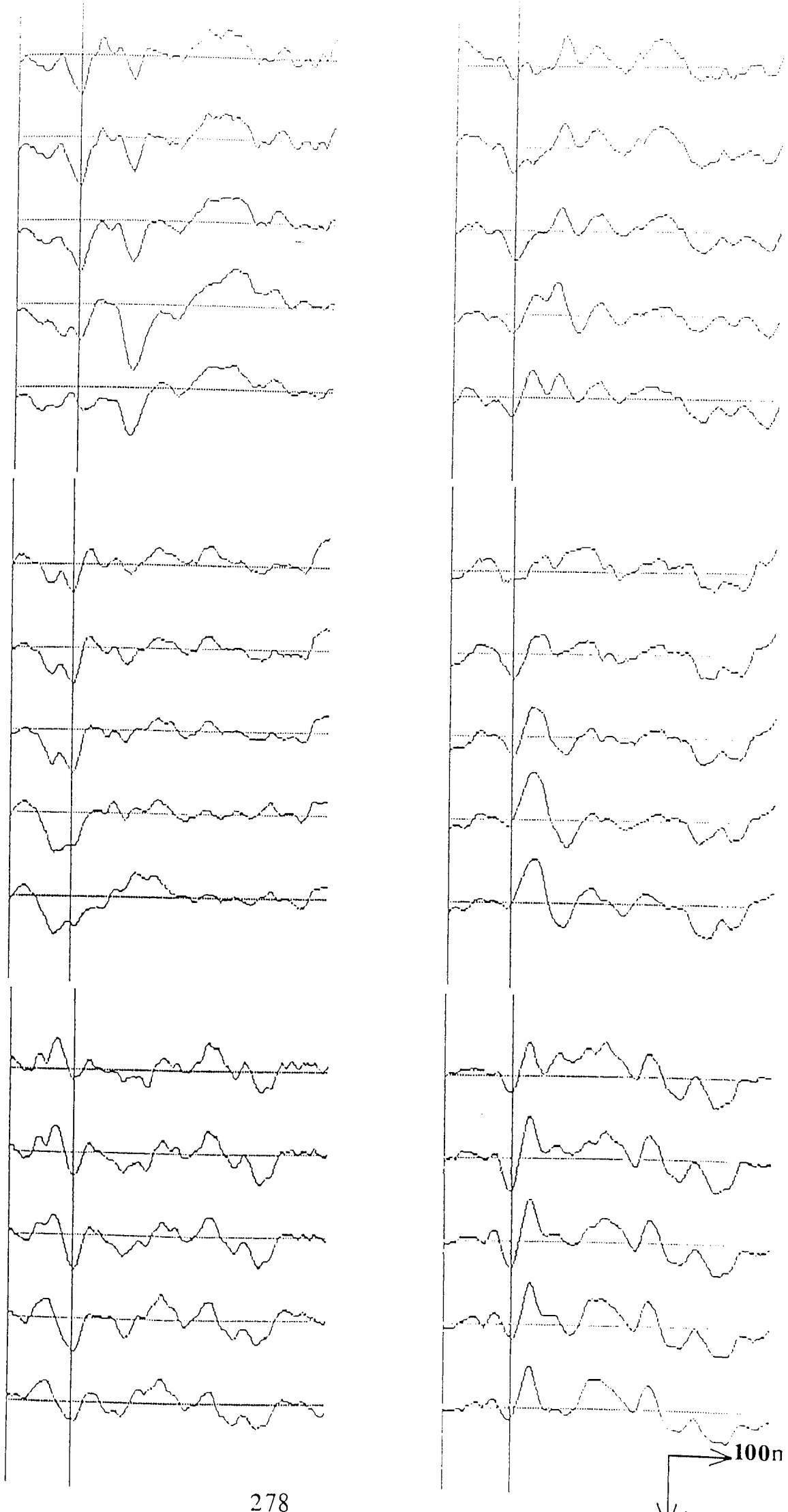
100m
10μV

Fig. 6.27. The pattern reversal VEP recorded from a row of five electrodes placed above the inion, waveforms from the top to bottom represent the response recorded from electrodes placed from the left to the right of the montage. Responses on the left are to left half field stimulation and those on the right are to right half field stimulation. The top group of responses are following 70', the middle group 34' and the lower 22' check stimulation. Responses are from subject AS.

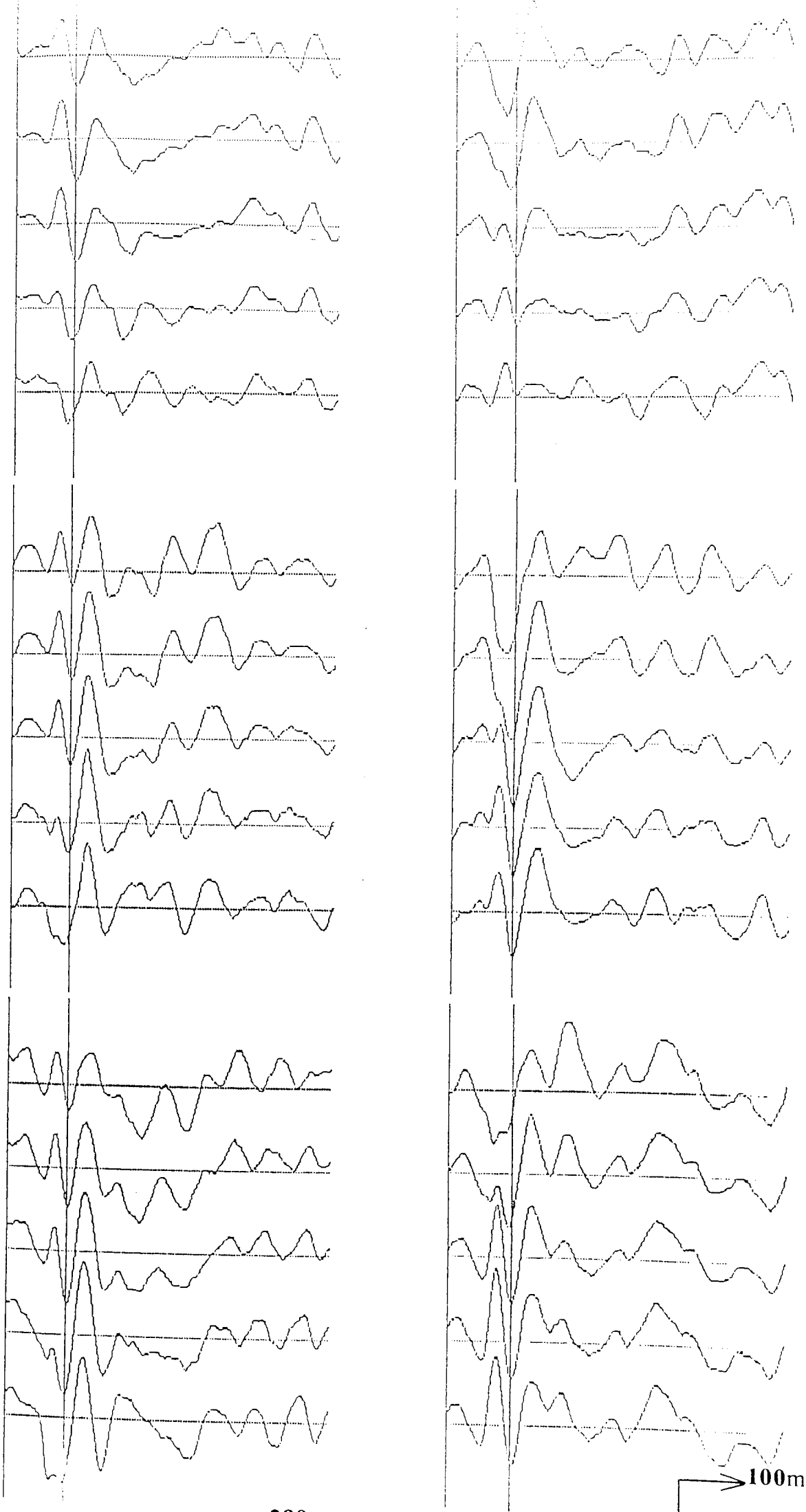
100ms

components with 34' check stimulation was equivalent to that recorded after right half field stimulation for all subjects.

A late contralateral positivity was recorded in one subject (CN) with all the check sizes, a low amplitude positivity was recorded from subject RA to small check stimulation a simultaneous posterior negativity was also present. With small checks this component had a more anterior distribution. This was followed by a positivity with the large and small checks. An ipsilateral negativity followed the P100 in subject CD. In contrast the P100 was followed by a positivity with the 34' and a negativity with the 22' checks from subject AS, a contralateral positivity was the last repeatable response with all check sizes. A contralateral negativity followed the P100 from subject RA with 70' and 22' checks, the negativity was bilateral with the 34' checks. This was followed by a later posterior negativity with RA70'.

6.5.4 Effect of Check Size on the Response Latency

The latency of the P100 was only found to increase consistently with an increase in check size in two subjects; CD and AS. In the remaining subjects the increase in latency was either variable or not present. Individual latencies are tabulated in the appendix table A.5.

6.5.5 Effect of Check Size and Half Field on the Response Amplitude

There did not appear to be any systematic effect of check size on the response amplitude, in two subjects the largest amplitude response was recorded with the large checks whereas in the other two the largest response was from the small and medium checks. In all four stimulus presentations the right half field stimulus elicited a larger response.

6.6 Discussion

The cruciform model has been proposed to aid the interpretation of half field responses (Harding, Janday, Armstrong 1991, Okada 1983, Spejkreijse 1980), see fig.6.28. The horizontal meridian of the visual field is represented in the calcarine fissure whereas the vertical meridian is represented along the longitudinal fissure. If a lateral half field is stimulated the dipoles set up along the calcarine fissure from the horizontal meridians act in opposition and so cancel. The signal recorded should therefore be the result of activation along the longitudinal fissure.

This is obviously a simplified approach as it will be appreciated that if the full field is stimulated a response is still recorded. It is likely that the dipoles do not cancel completely but may combine to reduce the signal. In addition there is evidence that two opposing dipoles may produce apparent phantom dipoles (Weinberg et al 1985).

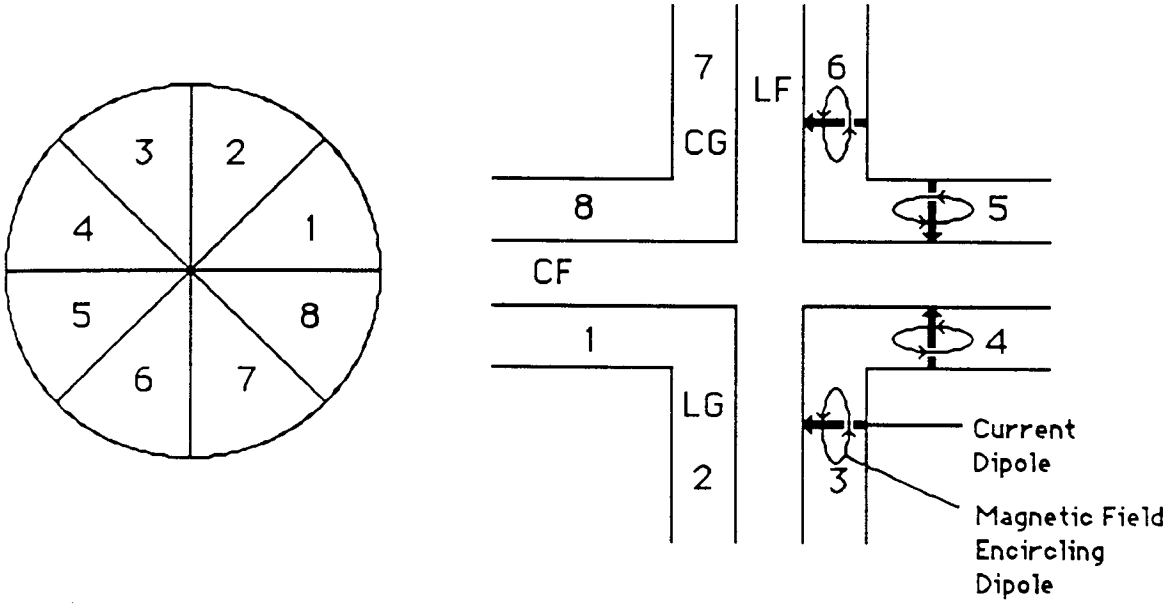

Fig. 6.28. The cruciform model demonstrating the projection of the visual field on the striate cortex. Activation of the left half field will result in the illustrated dipoles being activated and the concomitant magnetic field. LF= longitudinal fissure, CF= calcarine fissure, CG= cuneal gyrus and LG= lingual gyrus. After Harding, Janday and Armstrong (1991).

Due to the spatial tuning of the visual system larger check sizes should activate a greater proportion of the peripheral retina (Celesia and Meredith 1982) and as the peripheral visual field is represented more deeply larger check sizes should also activate deeper sources. As the depth of the source increases the VEMR signal is attenuated. In contrast the VEP amplitude is not thought to be as dependent on source depth. The field stimulated in the present study was 10°. There are various reports in the literature as to how much cortex represents a certain amount of visual field. It is well documented that a disproportionately large area of the visual cortex represents the fovea. Approximately 25% of the striate cortex is apparently devoted to processing the central 10°, although the amount varies between authors (see chapter 2). The foveal area, which represents approximately 4°, is represented on the posterior pole as shown in fig.6.29 and should in theory result in

predominantly radial dipoles which would not produce large VEMR responses. It is also known that the visual field is retinotopically projected onto area 18 and maybe area 19, and these may also be activated having an effect on the topography.

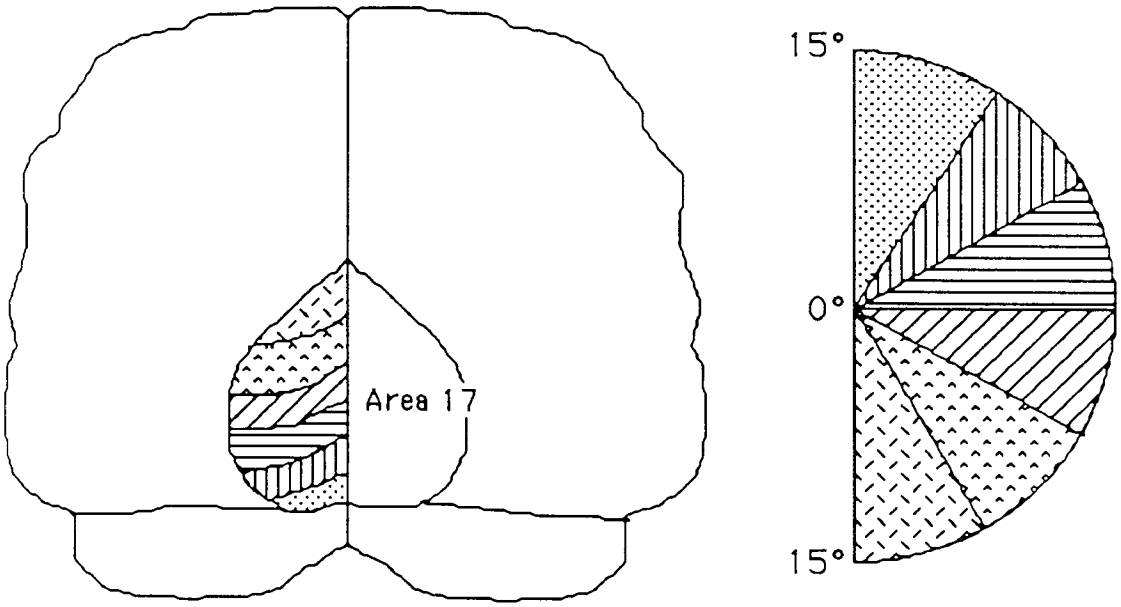

Fig.6.29. Coronal Section to Illustrate the Foveal Projection on Area 17. After Harrington (1981).

6.6.1 VEP Component Distribution

Half field VEP stimulation has been demonstrated previously to produce N75, P100, N145 components over the ipsilateral hemisphere similar to those found on full field stimulation. Contralaterally the components were P75, N105, P145 (Barratt et al 1976, Onofrj 1990, 1991). The P100 although recorded maximally over the 'wrong' hemisphere has been shown to originate from the correct hemisphere in hemispherectomised patients (Blumhardt et al 1977, Onofrj 1991).

6.6.1.i Half Field Distribution

The early ipsilateral negativity became increasingly more prominent when the check size was reduced for all subjects except for RALHF stimulation in which the amplitude was found to be relatively independent of check size. This confirms results of Onofrj et al (1990) who demonstrated that the distribution of N75 was more pronounced with a reduction in stimulus size. An early contralateral positivity was recorded in all stimulus presentations of subjects AS, CN, CDRHF and CDLHF70. For subject AS with large check stimulation the latency of this

positivity was greater than that of the ipsilateral negativity however, for the smaller checks the negativity appeared to become superimposed onto the contralateral positivity therefore producing a positivity with a central negative deflection. Peaks of cP75 and N75 have previously been demonstrated to possess slightly different peak latencies, suggesting they may arise from separate generators (Onofrj 1990). The distribution of the response from subject RA over the contralateral hemisphere was very similar to that from the ipsilateral hemisphere with a negative-positive-negative progression.

An alteration in the distribution of the half field response has been demonstrated to be dependent on the size of the stimulating field (Harding, Smith and Smith 1980, Lehmann and Skrandies 1982) however, no effect of check size was displayed. In contrast Brecelj and Cunningham (1985) and Edwards (1989) have demonstrated that when using a small foveal field, a reduction in check size exaggerates the field size effect. Attenuation of the ipsilateral P100 has been shown to occur with occlusion of the central area. In contrast the contralateral components were attenuated with a reduction in field size (Blumhardt et al 1978). Other workers have reported no effect of check or field size on the distribution of either the ipsilateral or contralateral components, the major positive still being maximal over the ipsilateral hemisphere and the contralateral negative response still present with a field size of 0-3° (Onofroj et al 1991). With central 6° occlusion the response consisted of contralateral components over the occipital derivations, ipsilateral components being recorded over temporal and anterior derivations (Onofroj et al 1991). The components of the response can not therefore be solely attributed to either peripheral or central stimulation (Onofroj et al 1991). Onofrj et al (1990) observed dispersion of the ipsilateral and contralateral components onto the opposite derivations in a number of normal controls, this did not however transpose onto the group average maps. This was thought to be due to anatomical variation in the representation of the fovea on the occipital pole, see fig 6.30.

The P100 was recorded from all subjects following full and half field stimulation. On half field stimulation the topographical distribution of the maximal positivity presented on the maps appears to shift from being maximal ipsilaterally with large checks to being mainly contralateral with small check stimulation. On examination of the waveforms it is evident that on reduction of check size the contralateral components, consisting of the positive-negative-positive progression, become increasingly less prominent and are replaced with components resembling the ipsilateral complex i.e. a negative-positive-negative progression of components.

Contralateral components were recorded from subjects CN, RA and CD with the 70' checks and with CN for the 34' checks.

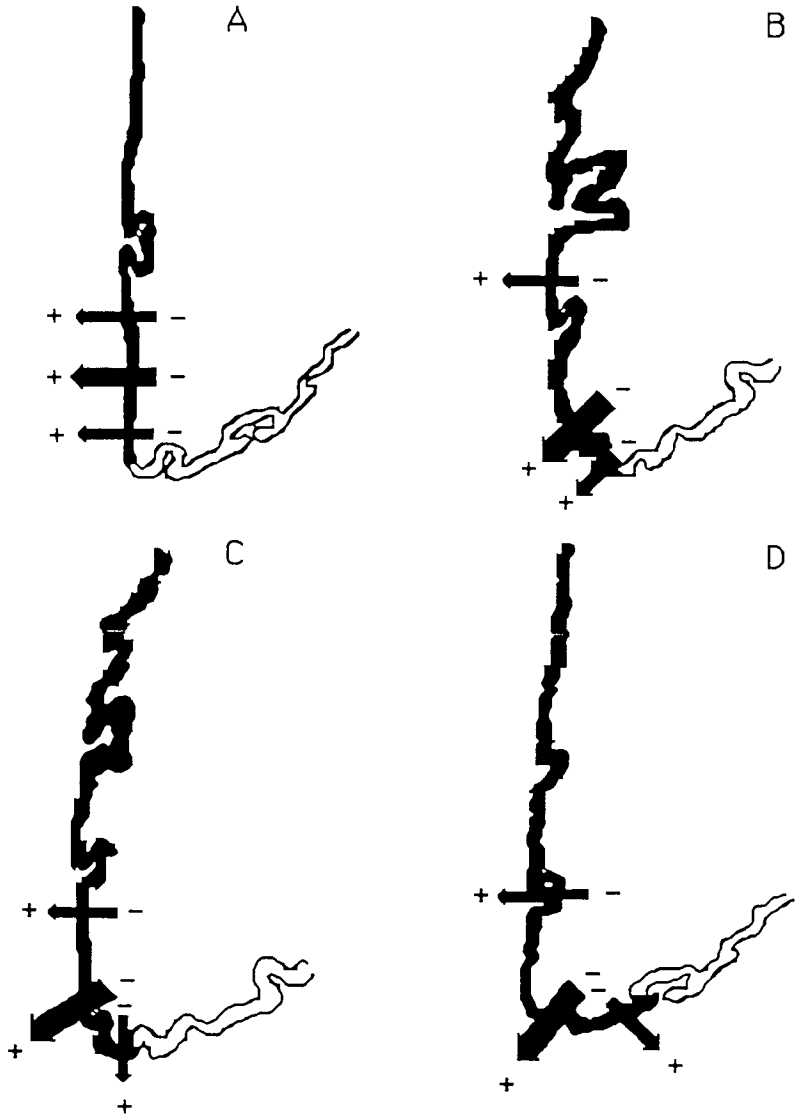

Fig. 6.30. The variation in the representation of the striate cortex on the occipital pole resulting in variations in the lateralisation of the half field VEP. The small dipoles represent the central and peripheral projections and the large dipole represents the vector sum. After Blumhardt et al (1991).

In subject AS a reduction in check size results in an enhancement of the contralateral early positivity this then masks the ipsilateral 'P100'. With reducing check size the ipsilateral negativity appears to become superimposed on the contralateral positivity therefore producing a negative deflection in the centre of this early peak. This would fit with a change in orientation of the N75 dipole with the source being projected more onto the contralateral hemisphere as observed with the P100, see fig 6.31 and 6.32.

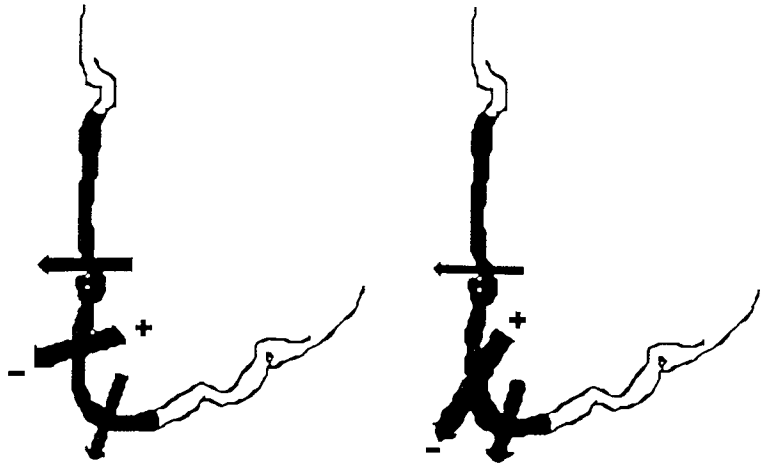

Fig. 6.31. Effect of reduction in check size on the equivalent dipolar source of N75. As check size is reduced the fovea is preferentially stimulated thus resulting in the orientation of the dipolar representing the sum of the fovea and periphery becoming increasingly radial.

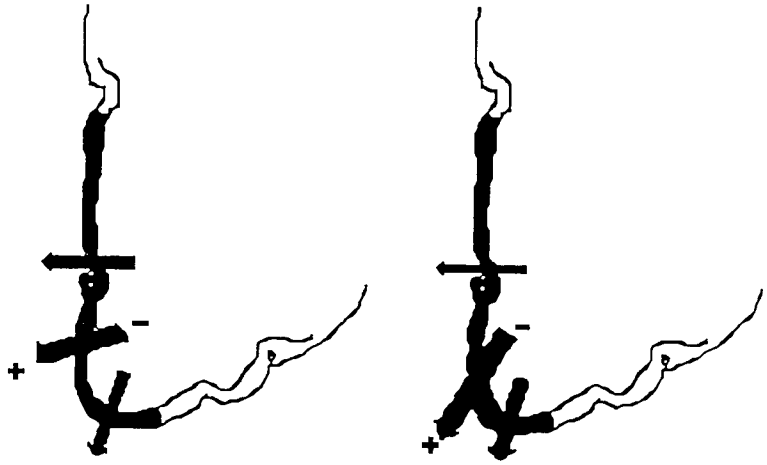

Fig. 6.32. Effect of reduction of check size on the equivalent dipolar source of the P100. As check size is reduced the foveal projection is preferentially stimulated thus resulting in the orientation of the dipolar representing the sum of the fovea and periphery becoming increasingly radial.

The fact that the early contralateral positivity appears to increase in amplitude independently of the ipsilateral negativity and the latencies differ may confirm suggestions that these components arise from separate generators (Onofrj 1991). No polarity reversals of the P100 were demonstrated on any of the maps, and although contralateral components were recorded these were not sufficiently large to be shown on the maps. Dipolar distributions following the P100 were found for all checks sizes and half fields from 1/4 subjects (CN) for RA and CD70' and RA22' to right half field stimulation and from RA22' and AS70' to left half field stimulation. A dipolar distribution has also been demonstrated by Onofrj et al

(1990) occuring at around 115ms, from the RHF to 1 and 4cpds and both the LHF and RHF for a 2cpd stimuli.

All the stimulation described has been binocular. It is thought that binocular stimulation should preferentially stimulate binocular driven cells which are more prevelant in the extrastriate cortex. The distribution of the VEP has however been shown to be the same whether the stimulus is viewed monocularly or binocularly (Onofrj 1991). In contrast Adachi-Usami and Lehmann (1983) have demonstrated a dependence of the location of the maxima on whether binocular or monocular stimulation is employed. Lower half field binocular stimulation was shown to produce the most anterior and binocular upper half field stimulation the most posterior response. This was postulated to be the result of binocular stimulation preferentially stimulating the extrastriate areas. The binocular amplitude has been reported to be approximately $\sqrt{2}$ greater than the monocular amplitude (Onofrj 1991, Trick, Dawson and Compton 1981, Srebro 1978, Wanger and Nilson 1978). Variations in binocular summation have been shown to be dependent on contrast, spatial and temporal properties of the stimulus (Apkarian et al 1981) and central and peripheral stimulation (Katsumi, Hirose and Tanino 1988). The components of the flashed on pattern stimulus have been shown to be independently affected by either dioptic or dichoptic stimulation, this may provide insight into their site of generation (Harter, Seiple and Salmon 1973). When compared with contrast stimuli, stereoscopic stimuli produce maxima closer together, this may indicate more superficial generators. With half field stimulation the stereoscopic stimuli produced maximal amplitudes over the contralateral hemisphere whereas the contrast stimuli produced maximal amplitudes over the ipsilateral hemisphere (Skrandies 1991). Stereoscopic stimuli activate cells with binocular disparity, predominantly located in the extrastriate cortex.

When stimulating the binocular half field a nasal and temporal half field are simultaneously stimulated. Addition of separate left and right eye half fields has been shown to produce a very similar morphology to the VEP to binocular half field stimulation and the crossed and uncrossed pathways have been shown to make equal contributions (Arruga et al 1980). Although the amplitudes were similar, nasal half field stimulation has been shown to have shorter latencies (Yanashima and Degering 1981).

6.6.2 VEMR Distributions

The full field responses for all checks and subjects are presented in figs. 6.4 - 6.7. The majority of the maps show a positivity over the midline at about 6cm above the inion, however for subject CD the outgoing field is slightly lateralised to the left and posterior for the 70' checks. The variability between subjects may relate to variation in the position of cortical structures, it has been shown that there is wide variability between individuals in the projection of area 17 onto the cortex (Brindley 1972). Further to this a large variability between individuals (absolute variation 4cm) in the position and angle of the calcarine fissure with respect to the inion has been demonstrated (Steinmetz 1989, Myslobodsky et al 1991). The right calcarine sulcus occupies a slightly higher position above the inion (6.6% v.7.4% of the nasion to inion line) and the left sulcus appeared to be slightly steeper than the right although both these results were insignificant (67.8 +/-8.69° v. 73.1+/-4.29°, angle measured with a line perpendicular to the nasion-inion line). A variation in the angle of the calcarine fissure can result in radial sources being silent in one recording location and producing a tangential effect at another recording site. For example foveal sources located around the occipital pole will be radial to the probe when positioned at the inion but will be tangential to the probe when positioned more anterior. This can lead to increased complexity in the field patterns when stimulating the fovea. When the periphery is activated the sources are more likely to be located along the cuneal and ligual gyri, thus producing tangentially orientated dipoles for the majority of the recording positions. Sources in the calcarine fissure will also be activated although these will probably be of low amplitude due to addition of opposing magnetic fields. This results in foveal stimulation producing more complicated maps whereas in contrast the interpretation of the maps should be more straightforward with parafoveal stimulation. The stimuli used in the present study have been used to preferentially stimulate the fovea and periphery. The distribution of the VEMR appeared to be more centrally distributed following right half field stimulation in contrast to that following left half field stimulation. A number of authors have documented differences between the left and right hemispheres, particularly in right handed individuals, which three of the subjects were (RA, CD, AS). Myslobodsky et al (1989) showed that scalp markers were skewed to the left with respect to the longitudinal fissure, in addition LeMay and Kido (1978) have shown that the left hemisphere extends more posteriorly with a wider parieto-occipital area. These would lead to the midline being more likely to lie over the left hemisphere i.e. over the site of activity after right half field stimulation. With large check stimulation

half field maps is similar to the full field distribution this is not apparent with small check stimulation. On full field foveal stimulation the sources around the occipital pole may predominate and lead to the full field distribution not resembling summation of the half fields. In contrast with the large checks the full field sources will preferentially stimulate the sources along the fissures and as a result summation will not be as complex. The method of recording the VEMR must also be considered, recording following the head contours results in some contribution from secondary sources (Meijs et al 1987). When the dipole is in the direction of sources in the longitudinal fissure these secondary sources will act so as to counteract the primary source, this effect increases with the source depth. Dipoles in the direction of sources in the calcarine fissure are reinforced by the secondary sources. This will therefore lead to further complications in the field distribution.

6.6.3 Effect of Check size on the Evoked Response Amplitude

No consistent change was observed in either the VEP or VEMR response amplitude with a change in check size. A maximum response was shown by 3/4 subjects with the full field small check VEMR stimuli, this would fit with the proposal that after cancellation the full field response is produced from the occipital pole which is more likely to be maximally stimulated with smaller checks. Small check stimulation also gave the largest amplitudes for the half field VEP responses, except for subject RA. The P100 has previously been shown to produce the highest amplitude with a large (1cpd) stimulus (Onofrj 1990). It may have been expected from the distribution of the VEP that with small check stimulation the strength of the VEMR would reduce as the dipolar source moves more radial, this was however not the case.

Maclin et al (1983) also failed to demonstrate any systematic change in signal strength with an increase in stimulus eccentricity. Conversely, Odaka (1991) demonstrated a decrease in response amplitude with an increase in eccentricity, however by increasing the check size an increase in the response amplitude was obtained, thus demonstrating the spatial tuning of the response. Even after spatial tuning George et al (1988) showed that the response amplitude was greater for central stimulation with high spatial frequency stimuli than peripheral stimulation with low spatial frequency stimuli. Reduction in amplitude with increased eccentricity has been demonstrated for the VEP (Rover, Schaubele and Berndt 1980, Celesia and Meredith 1982).

For the majority of the VEMR stimuli presented the right half field evoked larger amplitude signals, the distribution, however appeared to be more consistent between subjects on left half field stimulation (except for CN34' whose response was inconsistent from both left and right half fields). Kuriowa et al (1987) investigating the VEP half field reponse to pattern reversal transient and steady state stimulation showed the response to be maximal over the ipsilateral hemisphere with the right half field producing the largest amplitude signals. This has been confirmed by other authors; Pike and Polish (1988) and Abe and Kuriowa (1989), although not by Edwards (1989).

6.6.4 Comparison of the VEP and VEMR

The main difference between the VEP and VEMR is the fact that they are sensitive to different aspects of the source, the VEP reflecting both tangential and radial aspects of the source whereas the VEMR only detects the tangential aspects. The external magnetic field due to a radial dipole in a sphere has been shown to be zero (Baule and McFee 1965). Consequently the MEG cannot 'see' a dipole in the centre of the head because it will produce a radial source at all positions on the surface of the sphere (Cohen and Cuffin 1987). As a result the deeper the source the greater is the attenuation of the magnetic field, in contrast the electrical field should not be affected by changing depth. The maxima of the VEP are rotated through 90° when compared to the VEMR, the VEMR maxima are also more localised (Cohen and Cuffin 1983).

Further to this the two techniques are recording different aspects of the same electrical event. The magnetometer records the direct current flow in the head (Okada 1983) whereas the VEP records the extracellular current in the form of a potential difference between two positions on the scalp. Variation not only at the point of recording but at the reference point can alter the latency and amplitude of the reponse.

The maximal VEMR and VEP responses were produced at different latencies, the VEMR being later. This could be a result of the two methods of data collection used i.e. different filtering, which may affect the latencies and morphology of the reponses and could therefore make direct comparisons of the latencies of the two responses invalid (Skuse and Burke 1990). Power spectrum curves from half field VEP and VEMR stimulation have previously been shown to have different peak latencies, the VEP peaking at 78ms compared with 102ms for the magnetic field

(Janday et al 1987), in contrast other groups have observed the responses peaking at the same latencies (Seki et al 1990). Simultaneous recordings of the VEP and VEMR would have been preferable however preliminary studies in the department demonstrated that this resulted in the production of an intolerable amount of background noise.

The latency data from the two techniques was divided into three sets related to the different areas of visual field stimulated. Two factor analysis of variance in randomised blocks was then performed on the data. A significant latency difference between the visual evoked field and visual evoked potential was shown from all fields (full field $F = 73.9$, left half field $F = 73.88$, right half field $F = 45.27$, $p<0.001$), with the VEMR producing longer latencies. A significant effect of check size on the latency was also found on the data sets for full field ($F = 5.66$ $p<0.05$) and left half field stimulation ($F = 6.08$ $p<0.02$), the effect of check size however, failed to reach significance for right half field stimulation. The failure to reach a significance following right half field stimulation was most probably a result of the increased variablility of the data.

The same overall trends were shown to be produced for the two techniques (VEMR and VEP) after full and left half field stimulation i.e. an increase in latency with a reduction in check size. It could therefore be postulated that the two techniques are looking at similar events in the brain that are affected in a similar way to different visual stimuli. The results from right half field stimulation were found to be more variable especially the VEMR data.

A significant positive correlation was also demonstrated between the latencies of the VEMR and VEP over all subjects, check sizes and fields ($r=0.34$, $p<0.05$). Individually, however the correlation did not reach significance, this is probably a result of the small sample size in each separate group.

It has also been demonstrated that the VEMR is more variable over time than the VEP (Armstrong et al 1991). As the VEMR data sets for each subject could not be recorded in the same session and the responses from each point of the distribution were recorded consecutively variations both within a trial and between trials are inherent when mapping with a single channel magnetometer. The response to one stimulus could be recorded in a session of about an hour. In contrast the VEP distribution was recorded from all points simultaneously thus reducing the intratrial variation, all the stimulus parameters could also be recorded at one sitting consequently reducing between trial deviation. Due to the fact that the VEMR

recordings were made in an unshielded environment the recording time was limited to early morning and evening.

The VEMR and VEP are not equally susceptible to the filtering effects of the scalp, low frequency elements of the VEP are filtered by the scalp (Nunez 1988) and small dipoles are attenuated to a greater extent compared with large dipole layers (Nunez 1981, 1988). Due to the fact that the VEP is sensitive to radial sources it is more liable to detect the field of secondary sources produced at the interfaces of differing conductivities i.e. where the scalp meets the dura mater. The amplitude of the response will be transformed, either by falicitation or reduction depending on the relative conductivities.

Consistent trends however demonstrated in the VEP maps have been found to transpose onto the VEMR maps i.e. the distribution for the subject CD are shown to occupy a more posterior location on the scalp for both. In the VEP maps some of the subjects produce a dipolar distribution following the P100. The distribution of this response was compared with the VEMR maps to ascertain whether this distribution better fitted the VEMR distribution. In subject AS the P100 is followed by a negativity with a similar distribution for the 34' and 22' checks, there is therefore no difference in the fit of these two components to the VEMR maps. With the 70' maps the RHF and FF could maybe match the VEMR maps. In subject CN the 34' dipolar distributions could fit the VEMR distributions and in subject RA the LHF 22' distribution could also fit. In subject CD no dipolar distributions were produced following the P100. The fit of the dipolar distribution of the later VEP component with the VEMR for subject CN could explain the anomalous distribution of this map, however this could not explain why the dipolar distribution after 70' stimulation was not recorded in preference to the P100.

6.6.5 Source Localisation

The distribution of the VEMR to half field stimulation produced a response which was maximal over the contralateral hemisphere in all subjects, in accordance with results of Seki et al (1990). The VEMR distribution could be approximately described by a contralateral upper quadrant outgoing field and a contralateral lower quadrant ingoing field for left half field stimulation, the reverse being apparent for right half field stimulation. This pattern was observed in all the subjects apart from subject CN with 34' checks. The laterality of the response did not appear to be affected by check size. The source of the field could therefore be approximately

located in the contralateral hemisphere and directed towards the midline. The orientation of the 'dipole' appeared to rotate for some maps this may be due to a contribution from sources in the calcarine fissure. This was not a consistent finding in all subjects. Although the VEMR latencies were longer and more variable when compared with the VEP the distribution of the VEMR response would not fit with the distribution of the late contralteral positivity that follows the ipsilateral P100.

Source derivation investigations of the half field pattern reversal VEP have shown that the sink of the response is located over the contralateral hemisphere (Flanagan et al 1985, Biersdorf 1987, Thickbroom et al 1984). Sources (current out of the scalp) were located over the midline for both lateral half fields (Flanagan et al 1985). Conversely Biersdorf (1987) demonstrated an ipsilateral source from right half field stimulation. Thickbroom et al (1984) using brain mapping demonstrated a sink in the contralateral centrotemporal area. This would suggest a source rotated slightly, converting this to the distribution of the magnetic field would result in the field originating in the lower ipsilateral hemisphere and entering in the upper contralateral hemisphere, thus corresponding well with our results.

6.6.6 Visual Evoked Field Studies

The majority of VEMR studies appear to use a pattern onset stimulus. The locations of the ECDs generated by both the VEMR and VEP have been compared (Stok 1984). Occurence of the major components and their latencies with both techniques has also been investigated (Richer et al 1983). Two VEMR components have been observed, occuring at 120msec and 180 msec, termed M120 and M180 (Richer et al 1983). In the VEP a component was also observed at 80ms, it was concluded that this component must be orientated orthogonally to the scalp surface as it was not demonstrated in the VEMR. The data presented seems to be consistent with the theory that both M120 and N120 are related. It was not possible to show that the generators activated during the half field stimulation were located in just one hemisphere although the depth estimates indicated a superficial source which would suggest it was unilateral. The M180 exhibited greater intersubject variability and may be a result of activation of a diffuse source (Aine et al 1991).

The equivalent dipole from the VEMR (M-ED) has been compared to the tangential component of the equivalent dipole based on the VEP (E-tED), (Stok 1984). Equivalent dipoles were estimated at 5ms intervals by using a least squares fitting

procedure. A single dipole was used to model the source and four concentric spheres were used to model the volume conductor. Equivalent dipoles were estimated for the time courses of the two major components CI and CII. The M-EDs and E-tEDs were comparable in terms of position, orientation and time periods covered. Differences did occur between the equivalent dipoles but these were thought to be largely attributable to variations in individual cortical topography.

Kaufman and Williamson (1988) stimulated both the upper and lower right visual quadrants with a pattern onset grating stimulus. The upper quadrant gave an ECD whose orientation and position fitted with the model of representation of the visual field on the visual cortex. The lower quadrant ECD, was however, oriented in a direction not predicted, in that it was oriented in an upward direction. Both the ECD's were also situated at approximately the same level in the visual cortex, see fig 6.33.

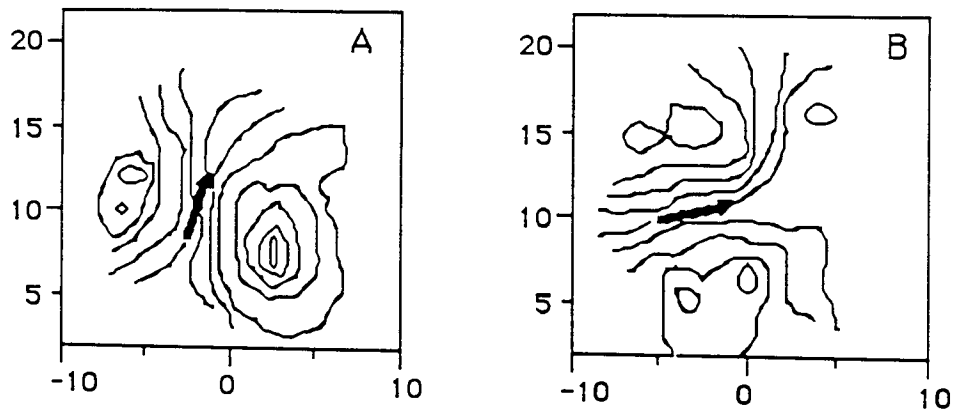

Fig. 6.33 Illustration of the location of the ECD's after A) lower quadrant stimulation and B) upper quadrant stimulation After Kaufman and Williamson (1988).

Peripheral stimulation of the half field has been shown to originate from deeper sources (George et al 1988, Maclin et al 1983). A source for the right half field stimulus was located several cms off the midline near the end of the calcarine fissure whereas a shallow source for central stimulation was located near the occipital pole (George et al 1988). Conversely Ahlfors et al (1991) could not demonstrate any systematic depth difference between stimuli located in the foveal and parafoveal regions. Using a checkerboard pattern onset stimulus a depth difference of the dipole, described after calculation from a sphere model, was shown between the upper and lower field stimuli, the depth of the lower field dipoles tended to be greater, see fig 6.35. Dipoles were located in the contralateral

hemisphere and for 1/2 subjects the parafoveal stimuli tended to be located more superiorly. Parafoveal ECDs tended to be located more superior than those of the fovea, see fig 6.34. In one subject the upper parafoveal ECDs were more superior than the lower field ECDs. Whereas the parafoveal lower field stimuli tended to be at a similar position to the foveal lower field stimuli. The foveal responses appeared to be localised more contralaterally.

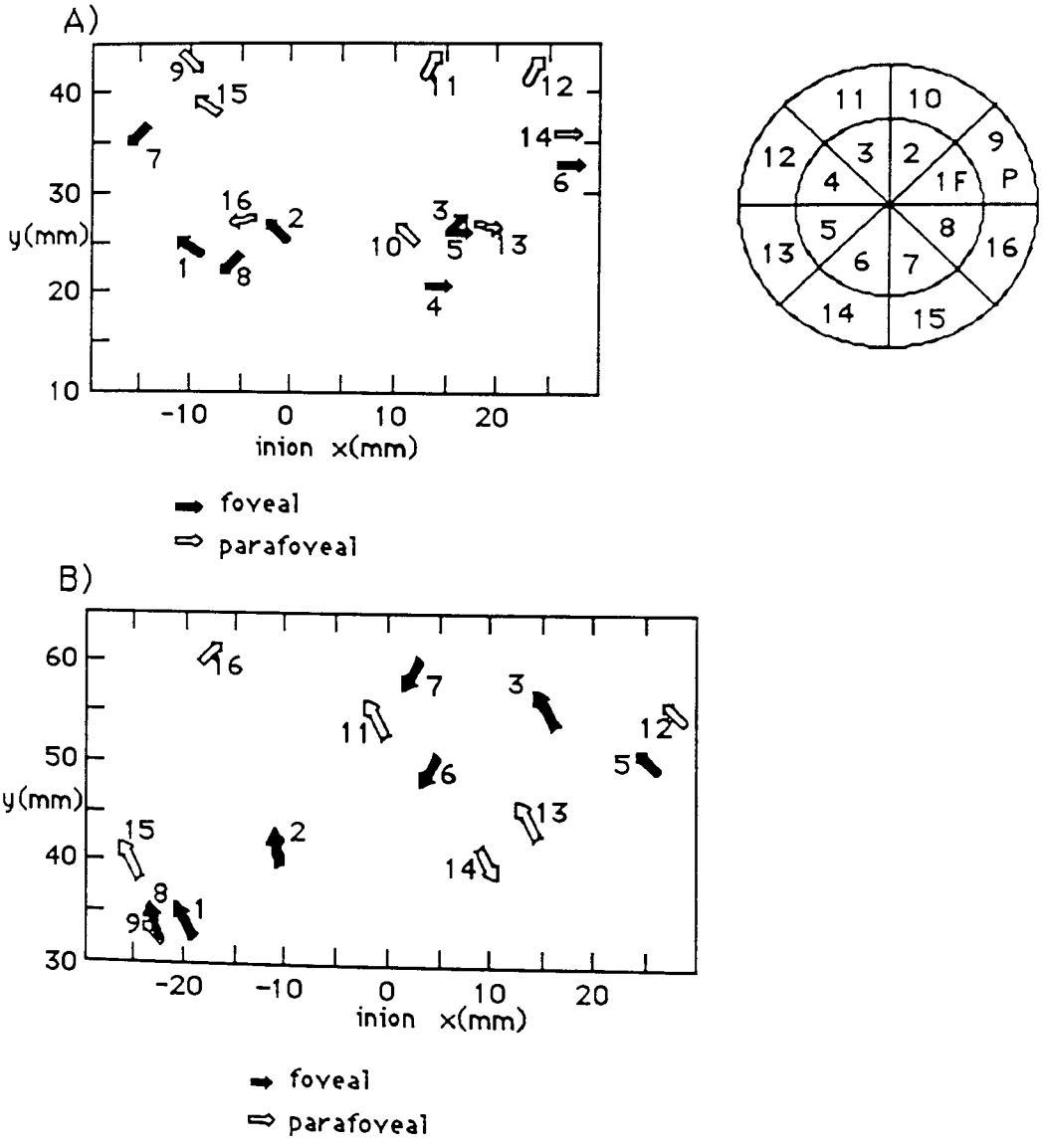

Fig 6.34. Position of the Equivalent current dipoles for the first major deflection in the pattern onset response. Upper plot of ECDs are at 80ms and the lower are at 100ms. After Ahlfors, Ilmoniemi and Hamalainen (in press).

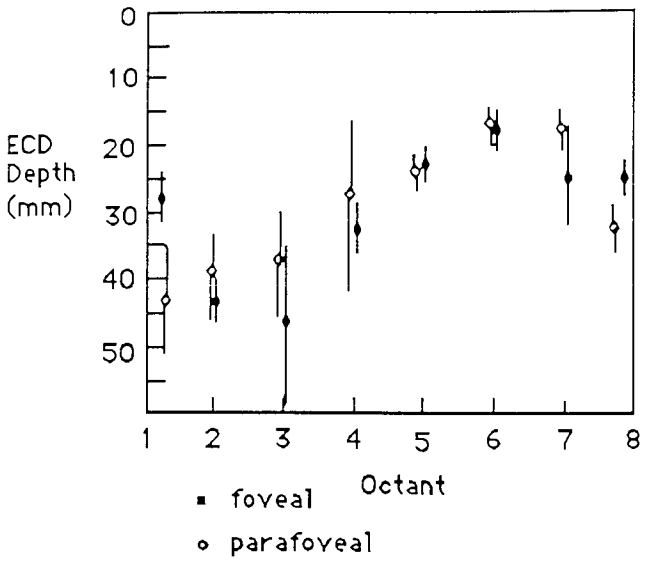

Fig 6.35 Plot of the depth of the ECD for one subject versus the octant stimulated. The bars denote the 95% confidence limits, calculated for an 8fT/(cm$\sqrt{Hz}$) total noise level. After Ahlfors, Illmoniemi and Hamalainen (in press).

Using a pattern reversal stimulus Janday et al (1987) compared the distribution of the VEP to that of the VEMR for right half field and right upper and lower quadrants. The field size used was 5° and the check size was 13'. Location of the equivalent current dipole was estimated by the iterative fitting procedure using the dipole in a sphere model. Dipoles for both the lower quadrant and half field were located contralaterally at depths of 2.92 and 3.67cm respectively, whereas the dipole for the upper quadrant was located ipsilaterally at a depth of 4.21cm. The dipole directions for both the upper and lower quadrants conform with the projection of these areas onto the cortex, the most anterior source was due to the lower quadrant however the most posterior was the result of half field stimulation. Conversely the lower quadrant distribution of the electrical response was more posterior than the upper quadrant, the distribution was however shown at the peak of the magnetic and not the electrical data. Dipoles were also constructed in a time window of 90-168ms from the peaks of the magnetic power curve. The orientation of the dipole for the upper quadrant did not change substantially, however the location moved from being ipsilateral to contralateral. With increasing time the dipole position for the half field stimulus became more contralateral and slightly shallower. The lower quadrant dipole also moved contralaterally but the depth increased with increasing time and the dipole orientation was rotated through aproximately 180° for the later peaks.

Dipole generators of the pattern onset VEP response have been extensively investigated (Darcey 1981, Butler 1985, Ossenblok and Spekreijse 1991). Foveal sources have been shown to result from dipoles located lateral to the midline and contralateral to the stimulating field, lower foveal quadrant dipoles were also shown to be positioned lower than those from the upper quadrant (Butler 1985). In addition dipoles fitted after upper quadrant stimulation have been shown to be more lateralised (Darcey 1981) and more tangentially orientated (Ossenblok and Spekreijse 1991). This could be in accordance with the dipole sheet model of the extrastriate cortex. No difference in the peak latencies of the upper and lower quadrants were demonstrated, the half field dipole fits were mainly radial, dominated by the lower quadrant, and located between the two quadrants (Ossenblok and Spekreijse 1991)

There has been much controversy in the literature as to the location of the neuronal generators of the pattern reversal VEP. A number of authors suggest a source in the extrastriate areas (Halliday and Michael 1971, Lehmann, Darcey and Skrandies 1982). Others suggest a source in both the striate and extrastriate areas (Celesia et al 1982, Phelps et 1981, Kushner et al 1988, Edwards 1989) or just the striate areas (Ducati et al 1988).

6.6.7 Dipole Source Localisation of the Present Data

Dipole localisation was performed on the present data using the forward solution of a single dipole in a sphere. The data points were first transformed from values on a sphere surface to values on a flat plane. These values were then inputed into the following equations to estimate the best fit dipole.

The general formula for the external field 'B' produced by a set of i current dipoles P_i in a piecewise homogeneous conducting body is:

$$B = \frac{\mu_0}{4\pi} \sum P_i \times \frac{R_i}{R_i^3} - \frac{\mu_0}{4\pi} \sum_{j=1} (\partial_j' - \partial_j'') f_{S_j} V(r') \, dS_j \times \frac{R'}{R'^3}$$

$\partial_j' - \partial_j''$ are the conductivities on the inner and outer sides of the n surfaces, Sj that separate regions of different conductivity. V(r') is the potential distribution found by solving a self consistent integral equation for the body. Five parameters were defined, three for dipole location (x_d,y_d,z_d), one for the angle between the projection of the dipole into the xy plane and the x axis and one for the strength. These are found by minimising the error parameter:

$$R = \Sigma_i (Se^i - St^i)^2 / \Sigma (Se^i)^2$$

Se^i and St^i are the measured and predicted SQUID signals at the i measurement sites. Dipole fits could not be performed with any confidence on the large check field maps or on the data from subject AS. Source localisation was however performed on the remaining data and the following fits were achieved, see table 6.1.

File	Sphere Centre	Dipole Location	Orientation	Strength	Rmin
22' Checks					
RAFF	0, 4, 10	-0.51, 2.86, -5.31	292°	3.1×10^{-7}	0.27
CNFF	0, 2, -8	2.69, 3.58, -6.26	53°	7.8×10^{-7}	0.12
CDFF	0, 4, -8	0.87, 1.96, -3.23	300°	12.9×10^{-7}	0.13
CDRHF	0, 2, -12	0.04, 3.12, -3.42	301°	8.5×10^{-7}	0.15
34' Checks					
RAFF	0, -4, -12	0.23, 3.70, -6.66	113°	8.0×10^{-7}	0.30
CNFF	0, 2, -12	-0.02, 1.22, -5.01	40°	3.8×10^{-7}	0.14
CNRHF	0, 4, -8	-0.74, 3.52, -3.68	121°	1.4×10^{-7}	0.21

Table 6.1 Locations, orientations and strengths of the dipole calculated from the topographical distributions. The sphere centre is given in the x, y, z directions. The last column indicates the error parameter.

The dipole sources were positioned close to the midline, apart from the data of subject CN with 22' full field stimulation. The dipole positions are shown in figs 6.36 - 6.38. Dipole fits for subject RA demonstrated an increase in the depth with an increase in the size of the checks. These dipoles would fit with a source located in the striate cortex and maybe bordering regions of the extrastriate cortex, area 18.

Fig. 6.36. Diagrammatic illustration of the position of the dipole fit following full field stimulation with the 34' and 22 checks, upper and lower figure respectively. Position 0,0 represents the inion. Subject R.A.

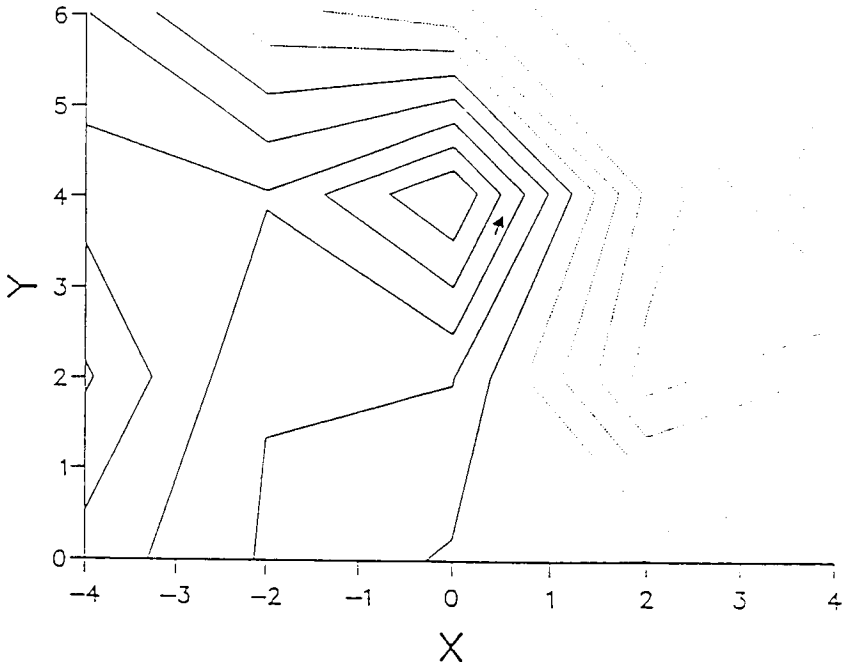
6
5
4
3
2
1
0
Y
−4
−3
−2
−1
0
1
2
3
4
X

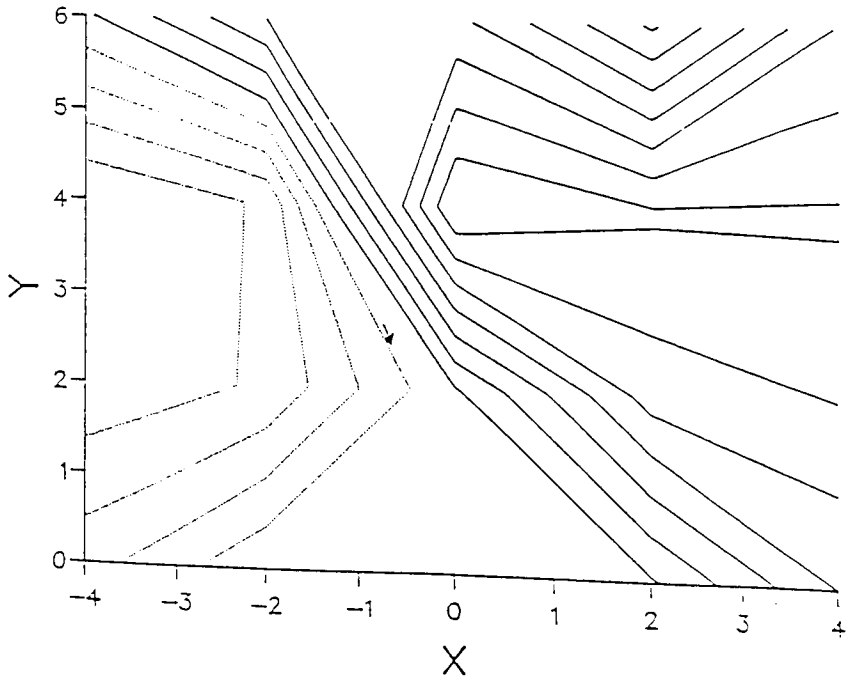
6
5
4
3
2
1
0
Y
−4
−3
−2
−1
0
1
2
3
4
X

Fig. 6.37. Diagrammatic illustration of the position of the dipole fit following full field stimulation with the 34' and 22 checks, upper and lower figure respectively. Position 0,0 represents the inion. Subject C.N.

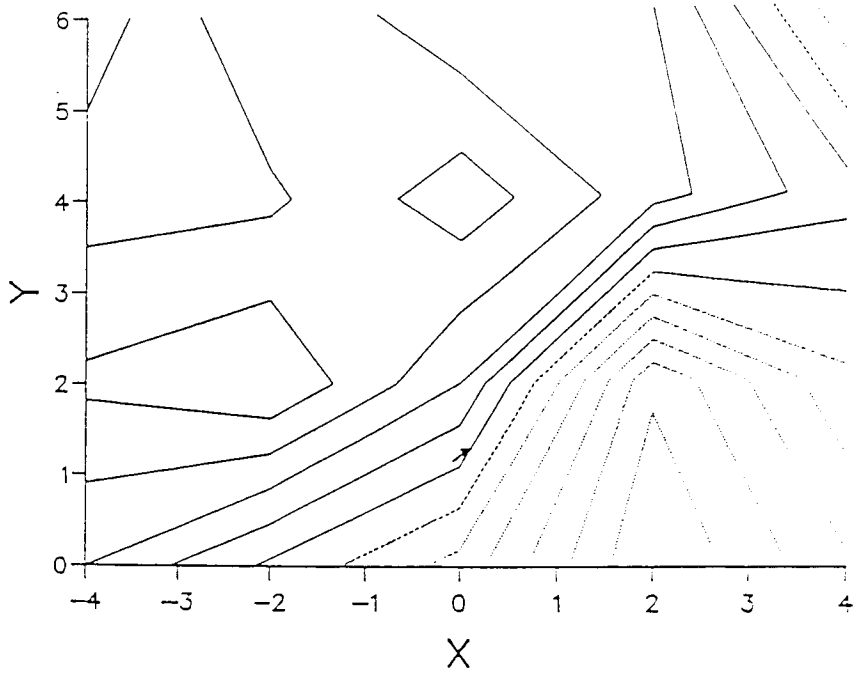
6
5
4
3
2
1
0
Y
−4
−3
−2
−1
0
1
2
3
4
X

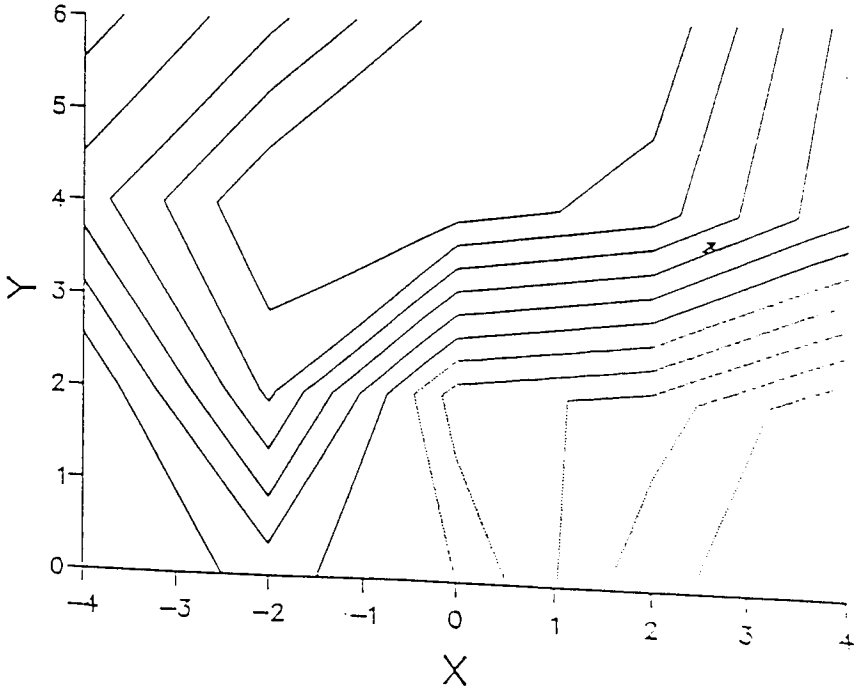
6
5
4
3
2
1
0
Y
−4
−3
−2
−1
0
1
2
3
4
X

Fig. 6.38. Diagrammatic illustration of the position of the dipole fit following right half field 34 check stimulation, subject C.N. Position 0.0 represents the inion.

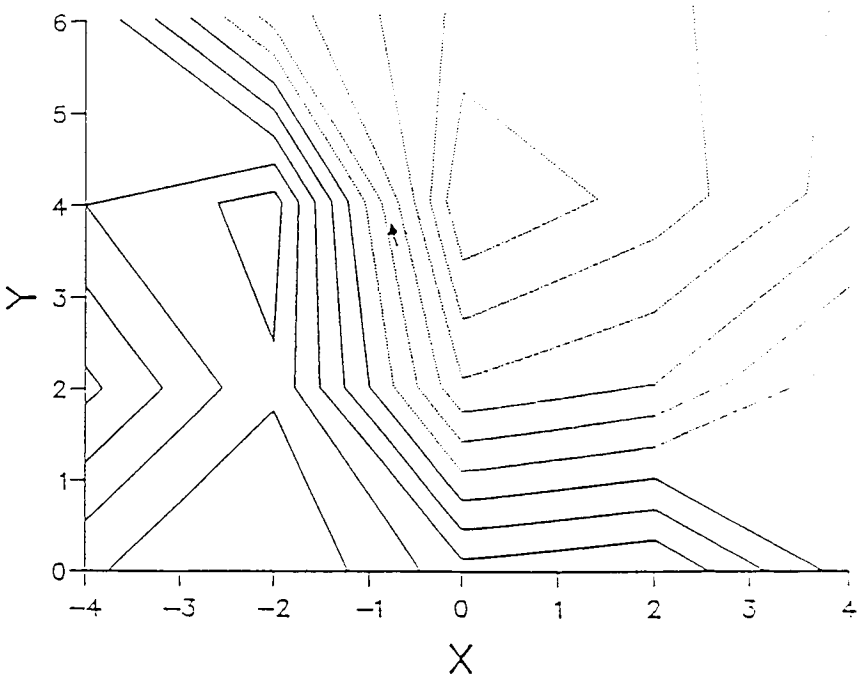
6
5
4
3
2
1
0
Y
−4
−3
−2
−1
0
1
2
3
4
X

6.7 Summary

1) The VEMR data collected could be the result of a dipolar source located in the contralateral hemisphere. The dipolar fits show a source close to the midline in the contralateral hemisphere directed towards the midline. This could be consistent with a source in the striate cortex or neighbouring area 18.

2) The VEP distributions were shown to be consistent with previous work, however the contralateral positivity recorded before the P100 was found to be dependent on check size. Variation in the contralateral components were demonstrated with one subject producing the ipsilateral progression of components over the contralateral hemisphere.

3) The latency of the two responses were found to vary, however the same trends were demonstrated in the two data sets to varying check sizes from left half field and full field stimulation. There was also a significant positive correlation of the latencies of the two groups over checks sizes, subjects and field location ($r=0.34$, $p<0.05$). This suggests that the two techniques may be recording similar events in the brain. The dipolar distribution succeeding the P100 could not be fitted to the VEMR distribution in all presentations.

4) From the location of the maximum early negativity and P100 it appears that as the check size reduces the orientation of the 'dipole' rotates to become directed toward the contralateral hemisphere.